Why is dihydrodipicolinate synthase a tetramer?

Thesis submitted in partial fulfilment of the requirements for the degree of

Doctor of Philosophy

at the

University of Canterbury

by

Michael D W Griffin

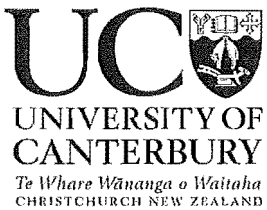

2005

to mum and dad...

Acknowledgements

Sincere thanks must first go to my supervisor Juliet Gerrard, whose enthusiasm, unwavering positivity, support, and friendship have kept me on track, even when I wasn't smiling. It has been a privilege. Stellar pauses are here to stay, Ren said it, and I don't really glow.

Thanks must also go to the people who saw fit to let me use bits of equipment that we don't have just lying around. To Matt Perugini, who so willingly offered his time and XL-A to a young kiwi. To the elusive Mike Morris, nuff said, and to Geoff Jameson for the opportunity to produce my -very own- crystal structures. Thanks also to my co-supervisors, and to all who have had input into this project, especially Ashley Sparrow, Khris Mahanty, Peter Steel, and Craig Hutton. Thanks, also, to Crop and Food research and especially Nigel Larsen for the funding.

To Ren, you have been an inspiration. The road would have been a very different one if you had not been around. My huge thanks for your friendship and help... and for taking me in when I needed a place to live. To the rest of Team-DHDPS, past and present, it has been a time. Tammy, thanks for keeping my car sealed and fresh while I did the show. Jen... we love you Jen. Laurence... no no no no no. To the rest of the lab crew especially Antonia and our surrogate lab member, Matt G, it has been fun. To the Morris lab, thanks for adopting me, and for all the NMRs. Thanks to Jackie for advice along the way and to Matt W who was always at the ready with a new poster layout or laser printer when they were needed.

To my dear friends, thank you for being patient. This is what it has all been about, and yes, I will no longer be a student. My love and thanks go to Trace, who joined the team late, but who has made the period spent producing this document a world apart from what I had expected.

To Mum, Dad, Nick, Pip, James, Kate, David, Kezia, and Diana, without your love and support over the years I would certainly not have arrived at the place where I am now.

Finally, Batman *is* a scientist...

Table of contents

Abbreviations

α	ratio of V and V'
A	alanine
A	concentration ofsubstrate A
Å	Angstrom
amp^r	gene conferring ampicillin resistance
(*S*)-ASA	(*S*)-asparate β-semialdehyde
B	concentration of substrate B
bd	broad doublet
BN-PAGE	blue-native polyacrylamide gel electrophoresis
BOC	*tert*-butoxycarbonyl
BOP.PF_6	(benzotriazol-1-yloxy) tris(dimethylamino)phosphonium hexafluorophosphate
bp	base pairs
BSA	bovine serum albumin
°C	degrees Celsius
CD	circular dichroism
cp	centipoise
c(s)	continuous sedimentation coefficient distribution
c(M)	continuous mass distribution
c(r)	concentration at radius r
$c(r_0)$	concentration at radius r_0
cm	centimetre
d	doublet
δ	chemical shift in parts per million downfield from tetramethylsilane
D	aspartate
Da	Daltons
DAP	*meso*-diaminopimelate
*dap*A	gene encoding dihydrodipicolinate synthase
*dap*B	gene encoding dihydrodipicolinate reductase
DHDP	dihydrodipicolinate
DHDPR	dihydrodipicolinate reductase

DHDPS	dihydrodipicolinate synthase
DIBAL	diisobutylaluminium hydride
DNA	deoxyribonucleic acid
ddNTP	(2',3')-dideoxynucleic acid triphosphate
dH_2O	distilled water
ddH_2O	double distilled water
dt	doublet of triplets
E	glutamate
E	baseline offset
ε	extinction coefficient
E. coli	*Escherichia coli*
EDTA	ethylenediaminetetraacetic acid
f/f_0	frictional ratio
g	gram
g	gravity
η	solvent viscosity
HEPES	N-2-hydroxyethylpiperazine-N'-2-ethane sulphonic acid
HIC	hydrophobic interaction chromatography
HTPA	(4*S*)-4-hydroxy-2,3,4,5-tetrahydro-(2*S*)-dipicolinate
I	inhibitor
[I]	inhibitor concentration
IC_{50}	inhibitor concentration giving 50% inhibition
IPTG	isopropyl β-*D*-thiogalactopyranoside
J	Joules
J	coupling constant
K	lysine
K	Kelvin
K_a	association constant
kb	kilobase
k_{cat}	catalytic constant
kDa	kiloDalton
K_i	inhibition constant
K_m	Michaelis-Menton constant

lac	operon encoding β-galactosidase
L	leucine
L	litre
LB	Luria-Bertani broth
µg	microgram
µl	microlitre
M	moles per litre
M	molecular mass
M_{app}	apparent molecular mass
M_{eq}	equivalent molecular mass
m/z	mass to charge ratio
min	minute
mg	milligram
ml	millilitre
ng	nanograms
nm	nanometre
N	asparagine
NADH	nicotamide adenine dinucleotide, reduced form
NADPH	nicotamide adenine dinucleotide phosphate, reduced form
NMR	nuclear magnetic resonance
N. sylvestris	*Nicotiana sylvestris*
P	confidence level/f-ratio
ρ	solvent density
PAGE	polyacrylamide gel electrophoresis
PCR	polymerase chain reaction
PDB	Protein Data Bank
pJG001	Bluescript plasmid containing the *dap*A gene encoding DHDPS
pJK001	Bluescript plasmid containing the *dap*B gene encoding DHDPR
ppm	parts per million
pyr	pyruvate
Q	glutamine
r	radius
R	arginine

R	the gas constant
*rec*A	gene encoding for the RecA protein
rpm	revolutions per min
r.m.s.d.	root mean square deviation
RNase	ribonuclease
r.t.	room temperature
s	sedimentation coefficient
S	Svedberg
S	substrate
[S]	substrate concentration
sec	second
SDS	sodium dodecyl sulphate
T	threonine
T	temperature in kelvin
TAE	tris-acetyl EDTA electrophoresis buffer
tet^r	tetracycline resistance gene
TFA	trifluoroacetic acid
THF	tetrahydrofuran
TIM	triosephosphate isomerase
Tris.HCl	tris(hydroxymethyl)methylamine
UV	ultraviolet
v	intial rate
$\bar{v}$	partial specific volume
V	maximum rate of reaction
V'	maximum rate of reaction in the presence of saturating inhibitor
V_e	elution volume
ω	angular velocity
X-gal	5-bromo-4-chloro-3-indolyl-(–δ-glactosidase
Y	tyrosine

Abstract

Dihydrodipicolinate synthase (DHDPS, E.C. 4.2.1.52) catalyses the final branch-point reaction in lysine biosynthesis and is feedback inhibited by lysine. The enzyme is a homotetramer of 125 kDa that is composed of a dimer of dimers, where two monomers associate strongly to form tight-dimer units and two of these units associate to form the wild-type tetrameric structure. Efficient catalysis by DHDPS requires the movement of protons between the active site and bulk solvent *via* a proton-relay triad. This motif is formed on association of the two monomers of the tight-dimer and is comprised of residues from both monomers, suggesting that establishment of the tight-dimer structure is required for optimal catalysis. However, there is no obvious function afforded by the association of tight-dimer units to form the tetramer.

To understand the functional and mechanistic contributions of the tetrameric structure of DHDPS, a suite of amino acid mutations of residues at the dimer-dimer interface was designed to produce dimeric variants of the enzyme for comparative functional analysis. A complete re-evaluation of the composition of the dimer-dimer interface contact surface was undertaken, identifying five intersubunit contact residues and a water-bridging network that had not previously been reported. The variants DHDPS-L197D, DHDPS-L197Y, DHDPS-Q196D, DHDPS-D193A, DHDPS-D193Y, and DHDPS-Q234D were produced by site-directed mutagenesis. Comprehensive biophysical characterisation suggested that all variants had altered quaternary structure with respect to wild-type DHDPS. DHDPS-L197D and DHDPS-L197Y were found to exist as stable obligate dimers in solution. DHDPS-Q196D and DHDPS-D193A were shown to exist in equilibrium between dimer and tetramer with K_a values of $10^{5.6}$ M^{-1} and $10^{5.8}$ M^{-1}, respectively.

Rigorous kinetic analysis showed that each variant retained catalytic activity, but that this activity was attenuated from the level of the wild-type enzyme. This was most pronounced in the dimeric variants, DHDPS-L197D and DHDPS-L197Y, which displayed 2.5% and 1.4% of wild-type activity, respectively. Each variant demonstrated a raised K_m value for the first binding substrate, pyruvate. In DHDPS-L197D and DHDPS-L197Y, K_{mPyr} values were raised four-fold and seven-fold over that of wild-type DHDPS. Interestingly, it was also found that incubation of these variants at raised temperature gradually increased the catalytic turnover rate of each enzyme.

Both DHDPS-L197D and DHDPS-L197Y were successfully crystallised and their structures solved to 2.0 Å and 1.7 Å resolutions, respectively. Both structures retained the tertiary and quaternary details of the wild-type tight-dimer with a very high degree of fidelity and no rearrangements at the active site were observed to account for the attenuation of catalysis in the variants.

Electron density suggested that pyruvate remained covalently attached at the active site, despite crystallisation and purification in the absence of the substrate. The pyruvate adduct was identified as the trapped tetrahedral intermediate of the reaction between pyruvate and K161. The dehydration of this intermediate is catalysed by the proton-relay triad that includes a tyrosine residue, Y107, that interdigitates into the active site from the neighbouring monomer.

In conclusion, it is proposed that a function of the tetrameric structure of *E. coli* DHDPS is to constrain dynamic movements of the monomers of the tight-dimer with respect to each other. This is thought to allow for correct positioning of Y107 in the proton-relay triad, resulting in optimal catalysis, and circumventing the trapping of the pyruvate reaction intermediate. Such constraint of protein dynamics may offer a general rationale for the oligomeric structure of many enzymes.

Chapter One

Introduction

The subject of this thesis is the tetrameric enzyme dihydrodipicolinate synthase (DHDPS) from *Escherichia coli*; the enzyme that catalyses the first committed step of the diaminopimelate pathway of lysine biosynthesis, and is feedback inhibited by lysine.

The work described in this thesis focuses on the elucidation of the mechanistic and functional advantages afforded by the homotetrameric structure of DHDPS. This research was undertaken in light of the fact that structural data indicate that a dimeric structure is the minimal unit necessary for the catalytic and regulatory function of the enzyme.

The mechanistic and functional advantages of the tetrameric structure of the *E. coli* enzyme are examined by alteration of the quaternary structure of the protein using site-directed mutagenesis, followed by characterisation of both the wild-type and variant forms of the enzyme by biophysical methods, steady state kinetics, and X-ray crystallography.

1.1 Background

In 1950, the identification of the novel amino acid, *meso*-diaminopimelate, in bacterial hydrolysates (1,2) prompted investigation into the biosynthesis and cellular role of this molecule. This eventually led to a full elucidation of bacterial biosynthesis of lysine (3) including the discovery and preliminary characterisation of the first enzyme unique to this pathway, DHDPS (4,5).

Lysine is a member of the aspartate family of amino acids, which also includes threonine, methionine, and isoleucine (Figure 1.1) (6,7). Biosynthesis of aspartic acid derived amino acids is restricted to plants, bacteria, and some fungi, and as such, these amino acids are essential dietary components for animals.

The lysine biosynthetic pathway has become the focus of two important avenues of research: as a target for antibiotics and herbicides and in efforts towards engineering lysine rich crops (7). As DHDPS catalyses the branchpoint and purported rate limiting step in the biosynthesis of lysine, this enzyme has largely been the focus of these two lines of investigation. Thus, a better understanding of the function and mechanisms of this enzyme may aid in furthering these efforts.

Figure 1.1 *The biosynthesis of the aspartate family of amino acids, highlighting the DAP pathway (red) and the products meso-diaminopimelate and* (S)*-lysine.*

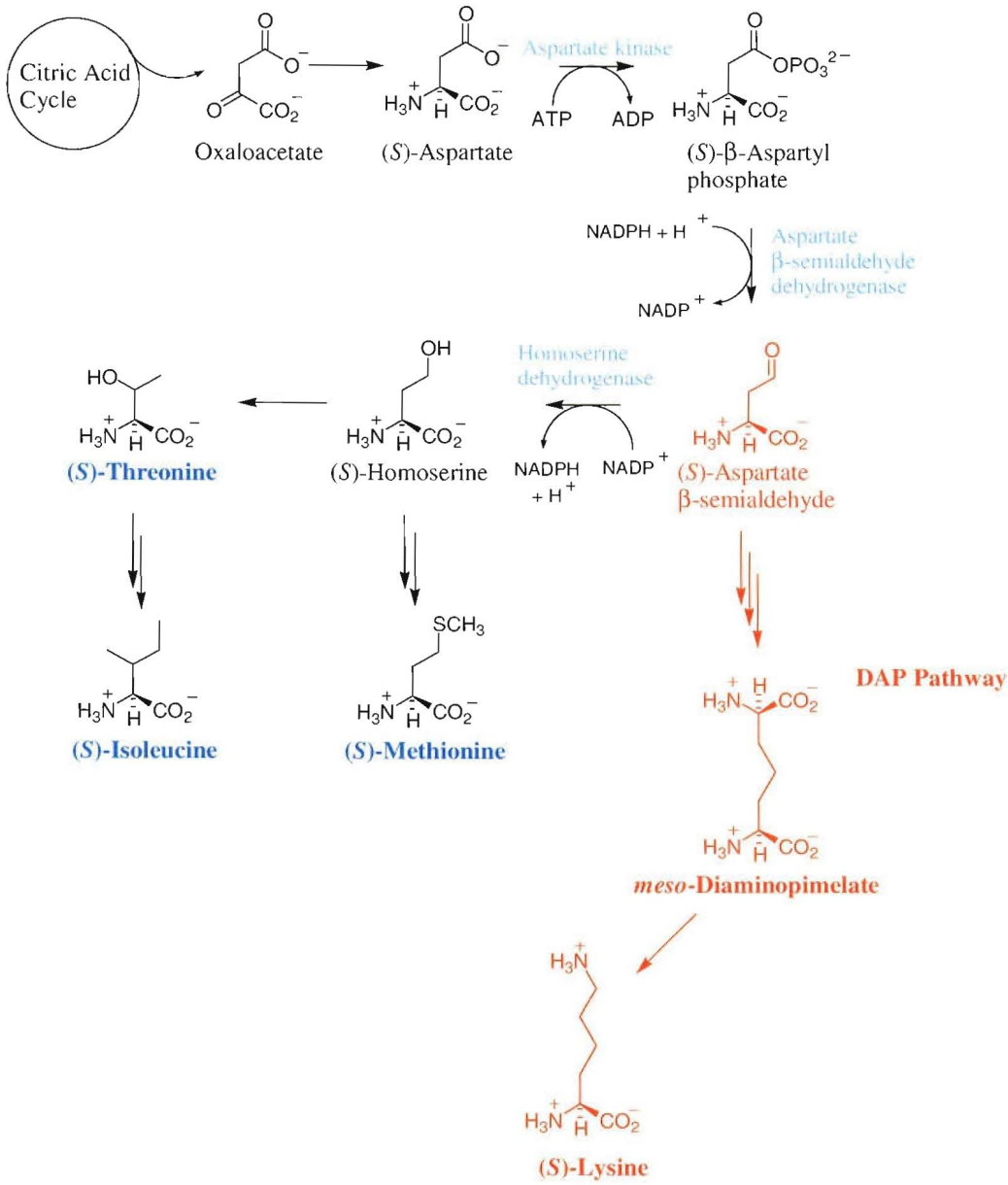

1.1.1 Antibiotics and herbicides

The recent increase in bacterial resistance to current antibiotic compounds has produced an urgent need for the development of new antibiotic agents (6). As lysine biosynthesis is restricted to plants and microbes, specific inhibitors of this pathway have the potential to be selectively toxic to these organisms with limited toxicity to mammals and other animals, and may thus, represent a novel class of antibiotic (6,8-10). However, despite substantial research, succcess in this field has been limited (8), and there are currently no commercial drugs or herbicides available that specifically inhibit lysine biosynthesis (6,8).

In addition to the final product, lysine biosynthesis *via* the diaminopimelate pathway is an important source of *meso*-diaminopimelate (DAP) (6) (Figure 1.1). Bacteria require either lysine or DAP as an essential component of the cell wall peptidoglycan layer (11,12). These amino acids form a crucial part of the crosslinking network that lends the cell wall its rigidity and strength. Many commonly used antibiotics act by inhibiting the crosslinking of the bacterial cell wall, which in turn causes cell lysis by intracellular osmotic pressure.

The herbicidal action of inhibition of lysine biosynthesis may be exerted by deprivation of the essential product of the pathway, which the plant has no other means of aquiring.

1.1.2 Lysine content of crop foods

Lysine is among the essential amino acids that humans and other animals are unable to synthesise, and thus must be taken in as a dietary component. However, many crop and cereal plants contain relatively low levels of lysine, and frequently lysine is the nutritionally limiting component of these foods (7,13). The manipulation of the biochemical and genetic regulation of lysine metabolism has been studied extensively in an effort to enhance the nutritional value of plant products (4,14-25).

Lysine biosynthesis in plants is primarily regulated by aspartate kinase and DHDPS. In order to increase cellular free lysine concentrations, flux through the lysine biosynthetic pathway must be increased. Bacterial DHDPS is less sensitive to feedback inhibition by lysine than plant enzymes, and thus, expression of bacterial

enzymes in plant systems has been shown to increase the total free lysine content of tobacco (19), barley (23), canola (22), and potato (26,27) plants.

Mutations causing insensitivity to feedback inhibition of DHDPS have also been shown to lead to over production of lysine (18,20) and this method has been used to increase the total lysine content of plants such as *Nicotiana sylvestris* (28,29). Plants with increased lysine content have also been produced by over expression of recombinant, lysine-rich proteins (30), which reduce feedback inhibition of DHDPS by sequestration of free lysine.

1.2 Lysine biosynthesis

Two unrelated pathways for the biosynthesis of lysine have been described; the α-aminoadipate pathway and the diaminopimelate pathway. The α-aminoadipate pathway is restricted to higher fungi and euglenoids (31,32). This pathway begins with the condensation of α-ketoglutarate and acetyl-CoA, and proceeds *via* the intermediate (*S*)-α-aminoadipate to lysine in eight steps (32).

In plants, bacteria and some phycomycetes, lysine is synthesised from aspartate *via* the diaminopimelate pathway. This route of lysine biosynthesis can be broken into two parts: the synthesis of (*S*)-aspartate β-semialdehyde ((*S*)-ASA), which is common to lysine, methionine, threonine and isoleucine biosynthesis (Figure 1.1), and the lysine-specific diaminopimelate pathway (Figure 1.2).

1.2.1 The aspartate family of amino acids

The family of (*S*)-aspartate-derived amino acids comprises lysine, methionine, threonine, and isoleucine (Figure 1.1). Aspartate itself is derived from oxaloacetate, and is initially phosphorylated by aspartate kinase to give (*S*)-β-aspartyl phosphate before an NADPH-dependent reduction to (*S*)-ASA (33). At this point, the pathway branches and (*S*)-ASA can then be reduced to give (*S*)-homoserine, the precursor to methionine, threonine, and isoleucine, or, alternatively, it can enter the diaminopimelate pathway to produce lysine (33).

1.2.2 The diaminopimelate pathway

The first committed step of lysine biosynthesis *via* the diaminopimelate pathway is the condensation of pyruvate and (*S*)-ASA to form (4*S*)-hydroxy-2,3,4,5-tetrahydro-(2*S*)-dipicolinic acid (HTPA) (34), which is then thought to undergo non-enzymatic dehydration to dihydrodipicolinate (DHDP) (34). This reaction is catalysed by the enzyme DHDPS and is a key point of regulation in the pathway, as DHDPS is feedback inhibited by the final product of the pathway, lysine.

DHDP is subsequently reduced by dihydrodipicolinate reductase (DHDPR) to tetrahydrodipicolinate in an NAD(P)H-dependent reaction. From this point, three alternative routes to *meso*-diaminopimelate have been identified and described (Figure 1.2) (35,36).

The most common route, and that found in *E. coli*, is the succinylase pathway (37). The tetrahydrodipicolinate ring is opened *via* N-succinylation of the α-amino group to form succinyl-ε-keto-α-aminopimelate (38). This ketopimelate then undergoes transamination, with glutamate as the amino group donor, to yield succinyl diaminopimelate (39). Succinyl diaminopimelate is then desuccinylated, forming (*S*,*S*)-diaminopimelate (40), which is epimerised to *meso*-diaminopimelate (41).

The chemistry of the acetylase pathway is directly related to that of the succinylase pathway. The two pathways proceed through an identical series of steps, and differ only in the protecting group utilised: the acetylase pathway involves N-acylated intermediates in place of N-succinylated intermediates (42). The acetylase pathway is extremely limited in its bacterial distribution but has been described in some *Bacillus* species (43).

In the shorter dehydrogenase pathway, tetrahydrodipicolinate is converted directly to *meso*-diaminopimelate by reductive amination, catalysed by diaminopimelate dehydrogenase (33). Again, this pathway has highly limited bacterial distribution (33,36) but has been found to be utilised in parallel with the succinylase pathway in the industrial (*S*)-lysine producer, *Corynebacterium glutamicum* (33,44).

Figure 1.2 *The three known variants of the diaminopimelate pathway to* (S)*-lysine.*

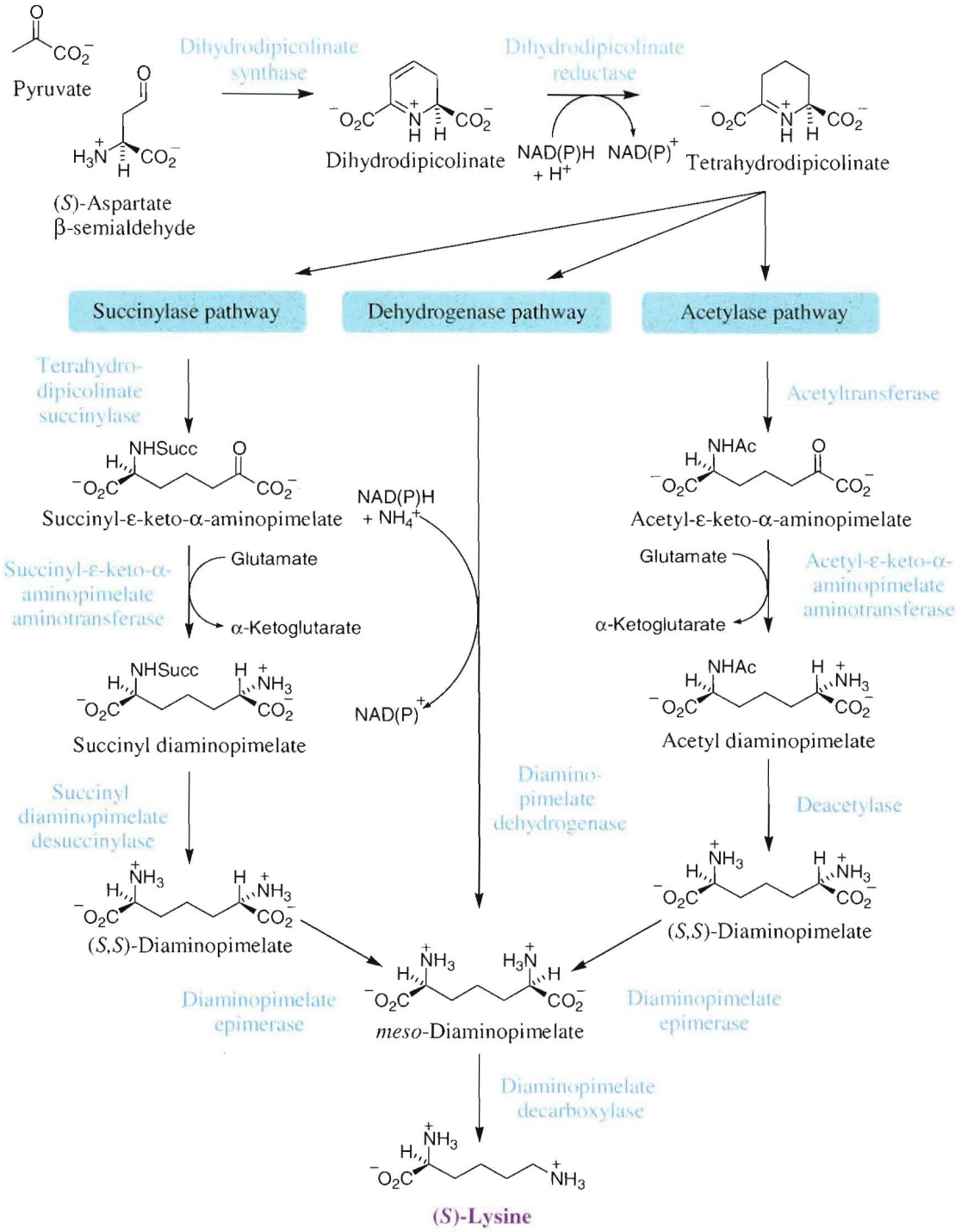

The decarboxylation of the common product of the three alternate routes, *meso*-diaminopimelate, to produce the end product, (*S*)-lysine (45), forms the final step of the DAP pathway.

1.3 Dihydrodipicolinate synthase

Dihydrodipicolinate synthase activity was first observed in *E. coli* cell lysates in 1965 by Yugari and Gilvarg (4). Since that time, the genetic, structural, and functional properties of DHDPS from numerous sources have been extensively studied. Despite this, many aspects of the structural and functional mechanisms of the enzyme remain inadequately understood, due, at least in part, to the complexity of these mechanisms. Thus, more rigorous structure-function studies are required in order to understand fully this enzyme and thereby acquire the tools needed to effect its manipulation.

1.3.1 Genetic studies

The *dap*A gene encoding DHDPS has been mapped to 53 minutes on the *E. coli* chromosome (46,47), cloned (48), and sequenced (47). In contrast to other enzymes in the DAP pathway, the expression of the *dap*A gene in *E. coli* is not regulated by cellular free lysine levels or by any other stimuli (49).

The *dap*A gene has also been cloned and sequenced from a variety of other bacterial (50-54) and plant (18,55-58) species. Sequence similarity at the amino acid level is high among plant enzymes; the wheat and maize sequences have approximately 90% identity (56). In contrast, bacterial enzymes appear to be more divergent, with the *E. coli* sequence showing 33% identity to both the *Brevibacterium lactofermentum* (53) and *Corynebacterium glutamicum* (51) sequences, and 55% identity to that of *Methylophilus methylotrophus* (54). Interestingly, sequence identities between bacterial and plant enzymes are similar to those between bacterial examples (53,54,59,60).

1.3.2 Enzymology

Early gel filtration and sucrose density gradient centrifugation experiments placed the molecular weight of *E. coli* DHDPS at approximately 126 kDa and 134 kDa, respectively (5). The published *dap*A sequence from *E. coli* predicts a polypeptide of 292 amino acid residues with a molecular mass of 31,372 Da (47), and thus, the enzyme was presumed to be a tetramer of four identical subunits. However, electrospray mass spectrometry experiments yielded a monomeric molecular weight of 31,272 Da (61,62), suggesting that errors existed in the predicted amino acid sequence. This latter mass was confirmed by X-ray crystallographic studies, which

also verified the correct amino acid sequence and quaternary structure of *E. coli* DHDPS (60).

DHDPS has been isolated from a range of bacterial (5,63-66) and plant (18,58,67-70) sources. At the outset of this work, all characterised DHDPS enzymes were reported to be tetrameric with one exception. In contrast to all other plant examples, a single set of gel filtration experiments suggests that DHDPS from *Pisum sativum* is trimeric (68), a result that has not been confirmed by other methods.

1.3.3 Kinetic studies

All kinetically characterised examples of DHDPS appear to exhibit the compulsory ordered, substituted kinetic mechanism, commonly called the 'ping-pong' mechanism (71).[⊥] This mechanism requires that the two substrates, (*S*)-ASA and pyruvate, bind to the enzyme in a defined order, that the reaction proceeds through a covalent enzyme-substrate intermediate, and that two independent products are released (Figure 1.3) (71).

Figure 1.3 *Schematic representation of the kinetic mechanism of DHDPS. E is unliganded enzyme, F is the covalent intermediate enzyme form, PYR is pyruvate, (S)-ASA is (S)-aspartate-β-semialdehyde, and HTPA is (4S)-hydroxy-2,3,4,5-tetrahydro-(2S)-dipicolinic acid (72).*

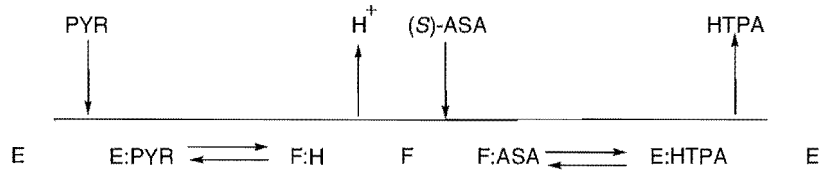

The assignment of the ping-pong mechanism to DHDPS is supported by a number of lines of evidence. Double reciprocal plots of steady state initial velocity data show the characteristic parallel lines with respect to each substrate, (4,72,73). The enzyme-pyruvate covalent intermediate has been identified in the absence of (*S*)-ASA by reduction of the complex with $NaBH_4$ (4,61), and product analogues have been reported to show predicted inhibition patterns with respect to the second binding substrate, (*S*)-ASA (72).

[⊥] The ping-pong kinetic mechanism is also known as the substituted enzyme, or the double displacement mechanism (71).

Substrate inhibition of DHDPS by (*S*)-ASA, which is predicted by the ping-pong mechanism, has been reported by a number of investigators (17,69,70,72,74). However, this behaviour has not been observed in work performed in this laboratory (8,75). Separate kinetic experiments using (*S*)-ASA synthesised by different methods were used to show unequivocally that the reported substrate inhibition was an artefact caused by an unidentified contaminant in the preparations of the substrate, which were produced by ozonolysis of allylglycine (75).

Reported Michaelis-Menten constants for both substrates vary greatly, depending on the source of the enzyme. In general, K_m values for (*S*)-ASA are much larger for DHDPS from bacterial sources than for DHDPS from plant sources. K_m values for pyruvate cover a broad range within both bacterial and plant examples (Table 1.1).

Published data for DHDPS from *E. coli* report a K_m for pyruvate of 0.19 mM and a K_m for (*S*)-ASA of 0.12 mM (72). These are significantly lower than values for enzymes from other sources, indicating that the *E. coli* enzyme has higher binding affinities for its substrates. The specificity of DHDPS for both of its substrates also appears high, as no alternative substrates have yet been found (4).

Table 1.1 *Kinetic constants of DHDPS from various sources.*

Organism	$K_{m\ Pyruvate}$ (mM)	$K_{m\ ASA}$ (mM)
Bacteria		
Escherichia coli (72)	0.19	0.12
Corynebacterium glutamicum (64)	6.2	–
Bacillus subtilis (65)	1.07	3.13
Bacillus licheniformis (66)	5.3	2.6
Bacillus sphericus (63)	9	5.1
Bacillus megaterium (76)	0.5	0.46
Plants		
Zea mays (58)	2.1	0.6
Pisum sativum (68)	1.7	0.4
Triticum aestivium (77)	11.8	0.8
Spinacia oleracea (69)	1.4	–

1.3.4 Regulation by lysine

As the enzyme that catalyses the first committed step of lysine biosynthesis *via* the diaminopimelate pathway, DHDPS represents the key point of regulation in the pathway (Figure 1.4). As such, the enzyme is subject to feedback inhibition by the final product of the pathway (*S*)-lysine. Kinetic and structural studies indicate that lysine acts allosterically on DHDPS (4,17,34,59,73,77); however, the precise mechanism by which lysine exerts regulatory control is yet to be elucidated fully, although recent studies carried out in this laboratory have produced significant advances in this area (78).

DHDPS from different sources display varying degrees of sensitivity to lysine inhibition, for example DHDPS from plants is generally 20- to 100-fold more sensitive to lysine than bacterial enzymes. It is, therefore, convenient to group DHDPS enzymes according to their regulatory properties with respect to lysine (79).

Figure 1.4 *Regulation of flux through the DAP pathway by lysine. ⊖ indicates feedback inhibition.*

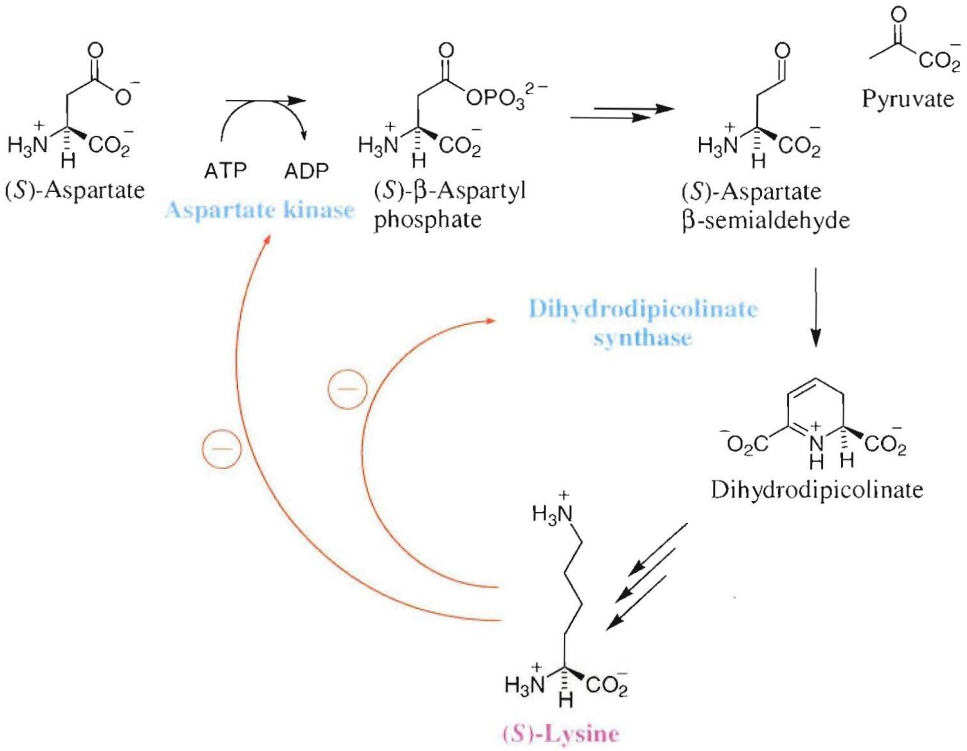

Plant enzymes are strongly inhibited by lysine with IC_{50} values between 0.01-0.05 mM (58,67-70,80). DHDPS from Gram negative bacteria such as *E. coli* are

more weakly inhibited by lysine, displaying IC_{50} values of 0.25-1.0 mM (63,72,81). Enzymes from Gram positive bacteria show little or no inhibition by lysine, with IC_{50} values of greater than 10 mM (17,51,65,76,82,83).

Structural studies, sequence alignment and random mutagenesis studies suggest that the observed differences in sensitivity to inhibition by lysine are due to modifications of the lysine binding site and that the underlying mechanism of inhibition is likely to be similar in all DHDPS enzymes.

1.3.5 The reaction mechanism of DHDPS

DHDPS has been classified as a type I aldolase (34,72), as the catalysed reaction proceeds through a Schiff base intermediate (84).

Central to the reaction mechanism of DHDPS, is a highly conserved motif that is involved in relaying protons into and out of the active site (34,59,62). The importance of this motif, in which the side chains of residues Y133, T44, and Y107 form a hydrogen bonded network, is demonstrated by the finding that mutation of any of the three residues severely attenuates catalytic function (62).

The reaction catalysed by DHDPS can be divided into three consecutive steps: Schiff base formation with pyruvate, aldol condensation of (*S*)-ASA with bound pyruvate, and finally transimination and cyclisation to form the product, HTPA (Figure 1.5) (34).

Schiff base formation

The reaction is initiated by formation of a Schiff base between pyruvate and the ε-amino group of the highly conserved active site lysine residue, K161. Nucleophilic attack of this ε-amino group on the keto group of pyruvate (step 1) results in formation of the Schiff base with the release of water (step 2). Y133 is proposed to play a major role in this reaction, firstly in the stabilisation of the oxyanion intermediate and secondly as a proton donor (34). Subsequent tautomerisation of the Schiff base to form the enamine has been shown to proceed in the absence of (*S*)-ASA (step 2) (5).

Figure 1.5 *The reaction mechanism of DHDPS as proposed by Blickling* et al.*(34) and Dobson* et al. *(62)*

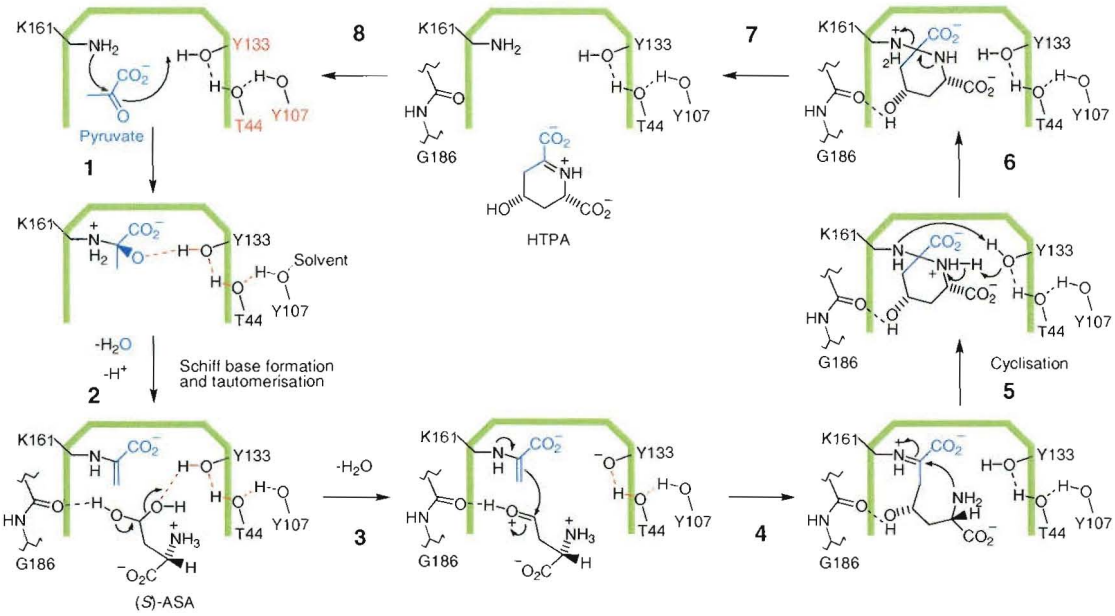

Aldol condensation

The binding of (*S*)-ASA to the pyruvate enzyme complex is followed by condensation with the enamine (step 4). (*S*)-ASA can exist in aqueous solution as a number of species and the identity of the biologically relevant form remains under debate (34,72,85). It has been observed that the predominant species in solution is the hydrate (85,86) and that the active site is spatially well configured to accommodate and coordinate this species (34). Thus, the hydrate of (*S*)-ASA is assumed throughout this thesis. If this is indeed the biologically relevant species, a dehydration step, generating the aldehyde, is required prior to aldol condensation (step 3).

Figure 1.6 *The possible solution structures of* (S)*-aspartate-β-semialdehyde*

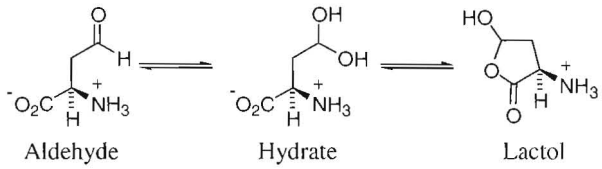

The new C-C bond is formed by nucleophilic attack of the enamine on the hydrate with the release of water. Stabilisation of the tyrosine anion is thought to be achieved *via* the proton relay to bulk solvent involving Y133, T44, and Y107 (34,59,62).

Cyclisation and product release

Nucleophilic attack of the amino group of the (*S*)-ASA moiety on the Schiff base (step 5) results in cyclisation and release of the product (step 7). This reaction requires the deprotonation of the attacking amino group and proton transfer to the ε-amino group of K161 (step 6). Again, here, Y133 is proposed to play a central role. The hydroxyl group of Y133 is well placed to coordinate the attacking amino group both before and after attack. Proton transfer to the ε-amino group of K161 is also proposed to be mediated by the proton-relay triad (34).

2,3-Dihydrodipicolinate was originally assumed to be the product released by DHDPS (4). However, more recent NMR studies suggest that the product released by the enzyme is the cyclic imine (4*S*)-hydroxy-2,3,4,5-tetrahydro-(2*S*)-dipicolinic acid (HTPA), and that elimination of water does not occur while the molecule is bound to the enzyme (34). This suggests that HTPA undergoes a non-enzymatic dehydration after release from the enzyme under physiological conditions, but this remains to be elucidated fully (6,34).

1.4 Structural studies of DHDPS

The crystal structures of DHDPS isolated from the bacterial species, *E. coli* and the plant species, *Nicotiana sylvestris*, have been solved by X-ray crystallography.

The crystal structure of *E. coli* DHDPS was determined to a resolution of 2.5 Å (60) and subsequent structures of the enzyme in complex with lysine, substrates, substrate analogues, and alternative inhibitiors have been solved (59). Recent work in this laboratory has resulted in the structures of the uncomplexed enzyme determined to 1.9 Å and the lysine bound enzyme determined to 2.0 Å (87). The structure of the *N. sylvestris* enzyme with and without lysine bound has been determined to a resolution of 2.8 Å (59).

Recently, the crystal structure of DHDPS isolated from the hyperthermophilic bacteria *Thermotoga maritima* has been deposited in the Protein Data Bank (PDB code 105K); however, at this time, no supporting publication has been released. This will be discussed further in Chapter seven.

1.4.1 The structure of *E. coli* DHDPS

The crystal structure of *E. coli* DHDPS confirms the homotetrameric structure of the enzyme.

The monomer

Each monomer is composed of two domains (Figure 1.7). The N-terminal domain consists of residues 1 to 224 and forms a parallel $(\alpha/\beta)_8$-barrel, analogous to that of triosephosphate isomerase (88). The hydrophobic core of the barrel is formed by irregular layers of side chains pointing inwards from the β-barrel. The C-terminal domain is much smaller, consisting of residues 224 to 292, and forms three α-helices (60). This domain has no obvious function for the catalytic or regulatory mechanisms of the enzyme.

Figure 1.7 *The structure of the* E.coli *DHDPS monomer. The catalytic site residue, K161, is shown in stick representation (yellow). a) show a view looking through the $(\alpha/\beta)_8$ barrel. b) shows a view of the side of the $(\alpha/\beta)_8$-barrel.*

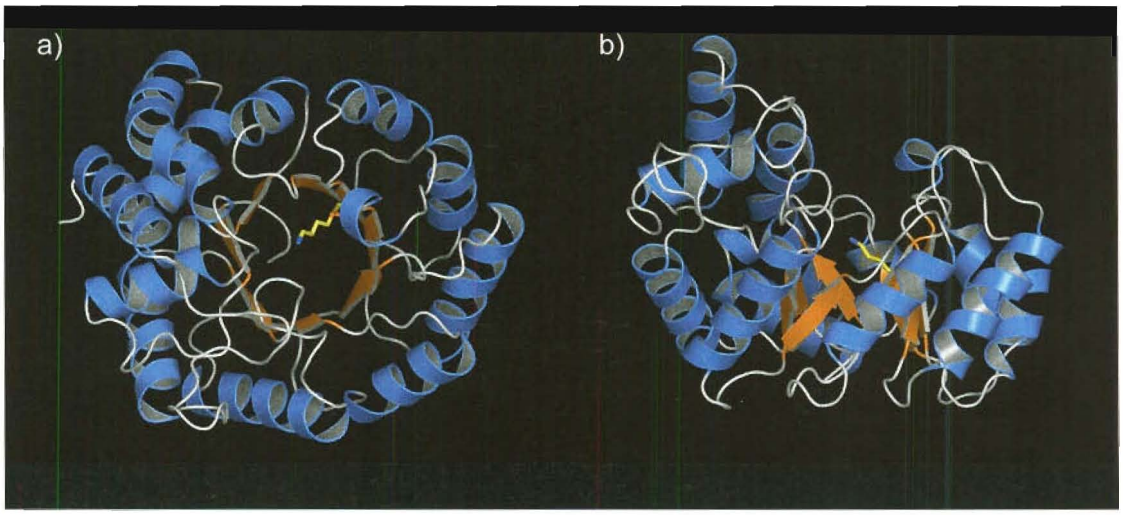

The catalytic site of DHDPS is situated at the C-terminal end of the barrel where the pyruvate binding residue, K161, lies in a 30 Å long by 10 Å deep solvent accessible cleft.

The tetramer

The quaternary structure of *E. coli* DHDPS is that of a homotetramer composed of a dimer of dimers (Figure 1.8). Two monomers associate *via* an extensive interface to

form a tight-dimer unit and two of these tight-dimers associate *via* a more limited contact area to form the wild-type tetrameric enzyme. Each of the four monomers has contacts with only two neighbouring monomers, resulting in a large solvent filled cavity in the centre of the tetramer (60).

Figure 1.8 *The tetrameric structure of* E. coli *DHDPS. Subunits A and B, and subunits C and D associate strongly to form tight-dimers that associate via two smaller interfaces.*

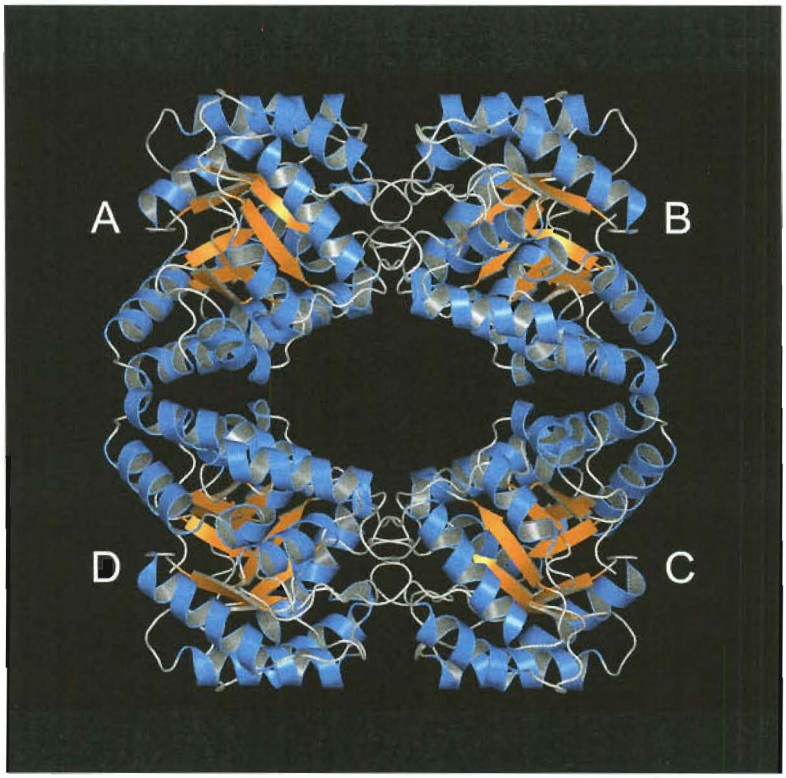

The interface between the two monomers of each tight-dimer consists of 25 contact residues per monomer and buries 12.4% (1,400 $Å^2$) of the total monomeric surface area. In contrast, the interfaces formed between the two dimers of the tetramer bury only 5.8% (650 $Å^2$) of the total monomeric surface area (59,60). Only three residues, L167, T168, and L197, were originally reported to be involved in this weaker interface (59).

The catalytic site

The *E. coli* DHDPS tetramer has four complete active sites. The conserved pyruvate binding residue, K161, lies in a cavity formed by the two monomers of the tight-dimer and is positioned proximal to Y133, which is involved in coordination of the

keto-oxygen of pyruvate. R138 lies at the entrance to the active site cavity and is responsible for coordination of the carboxyl group of (*S*)-ASA (34,59).

As discussed in section 1.3.5, Y133 is part of an essential proton-relay triad (59,62). This triad involves residues from both monomers of the tight-dimer: Y133 is hydrogen bonded *via* T44 of the same monomer to Y107 of the other dimer-forming monomer. The interface between the monomers is such that the sidechain of each Y107 protrudes into a cleft in the adjacent monomer, forming an interdigitating configuration. Thus, formation of this important motif requires the association of the two monomers of the tight-dimer, suggesting that this is the minimal structural unit necessary for full catalytic function.

The lysine binding site

The allosteric lysine binding site is situated in the cleft formed between the two monomers of the tight-dimer, on the exterior of the tetramer. Two inhibitory lysines bind in this pocket, in van der Waals contact with each other, and each lysine molecule is coordinated by residues from both monomers of the tight-dimer (59,79). The carboxyl group of each (*S*)-lysine is coordinated by residue Y106 and the ε-amino group is coordinated by H53, H56, and the main chain oxygen of G78 *via* a water molecule. Coordination of the α-amino group is achieved by residues N80 and E84 of the neighbouring dimer-forming monomer (59). The fact that the lysine binding site is shared between the two monomers of the tight-dimer suggests that this tight-dimer unit is the minimum structure required for regulatory function.

A slight twisting of Y106 occurs on binding of (*S*)-lysine. The side chain of Y106 forms an aromatic stack with Y107 and modulation of the catalytic function of the proton relay is proposed to play a part in the mechanism of inhibition of *E. coli* DHDPS (34,79). Proton relay to bulk solvent may be further impeded by steric blockage of a channel of ordered water molecules, thought to also be involved in proton movement, by the bound (*S*)-lysine (78). (*S*)-Lysine coordination also results in rigidification of the sidechain of R138 *via* the sidechains of N80 and Y107. As R138 is thought to be involved in product cyclisation, this reduction of flexibility may attenuate product release from the enzyme by inhibiting ring closure (34,79).

Structural movements within the protein upon lysine binding are confined to the lysine binding site and to helix α2, which is neither connected to another monomer nor to the active site. This suggests that structural shifts are not communicated between the monomers of the enzyme (34,79). This finding adds weight to the proposal that the tight-dimer is the minimal structural unit required for full lysine regulatory function.

1.4.2 The structure of *N. sylvestris* DHDPS

DHDPS from *N. sylvestris*, like that of *E. coli*, is a tetramer of four identical subunits (Figure 1.9). The monomers of *N. sylvestris* DHDPS share a high level of structural homology with those of the *E. coli* enzyme, consisting of the same arrangement of an N-terminal $(\alpha/\beta)_8$-barrel domain and a C-terminal α-helical domain (59).

Figure 1.9 *The tetrameric structure of* N. sylvestris *DHDPS. Subunits A and B, and subunits C and D associate strongly to form tight-dimers. These dimers are arranged in a back to back fashion with respect to the dimers of the* E. coli *DHDPS tetramer.*

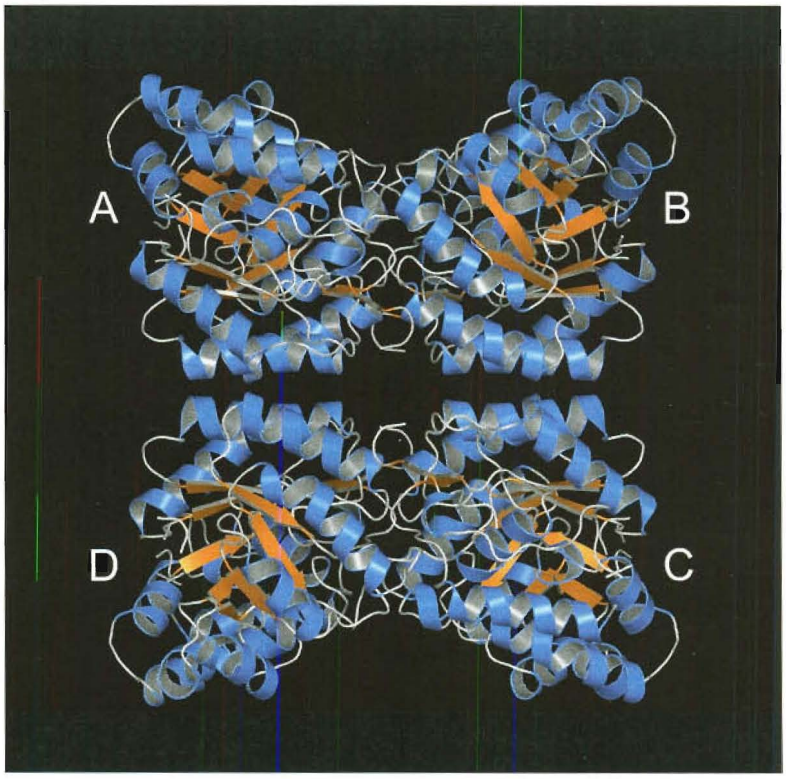

Again, the quaternary structure of the protein is best described as a dimer of dimers. The details of the association of the two monomers forming the tight-dimer remain similar to those of *E. coli* DHDPS and the shared lysine binding site and catalytic site

have almost identical configurations (59). However, the way in which the two tight-dimers associate to form the tetramer is radically different to the *E. coli* enzyme.

Contacts between the two tight-dimers of *N. sylvestris* DHDPS are formed by residues of helices α2 and α3 (59), which lie on the opposite face of the monomer to the dimer-dimer contact residues of the *E. coli* enzyme. Thus, the tight-dimers of *N. sylvestris* DHDPS associate in a back-to-back fashion with respect to those of *E. coli* DHDPS.

As a result of this shift in quaternary structure, the number of residues involved in dimer-dimer contacts is higher and the buried surface area is significantly larger (59), indicating that dimer-dimer association may be stronger in this structure than in the *E. coli* enzyme.

Another important consequence of this alternative arrangement of the dimers is the communication of structural movements between all four subunits upon inhibitory lysine binding. Displacement of helix α2 on lysine binding leads to a slight movement of the tight-dimers relative to each other, coupled with movements in helix α5 away from the active site. It is helix α5 that is responsible for positioning R160 (*E. coli*: R138) at the active site and this displacement is thought to act in combination with rigidification of R160 to enhance inhibition (59). The complementation of the underlying inhibition mechanisms present in bacterial DHDPS with these cooperative structural movements, results in a plant enzyme that is more strongly feedback inhibited by lysine (59).

This structural communication provides an obvious requirement for the tetrameric quaternary structure of the plant enzyme. Evolutionary pressure for more stringent regulation of lysine biosynthesis in the plant system appears to have produced an enzyme with homologous tertiary structure, catalytic site, and allosteric regulation site, but altered quaternary structure, resulting in greatly altered regulatory properties.

The functional or mechanistic contributions offered by the tetrameric configuration of *E. coli* DHDPS that were responsible for the evolution of this architecture are yet to be identified. The existence of two alternative tetramers, consisting of essentially identical tight-dimer units, hints that these structures have evolved from a common early dimeric precursor. Additionally, the independent selection of the two different

tetrameric forms suggests that generic, rather than specific, advantages of a tetrameric structure have been the driving force behind this evolution.

1.5 Sequence alignments

Strictly conserved and highly conserved residues reported in published amino acid sequence alignments of DHDPS can be identified as those residues forming catalytic site motifs, residues important in maintenance of tertiary structure, residues contributing to the tight-dimer interface, and in lysine sensitive enzymes, residues forming the lysine binding site (53,59,60). Another group of highly conserved residues that is apparent from alignment of bacterial sequences is the three residues that form the closely packed hydrophobic core of the interfaces between the tight-dimers. Of these residues, the *E. coli* positions L197 and L167 appear highly conserved. Where the third interface residue, T168, is substituted, in most cases the contacting methyl group is conserved (60).

That the tetrameric quaternary structure of DHDPS should be highly conserved indicates that it is an important and functional feature of the protein and therefore warrants further investigation.

1.6 Summary and aims of this research

The structure, stability, and function of oligomeric proteins are determined both by their constituent monomeric subunits, and the interactions between these monomers. Thus, any rigorous structure-function study must include investigation of the functional and mechanistic contributions of the quaternary structure of that protein.

The specific details, and highly conserved nature, of the tetrameric quaternary structure of DHDPS suggest that the association of two tight-dimers to form the tetramer offers some advantage not present in the dimeric structure. Furthermore, the existence of at least two distinct tetrameric forms of the enzyme suggests that generic advantages, which may be relevant to a wide range of multimeric proteins, underlie the evolution of these structures.

The primary aim of this study has, therefore, been to identify and understand the functional and mechanistic advantages afforded by the quaternary structure of

DHDPS from *E. coli*. This has been achieved by engineering of the quaternary structure of the enzyme coupled with rigorous functional, biophysical, and solid-state structural analysis of both the wild-type and mutant enzymes.

1.7 References

1. Work, E. (1950) A new naturally occurring amino acid. *Nature* **165**, 74
2. Work, E. (1951) The isolation of α,ε-diaminopimelic acid from *Corynebacterium diphtheriae* and *Mycobacterium tuberculosis*. *J Biochem* **49**, 17-23
3. Gilvarg, C. (1960) Biosynthesis of diaminopimelic acid. *Fin Lakaresallsk Handl* **19**, 948-952
4. Yugari, Y., and Gilvarg, C. (1965) The condensation step in diaminopimelate synthesis. *J Biol Chem* **240**, 4710-4716
5. Shedlarski, J. G., and Gilvarg, C. (1970) The pyruvate-aspartic semialdehyde condensing enzyme of *Escherichia coli*. *J Biol Chem* **245**, 1362-1373
6. Cox, R. J., Sutherland, A., and Vederas, J. C. (2000) Bacterial diaminopimelate metabolism as a target for antibiotic design. *Bioorg Med Chem* **8**, 843-871
7. Viola, R. E. (2001) The central enzymes of the aspartate family of amino acid biosynthesis. *Acc Chem Res* **34**, 339-349
8. Coulter, C. V., Gerrard, J. A., Kraunsoe, J. A. E., and Pratt, A. J. (1999) *Escherichia coli* dihydrodipicolinate synthase and dihydrodipicolinate reductase: kinetic and inhibition studies of two putative herbicide targets. *Pestic Sci* **55**, 887-895
9. Cox, R. J. (1996) The DAP pathway to lysine as a target for antimicrobial agents. *Nat Prod Rep* **13**, 29-43
10. Walters, D. R., McPherson, A., and Robins, D. J. (1997) Inhibition of lysine biosynthesis in *Phytophthora infestans*. *Mycol Res* **101**, 329-333
11. Cummins, C. S., and Harris, H. (1956) The chemical composition of the cell wall in some Gram-positive bacteria and its possible value as a taxonomic character. *J Gen Microbiol* **14**, 583-600
12. Work, E. (1957) Biochemistry of the bacterial cell wall. *Nature* **179**, 841-847
13. Bright, S. W. J., and Shewry, P. R. (1983) Improvement of protein quality in cereals. *CRC Crit Rev Plant Sci* **1**, 49-93
14. Azevedo, R. A., Arruda, P., Turner, W. L., and Lea, P. J. (1997) The biosynthesis and metabolism of the aspartate derived amino acids in higher plants. *Phytochemistry* **46**, 395-419
15. Azevedo, R. A. (2002) Analysis of the aspartic acid metabolic pathway using mutant genes. *Amino Acids* **22**, 217-230

16. Galili, G. (1995) Regulation of lysine and threonine synthesis. *Plant Cell* **7**, 899-906

17. Stahly, D. P. (1969) Dihydrodipicolinic acid synthase of *Bacillus licheniformis*. *Biochim Biophys Acta* **191**, 439-451

18. Ghislain, M., Frankard, V., and Jacobs, M. (1995) A dinucleotide mutation in dihydrodipicolinate synthase of *Nicotiana sylvestris* leads to lysine overproduction. *Plant J* **8**, 733-743

19. Kwon, T., Sasahara, T., and Abe, T. (1995) Lysine accumulation in transgenic tobacco expressing dihydrodipicolinate synthase of *Escherichia coli*. *J Plant Physiol* **146**, 615-621

20. Silk, G. W., and Matthews, B. F. (1997) Soybean *dap*A mutations encoding lysine-insensitive dihydrodipicolinate synthase. *Plant Mol Biol* **33**, 931-933

21. Shaver, J. M., Bittel, D. C., Sellner, J. M., Frisch, D. A., Somers, D. A., and Gengenbach, B. G. (1996) Single amino acid substitutions eliminate lysine inhibition of maize dihydrodipicolinate synthase. *Proc Natl Acad Sci, U S A* **93**, 1962-1966

22. Falco, S. C., Guida, T., Locke, M., Mauvais, J., Sanders, C., Ward, R. T., and Webber, P. (1995) Transgenic canola and soybean seeds with increased lysine. *Biotechnology* **13**, 577-582

23. Brinch-Pedersen, H., Galili, G., Knudsen, S., and Holm, P. B. (1996) Engineering of the aspartate family biosynthetic pathway in barley (*Hordeum vulgare L.*) by transformation with heterologous genes encoding feedback insensitive aspartate kinase and dihydrodipicolinate synthase. *Plant Mol Biol* **32**, 611-620

24. Miflin, B., Napier, J., and Shewry, P. (1999) Improving plant product quality. *Nat Biotechnol* **17**, 13-14

25. Amir, R., and Galili, G. (1999) Regulation of lysine and threonine metabolism in plants. *Genet Eng* **21**, 57-77

26. Perl, A., Shaul, O., and Galili, G. (1992) Regulation of lysine synthesis in transgenic potato plants expressing a bacterial dihydrodipicolinate synthase in their chloroplasts. *Plant Mol Biol* **19**, 815-823

27. Perl, A., Galili, S., Shaul, O., Bentzvi, I., and Galili, G. (1993) Bacterial dihydrodipicolinate synthase and desensitized aspartate kinase: two novel selectable markers for plant transformation. *Biotechnology* **11**, 715-718

28. Frankard, V., Ghislain, M., and Jacobs, M. (1992) Two feedback insensitive enzymes of the aspartate pathway in *Nicotiana-sylvestris*. *Plant Physiol* **99**, 1285-1293

29. Azevedo, R. A., and Lea, P. J. (2001) Lysine metabolism in higher plants. *Amino Acids* **20**, 261-279

30. Keeler, S. J., Maloney, C. L., Webber, P. Y., Patterson, C., Hirata, L. T., Falco, S. C., and Rice, J. A. (1997) Expression of *de novo* high-lysine α-helical coiled-coil proteins may significantly increase the accumulated levels of lysine in mature seeds of transgenic tobacco plants. *Plant Mol Biol* **34**, 15-29

31. Girodeau, J. M., Agouridas, C., Masson, M., Pineau, R., and Le Goffic, F. (1986) The lysine pathway as a target for a new genera of synthetic antibacterial antibiotics. *J Med Chem* **29**, 1023-1030

32. Zabriskie, T. M., and Jackson, M. D. (2000) Lysine biosynthesis and metabolism in fungi. *Nat Prod Rep* **17**, 85-97

33. Scapin, G., and Blanchard, J. S. (1998) Enzymology of bacterial lysine biosynthesis. *Adv Enzymol Relat Areas Mol Biol* **72**, 279-324

34. Blickling, S., Renner, C., Laber, B., Pohlenz, H. D., Holak, T. A., and Huber, R. (1997) Reaction mechanism of *Escherichia coli* dihydrodipicolinate synthase investigated by X-ray crystallography and NMR spectroscopy. *Biochemistry* **36**, 24-33

35. Pavelka, M. S., Jr., Weisbrod, T. R., and Jacobs, W. R., Jr. (1997) Cloning of the *dap*B gene, encoding dihydrodipicolinate reductase, from *Mycobacterium tuberculosis*. *J Bacteriol* **179**, 2777-2782

36. Scapin, G., Blanchard, J. S., and Sacchettini, J. C. (1995) Three-dimensional structure of *Escherichia coli* dihydrodipicolinate reductase. *Biochemistry* **34**, 3502-3512

37. Kindler, S. H., and Gilvarg, C. (1960) N-Succinyl-*L*-2,6-diaminopimelic acid deacylase. *J Biol Chem* **235**, 3532-3535

38. Simms, S. A., Voige, W. H., and Gilvarg, C. (1984) Purification and characterization of succinyl-CoA: tetrahydrodipicolinate N-succinyltransferase from *Escherichia coli*. *J Biol Chem* **259**, 2734-2741

39. Peterkofsky, B., and Gilvarg, C. (1961) N-Succinyl-*L*-diaminopimelic-glutamic transaminase. *J Biol Chem* **236**, 1432-1438

40. Lin, Y. K., Myhrman, R., Schrag, M. L., and Gelb, M. H. (1988) Bacterial *N*-succinyl-*L*-diaminopimelic acid desuccinylase. Purification, partial characterization, and substrate specificity. *J Biol Chem* **263**, 1622-1627

41. Wiseman, J. S., and Nichols, J. S. (1984) Purification and properties of diaminopimelic acid epimerase from *Escherichia coli*. *J Biol Chem* **259**, 8907-8914

42. Sundharadas, G., and Gilvarg, C. (1967) Biosynthesis of α,ε-diaminopimelic acid in *Bacillus megaterium*. *J Biol Chem* **242**, 3983-3984

43. Weinberger, S., and Gilvarg, C. (1970) Bacterial distribution of the use of succinyl and acetyl blocking groups in diaminopimelic acid biosynthesis. *J Bacteriol* **101**, 323-324

44. Wehrmann, A., Phillipp, B., Sahm, H., and Eggeling, L. (1998) Different modes of diaminopimelate synthesis and their role in cell wall integrity: a study with *Corynebacterium glutamicum*. *J Bacteriol* **180**, 3159-3165

45. White, P. J., and Kelly, B. (1965) Purification and properties of diaminopimelate decarboxylase from *Escherichia coli*. *Biochem J* **96**, 75-84

46. Bachmann, B. J. (1983) Linkage map of *Escherichia coli* K-12, edition 7. *Microbiol Rev* **47**, 180-230

47. Richaud, F., Richaud, C., Ratet, P., and Patte, J. C. (1986) Chromosomal location and nucleotide sequence of the *Escherichia coli dap*A gene. *J Bacteriol* **166**, 297-300

48. Richaud, F., Richaud, C., Haziza, C., and Patte, J. C. (1981) Isolation and purification of *Escherichia coli* K12 genes involved in the biosynthesis of lysine. *C R Seances Acad Sci III* **293**, 507-512

49. Butour, J. L., Felenbok, B., and Patte, J. C. (1974) Synthesis of dihydrodipicolinate synthetase in *Escherichia coli* K12. *Ann Microbiol (Paris)* **125**, 459-462

50. Chen, N. Y., Jiang, S. Q., Klein, D. A., and Paulus, H. (1993) Organization and nucleotide sequence of the *Bacillus subtilis* diaminopimelate operon, a cluster of genes encoding the first three enzymes of diaminopimelate synthesis and dipicolinate synthase. *J Biol Chem* **268**, 9448-9465

51. Cremer, J., Eggeling, L., and Sahm, H. (1990) Cloning the *dap*A *dap*B cluster of the lysine-secreting bacterium *Corynebacterium glutamicum*. *Mol Gen Genet* **220**, 478-480

52. Garcia-Rodriguez, F. M., Zekri, S., and Toro, N. (2000) Characterization of the *Sinorhizobium meliloti* genes encoding a functional dihydrodipicolinate synthase (*dap*A) and dihydrodipicolinate reductase (*dap*B). *Arch Microbiol* **173**, 438-444

53. Pisabarro, A., Malumbres, M., Mateos, L. M., Oguiza, J. A., and Martin, J. F. (1993) A cluster of three genes (*dap*A, *orf*2, and *dap*B) of *Brevibacterium lactofermentum* encodes dihydrodipicolinate synthase, dihydrodipicolinate reductase, and a third polypeptide of unknown function. *J Bacteriol* **175**, 2743-2749

54. Gunji, Y., Tsujimoto, N., Shimaoka, M., Ogawa-Miyata, Y., Sugimoto, S., and Yasueda, H. (2004) Characterization of the *L*-lysine biosynthetic pathway in the obligate methylotroph *Methylophilus methylotrophus*. *Biosci Biotechnol Biochem* **68**, 1449-1460

55. Vauterin, M., and Jacobs, M. (1994) Isolation of a poplar and an *Arabidopsis thaliana* dihydrodipicolinate synthase cDNA clone. *Plant Mol Biol* **25**, 545-550

56. Kaneko, T., Hashimoto, T., Kumpaisal, R., and Yamada, Y. (1990) Molecular cloning of wheat dihydrodipicolinate synthase. *J Biol Chem* **265**, 17451-17455

57. Silk, G. W., Matthews, B. F., Somers, D. A., and Gengenbach, B. G. (1994) Cloning and expression of the soybean *dap*A gene encoding dihydrodipicolinate synthase. *Plant Mol Biol* **26**, 989-993

58. Frisch, D. A., Gengenbach, B. G., Tommey, A. M., Sellner, J. M., Somers, D. A., and Myers, D. E. (1991) Isolation and characterization of dihydrodipicolinate synthase from maize. *Plant Physiol* **96**, 444-452

59. Blickling, S., Beisel, H. G., Bozic, D., Knablein, J., Laber, B., and Huber, R. (1997) Structure of dihydrodipicolinate synthase of *Nicotiana sylvestris* reveals novel quaternary structure. *J Mol Biol* **274**, 608-621

60. Mirwaldt, C., Korndorfer, I., and Huber, R. (1995) The crystal structure of dihydrodipicolinate synthase from *Escherichia coli* at 2.5 Å resolution. *J Mol Biol* **246**, 227-239

61. Borthwick, E. B., Connell, S. J., Tudor, D. W., Robins, D. J., Shneier, A., Abell, C., and Coggins, J. R. (1995) *Escherichia coli* dihydrodipicolinate synthase: characterization of the imine intermediate and the product of bromopyruvate treatment by electrospray mass spectrometry. *Biochem J* **305**, 521-524

62. Dobson, R. C., Valegard, K., and Gerrard, J. A. (2004) The crystal structure of three site-directed mutants of *Escherichia coli* dihydrodipicolinate synthase: further evidence for a catalytic triad. *J Mol Biol* **338**, 329-339

63. Bartlett, A. T. M., and White, P. J. (1986) Regulation of the enzymes of lysine biosynthesis in *Bacillus sphaericus* Nctc 9602 during vegetative growth. *J Gen Microbiol* **132**, 3169-3177

64. Eggeling, L., Oberle, S., and Sahm, H. (1998) Improved *L*-lysine yield with *Corynebacterium glutamicum*: use of *dap*A resulting in increased flux combined with growth limitation. *Appl Microbiol Biotechnol* **49**, 24-30

65. Yamakura, F., Ikeda, Y., Kimura, K., and Sasakawa, T. (1974) Partial purification and some properties of pyruvate-aspartic semialdehyde condensing enzyme from sporulating *Bacillus subtilis*. *J Biochem* **76**, 611-621

66. Halling, S. M., and Stahly, D. P. (1976) Dihydrodipicolinic acid synthase of *Bacillus licheniformis*. Quaternary structure, kinetics, and stability in the presence of sodium chloride and substrates. *Biochim Biophys Acta* **452**, 580-596

67. Ghislain, M., Frankard, V., and Jacobs, M. (1990) Dihydrodipicolinate synthase of *Nicotiana sylvestris*, a chloroplast localized enzyme of the lysine pathway. *Planta* **180**, 480-486

68. Dereppe, C., Bold, G., Ghisalba, O., Ebert, E., and Schar, H. P. (1992) Purification and characterization of dihydrodipicolinate synthase from pea. *Plant Physiol* **98**, 813-821

69. Wallsgrove, R. M., and Mazelis, M. (1981) Spinach leaf dihydrodipicolinate synthase: partial purification and characterization. *Phytochemistry* **20**, 2651-2655

70. Kumpaisal, R., Hashimoto, T., and Yamada, Y. (1987) Purification and characterization of dihydrodipicolinate synthase from wheat suspension-cultures. *Plant Physiol* **85**, 145-151

71. Cornish-Bowden, A. (1999) *Fundamentals of enzyme kinetics*, 2nd Ed., Portland Press Ltd, London

72. Karsten, W. E. (1997) Dihydrodipicolinate synthase from *Escherichia coli*: pH dependent changes in the kinetic mechanism and kinetic mechanism of allosteric inhibition by *L*-lysine. *Biochemistry* **36**, 1730-1739

73. Laber, B., Gomis-Ruth, F. X., Romao, M. J., and Huber, R. (1992) *Escherichia coli* dihydrodipicolinate synthase. Identification of the active site and crystallization. *Biochem J* **288**, 691-695

74. Mazelis, M., Whatley, F. R., and Whatley, J. (1977) The enzymology of lysine biosynthesis in higher plants. The occurrence, characterization and some regulatory properties of dihydrodipicolinate synthase. *FEBS Lett* **84**, 236-240

75. Dobson, R. C., Gerrard, J. A., and Pearce, F. G. (2004) Dihydrodipicolinate synthase is not inhibited by its substrate, (*S*)-aspartate β-semialdehyde. *Biochem J* **377**, 757-762

76. Webster, F. H., and Lechowich, R. V. (1970) Partial purification and characterization of dihydrodipicolinic acid synthetase from sporulating *Bacillus megaterium*. *J Bacteriol* **101**, 118-126

77. Kumpaisal, R., Hashimoto, T., and Yamada, Y. (1989) Inactivation of wheat dihydrodipicolinate synthase by 3-bromopyruvate. *Agric Biol Chem* **53**, 355-359

78. Dobson, R. C. J. (2003) Investigating the catalytic and regulatory mechanisms of dihydrodipicolinate synthase. *D. Phil. thesis*, University of Canterbury

79. Blickling, S., and Knablein, J. (1997) Feedback inhibition of dihydrodipicolinate synthase enzymes by *L*-lysine. *Biol Chem* **378**, 207-210

80. Matthews, B., and Widholm, J. (1978) Regulation of lysine and threonine synthesis in roots and cell-cultures of garden carrot (*Daucus carota L.*). *Plant Physiol* **61**, 47-47

81. Bakhiet, N., Forney, F. W., Stahly, D. P., and Daniels, L. (1984) Lysine biosynthesis in *Methanobacterium thermoautotrophicum* is by the diaminopimelic acid pathway. *Curr Microbiol* **10**, 195-198

82. Tosaka, O., and Takinami, K. (1978) Biosynthesis of *L*-lysine and *L*-threonine in *Brevibacterium*. 1. Pathway and regulation of lysine biosynthesis in *Brevibacterium lactofermentum*. *Agr Biol Chem* **42**, 95-1000

83. Hoganson, D. A., and Stahly, D. P. (1975) Regulation of dihydrodipicolinate synthase during growth and sporulation of *Bacillus cereus*. *J Bacteriol* **124**, 1344-1350

84. Grazi, E., Rowley, P. T., Cheng, T., Tchola, O., and Horecker, B. L. (1962) The mechanism of action of aldolases. III. Schiff base formation with lysine. *Biochem Biophys Res Commun* **9**, 38-43

85. Coulter, C. V., Gerrard, J. A., Kraunsoe, J. A. E., Moore, D. J., and Pratt, A. J. (1996) (*S*)-Aspartate semi-aldehyde: synthetic and structural studies. *Tetrahedron* **52**, 7127-7136

86. Tudor, D. W., Lewis, T., and Robins, D. J. (1993) Synthesis of the trifluoroacetate salt of aspartic-acid β-semialdehyde, an intermediate in the biosynthesis of *L*-lysine, *L*-threonine, and *L*-methionine. *Synthesis* **11**, 1061-1062

87. Dobson, R. C. J., Griffin, M. D. W., Jameson, G. B., and Gerrard, J. A. (2005) The crystal structures of native and (*S*)-lysine bound dihydrodipicolinate synthase from *Escherichia coli* with improved resolution show new features of biological significance. *Acta Crystallogr D Biol Crystallogr*, (Submitted)

88. Banner, D. W., Bloomer, A. C., Petsko, G. A., Phillips, D. C., Pogson, C. I., Wilson, I. A., Corran, P. H., Furth, A. J., Milman, J. D., Offord, R. E., Priddle,

J. D., and Waley, S. G. (1975) Structure of chicken muscle triose phosphate isomerase determined crystallographically at 2.5 Å resolution using amino acid sequence data. *Nature* **255**, 609-614

Chapter Two

The quaternary complex and design of the dimeric mutants of *E. coli* DHDPS

2.1 Introduction

While the existence of multisubunit proteins is well documented, our understanding of the principles behind the supramolecular assembly of proteins into quaternary complexes remains rudimentary compared to our sophisticated knowledge of protein tertiary structure. The question of why such a large proportion of proteins are composed of subunits in this way has stimulated great interest in the delineation of the structural and functional roles of subunits in oligomeric proteins (1); however, knowledge in this field has progressed little since early work in the area (2). Understanding the functional roles of protein oligomerisation has proved difficult, in part because of the relative paucity of biophysical data: the proportion of known proteins that are well characterised in terms of their quaternary structure is notably low (3).

Investigations of the biophysics and mechanistic contributions of intersubunit interactions are, therefore, critical to our understanding of how the quaternary structures of these proteins endow them with their unique biological properties (1). Studies of this sort have the potential to provide insight, not only into the details of specific multimeric systems, but also into characteristic factors that may be applied to broad classes of proteins by relation of tertiary and quaternary structural features.

This chapter details the current literature concerning quaternary structure and reviews the reports of quaternary structural engineering. Re-evaluation of the structural details of the interfaces between the two tight-dimers of the *E. coli* DHDPS tetramer, which was conducted as part of this study, is also described. Finally, the rational design of mutations to produce dimeric variants of *E. coli* DHDPS is detailed.

2.2 The quaternary complex and protein-protein interactions

The self-association of proteins to form quaternary complexes (oligomers) is a very common phenomenon. 70-80% of proteins are comprised of a number of monomeric subunits that associate noncovalently to form functional oligomeric proteins (4-6). These multimeric proteins vary enormously in complexity, ranging from dimers to giant holo-enzymes composed of large numbers of subunits (1), and each may consist of identical monomers or two or more different types of subunit. However, the large majority of multimeric proteins are either homodimeric, consiting of two identical monomers, or homotetrameric, consisting of four identical monomers. A recent poll of the Brenda enzyme database revealed that of 311 characterised oligomeric human proteins 199 form homo-multimers and that over a quarter of these are homotetrameric (3).

2.2.1 Homo- and hetero-complexes

Protein quaternary complexes can be composed of identical (homo-) or non-identical (hetero-) protein units. In the case of homo-complexes, these protein units can be organised in an isologous or heterologous manner (7,8) with associated symmetry (9) (Figure 2.1).

Figure 2.1 *Examples of isologous and heterologous arrangements of identical subunits. (a) Homotetramer with isologous interfaces. Two two-fold symmetry axes are shown as dashed lines, the third is orthogonal to the page at the centre of the structure. (b) Homotetramer with heterologous interfaces. (c) Heterologous association without cyclic symmetry allows unrestricted aggregation.*

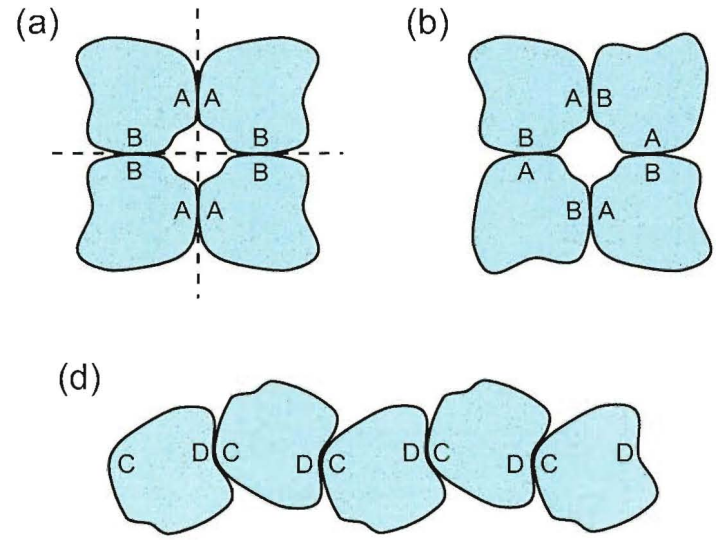

An isologous association involves the same surface, and hence the same contact residues, of both monomers, which are related by a two-fold symmetry axis. Further oligomerisation of an isologous association can only be achieved by a different interface, for example, to produce a dimer of dimers with three two-fold axes of symmetry, as is the case with *E. coli* DHDPS.

In contrast, heterologous assemblies involve association of non-identical surfaces, which, without closed, cyclic, symmetry, can lead to infinite aggregation. By their nature, hetero-oligomers must form heterologous associations.

2.2.2 Obligate and non-obligate associations

Multimeric protein structures are also distinguished on the basis of whether a complex is obligate or non-obligate (8). An obligate interaction is usually very stable, and thus, normally only exists in its complexed form; hence, the components of the complex are not found as stable structures on their own *in vivo* (8). These complexes are generally also thought to be functionally obligate; however, this may not always be the case.

Non-obligate multimeric structures form transient complexes that associate and dissociate *in vivo*. These complexes can be further classified as those in which weak interactions produce a dynamic oligomeric equilibrium in solution, and those in which stronger transient interactions require a molecular or physiological trigger to alter the oligomeric state (8).

Of course, these classifications are not mutually exclusive, as equilibrium between varying oligomeric orders is a feature of all multimeric structures; however, the position and nature of the equilibrium is important.

2.2.3 Structural characteristics of protein-protein interfaces

The increasing volume of structural data available for various protein quaternary complexes has allowed comparative analysis of the structural characteristics of protein-protein interfaces. Most recently, the interfaces of wide ranges of protein oligomers have been assessed by parameters such as the size and shape of the contact area, protrusion or flatness of the interface, the chemical and physical properties of the surface, and the amino acid composition of contact residues (10-17). This has lead to limited success in prediction of protein interface sites from structural and sequence

data (12,18-20). From these studies, it is possible to extract a number of general features of protein-protein interfaces.

The interfaces of both hetero-complexes and homo-complexes are generally circular and planar (3,13,14), and a clear, though scattered, correlation exists between the size of the interface and the molecular weight of the monomer, with larger subunits generally having larger interfaces (13,14). However, the overall binding energy between monomers does not appear to be correlated to the size of the interface (17,21). The interfaces of obligate complexes are generally larger and more hydrophobic in nature than those involved in non-obligate complexes (13,14,16), which generally exhibit a more polar interface, presumably to meet the requirements for independent monomer folding and solubility.

Oligomeric structures with interface areas of less than 1,000 $Å^2$ are unlikely to undergo large scale conformational changes on complex formation (8,16,17). This latter point has implications when considering the structural features of *E. coli* DHDPS as the monomer-monomer contact area at the dimer-dimer interface is only 650 $Å^2$. This suggests that domain movements on dimer-dimer association do not play a functional role in this enzyme.

2.2.4 Evolution of protein-protein interfaces

The structure and affinity of a protein-protein association is tuned to its biological function and/or mechanism (8). Thus, protein-protein interfaces presumably evolve to optimise association with respect to functional efficacy.

Although it has not been clearly established how specific protein-protein associations have evolved, it is reasonable to assume that weak, non-specific interactions that confer a functional advantage for an organism may be expanded by fine tuning of the physics of association and thus evolve into specific associative interfaces (3). This evolutionary process, as any, requires significant selective pressure, implying that the advantage conferred must outweigh the disadvantages of the evolutionary process. Thus quaternary complexes are unlikely to evolve 'by accident'.

Given the structural and functional homology between the tight-dimers of DHDPS from *E. coli* and *N. sylvestris* (22), this also suggests that the distinct quaternary structures of the two enzymes evolved from a common dimeric precursor. Examples, such as this, of distinct quarternary structures, with equivalent order, consisting of essentially identical monomer units are extremely rare (23) and have only been observed in a handful of cases (22-25).

2.3 The roles of quaternary structure in protein function

A range of factors has been proposed to account for the high incidence of multimeric proteins. The most familiar of these are the facilitation of regulatory or substrate induced cooperativity between the subunits of an oligomer and the formation of shared active sites (1,3) (Figure 2.2). Structural proteins that form large filamentous or scaffold structures (Figure 2.2a) within the cell present a special case of a functional consequence of oligomerisation that is beyond the scope of this discussion.

2.3.1 Specific functional advantages

The haemoglobin tetramer provides the archetypal example of a protein that undergoes structural change on ligand binding to any monomer, leading to the generation of a tetrameric conformation with increased ligand binding affinity (26) (Figure 2.2b). The delineation of these complex mechanisms of concerted cooperativity represents the original demonstration of the requirement of specific quaternary structure for biological function, and a range of multimeric proteins have since been found to display this sort of regulatory mechanism. However, these proteins are predominantly hetero-complexes, composed of non-identical monomers, and account for only about 30% of all oligomeric proteins (5,6).

Shared active sites, in which the active site is formed at the interface of two monomers of an oligomeric enzyme, and is contributed to by both monomers has frequently been observed (3) (Figure 2.2c). This feature places enzyme activity under the regulation of oligomerisation: if the protein concentration drops below the threshold of association, or some molecular trigger causes disruption of the oligomeric structure, inactive monomers are formed (3). Similarly, monomer-monomer association may cause blocking of the active site. In this case, the monomer is the active species (Figure 2.2d).

Figure 2.2 *Familiar functional consequences of protein oligomerisation. (a) Dimerisation of the monomer (i), allows aggregation of stable structural elements in the cell (ii). (b) Binding of a cofactor or substrate to a single subunit of an oligomer can alter the conformation of that subunit (i), and can cooperatively induce structural changes in the remaining subunits (ii). (c) Oligomerisation can generate complete active or binding sites at the interface. (d) Alternatively, oligomerisation can block existing active or binding sites of the monomer. Adapted from Marianayagam* et al. *(3).*

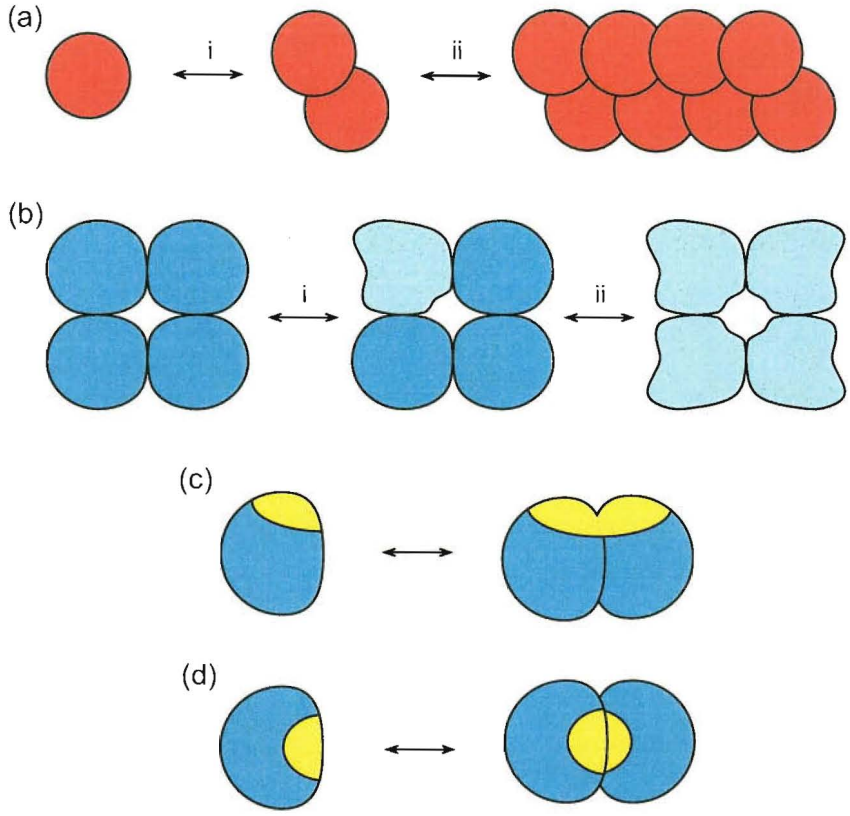

An elegant example of active site sharing can be found in the dimeric type II restriction endonucleases, which bind and cleave palindromic DNA sequences. The binding sites of each monomer of the homodimer are arranged symmetrically across the interface such that each subunit binds half of the palindrome (3).

While active site sharing can provide a rationale for monomer-monomer association, it may not explain the full order of the quaternary complex, as is the case with *E. coli* DHDPS, in which the tight-dimer structure is required for full configuration of active site and regulatory motifs, but the association of two dimers to form the tetramer has no known function.

2.3.2 Generic advantages

In other oligomeric proteins, most notably those composed of identical subunits, the functional properties conferred by the quaternary structure are not immediately obvious from structural data or functional studies (1). In these cases, a range of generic benefits have been ascribed in an effort to justify their existence as quaternary complexes. These include factors relating to the increased size of the complexes relative to the monomers, and economy of scale with respect to protein synthesis and genome size (9).

Burial of hydrophobic domains within interfaces that would otherwise be exposed leading to insolubility has been put forward as a possible justification for the formation of oligomeric structures (1). Consideration of the evidence presented above would suggest that the hydrophobic nature of the contact surfaces of obligatory quaternary complexes is a consequence of, rather than a cause of, the formation of these interfaces. In order for a protein to develop higher order oligomers, it must itself have an intrinsic level of stability and solubility.

Large proteins with extensive internal interactions generally have more stable folded structures than small proteins (9). This is because in large proteins the enthalpic contribution of the many weak internal interactions far outweighs the entropic cost of the constrained conformation, whereas, in smaller proteins this balance is not as pronounced (9). The oligomerisation of multiple identical monomers provides a relatively simple and economical method of forming large protein structures and may be a general means for increasing stability against denaturation. Here it must be noted that the effect of oligomerisation on the stability of a protein is highly dependent on the characteristics of the interface and the nature of the interactions between monomers. A number of cases have been documented in which monomeric forms of obligate quaternary complexes show equal or increased stability when compared to the oligomeric structure (27-30).

Another facet of stability that may be offered by oligomeric structure is protection against misfolding and formation of potentially pathogenic protein aggregates such as amyloid fibrils, which have been implicated in a number of neurodegenerative diseases (31). In the amyloidogenic proteins insulin and transthyretin, it has been shown that break down of the natural oligomeric complexes into monomers is

necessary for nucleation of amyloid fibrils (32,33), and that non-covalent stabilisation of the oligomeric structures inhibits amyloid formation .(34). Further, hereditary mutations in the tetrameric human transthyretin that cause disruption of the tetramer into dimers (35) or monomers (36) increases the propensity of the protein to form amyloid, even where the stability of the monomeric units is unaltered (35).

The increased size of oligomeric complexes with respect to the free constituent monomers also has implications for the water regulation of a cell or organelle. The larger protein structures have lower membrane permeability and therefore reduced osmotic pressure (1). Formation of complexes also reduces the available protein surface area, thereby significantly reducing the amount of water required for full hydration of the protein (9). These factors may not present a major evolutionary driving force, however, as it has been shown that many cell types can loose over half of their water without adverse effects (9,37).

Related to these considerations of size is the error management and efficiency of coding offered by homo-oligomeric proteins (1,9). As the protein is made up of a number of polypeptide chains, translation errors may be reduced by discarding individual protein chains with sequence defects, as opposed to rejecting one large chain. Also, the assembly of a number of identical protein monomers into a quaternary complex allows creation of a large structure using the minimum amount of genetic material. However, the large amount of non-coding DNA in eukaryotic genomes suggests that this may not be a driving force in higher organisms.

2.4 Quaternary structural engineering

Over the past two decades, protein engineering has become a major tool in the study of the catalytic mechanisms of enzymes (38-40). Routinely, active site amino acid residues are substituted in order to ascertain their function in the catalysis of the enzyme. More recently, the powerful technique of site-directed mutagenesis has been utilised to study the structural properties of proteins, including folding processes (41), thermal stability (42-44) and, in a limited number of studies, the roles of quaternary structure.

Structural engineering of the interfaces of oligomeric proteins has concentrated on two separate lines of investigation: engineering thermal stability and the disruption of intersubunit interfaces, in order to investigate the functional contributions of the quaternary structure of the protein, or to produce lower order oligomers to meet specific purposes.

2.4.1 Engineering of thermostable interfaces

Interest in the mechanisms by which proteins from thermophilic bacteria achieve their remarkable thermal tolerance prompted examination of the characteristics of the intersubunit interfaces of the proteins form these organisms (45,46). It was found that increased density of hydrophobic packing and more extensive ion-pair networks were commonplace in the intersubunit interfaces of these proteins when compared to their non thermally resistant homologues (47,48).

Applying these principles, the thermal stability of a hexameric enzyme, glutamate dehydrogenase, from two bacterial species was significantly enhanced by the introduction of amino acid residues forming complex ion-pair networks within the interfaces of these proteins (49,50). The stability of the non-obligate dimeric TATA-binding protein from yeast was also shown to increase subsequent to introduction of two additional ion pairs at the interface of the complex (51). Improvement of the hydrophobic packing within the interface of the dimeric Lac repressor of *E. coli* has resulted in a remarkable increase in thermostability from 47°C to 87°C (48). Mutation of residues at the dimer interface of yeast triosephosphate isomerase based on their chemical properties and contribution to association of the two monomers was shown to double the half life of the enzyme at 100°C (52,53).

2.5 Engineering of lower order quaternary structures from existing oligomers

The literature contains a limited number of reports of studies directed towards altering the quaternary structure of oligomeric proteins by site-directed mutagenesis. These investigations have been undertaken for a number of reasons, including examination of the functional properties of proteins and production of improved clinical therapeutic agents.

2.5.1 Early studies

The earliest reported investigation into the possibility of dissociation of an obligate oligomeric protein into stable, independent monomers by site-directed mutagenesis of interface residues was carried out by Jones *et al.* (54). The study focussed on the homodimeric enzyme tyrosyl-tRNA synthetase from *Bacillus stearothermophilus*, which contains two complete and separate active sites, but binds only one equivalent of tyrosine and one equivalent of t-RNA per dimer. This half-of-sites reactivity was presumed to involve negative cooperativity of substrate binding between the two monomers, but had no known mechanistic function. Protein engineering was therefore applied in an effort to create stable and active monomeric units of the enzyme by disruption of the dimeric structure, and thereby shed light on the functional contribution of the protein complex.

Disruption of the monomer-monomer interface was achieved by introduction of negatively charged groups at previously interacting positions in the interface, thus producing electrostatic repulsion between the two subunits at this location. The mutant form of t-RNA synthetase produced by this strategy was found to display pH dependent dissociation into stable monomers, consistent with the ionisation of the carboxyl groups producing repulsion. The monomeric form of the enzyme was found to be inactive and was therefore not amenable to the kinetic characterisation necessary for functional analysis. However, subsequent work, in which active heterodimers consisting of this monomeric mutant complexed with a truncated form of the enzyme with an engineered complementary charge at the interface (55,56), assisted in the elucidation of the binding mode of t-RNA with the dimer (57).

Subsequent to this study, the technology of alteration of the quaternary structure of proteins by rational design has been applied to a limited range of oligomeric systems for a number of different purposes.

2.5.2 Quaternary structural engineering in medical science

Insulin

The implications of quaternary structural engineering for the pharmacokinetics of insulin administration in diabetics were seized upon quickly (58,59). The treatment of type I diabetes requires the subcutaneous injection of the hormone insulin at meal

times, in order to control resultant blood glucose levels. Human insulin exists largely as a homohexameric structure, composed of a trimer of dimers, and, therefore, exerts a relatively low osmotic pressure. Thus, early insulin therapy was limited by slow absorption of insulin from the subcutaneous tissue into the bloodstream, and slow clearance of blood insulin levels, resulting in abnormal diurnal insulin patterns.

It was recognised that smaller forms of the hormone were likely to be absorbed faster into the bloodstream. Monomeric forms of human insulin were, therefore, produced by engineering single and double mutations at the dimer interface of the monomer (58,59). These monomeric analogues were found to be absorbed up to three times faster than the wild-type insulin and show a more natural clearance profile. It was also found that most of these mutations did not significantly effect the *in vivo* potency of the hormone (59). As a result of these studies a number of engineered monomeric insulin analogues are commercially available and in common use today (60,61).

Interleukin

Another example where interface engineering has found a medical application is human interleukin-5, a homodimeric cytokine protein that is central in the pathogenesis of allergies and asthma (62). Mutation of cysteine residues that form intermonomer disulphide bonds in the wild-type protein produced monomers that lack biological activity (63). This lack of bioactivity was predicted to be due to a short loop between two helices that physically prevented complete folding of one of the helices (64), which lies across the surface of the other monomer in the wild-type protein. Extension of this loop to allow full unimolecular folding of the constrained helix resulted in a bioactive monomeric interleukin-5 (64). In this way, the constrained helix was identified as a functional epitope of the protein, a finding that was later confirmed (65), providing the framework for development of agonists and antagonists of interleukin-5 (66).

2.5.3 Functional studies by quaternary structural engineering

Serratia marcessens endonuclease

The design of monomeric variants of the *Serratia marcessens* nonspecific endonuclease was originally directed towards commercial applications, as the enzyme is utilised for removal of nucleic acids from biochemical and pharmaceutical

preparations (27,67). Efficient immobilisation of the wild-type homodimer proved problematic and thus a stable, active monomer was sought and created (27). However, detailed functional analysis of the resulting monomeric forms revealed an interesting mechanistic advantage afforded by the dimeric structure of the enzyme.

The monomeric form of the nuclease showed the same specific activity as the wild-type dimer when polynucleotide substrate concentration was high. However, as substrate concentration became limiting, the dimer showed relatively higher activity (68). The two active sites of the wild-type *S. marcessens* nuclease dimer are separate and operate independently. Thus, a binding event at one active site will raise the apparent local concentration of substrate for the other binding site of the dimer due to the protruding nucleic acid strands either side of the cleavage site, raising the probability of a binding event at the other active site. A processive mechanism of nucleic acid degradation is, therefore, produced when substrate concentration is low (68), allowing more efficient degradation of nucleic acids.

Biotin-binding proteins

The structurally analogous tetrameric biotin-binding proteins avidin and streptavidin have attracted considerable interest due to their remarkably high affinity for biotin (k_d ~ 10^{-15} M) and, hence, the possibility of their use as biotin-binding components of affinity columns or fusion proteins. Early attempts to produce independent dimeric variants of streptavidin resulted in protein chains that folded into dimeric structures only in the presence of biotin (69). Subsequent efforts were more successful, producing independent and stable biotin binding dimers of both streptavidin and avidin by single residue mutation (70). This point mutation was complemented by a second substitution to produce a stable monomeric mutant of avidin which retains a high affinity for biotin (k_d ~ 10^{-7} M) and may therefore be utilised for its affinity properties (71). Crystal structures of the stable dimeric forms of streptavidin and avidin revealed tetrameric quaternary structure, analogous to that of the wild type protein, indicating that tetramerisation of these dimers occurred at high concentration (72).

Inorganic pyrophosphatase

Various lower order oligomers of hexameric inorganic pyrophosphatase have been produced from both the *Bacillus stearothermophilus* (73) and the *E. coli* enzyme (74,75). Kinetic analysis of the variant forms of *E. coli* pyrophosphatase revealed that substrate binding was progressively weakened in the transition from hexamer to monomer, with little change in k_{cat}. Additionally, hexameric variants with impaired subunit association displayed strong substrate binding cooperativity, which was not observed in the wild-type enzyme. These observations led to the proposal that the hexameric structure of the wild-type enzyme produces constraint of the active sites in an optimal substrate binding conformation (76); breakdown of the oligomeric structure of the enzyme leads to progressive and communicated conformational relaxation of the monomers that can be reversed by the binding of substrate.

Eco*R I*

Monomeric mutants of the restriction endonuclease, *Eco*R I, were engineered with a view to producing heterodimers with novel site specificity (77), by the method of Jones *et al.* (54,55). The observed nickase activity of the monomeric variants, where only one strand of the DNA duplex is cleaved, is consistent with the single catalytic centre of the monomer. Surprisingly, this nickase activity was found to be non-specific, in contrast to the expected half recognition site specificity (77), suggesting that the monomer alone was unable to form specific interactions with the DNA bases, perhaps due to an inability to bend the DNA molecule and open the major groove.

λ Cro

In contrast, a monomeric form of the homodimeric DNA binding protein λ Cro, produced by extension of the C-terminal, β-strand forming dimerisation domain, was found to have half operator binding specificity (28). Interestingly, this mutant, in which two β-turn residues were optimised for β-strand formation, is significantly more stable than the wild type-dimer.

Triosephosphate isomerase

The homodimeric enzyme triosephosphate isomerase (TIM) has undergone rigorous characterisation by quaternary structural engineering. The report of the crystal

structure of recombinant derived trypanosomal TIM (78) also described a study in which an interface histidine residue, forming water-mediated hydrogen bonds between the two monomers, had been mutated producing a dimer that dissociates at low protein concentration and displays concentration dependent activity (78,79). This study was quickly followed up by the creation of an obligate monomeric form of the enzyme, designated monoTIM, by shortening of the 15 residue major interface loop (29). This monomer was catalytically active, however, the k_{cat} was approximately 1000-fold lower than the wild-type enzyme and was independent of protein concentration. The crystal structure of monoTIM indicated that this large reduction in activity was likely to be due to the reordering of two minor interface loops which contain two of the four essential catalytic residues (80). This indicates that the dimeric state of the enzyme is necessary for maintenance of the correct conformation of these loops and therefore the positioning of these essential residues.

Subsequent introduction of more conservative double point substitutions of interface residues of trypanosomal TIM resulted in an alternative monomeric variant (81), with kinetic and physical properties similar to those of monoTIM. Further single and double point mutant monomeric forms were crystallised, in the presence and absence of substrate analogue inhibitors (82). The resulting structures showed that, on complexation with the inhibitiors, the reordered catalytic residue containing loops adopt conformations similar to those observed in the wild-type enzyme, suggesting that it is the rigidity of these loops, resulting from interface formation, that is important for optimal catalysis (82).

In contrast to these studies, where the thermal stability of monomeric variants of trypanosomal TIM was found to be similar to that of the wild-type (29,81), an obligate monomeric variant of human TIM produced by double point substitution was shown to have greatly reduced conformational stability (83). Detailed fluorescence spectroscopic denaturation analysis indicated a conformational stability of 2.5 kcal/mol for the monomer, reduced from 19.3 kcal/mol for the wild-type dimer. However, subsequent introduction of α-helix stabilising mutations produced a partial return of conformational stability of the monomer, to 3.9 kcal/mol (84).

Superoxide dismutase

As with the monomeric trypanosomal TIM mutants, the NMR solution structure (76) of a monomeric form of the dimeric human Cu/Zn superoxide dismutase (85,86) showed significant disorder in regions previously involved in monomer-monomer association. In particular, the electrostatic loop that is responsible for driving superoxide anions toward the reactive copper site was found to have high disorder and altered conformation with respect to that of the wild-type dimeric protein. This reordering of a critical loop due to the absence of a second, contacting subunit formed the basis of a mechanism used to explain the 10-fold reduction of activity found in the monomeric variant (76).

Further examples of reduced activity in quaternary structural engineered proteins

Reduction of catalytic activity has been a common observation in studies of the alteration of the quaternary structure of enzymes. Rat prostatic acid phosphatase showed complete loss of activity on monomerisation of the wild-type dimer (87), the activity of monomeric mutants of the dimeric malate dehydrogenase from *E. coli* was four orders of magnitude lower than that of the wild-type (88), and a 20-fold reduction of activity was observed in a dimeric variant of the tetrameric *D*-hydantoinase (89). Stability conferred by the homodimeric structure of RNA triphosphatase was used to explain the *in vitro* thermolability of activity and the *in vivo* lethality of monomer producing mutations in the protein (90,91).

Often the attenuation of activity has been difficult to explain and has, therefore, been ascribed to reduced stability in the protein structure. It is then easy to reach the conclusion that the primary function of the quaternary structure of these enzymes is to confer generalised structural stability and consequentially catalytic efficiency. However, contrary to this, cases have been described where reduced stability does not correlate with reduced activity. Dimeric and monomeric variants of the fructose-1,6-bisphosphate aldolase tetramer show progressively reduced stability against denaturation, while the specific activity of each variant is similar to that of the wild-type (92-94). Other cases have seen no change in either stability or activity (30,95).

2.6 Rational design of mutations to disrupt the dimer-dimer interface of *E. coli* DHDPS

In order to investigate the functional and mechanistic contributions of the tetrameric structure of *E. coli* DHDPS, variants of the protein with altered quaternary structure were designed using site-directed mutagenesis of residues involved in the minor, inter-dimeric interface of the enzyme. Previous studies on the alteration of protein quaternary structure (section 2.5) were used to inform the design.

The primary aim of this section of work was to produce one or more stable, obligate dimeric forms of the enzyme, corresponding to the tight-dimer unit of wild-type DHDPS. As a secondary aim, amino acid residues at the dimer-dimer interface were mutated in order to establish their importance in the formation of the interface. This had the added benefit of producing proteins that displayed dimer-tetramer equilibrium.

2.6.1 The dimer-dimer interface of *E. coli* DHDPS

The tight-dimer units of the *E. coli* DHDPS tetramer associate *via* two isologous interfaces formed between corresponding monomers of the dimer units. Published analyses of crystal structures of wild-type DHDPS stated that intersubunit contacts at this dimer-dimer interface are comprised of only three amino acid residues: L167, T168, and L197 (22,96). This result was obtained using the program CoPS (unpublished) with a distance cut-off of 3.9 Å.

L197-L197

These residues form mainly hydrophobic intersubunit interactions. The γ- and δ-carbons of the side chain of L197 from one monomer are in direct van der Waals contact with the same carbon atoms of the side chain of L197 from the neighbouring monomer (Figure 2.3).

L167 and T168

Similarly, the side chains of both L167 residues interact directly in a symmetrical manner, with the β-carbon in van der Waals contact with the β-carbon and exposed δ-carbon of the neighbouring residue. This exposed δ-carbon is also in van der Waals

contact with the main chain atoms between the side chains of L167 and T168 and the γ-carbon of the threonine side chain (Figure 2.4).

Figure 2.3 *The contact between L197 residues of neighbouring subunits.*

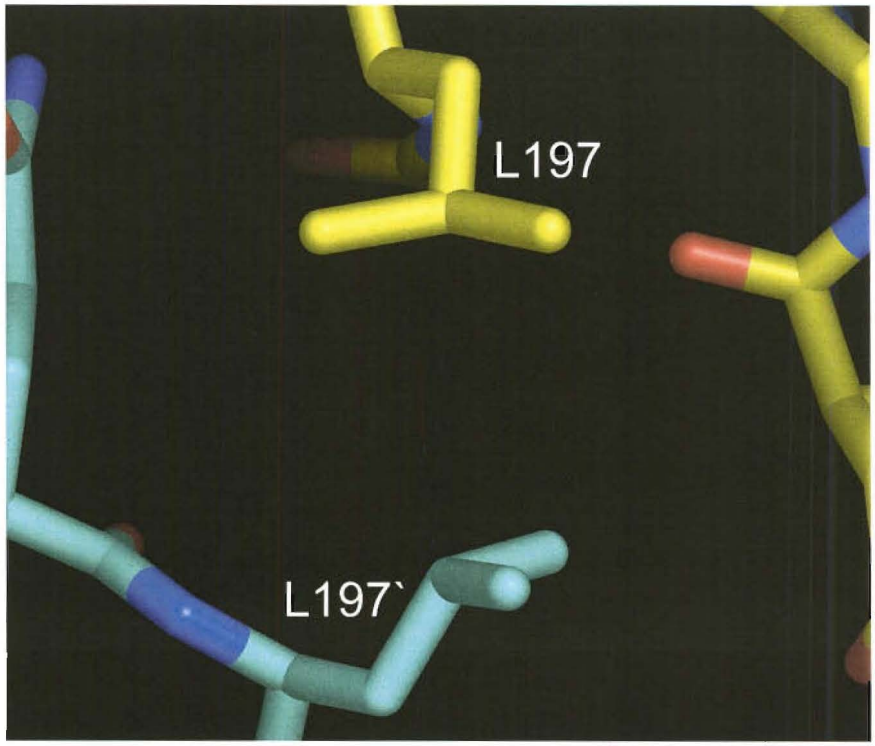

Figure 2.4 *The contact between residues L167 and T168 from neighbouring subunits.*

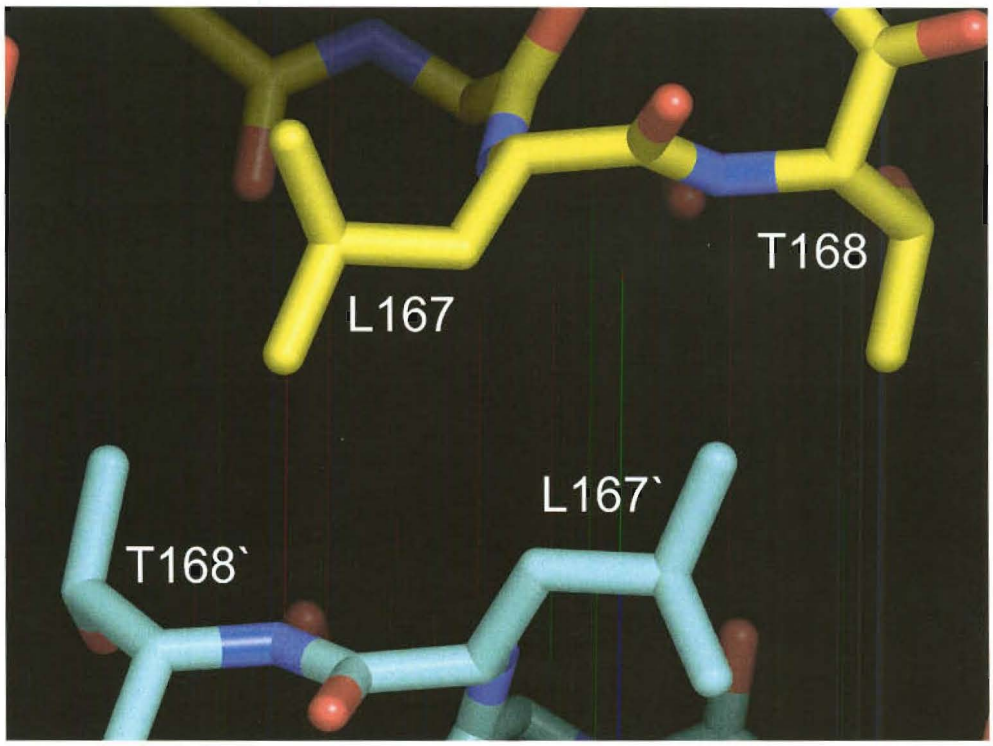

2.6.2 Re-evaluation of the dimer-dimer interface of *E. coli* DHDPS

Three-dimensional visual analysis of both the published structure and the higher resolution wild-type structure solved in this lab during this work (97) has revealed that the dimer-dimer interfaces are significantly more extensive than these published reports.

Additional to the three reported contacts, three new direct intersubunit contacts, involving five amino acid residues, and a water-bridging network, in which water molecules participate in intersubunit hydrogen bonding, were identified during this work. These are summarised below.

Q196-Q196

Figure 2.5 *Hydrogen bonding between Q196 residues from contacting subunits.*

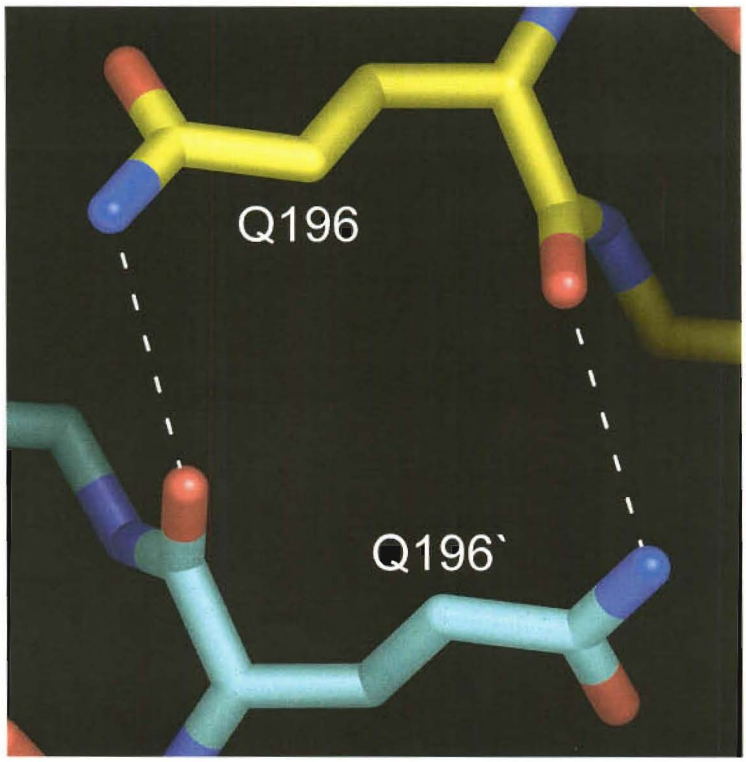

Perhaps the most important of the newly identified contacts is the symmetrical contact between the Q196 residues of neighbouring subunits, which form two inter-subunit hydrogen bonds (Figure 2.5). In the published structure, the orientation of the ε-nitrogen and oxygen atoms of this residue is incorrect, and, in fact, these atoms should be flipped 180°, producing the correct geometry for inter-monomer hydrogen

bonding between the epsilon nitrogen and the main chain oxygen of the neighbouring residue. This also allows for formation of an intra-subunit hydrogen bond between the ε-oxygen of Q196 and an NH_2 group of R230 from the same monomer.

D193

Water-mediated hydrogen bonds are also formed between the two monomers at the interface. D193 has strong hydrogen bonds to two well-defined water molecules that occupy cavities formed by the interface of the two monomers, and are, in turn, hydrogen bonded to residues of the neighbouring monomer (Figure 2.6). One of these water molecules forms three separate hydrogen bonds to the other monomer, involving the main chain nitrogen of N171, the side chain δ-nitrogen of N171, and the main chain oxygen of L167. The second water molecule forms one further hydrogen bond to the main chain oxygen of T168 from the other monomer. Since D193 does not interact directly or indirectly with D193 from the neighbouring subunit, each inter-dimer interface contains two complete water-mediated hydrogen bonding networks.

Figure 2.6 *Water-mediated hydrogen bonds between two neighbouring subunits.*

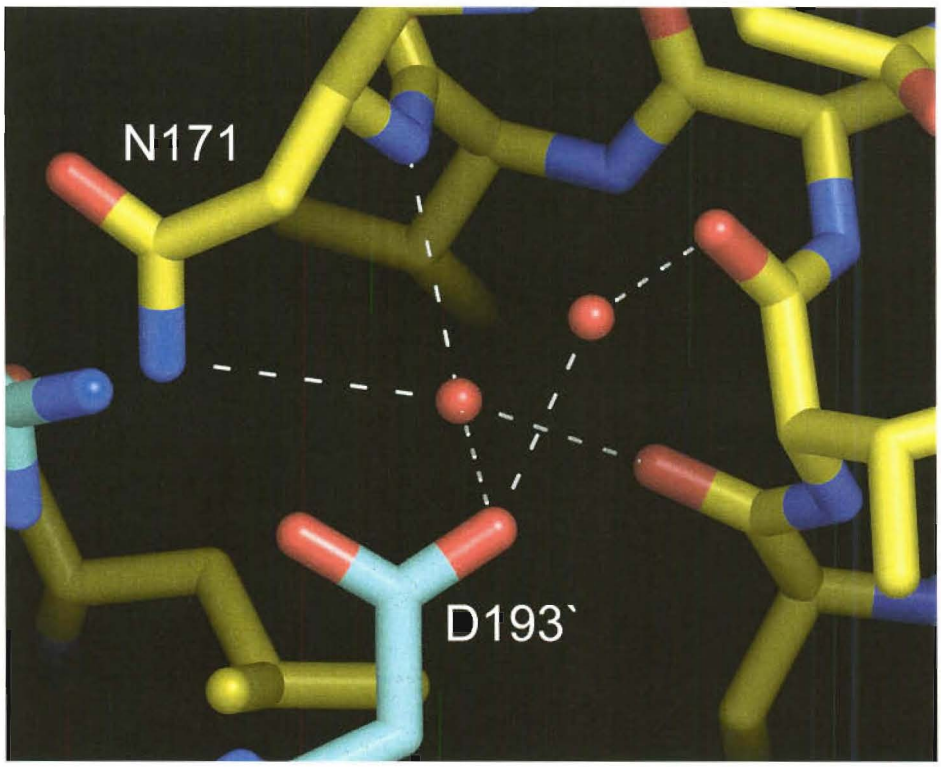

E175-Q234

The side chains of the two residues E175 and Q234 protrude away from the surface of the monomer at the edge of the contact area between the two monomers and form hydrogen bonded contacts that are separate from the main interface. These side chains are not constrained by other structural elements and are surrounded by solvent. They would, therefore, be expected to show flexibility and interact directly only transiently. This is borne out by the high B-factors of these side chains indicated in the published structure. However, the correct geometry for hydrogen bonding between the ε-oxygen of E175 and the ε-nitrogen of Q234 from the contacting subunit is conserved in each contact in our improved resolution structure, suggesting that this is an important inter-subunit hydrogen bond (Figure 2.7).

Figure 2.7 *Hydrogen bonding between E175 and Q234 of the neighbouring subunit.*

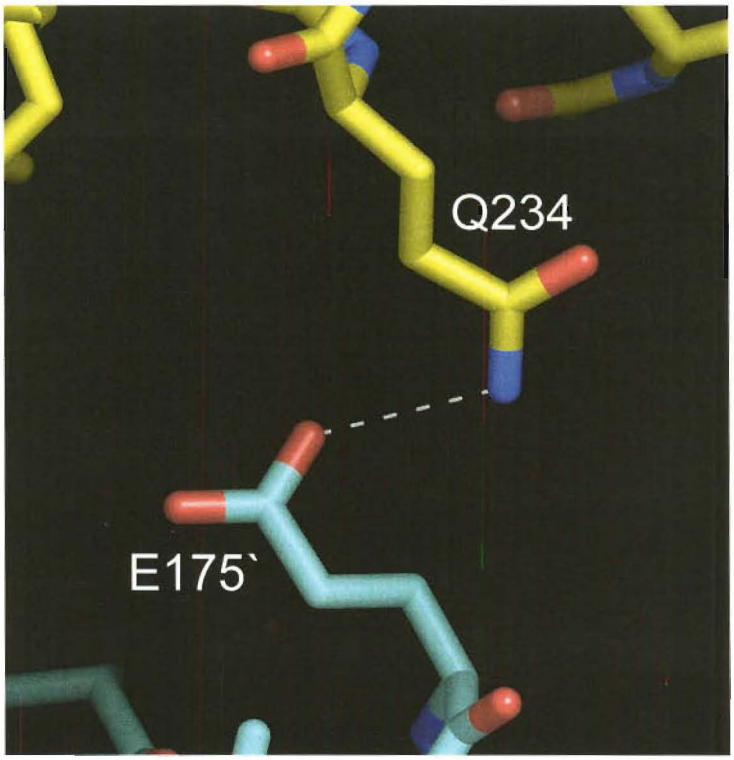

N171-R230

Contact is also made at the interface by the side chains of N171 and R230, which are positioned at the edge of the interface between the two monomers. The extremities of the side chains abut, resulting in close van der Waals contact between the last four atoms of each side chain (Figure 2.8). Despite the presence of appropriate groups for

hydrogen bonding, the geometric configuration of these groups is incorrect for inter-subunit hydrogen bond formation and thus this contact appears to be van der Waals in nature.

Figure 2.8 *Contact between N171 and R230 at the dimer-dimer interface*

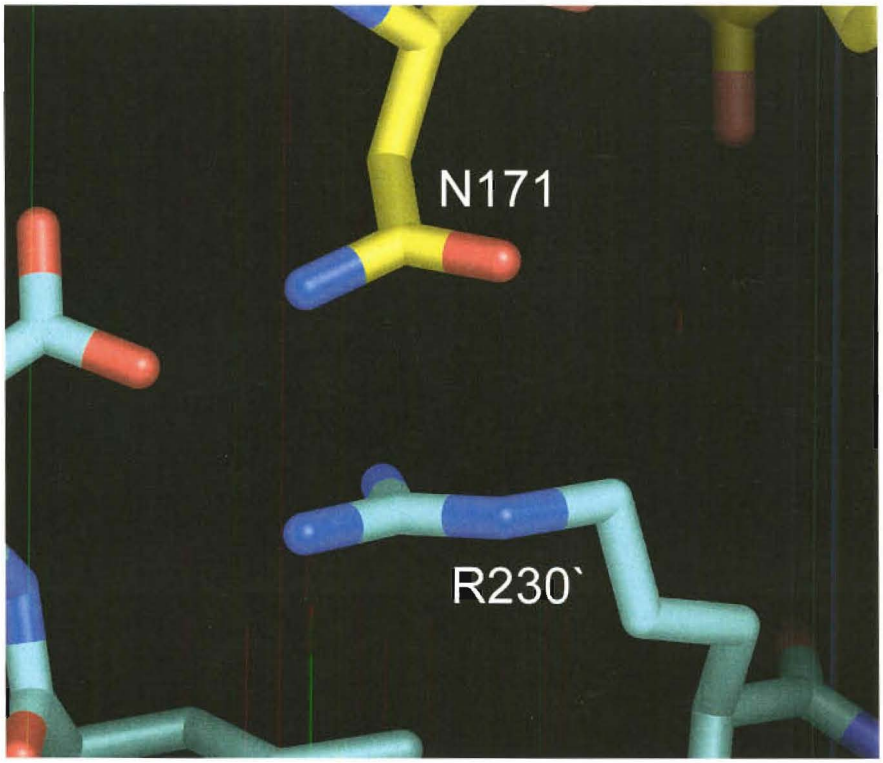

The 'new' interface

It is clear from this re-inspection of the dimer-dimer interface that the number and range of contacts between the two monomers involved is much larger than the purely hydrophobic interactions reported (Figure 2.9) (22).

Figure 2.9 *Re-evaluation of the dimer-dimer interface of* E. coli *DHDPS. Hydrophobic contacts are indicated by black lines, van der Waals contacts are indicated by green lines, and hydrogen bonds are indicated by dashed red lines. Water molecules are represented by red circles.*

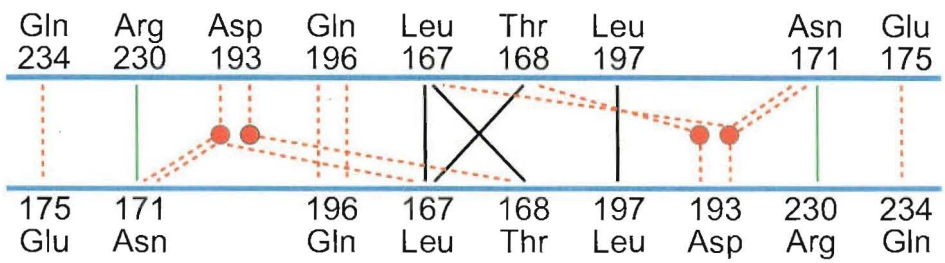

2.6.3 Mutation strategies for the disruption of protein-protein interfaces

Among the published studies (section 2.5), four different approaches have been taken to destabilising subunit interfaces.

Loop deletion/insertion.

In many oligomeric proteins, amino acid residues that form the inter-monomer interfaces are located on extended loop regions. By replacing these regions with alternative shorter fragments, associative interactions between subunits can be eliminated. Alternatively, by lengthening the loop region, association of two monomers can be blocked by steric hinderance.

Small residues mutated to large residues

By mutating small amino acid residues that form tightly packed contacts in the subunit interfaces to more bulky amino acids, for example, tyrosine, subunits can be sterically forced apart, disallowing the formation of attractive interactions between subunits.

Hydrophobic residues mutated to hydrophilic residues

In cases where subunit interfaces are composed mainly of hydrophobic contacts, simply mutating these residues to hydrophilic amino acids can destabilise the interface sufficiently to cause dissociation.

Charged residue substitution

This approach uses the property of electrostatic repulsion of like charge. Interface contact residues are mutated to amino acids with ionisable side chain groups that are placed in positions adjacent to residues of the same charge in the neighbouring subunit (if the interface were allowed to form) thus creating electrostatic repulsion between the two subunits.

2.6.4 Considerations for the design of mutations

As discussed in sections 2.5 and 2.6.3, the disruption of the interfaces of a multimeric protein with the aim of producing stable, folded, and active protomer units is not a trivial task. The planning of mutations designed to disrupt the quaternary structure of an enzyme requires the consideration of three well-defined problems (69).

First, subunit-subunit association must be prevented, preferably by introduction of the least possible alteration to the primary structure of the protein. Thus, the smallest number of mutations that is able to produce the desired result of disallowing the associative interface to form must be used to ensure that possible resultant secondary or tertiary structural changes are kept to a minimum. Related to this consideration is the nature of the amino acid substitutions utilised; clearly, it is possible to minimise any structural disturbance to subunits by careful selection of structurally similar amino acids for substitutions. Isosteric replacements are more desirable than otherwise in this respect.

Second, substitutions must be selected that will have minimum impact on any ligand binding or active sites of the protein. Potential positions for alteration must be selected that are distal to any effector binding site or active site to minimise the possibility that potential structural rearrangements caused by the mutation are transmitted to these sites.

Third, separation of the subunits of an oligomeric protein exposes to solvent the side chains of a number of hydrophobic amino acid residues that would normally be buried within subunit-subunit interfaces. This has implications for the aqueous solubility of the subunits and sufficient solubility of the mutant may only be achieved by significant reduction of the hydrophobicity of the exposed interfaces.

2.6.5 Design of the mutations

In light of the considerations above, mutations of contact residues at the dimer-dimer interface of *E. coli* DHDPS were designed. In order to minimise structural effects of the mutations, it was decided that the disruption of the interface would first be attempted using only single residue mutations. The centre of the dimer-dimer interface area, as defined by L197, is approximately 20 Å distant from the active site, as defined by K161, and over 30 Å distant form the closest lysine binding residues. Thus mutation of interface residues would seem unlikely to directly affect these ligand binding sites.

As the two inter-subunit contact surfaces of the tight-dimer are separated by the water filled cavity at the centre of the *E. coli* DHDPS tetramer, large contiguous hydrophobic patches are absent from the surface of the tight-dimer unit. Inspection of

the surface character of the dimer-dimer interface area reveals a small hydrophobic patch surrounded by hydrophilic groups. Thus, while the exposure of this surface was considered in choosing possible mutations, it was not expected that insurmountable solubility issues would be encountered on exposure of this relatively small, isolated hydrophobic area.

Initially, a single mutation of L197 to the charged residue, aspartate, was produced in order to gauge the validity of a single residue substitution approach. Based on the success of this strategy in production of a stable dimeric form of *E. coli* DHDPS (Chapter four), five further mutations of interface residues were subsequently created with the intention of characterising the interface, and producing additional dimeric and partially-dimeric variants.

L197 to aspartate

The configuration of the two L197 residues at the interface, in which the side chains abut directly, made this residue a perfect candidate for replacement with a charged amino acid. By replacing this residue with the isosteric amino acid, aspartate, negative charge was placed on the interface surface at the previously interacting positions. Electrostatic repulsion of the two charged moieties would presumably prevent complementary interaction between monomers at this position disrupting formation of the interface.

L197 to tyrosine

As the mutation of L197 to aspartate was found to produce a stable dimeric form of DHDPS (Chapter four), it was decided to introduce steric bulk at this same position. The large aromatic side chain of tyrosine had the potential to sufficiently alter the topology, and, therefore, the complementarity, of the interface surfaces so as to disallow association of the dimers.

Q196 to aspartate

Q196 makes contact with Q196 from the neighbouring subunit, presenting a good candidate for charged residue substitution. However, the positioning of the side chains in this case would place the charged moieties distal if an isosteric substitution was made. Substitution of this residue with aspartate, which is negatively charged, but has a shorter side chain, was likely to place the charged groups in closely interacting

positions, if the interface was formed, thus producing electrostatic repulsion between the monomers.

Q234 to aspartate

Q234 interacts with the negatively charged E175. By mutating Q234 to the negatively charged aspartate, electrostatic repulsion can be created at this position. The mobile nature of the side chains of these residues was expected to attenuate repulsion by rearrangement of the side chain conformations.

D193 to alanine

Substitution of D193 with the hydrophobic amino acid alanine will remove the hydrogen bonds previously made by the hydrophilic side chain of this residue to the bound waters within the dimer-dimer interface, thus removing the intersubunit bonding afforded by this residue. It was hoped that this would be sufficient to disrupt the interface.

D193 to tyrosine

In addition to removing the intersubunit, water-mediated hydrogen bonding, introduction of the bulky side chain of tyrosine at this position was designed to produce an additional steric hindrance to the formation of the interface between the two subunits.

2.7 Summary

The literature describing the structural details and functional advantages of protein quaternary structure has been surveyed. In addition, literature describing the engineering of the quaternary structure of proteins has been comprehensively reviewed.

Extensive analysis of the crystal structures of *E. coli* DHDPS revealed that the dimer-dimer interface comprises a much larger set of contact residues than has been indicated in published reports. Based on this investigation, rational design of single-point amino acid mutations in the *E. coli* DHDPS sequence was undertaken to produce dimeric variants of the protein for functional analysis, and to confirm the importance of the newly identified interface residues to the tetramerisation of the protein.

2.8 References

1. Eisenstein, E., and Schachman, H. K. (1989) in *Protein Function* (Creighton, T. E., ed), IRL Press, Oxford
2. Perham, R. N. (1975) Self-assembly of biological macromolecules. *Philos Trans R Soc Lond B Biol Sci* **272**, 123-136
3. Marianayagam, N. J., Sunde, M., and Matthews, J. M. (2004) The power of two: protein dimerization in biology. *Trends Biochem Sci* **29**, 618-625
4. Klotz, I. M., Darnall, D. W., and Langerman, N. R. (1975) in *The proteins* (Hill, R. L., ed), Academic Press, New York
5. Beernink, P. T., and Tolan, D. R. (1996) Disruption of the aldolase A tetramer into catalytically active monomers. *Proc Natl Acad Sci U S A* **93**, 5374-5379
6. Traut, T. W. (1994) Dissociation of enzyme oligomers: a mechanism for allosteric regulation. *Crit Rev Biochem Mol Biol* **29**, 125-163
7. Monod, J., Wyman, J., and Changeux, J. P. (1965) On the nature of allosteric transitions: a plausible model. *J Mol Biol* **12**, 88-118
8. Nooren, I. M., and Thornton, J. M. (2003) Diversity of protein-protein interactions. *EMBO J* **22**, 3486-3492
9. Goodsell, D. S., and Olson, A. J. (2000) Structural symmetry and protein function. *Annu Rev Biophys Biomol Struct* **29**, 105-153
10. Papoian, G. A., Ulander, J., and Wolynes, P. G. (2003) Role of water mediated interactions in protein-protein recognition landscapes. *J Am Chem Soc* **125**, 9170-9178
11. Ma, B., Elkayam, T., Wolfson, H., and Nussinov, R. (2003) Protein-protein interactions: structurally conserved residues distinguish between binding sites and exposed protein surfaces. *Proc Natl Acad Sci, U S A* **100**, 5772-5777
12. Ofran, Y., and Rost, B. (2003) Analysing six types of protein-protein interfaces. *J Mol Biol* **325**, 377-387
13. Jones, S., and Thornton, J. M. (1996) Principles of protein-protein interactions. *Proc Natl Acad Sci, U S A* **93**, 13-20
14. Jones, S., and Thornton, J. M. (1997) Analysis of protein-protein interaction sites using surface patches. *J Mol Biol* **272**, 121-132
15. Jones, S., and Thornton, J. M. (1995) Protein-protein interactions: a review of protein dimer structures. *Prog Biophys Mol Biol* **63**, 31-65
16. Lo Conte, L., Chothia, C., and Janin, J. (1999) The atomic structure of protein-protein recognition sites. *J Mol Biol* **285**, 2177-2198
17. Nooren, I. M., and Thornton, J. M. (2003) Structural characterisation and functional significance of transient protein-protein interactions. *J Mol Biol* **325**, 991-1018
18. Jones, S., and Thornton, J. M. (1997) Prediction of protein-protein interaction sites using patch analysis. *J Mol Biol* **272**, 133-143

19. Salwinski, L., and Eisenberg, D. (2003) Computational methods of analysis of protein-protein interactions. *Curr Opin Struct Biol* **13**, 377-382

20. Ofran, Y., and Rost, B. (2003) Predicted protein-protein interaction sites from local sequence information. *FEBS Lett* **544**, 236-239

21. Brooijmans, N., Sharp, K. A., and Kuntz, I. D. (2002) Stability of macromolecular complexes. *Proteins* **48**, 645-653

22. Blickling, S., Beisel, H. G., Bozic, D., Knablein, J., Laber, B., and Huber, R. (1997) Structure of dihydrodipicolinate synthase of *Nicotiana sylvestris* reveals novel quaternary structure. *J Mol Biol* **274**, 608-621

23. Clore, G. M., and Gronenborn, A. M. (1995) Three-dimensional structures of α and β chemokines. *FASEB J* **9**, 57-62

24. Royer, W. E., Jr., Love, W. E., and Fenderson, F. F. (1985) Cooperative dimeric and tetrameric clam haemoglobins are novel assemblages of myoglobin folds. *Nature* **316**, 277-280

25. Shaanan, B., Lis, H., and Sharon, N. (1991) Structure of a legume lectin with an ordered N-linked carbohydrate in complex with lactose. *Science* **254**, 862-866

26. Perutz, M. F. (1997) *Science is not a quiet life: Unravelling the atomic mechanism of haemoglobin*, Imperial College Press, Singapore

27. Franke, I., Meiss, G., Blecher, D., Gimadutdinow, O., Urbanke, C., and Pingoud, A. (1998) Genetic engineering, production and characterisation of monomeric variants of the dimeric *Serratia marcescens* endonuclease. *FEBS Lett* **425**, 517-522

28. Mossing, M. C., and Sauer, R. T. (1990) Stable, monomeric variants of λ Cro obtained by insertion of a designed β-hairpin sequence. *Science* **250**, 1712-1715

29. Borchert, T. V., Abagyan, R., Jaenicke, R., and Wierenga, R. K. (1994) Design, creation, and characterization of a stable, monomeric triosephosphate isomerase. *Proc Natl Acad Sci, U S A* **91**, 1515-1518

30. Jackson, R. M., Gelpi, J. L., Cortes, A., Emery, D. C., Wilks, H. M., Moreton, K. M., Halsall, D. J., Sleigh, R. N., Behan-Martin, M., and Jones, G. R. (1992) Construction of a stable dimer of *Bacillus stearothermophilus* lactate dehydrogenase. *Biochemistry* **31**, 8307-8314

31. Dobson, C. M. (2002) Getting out of shape. *Nature* **418**, 729-730

32. Nielsen, L., Khurana, R., Coats, A., Frokjaer, S., Brange, J., Vyas, S., Uversky, V. N., and Fink, A. L. (2001) Effect of environmental factors on the kinetics of insulin fibril formation: elucidation of the molecular mechanism. *Biochemistry* **40**, 6036-6046

33. Lashuel, H. A., Lai, Z., and Kelly, J. W. (1998) Characterization of the transthyretin acid denaturation pathways by analytical ultracentrifugation: implications for wild-type, V30M, and L55P amyloid fibril formation. *Biochemistry* **37**, 17851-17864

34. Raghu, P., Reddy, G. B., and Sivakumar, B. (2002) Inhibition of transthyretin amyloid fibril formation by 2,4-dinitrophenol through tetramer stabilization. *Arch Biochem Biophys* **400**, 43-47

35. Jenne, D. E., Denzel, K., Blatzinger, P., Winter, P., Obermaier, B., Linke, R. P., and Altland, K. (1996) A new isoleucine substitution of Val-20 in transthyretin tetramers selectively impairs dimer-dimer contacts and causes systemic amyloidosis. *Proc Natl Acad Sci, U S A* **93**, 6302-6307

36. Hammarstrom, P., Sekijima, Y., White, J. T., Wiseman, R. L., Lim, A., Costello, C. E., Altland, K., Garzuly, F., Budka, H., and Kelly, J. W. (2003) D18G transthyretin is monomeric, aggregation prone, and not detectable in plasma and cerebrospinal fluid: a prescription for central nervous system amyloidosis? *Biochemistry* **42**, 6656-6663

37. Clegg, J. S. (1984) Properties and metabolism of the aqueous cytoplasm and its boundaries. *Am J Physiol* **246**, R133-151

38. Fersht, A., and Winter, G. (1992) Protein engineering. *Trends Biochem Sci* **17**, 292-295

39. Gerlt, J. A. (1994) Protein engineering to study enzyme catalytic mechanisms. *Curr Opin Struct Biol* **4**, 593-600

40. Regan, L., and Jackson, S. E. (2003) Engineering and design - protein design: theory and practice - editorial overview. *Curr Opin Struct Biol* **13**, 479-481

41. Fersht, A. R., Matouschek, A., and Serrano, L. (1992) The folding of an enzyme. I. Theory of protein engineering analysis of stability and pathway of protein folding. *J Mol Biol* **224**, 771-782

42. Matthews, B. W., Nicholson, H., and Becktel, W. J. (1987) Enhanced protein thermostability from site-directed mutations that decrease the entropy of unfolding. *Proc Natl Acad Sci, U S A* **84**, 6663-6667

43. Matthews, B. W. (1987) Genetic and structural analysis of the protein stability problem. *Biochemistry* **26**, 6885-6888

44. Alber, T. (1989) Mutational effects on protein stability. *Annu Rev Biochem* **58**, 765-798

45. Makhatadze, G. I., Loladze, V. V., Ermolenko, D. N., Chen, X., and Thomas, S. T. (2003) Contribution of surface salt bridges to protein stability: guidelines for protein engineering. *J Mol Biol* **327**, 1135-1148

46. Karshikoff, A., and Ladenstein, R. (2001) Ion pairs and the thermotolerance of proteins from hyperthermophiles: a "traffic rule" for hot roads. *Trends Biochem Sci* **26**, 550-556

47. Yip, K. S., Britton, K. L., Stillman, T. J., Lebbink, J., de Vos, W. M., Robb, F. T., Vetriani, C., Maeder, D., and Rice, D. W. (1998) Insights into the molecular basis of thermal stability from the analysis of ion-pair networks in the glutamate dehydrogenase family. *Eur J Biochem* **255**, 336-346

48. Gerk, L. P., Leven, O., and Muller-Hill, B. (2000) Strengthening the dimerisation interface of Lac repressor increases its thermostability by 40°C. *J Mol Biol* **299**, 805-812

49. Vetriani, C., Maeder, D. L., Tolliday, N., Yip, K. S., Stillman, T. J., Britton, K. L., Rice, D. W., Klump, H. H., and Robb, F. T. (1998) Protein thermostability above 100°C: a key role for ionic interactions. *Proc Natl Acad Sci, U S A* **95**, 12300-12305

50. Lebbink, J. H., Knapp, S., van der Oost, J., Rice, D., Ladenstein, R., and de Vos, W. M. (1999) Engineering activity and stability of *Thermotoga maritima* glutamate dehydrogenase. II: construction of a 16-residue ion-pair network at the subunit interface. *J Mol Biol* **289**, 357-369

51. Kou, H., and Pugh, B. F. (2004) Engineering dimer-stabilizing mutations in the TATA-binding protein. *J Biol Chem* **279**, 20966-20973

52. Ahern, T. J., Casal, J. I., Petsko, G. A., and Klibanov, A. M. (1987) Control of oligomeric enzyme thermostability by protein engineering. *Proc Natl Acad Sci, U S A* **84**, 675-679

53. Casal, J. I., Ahern, T. J., Davenport, R. C., Petsko, G. A., and Klibanov, A. M. (1987) Subunit interface of triosephosphate isomerase: site-directed mutagenesis and characterization of the altered enzyme. *Biochemistry* **26**, 1258-1264

54. Jones, D. H., McMillan, A. J., Fersht, A. R., and Winter, G. (1985) Reversible dissociation of dimeric tyrosyl-tRNA synthetase by mutagenesis at the subunit interface. *Biochemistry* **24**, 5852-5857

55. Ward, W. H., Jones, D. H., and Fersht, A. R. (1986) Protein engineering of homodimeric tyrosyl-tRNA synthetase to produce active heterodimers. *J Biol Chem* **261**, 9576-9578

56. Ward, W. H., Jones, D. H., and Fersht, A. R. (1987) Effects of engineering complementary charged residues into the hydrophobic subunit interface of tyrosyl-tRNA synthetase. Appendix: Kinetic analysis of dimeric enzymes that reversibly dissociate into inactive subunits. *Biochemistry* **26**, 4131-4138

57. Carter, P., Bedouelle, H., and Winter, G. (1986) Construction of heterodimer tyrosyl-tRNA synthetase shows tRNATyr interacts with both subunits. *Proc Natl Acad Sci, U S A* **83**, 1189-1192

58. Vora, J. P., Owens, D. R., Dolben, J., Atiea, J. A., Dean, J. D., Kang, S., Burch, A., and Brange, J. (1988) Recombinant DNA derived monomeric insulin analogue: Comparison with soluble human insulin in normal subjects. *Bmj* **297**, 1236-1239

59. Brange, J., Ribel, U., Hansen, J. F., Dodson, G., Hansen, M. T., Havelund, S., Melberg, S. G., Norris, F., Norris, K., and Snel, L. (1988) Monomeric insulins obtained by protein engineering and their medical implications. *Nature* **333**, 679-682

60. Hoffman, A., and Ziv, E. (1997) Pharmacokinetic considerations of new insulin formulations and routes of administration. *Clin Pharmacokinet* **33**, 285-301

61. DeFelippis, M. R., Chance, R. E., and Frank, B. H. (2001) Insulin self-association and the relationship to pharmacokinetics and pharmacodynamics. *Crit Rev Ther Drug Carrier Syst* **18**, 201-264

62. Robinson, D. S. (2003) New therapies for asthma: where next? *Pediatr Pulmonol* **36**, 369-375

63. McKenzie, A. N., Ely, B., and Sanderson, C. J. (1991) Mutated interleukin-5 monomers are biologically inactive. *Mol Immunol* **28**, 155-158

64. Dickason, R. R., and Huston, D. P. (1996) Creation of a biologically active interleukin-5 monomer. *Nature* **379**, 652-655

65. Dickason, R. R., Huston, M. M., and Huston, D. P. (1996) Delineation of IL-5 domains predicted to engage the IL-5 receptor complex. *J Immunol* **156**, 1030-1037

66. Dickason, R. R., English, J. D., and Huston, D. P. (1996) Engineering of a functional interleukin-5 monomer: a paradigm for redesigning helical bundle cytokines with therapeutic potential in allergy and asthma. *J Mol Med* **74**, 535-546

67. Miller, M. D., and Krause, K. L. (1996) Identification of the *Serratia* endonuclease dimer: structural basis and implications for catalysis. *Protein Sci* **5**, 24-33

68. Franke, I., Meiss, G., and Pingoud, A. (1999) On the advantage of being a dimer, a case study using the dimeric *Serratia* nuclease and the monomeric nuclease from *Anabaena sp.* strain PCC 7120. *J Biol Chem* **274**, 825-832

69. Sano, T., Vajda, S., Smith, C. L., and Cantor, C. R. (1997) Engineering subunit association of multisubunit proteins: a dimeric streptavidin. *Proc Natl Acad Sci, U S A* **94**, 6153-6158

70. Laitinen, O. H., Airenne, K. J., Marttila, A. T., Kulik, T., Porkka, E., Bayer, E. A., Wilchek, M., and Kulomaa, M. S. (1999) Mutation of a critical tryptophan to lysine in avidin or streptavidin may explain why sea urchin fibropellin adopts an avidin-like domain. *FEBS Lett* **461**, 52-58

71. Laitinen, O. H., Nordlund, H. R., Hytonen, V. P., Uotila, S. T., Marttila, A. T., Savolainen, J., Airenne, K. J., Livnah, O., Bayer, E. A., Wilchek, M., and Kulomaa, M. S. (2003) Rational design of an active avidin monomer. *J Biol Chem* **278**, 4010-4014

72. Pazy, Y., Eisenberg-Domovich, Y., Laitinen, O. H., Kulomaa, M. S., Bayer, E. A., Wilchek, M., and Livnah, O. (2003) Dimer-tetramer transition between solution and crystalline states of streptavidin and avidin mutants. *J Bacteriol* **185**, 4050-4056

73. Shinoda, H., Hattori, M., Shimizu, A., Samejima, T., and Satoh, T. (1999) Hydrophobic interactions of Val75 are critical for oligomeric thermostability of inorganic pyrophosphatase from *Bacillus stearothermophilus*. *J Biochem (Tokyo)* **125**, 58-63

74. Salminen, A., Efimova, I. S., Parfenyev, A. N., Magretova, N. N., Mikalahti, K., Goldman, A., Baykov, A. A., and Lahti, R. (1999) Reciprocal effects of substitutions at the subunit interfaces in hexameric pyrophosphatase of *Escherichia coli*. Dimeric and monomeric forms of the enzyme. *J Biol Chem* **274**, 33898-33904

75. Velichko, I. S., Mikalahti, K., Kasho, V. N., Dudarenkov, V. Y., Hyytia, T., Goldman, A., Cooperman, B. S., Lahti, R., and Baykov, A. A. (1998) Trimeric inorganic pyrophosphatase of *Escherichia coli* obtained by directed mutagenesis. *Biochemistry* **37**, 734-740

76. Banci, L., Benedetto, M., Bertini, I., Del Conte, R., Piccioli, M., and Viezzoli, M. S. (1998) Solution structure of reduced monomeric Q133M2 copper, zinc superoxide dismutase (SOD). Why is SOD a dimeric enzyme? *Biochemistry* **37**, 11780-11791

77. Fritsche, P., and Alves, J. (2004) A monomeric mutant of restriction endonuclease *Eco*R I nicks DNA without sequence specificity. *Biol Chem* **385**, 975-985

78. Borchert, T. V., Pratt, K., Zeelen, J. P., Callens, M., Noble, M. E., Opperdoes, F. R., Michels, P. A., and Wierenga, R. K. (1993) Overexpression of trypanosomal triosephosphate isomerase in *Escherichia coli* and characterisation of a dimer-interface mutant. *Eur J Biochem* **211**, 703-710

79. Borchert, T. V., Zeelen, J. P., Schliebs, W., Callens, M., Minke, W., Jaenicke, R., and Wierenga, R. K. (1995) An interface point-mutation variant of triosephosphate isomerase is compactly folded and monomeric at low protein concentrations. *FEBS Lett* **367**, 315-318

80. Borchert, T. V., Abagyan, R., Kishan, K. V. R., Zeelen, J. P., and Wierenga, R. K. (1993) The crystal structure of an engineered monomeric triosephosphate isomerase, monoTIM: the correct modeling of an 8-residue loop. *Structure* **1**, 205-213

81. Schliebs, W., Thanki, N., Jaenicke, R., and Wierenga, R. K. (1997) A double mutation at the tip of the dimer interface loop of triosephosphate isomerase generates active monomers with reduced stability. *Biochemistry* **36**, 9655-9662

82. Borchert, T. V., Kishan, K. V., Zeelen, J. P., Schliebs, W., Thanki, N., Abagyan, R., Jaenicke, R., and Wierenga, R. K. (1995) Three new crystal structures of point mutation variants of monoTIM: conformational flexibility of loop-1, loop-4 and loop-8. *Structure* **3**, 669-679

83. Mainfroid, V., Terpstra, P., Beauregard, M., Frere, J. M., Mande, S. C., Hol, W. G., Martial, J. A., and Goraj, K. (1996) Three hTIM mutants that provide new insights on why TIM is a dimer. *J Mol Biol* **257**, 441-456

84. Mainfroid, V., Mande, S. C., Hol, W. G., Martial, J. A., and Goraj, K. (1996) Stabilization of human triosephosphate isomerase by improvement of the stability of individual α-helices in dimeric as well as monomeric forms of the protein. *Biochemistry* **35**, 4110-4117

85. Bertini, I., Piccioli, M., Viezzoli, M. S., Chiu, C. Y., and Mullenbach, G. T. (1994) A spectroscopic characterization of a monomeric analog of copper, zinc superoxide dismutase. *Eur Biophys J* **23**, 167-176

86. Banci, L., Bertini, I., Chiu, C. Y., Mullenbach, G. T., and Viezzoli, M. S. (1995) Synthesis and characterization of a monomeric mutant Cu/Zn superoxide dismutase with partially reconstituted enzymic activity. *Eur J Biochem* **234**, 855-860

87. Porvari, K. S., Herrala, A. M., Kurkela, R. M., Taavitsainen, P. A., Lindqvist, Y., Schneider, G., and Vihko, P. T. (1994) Site-directed mutagenesis of prostatic acid phosphatase. Catalytically important aspartic acid 258, substrate specificity, and oligomerization. *J Biol Chem* **269**, 22642-22646

88. Breiter, D. R., Resnik, E., and Banaszak, L. J. (1994) Engineering the quaternary structure of an enzyme: construction and analysis of a monomeric form of malate dehydrogenase from *Escherichia coli*. *Protein Sci* **3**, 2023-2032

89. Yoon, J., Oh, B., Kim, K., Park, J. E., Wang, J., Kim, H. S., and Kim, Y. (2003) Modifying the oligomeric state of cyclic amidase and its effect on enzymatic catalysis. *Biochem Biophys Res Commun* **310**, 651-659

90. Hausmann, S., Pei, Y., and Shuman, S. (2003) Homodimeric quaternary structure is required for the in vivo function and thermal stability of *Saccharomyces cerevisiae* and *Schizosaccharomyces pombe* RNA triphosphatases. *J Biol Chem* **278**, 30487-30496

91. Lehman, K., Ho, C. K., and Shuman, S. (2001) Importance of homodimerization for the *in vivo* function of yeast RNA triphosphatase. *J Biol Chem* **276**, 14996-15002

92. Beernink, P. T., and Tolan, D. R. (1994) Subunit interface mutants of rabbit muscle aldolase form active dimers. *Protein Sci* **3**, 1383-1391

93. Beernink, P. T., and Tolan, D. R. (1996) Disruption of the aldolase A tetramer into catalytically active monomers. *Proc Natl Acad Sci, U S A* **93**, 5374-5379

94. Tolan, D. R., Schuler, B., Beernink, P. T., and Jaenicke, R. (2003) Thermodynamic analysis of the dissociation of the aldolase tetramer substituted at one or both of the subunit interfaces. *Biol Chem* **384**, 1463-1471

95. Bailey, D. L., Fraser, M. E., Bridger, W. A., James, M. N., and Wolodko, W. T. (1999) A dimeric form of *Escherichia coli* succinyl-CoA synthetase produced by site-directed mutagenesis. *J Mol Biol* **285**, 1655-1666

96. Mirwaldt, C., Korndorfer, I., and Huber, R. (1995) The crystal structure of dihydrodipicolinate synthase from *Escherichia coli* at 2.5 Å resolution. *J Mol Biol* **246**, 227-239

97. Dobson, R. C. J., Griffin, M. D. W., Jameson, G. B., and Gerrard, J. A. (2005) The crystal structures of native and (*S*)-lysine bound dihydrodipicolinate synthase from *Escherichia coli* with improved resolution show new features of biological significance. *Acta Crystallogr D Biol Crystallogr*, (Submitted)

Chapter Three

Site-directed mutagenesis, enzyme purification, and (*S*)-ASA synthesis

3.1 Introduction

The proposed investigation of the functional advantages afforded by the tetrameric structure of *E. coli* DHDPS required the creation of specific mutations in the amino acid sequence of the enzyme. Site-directed mutagenesis was employed in order to produce variants of DHDPS containing the amino acid substitutions described in the previous chapter.

The rigorous functional and biophysical characterisation of wild-type and mutant DHDPS required production and purification of milligram quantities of the proteins. Additionally, the assay utilised in this study to collect initial rate data employed DHDPR as a coupling enzyme and thus sufficient amounts of this enzyme were also required. Separate high copy-number plasmids carrying the genes for *E. coli* DHDPS and DHDPR allowed purification of both enzymes from a simple bacterial expression system.

As described in Chapter one, DHDPS catalyses the condensation of pyruvate and (*S*)-ASA. Kinetic analysis of wild-type DHDPS and the variants, therefore, requires pure stocks of both of these substrates. While pyruvate is commercially available as an analysis grade reagent, (*S*)-ASA must be synthesised. Several syntheses of (*S*)-ASA have been reported; however, these are generally protracted procedures or produce impure product. For the purposes of this study, (*S*)-ASA was synthesised using a novel three step protocol developed in this laboratory (1), which produces product of extremely high quality.

3.2 Site-directed mutagenesis

In vitro site-directed mutagenesis is an invaluable tool that utilises the polymerase chain reaction (PCR) to generate copies of a template DNA molecule while

incorporating the desired mutation (2). Thus, the technique provides an efficient method of introducing defined mutations into the *dap*A gene encoding *E. coli* DHDPS, which will translate into the specific single point amino acid mutations described in section 2.6.5.

Numerous methods for the site-directed mutagenesis of both linear and circular DNA have been reported (2). Many of these protocols require linearised single stranded template DNA (3) and are therefore labour intensive or technically difficult. The *dap*A gene is carried on a circular plasmid, and thus a method that allows site-specific mutation of the intact double-stranded, circular, DNA was sought for use in this study.

The QuikChange site-directed mutagenesis kit (Stratagene) allows simple mutation of supercoiled double-stranded plasmid DNA. This is achieved by PCR extension of primers containing the required mutation using the high fidelity *Pfu* DNA polymerase (Figure 3.1). In this process, both strands of the plasmid are replicated, incorporating the primers, and resulting in nicked, mutated plasmid DNA. Following amplification, the wild-type template DNA is specifically digested using the methylated DNA specific endonuclease, *Dpn* I, as DNA isolated from *E. coli* is generally dam-methylated and, therefore, susceptible to digestion by *Dpn* I. The resulting mutated DNA is then transformed into *E. coli* XL-1 Blue cells where the nicks are repaired producing intact mutated plasmid DNA.

Figure 3.1 *Overview of the QuikChange site-directed mutagenesis method. The template plasmid (i) with target site for mutation (grey circles). Complementary primers containing the desired mutation (red circle) anneal to the template DNA (ii) and are extended during PCR (iii) producing nicked circular DNA. (iv). Following amplification, wild-type template DNA is digested by* Dpn *I. Transformation of amplified DNA into XL-1 Blue cells repairs nicks in the plasmid containing the new mutation (v).*

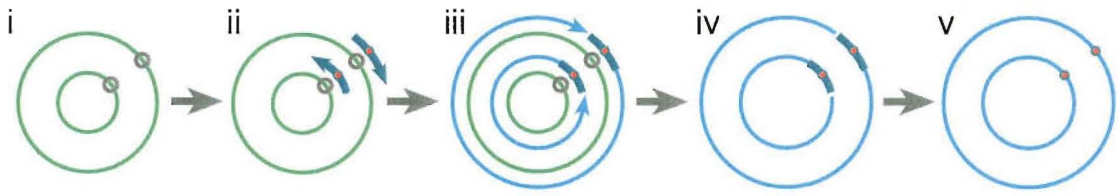

3.2.1 Mutagenic primer design

Oligonucleotide primers containing mutations designed to produce the specific amino acid substitutions described in section 2.6.5 were designed according to the guidelines

in the QuikChange kit manual (4). These primers were based on the nucleotide sequence of the *dap*A insert carried on the pBluescript based plasmid designated pJG001 (5), which was used as the template for the mutagenesis PCR reactions.

Primers for use with the QuikChange kit are required to meet a number of conditions. Both primers must anneal to the same sequence on opposite strands of the plasmid, and be 25-45 bases in length, with the desired mutation close to the centre of each. Additionally, primers should have a calculated melting temperature of greater than 78°C, contain a minimum GC content of 40%, and terminate in one or more C or G bases (4).

Table 3.1 *Oligonucleotide primer sequences used for site-directed mutagenesis of* dap*A harboured on plasmid pJG001. Substituted bases are shown in blue and the codon of the altered amino acid is underlined. The introduced recognition sequence for* Fok *I is italicised in the L197D primer sequences. Primers labelled #1 show nontemplate strand sequence and primers labelled #2 show template strand sequence.*

Primer name	Primer sequence
L197D #1	$^{5'}$GCG AGC GCG CTG GAC TTC ATG CA*G GAT* GGC GGT CAT GGG G$^{3'}$
L197D #2	$^{5'}$C CCC ATG ACC GC*C ATC* CTG CAT GAA GTC CAG CGC GCT CGC$^{3'}$
L197Y #1	$^{5'}$CTG GAC TTC ATG CAA TAC GGC GGT CAT GGG GTT ATT TC$^{3'}$
L197Y #2	$^{5'}$GA AAT AAC CCC ATG ACC GCC GTA TTG CAT GAA GTC CAG$^{3'}$
Q196D #1	$^{5'}$GCG CTG GAC TTC ATG GAT TTG GGC GGT CAT GGG$^{3'}$
Q196D #2	$^{5'}$CCC ATG ACC GCC CAA ATC CAT GAA GTC CAG CGC$^{3'}$
D193A #1	$^{5'}$GAT GCG AGC GCG CTG GCC TTC ATG CAA TTG G$^{3'}$
D193A #2	$^{5'}$C CAA TTG CAT GAA GGC CAG CGC GCT CGC ATC$^{3'}$
D193Y #1	$^{5'}$GAT GCG AGC GCG CTG TAC TTC ATG CAA TTG G$^{3'}$
D193Y #2	$^{5'}$C CAA TTG CAT GAA GTA CAG CGC GCT CGC ATC$^{3'}$
Q234D #1	$^{5'}$C GAG GCA CGC GTT ATT AAT GAT CGT CTG ATG CCA TTA CAC$^{3'}$
Q234D #2	$^{5'}$GTG TAA TGG CAT CAG ACG ATC ATT AAT AAC GCG TGC CTC G$^{3'}$

In the case of the L197D mutation, which was produced first, the primers were designed to incorporate a new restriction site, allowing rapid and easy confirmation of successful mutagenesis. This required the introduction of a silent mutation in the codon for amino acid position 196. Base substitutions for all other mutations were

kept to the minimum required for codon alteration. The sequences of all primers used are shown in Table 3.1.

3.2.2 PCR mutagenesis of plasmid pJG001

A pure preparation of plasmid pJG001, isolated from *E. coli* XL-1 Blue using standard DNA mini-prep methods (6), was used as template DNA for mutagenic PCR. In order to optimise for amplification, mutagenesis reactions were set up with several template DNA concentrations while holding the concentrations of both primers constant. A control mutagenesis reaction was also prepared using supplied primers and pWhitescript vector to test the efficiency of amplification and mutant plasmid generation.

Figure 3.2 *Agarose gel of mutagenic amplifications of pJG001. Lane 1 shows size standards with relevant bands indicated. Lane 2 was loaded with 50 ng of pJG001 and shows no significant staining at this DNA concentration. Lane 3 shows amplification of the control pWhitescript mutagenesis (4.5 Kb). Lanes 4-6 show amplification of pJG001 using primers incorporating the L197D mutation, from 10 ng (lane 4), 20 ng (lane 5), and 50 ng (lane 6) of template DNA. The strong staining of the band at approximately 4.1 kb indicates high amplification of in all reactions.*

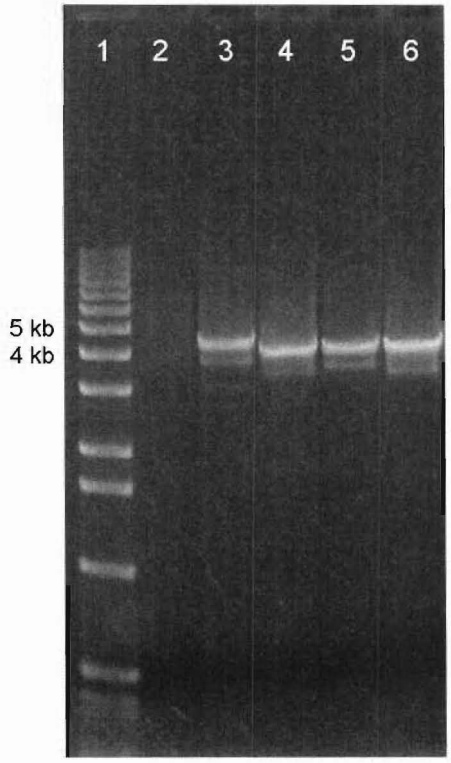

Amplification was achieved by thermal cycling of the reaction mixtures using a melting temperature of 95°C and an annealing temperature of 55 °C, followed by an

elongation step at 68°C (4). Amplification was then confirmed by agarose gel electrophoresis (Figure 3.2) before treatment of the reaction mixtures with *Dpn* I. Mutated plasmids were labelled according to the mutation carried. For example, the plasmid carrying the L197D mutation was designated pL197D.

3.2.3 Transformation of XL-1 Blue with mutated DNA

Amplified DNA from all PCR experiments was transformed into *E. coli* XL-1 Blue supercompetent cells by the heat shock method. Transformation controls were run without DNA, to ensure effective selection for transformants, and using the vector pUC18, to verify the viability of the competent cells. Transformed cells were then elaborated and cultured on LB agar plates containing ampicillin. From these plates, 5-10 potential transformant colonies from each mutagenesis reaction were subcultured and stored in LB media containing glycerol at -80°C.

In addition to the verification of efficient amplification of template DNA during the PCR reactions, the pWhitescript control mutagenesis allowed assessment of the efficiency of mutant plasmid generation under the conditions used. Since correct mutagenesis of the pWhitescript vector confers a β-gal$^+$ phenotype on transformation into *E. coli* XL-1 Blue, the proportion of mutagenised plasmids present in the final DNA preparation could be quantified by blue/white screening of transformed colonies on plates containing X-gal and IPTG. By this method, mutation efficiency was judged to be greater than 91% in all experiments carried out in this study.

3.2.4 Confirmation of the L197D mutation by restriction digest

The first variant produced for this study, the L197D mutation, was designed to incorporate the recognition sequence of the restriction endonuclease *Fok* I at the position of the mutation (Table 3.1). Thus, analysis of the *Fok* I restriction patterns of the wild-type and mutated *dap*A genes by gel electrophoresis allowed rapid initial screening for transformants containing the correct mutation.

Fok I restriction fragments of the wild-type pJG001 plasmid were predicted from the pBluescript plasmid sequence (Stratagene) with the *dap*A sequence (5) inserted appropriately. The four-base mutation designed for the L197D substitution was predicted to result in the cleaveage of a 1035 bp fragment, present in the wild-type restriction pattern, into 487 bp and 549 bp fragments. The presence of these new

fragments, and the loss of the 1035 bp fragment was confirmed in the first transformant analysed (Figure 3.3) indicating the presence of the correct mutation.

Figure 3.3 *The* Fok *I restriction patterns of pL197D (lane 2) and pJG001 (lane 3). Lanes 1 and 4 show the 1 kb+ lader with relevant bands marked. Lane 2 clearly shows the 487 bp and 549 bp expected for the mutated plasmid. The doublet expected at ~1035 bp in pJG001 is visible in lane 3, and is absent from lane 2, as predicted.*

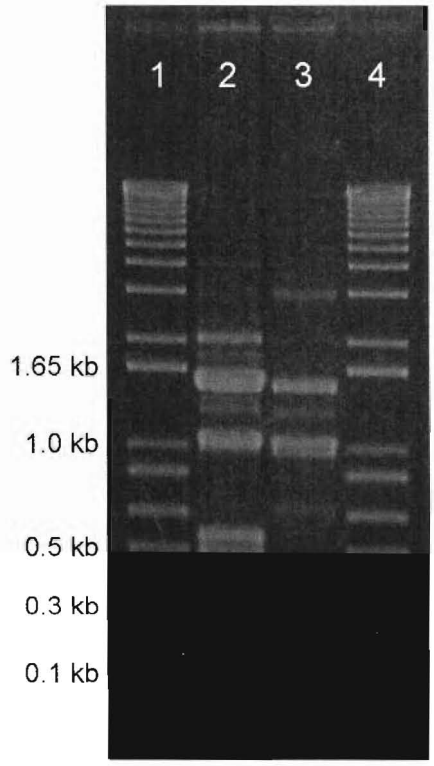

3.2.5 Sequencing of the mutated *dapA* genes

All mutant plasmids were sequenced to confirm both the presence of the correct mutation and the integrity of the full length of the *dap*A insert after mutagenesis. Bi-directional sequencing of the *dap*A insert was performed by the Auckland Genomics Unit, using BigDye dye terminator chemistry (Applied Biosystems). Sequencing quality DNA samples were produced and purified by standard methods resulting in sequence reads of 900 to 1100 bp. Consensus of sequence data from both DNA strands allowed accurate construction of the full sequence of all mutated inserts. Sequence data from plasmids to be used for expression of the enzyme variants confirmed incorporation of the desired mutations (Figure 3.4) and verified the correct sequence for the remainder of the *dap*A insert.

Figure 3.4 *Chromatograms and sequence assignment around the site of each mutation. Sequence data from the best resolved sequencing direction is shown. The mutated amino acid codon or anticodon is underlined.*

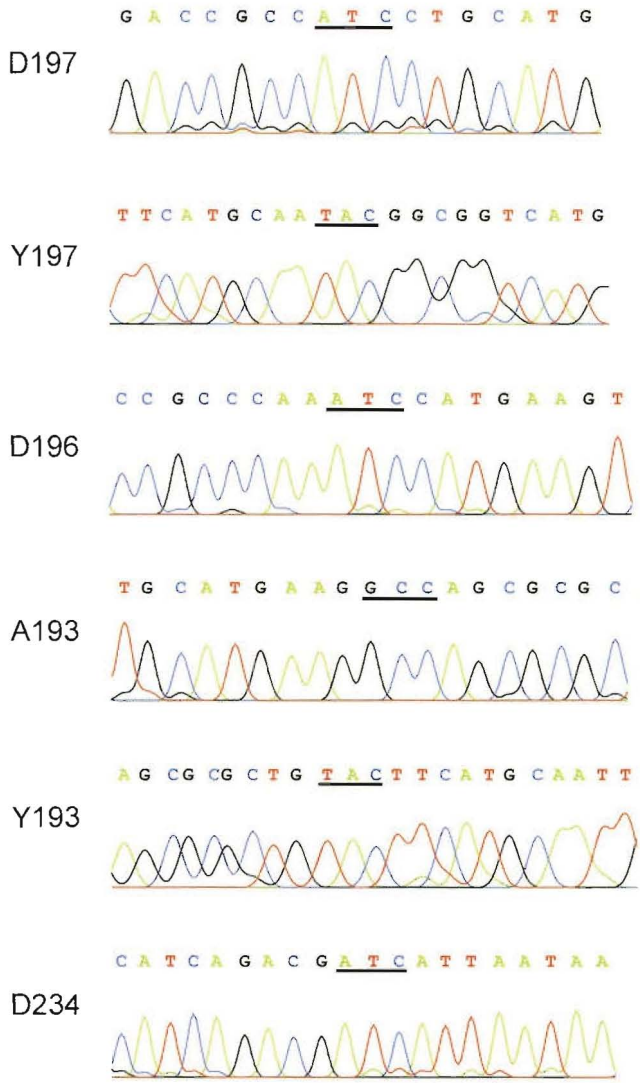

3.3 Production of wild-type DHDPS and DHDPR

3.3.1 Overexpression of wild-type DHDPS and DHDPR

Expression of both *E. coli* DHDPS and DHDPR was achieved using the *E. coli* strain XL-1 Blue containing plasmid pJG001 (5), and pJK001 (7) respectively. These pBluescript based vectors are maintained at levels of 500-700 copies per cell (6) allowing many-fold overexpression of the constitutively promoted plasmid borne *dap*A and *dap*B (DHDPR) inserts. Prior to purification of either enzyme, the integrity

of the pJG001 or pJK001 plasmids was routinely confirmed by restriction digest using both *Eco*R I and *Hin*d III, which cut each plasmid either side of the insert.

Large scale broth cultures of XL-1-pJG001 or XL-1-pJK001 were grown for 20 hours and cells were harvested by centrifugation and suspended in buffer. Crude, cell-free lysates were then produced by ultrasonication of cells, followed by clarification by centrifugation. In the past, preparation of crude DHDPS extract from XL-1-pJG001 has been routinely achieved by other workers utilising freeze-thaw cycles to gently disrupt harvested cells (5,8,9). However, investigation during this study revealed significantly higher target protein yield, with no loss of final purity, by ultrasonication, and this method was adopted.

3.3.2 Purification of wild-type DHDPS

The protocol employed for purification of wild-type DHDPS was modified from the procedure used by Mirwaldt *et al.* (10) for crystallisation of the enzyme. Initially, small aliquots of the crude extract from XL-1-pJG001 cells were subjected to heat-shock at 70°C. The relative stability of DHDPS to heat denaturation meant that this step resulted in a greater than two-fold reduction of protein background levels with little loss of DHDPS activity (Table 3.2).

Table 3.2 *Typical purification of wild-type DHDPS from* E. coli *XL-1-pJG001 from 17g wet-weight of cells (4.5 L of culture).*

	Protein (mg)	Total activity[a] (units[b])	Specific activity (units/mg)	Yield (%)	Degree of purification (fold)
Crude extract	896.0	391.5	0.44	-	-
Heat shock	295.3	283.9	0.96	72.51	2.20
Ion exchange	232.8	325.9	1.40	83.24	3.20
Hydrophobic interaction	127.9	241.6	1.89	61.71	4.32

[a] Activity was determined using the quantitative coupled assay.
[b] 1 unit is defined as the consumption of 1 µmol NADPH per sec.

Purification was continued by anion exchange chromatography: a Q Sepharose (GE Biosciences) column of approximately 100 ml bed volume was loaded with the clarified heat-shocked lysate. The column was then washed with 5 bed volumes of

wash buffer and eluted with a linear gradient of 0 to 1.0 M NaCl in buffer over 4 bed volumes. Active fractions were detected using the *o*-aminobenzaldehyde assay (section 5.2.1) and pooled. This sample was brought to 0.5 M ammonium sulfate in preparation for hydrophobic interaction chromatography on phenyl Sepharose (GE Biosciences). A column of approximately 150 ml bed volume was pre-equilibrated with 0.5 M ammonium sulphate in buffer and loaded with the pooled ion exchange fractions. The column was then washed with 0.5 M ammonium sulfate in buffer and eluted with a gradient of 0.5 to 0 M ammonium sulfate in buffer. Active fractions were again pooled and subsequently dialysed twice against 100 volumes of buffer for 2 hours.

Figure 3.5 *SDS-PAGE of a typical wild-type DHDPS preparation. Lane 1 shows molecular weight marker with relevant bands indicated. Lanes 2-6 were loaded with the protein preparation at various stages of the purification as follows: 2 - crude cell free extract, 3 - after heat shock, 4 - after ion exchange chromatography, 5 - after hydrophobic interaction chromatography, 6 - after final dialysis.*

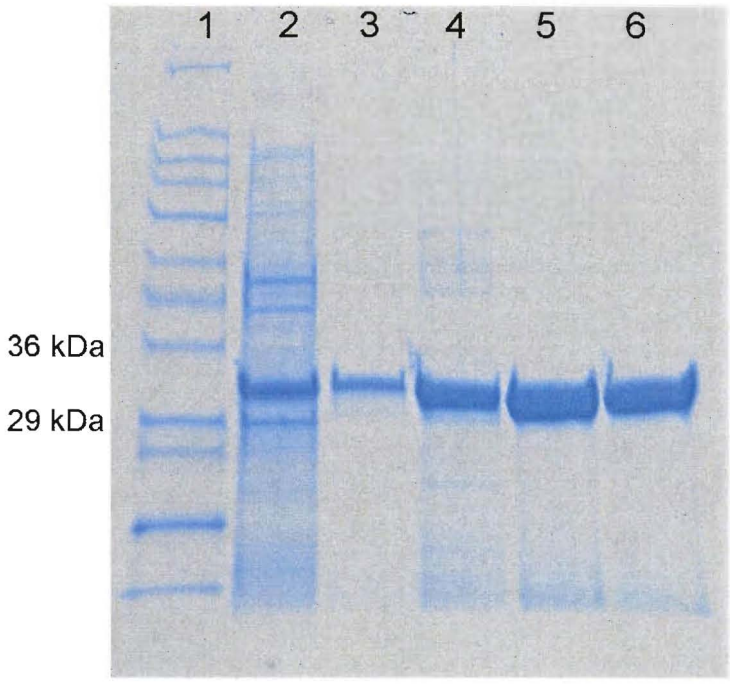

This protocol resulted in homogenous wild-type DHDPS, as judged by SDS-PAGE with Coomasie blue staining (Figure 3.5), with a specific activity of 1.89 units/mg, (1 unit is equal to the consumption of 1 µmol of NADPH per second) as judged by the coupled assay (section 5.2.3). Greater than four-fold purification of the enzyme was routinely achieved with a total yield of DHDPS activity of around 60% (Table 3.2).

The results presented in Table 3.2 show that around 14% of the total protein contained in the cell lysate obtained by this method was DHDPS, demonstrating the efficiency of this overexpression system for this enzyme.

The purified protein solution was aliquotted and stored at -20°C. Under these conditions, wild-type DHDPS was found to show no detectable loss of activity over 3 months.

3.3.3 Purification of DHDPR

The purification of DHDPR was achieved using a protocol that was loosely based on previously published reports (9,11,12). Significant modifications to these procedures were made, introducing an affinity chromatography step and eliminating a time-consuming ammonium sulfate fractionation, in order to streamline the purification and increase the purity of the final product.

Figure 3.6 *SDS-PAGE of a typical DHDPR preparation. Lanes 1 and 7 show molecular weight marker with relevant bands indicated. Lanes 2-6 were loaded with the protein preparation at various stages of the purification as follows: 2 - crude cell free extract, 3 - after heat shock, 4 - after ion exchange chromatography, 5 - after dialysis, 6 - after blue-Sepharose affinity chromatography and final dialysis.*

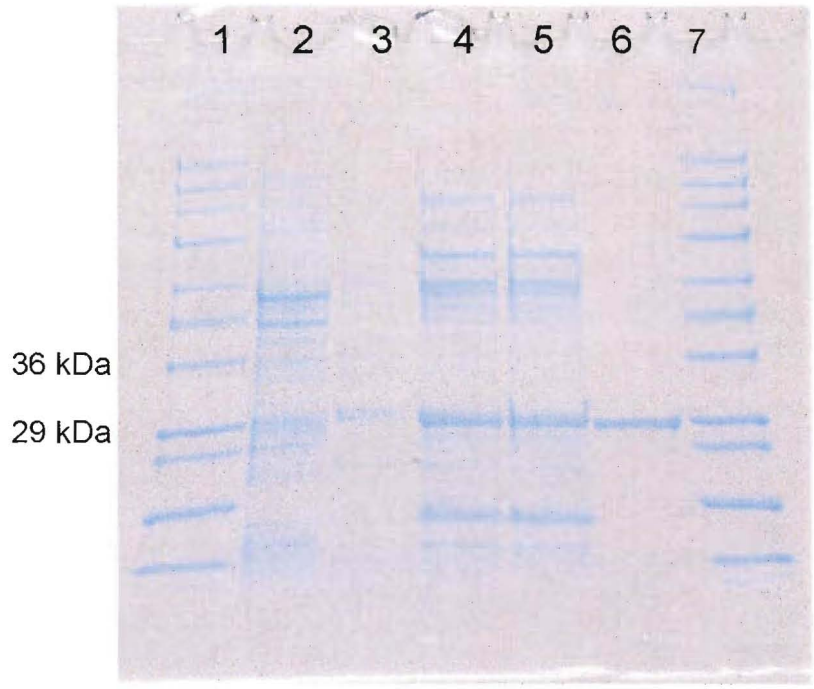

Like DHDPS, DHDPR displays unusually high stability against thermal denaturation (13), allowing initial reduction of background protein contaminants in crude extracts

from XL-1-Blue-pJK001 by heat shock at 70°C. Charge-based separation of the remaining soluble components of the crude extract was then carried out on a Q Sepharose column, as for DHDPS. Active fractions from the ion exchange chromatography were detected using the coupled assay for DHDPR activity, pooled, and dialysed. SDS-PAGE of the pooled ion exchange fractions revealed a major protein component of around 29 kDa, corresponding to the monomeric molecular weight of DHDPR (Figure 3.6). However, significant background contamination still remained, and thus, a further, highly selective, separation technique was needed.

Table 3.3 *Typical purification of wild-type DHDPR from* E. coli *XL-1-pJK001 from 17 g wet-weight of cells (4.5 L of culture).*

	Protein (mg)	Total activity[a] (units[b])	Specific activity (units/mg)	Yield (%)	Degree of purification (fold)
Crude extract	748.6	58.0	0.08	-	-
Heat shock	111.6	43.3	0.39	74.70	5.01
Ion exchange	57.7	48.9	0.85	84.26	10.93
Blue-Sepharose	12.5	46.0	3.67	79.39	47.30

[a] Activity was determined using the quantitative coupled assay.
[b] 1 unit is defined as the consumption of 1 µmol NADPH per sec.

As DHDPR can utilise both NADH and NADPH as cofactors (11,12), a purification step based on the affinity of the enzyme for these molecules was employed. The Cibacron Blue dye attached to the chromatography matrix Blue Sepharose (GE Biosciences) has structural similarities to nucleotide cofactors and thus will specifically bind to enzymes that utilise these molecules. Thus, purification of DHDPR was completed by loading a 5 ml bed volume column of Blue Sepharose with a quantity of the pooled dialysed ion exchange fractions. Elution of the column with 1 M NaCl, after washing, produced homogenous DHDPR, as judged by SDS-PAGE with Coomasie Blue staining (Figure 3.6), while concentrating the sample considerably. After dialysis, the pooled affinity chromatography fractions displayed a specific activity of 3.67 units/mg reflecting a 47.4-fold purification (Table 3.3). This is a higher specific activity than that reported previously (12) indicating that improved purity was achieved due to the affinity chromatography step.

Importantly, preparations of DHDPR produced in this manner did not consume NADPH in the presence of the substrates of the DHDPS reaction, indicating that chromosomally-derived wild-type DHDPS was not present in the final product of this purification.

3.4 Overexpression and purification of DHDPS variants

Accurate analysis of the DHDPS variants required preparations of these proteins that were free of wild-type DHDPS derived from the chromosome of the expressing organism, since its presence would be detected in biochemical measurements. For this reason, a strain of *E. coli* that contains a non-functional chromosomal *dap*A gene was selected for overexpression of the DHDPS mutants. *E. coli* strain AT997 (14) has been characterised as *dap*A$^-$ (15) and can be grown and maintained only on media supplemented with DAP. As the nature of the mutation producing the *dap*A$^-$ phenotype is unknown, a *dap*A$^-$ *rec*A$^-$ strain, designated AT997r$^-$, has been created to ensure that plasmid-borne *dap*A sequences are unable to recombine with the chromosome, which may potentially cause reversion of the chromosomal mutation (16).

3.4.1 Transformation of AT997r$^-$ with the mutated plasmids

Each mutated plasmid was prepared from the appropriate *E. coli* XL-1 Blue strain from the mutagenesis experiment. Transformation of AT997r$^-$ with each of these plasmids was attempted by standard electroporation and chemical ($CaCl_2$) methods (6). However, control transformations performed with these experiments, which contained no plasmid DNA, indicated that the *dap*A$^-$ phenotype was reverting in a very small proportion (<0.1%) of cells, resulting in colonies growing on the unsupplemented media. These were confirmed as revertants by subculturing on media with and without DAP, and repetition of the procedure produced identical results consistently. Despite the fact that this reversion rate was very low, the implication that the same rate of reversion may have occurred in the cells transformed with plasmid DNA was clear and there was no easy way by which to confirm the chromosomal genotype once the transformation has been carried out.

Verification of the phenotype of competent cells at all steps of the transformation protocols revealed that revertants only appeared after the electroporation step or the

heat-shock step of the respective procedures. These findings are consistent with the suggestion of Yeh *et al.* that the *dap*A mutation present in this strain may be temperature sensitive (15). Thus, the $CaCl_2$ transformation protocol was modified to allow omission of the heat-shock step.

Transformation of AT997r⁻ by the $CaCl_2$ method

The main purpose of the standard 42°C heat shock step employed during transformation of $CaCl_2$ competent cells is to destroy endogenous nucleases, thereby reducing breakdown of the introduced DNA and increasing transformation efficiency (Mahanty, H. K. *pers comm.*). Parameters for the transformation of AT997r⁻ were optimised in order to achieve satisfactory transformation efficiency using $CaCl_2$ competent cells, while omitting the heat-shock step.

Extending the incubation of prepared AT997r⁻ competent cells in 100 mM $CaCl_2$ produced a steady increase in transformation efficiency over a period of approximately 5 hours, followed by a steep reduction in transformation efficiency. Likewise, extension of the period of incubation of cells with plasmid DNA resulted in an increase, followed by a decline in transformation efficiency. Alteration of these incubation times allowed successful transformation of AT997r⁻ with up to 30% efficiency. No evidence of reversion was seen in control transformations performed in parallel with all transformation experiments.

All DHDPS variants were overexpressed in AT997r⁻ containing the appropriate plasmid in the same manner as wild type DHDPS and DHDPR (section 3.3.1).

3.4.2 Method development for the purification of the DHDPS-L197D

The first step of a protein purification protocol generally involves a straightforward process by which the bulk impurities of a crude sample are removed from solution while retaining as much of the target protein as possible. In the case of wild-type DHDPS, this is a heat-shock step that is followed by removal of precipitated proteins. As the physical properties of the variant forms of DHDPS were likely to be altered from those of the wild-type enzyme, it was necessary to assess a number of different initial capture methods. As the L197D variant was the first produced during this study, the method employed for the purification of the quaternary structural mutants was based on initial work on this enzyme.

Heat-shock of AT997r⁻-pL197D lysate

Samples of crude cell free lysate from AT997r⁻-pL197D were initially subjected to heat shock at 70°C for one, two, and three minute periods. Measurements performed on the resulting protein samples showed that after only one minute DHDPS activity had been reduced to less than 50% of that of the crude untreated sample, indicating that DHDPS-L197D was being denatured or digested by proteases. Given that an incubation period of two minutes is required to remove significant levels of background protein contaminants, this heat-shock capture method was clearly unsuitable for the purification of DHDPS-L197D. This result was interesting, however, as it suggested that DHDPS-L197D was less heat resistant than wild-type DHDPS presumably due to the altered quarternary structure.

Freeze thawing of AT997r⁻-pL197D cells

Freeze thaw cycling of harvested AT997r⁻-pL197D cells, allowing semi-selective release of cellular proteins, was also trialled as a method of target protein capture. Seven over night freeze thaw cycles were performed, as in reported methods (5,8,9). This approach was discarded as the step is highly time consuming and the yield of target protein activity was far lower than that of whole cell lysates, with little increase in specific DHDPS activity.

Ammonium sulfate fractionation of AT997r⁻-pL197D lysate

Ammonium sulfate precipitation of protein fractions is commonly used as a first purification step and has been employed in reported purifications of DHDPS (17). High concentrations of ammonium sulfate facilitate the precipitation of less soluble protein fractions without denaturation (18). As various proteins will precipitate at different concentrations of the salt, a range of ammonium sulfate concentrations can be found within which the target protein can be selectively precipitated and collected.

This range was determined for DHDPS-L197D by small scale precipitation experiments. Ammonium sulfate concentrations between 20% w/v and 50% w/v were added to small aliquots of cell-free AT997r⁻-pL197D lysate, and incubated at 4°C. Precipitated proteins were then pelleted and redisolved in buffer before being assayed for DHDPS activity. Figure 3.7 shows that the majority of the DHDPS-L197D in solution precipitates within the range of 30 to 40% w/v ammonium sulfate.

Figure 3.7 *DHDPS activity recovered from the precipitated fraction of a crude cell free preparation of DHDPS-L197D over a range of ammonium sulfate concentrations.*

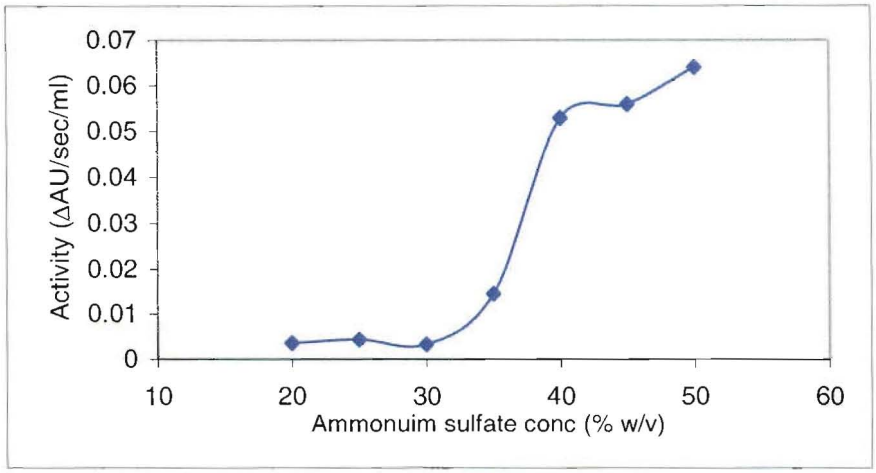

Based on these data, a trial preparative scale fractionation protocol was devised to allow the recovery of proteins precipitating between 30 to 40% w/v ammonium sulfate. Cell free lysate from AT997r⁻-pL197D was brought to 30% w/v ammonium sulfate by incremental addition of solid ammonium sulfate and incubated with mixing. Precipitated proteins were removed and discarded before addition of a further 10% w/v ammonium sulfate to the remaining solution. Recovered precipitated proteins at this stage were redissolved in buffer and dialysed before further purification. By this method, a two-fold enrichment of the target protein, at high yield, could routinely be achieved.

Further purification

From this point, purification of DHDPS-L197D proceeded in a similar fashion to that of wild-type DHDPS. Minor modifications to ion exchange and hydrophobic interaction chromatography procedures were necessary to allow for differences in loading and elution behaviour observed in the mutant (section 8.4).

3.4.3 Circular dichroism spectroscopy

The secondary structures of wild-type DHDPS and the DHDPS-L197D were compared in solution by circular dichroism (CD) spectroscopy. The CD spectrum of *E. coli* DHDPS has not previously been reported. Figure 3.8 shows that the CD spectra of wild-type DHDPS and DHDPS-L197D are almost identical, demonstrating that DHDPS-L197D is fully folded in solution. Both spectra are comprised of a

double minima at approximately 208 nm and 222 nm, which is characteristic of predominantly α-helical structure.

Figure 3.8 *Circular dichroism spectroscopy of wild-type DHDPS (●) and DHDPS-L197D (○).Mean residue elipticity ([θ]) is plotted as a function of wavelength.*

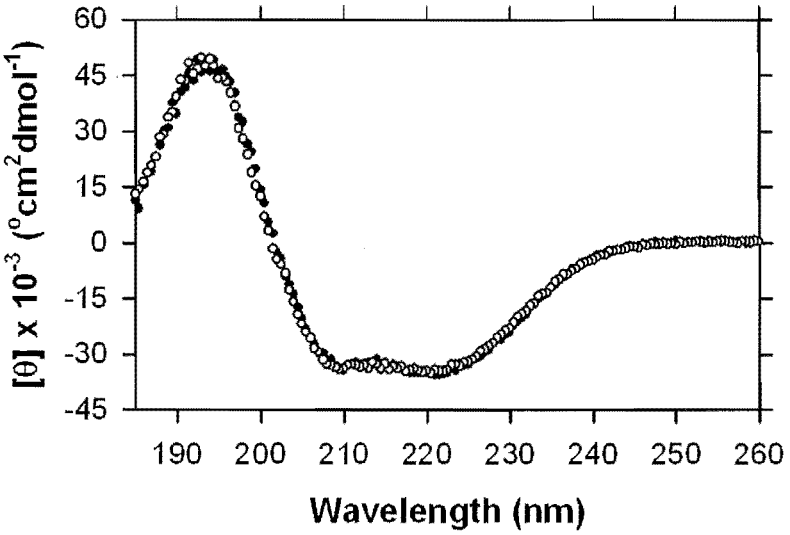

3.4.4 Purification of DHDPS variants

The purification of all DHDPS variants was based on the protocol devised for DHDPS-L197D (section 3.4.2). Only small alterations were necessary when applying this procedure to other DHDPS variants to allow for differences in physical behaviour, and these were largely made on an empirical basis. Final specific activities of all variants reflected significant enrichment of target proteins from the cell lysates (Table 3.4) and all preparations were judged to be homogenous by SDS-PAGE with Coomasie blue staining (Figure 3.9).

Table 3.4 *Typical purifications of the DHDPS variants from 4.5 L of cell culture.*

	Protein (mg)	Total activity[a] (units[b])	Specific activity (units/mg[b])	Yield (%)	Degree of purification (fold)
DHDPS-L197D					
Crude extract	1038.3	10.3	0.010	-	-
$(NH_4)_2SO_4$ fractionation	448.45	8.9	0.020	85.8	1.99
Ion exchange	276.61	6.2	0.022	60.0	2.25
Hydrophobic interaction	41.78	1.5	0.036	14.4	3.58
DHDPS-L197Y					
Crude extract	541.5	7.0	0.013	-	-
$(NH_4)_2SO_4$ fractionation	221.3	4.3	0.019	60.9	1.49
Ion exchange	105.3	3.4	0.032	48.0	2.47
Hydrophobic interaction	28.4	1.8	0.063	25.7	4.91
DHDPS-Q196D					
Crude extract	829.8	25.911	0.031	-	-
$(NH_4)_2SO_4$ fractionation	363.6	18.572	0.051	71.6	1.64
Ion exchange	136.3	12.374	0.091	47.7	2.91
Hydrophobic interaction	48.6	12.269	0.252	47.3	8.08
DHDPS-D193A					
Crude extract	756.9	16.50	0.022	-	-
$(NH_4)_2SO_4$ fractionation	126.6	14.54	0.115	88.1	5.27
Ion exchange	139.3	10.45	0.075	63.3	3.44
Hydrophobic interaction	70.2	11.96	0.170	72.5	7.81
DHDPS-D193Y					
Crude extract	777.9	25.89	0.033	-	-
$(NH_4)_2SO_4$ fractionation	300.0	21.88	0.073	84.5	2.19
Ion exchange	170.3	18.25	0.107	70.5	3.22
Hydrophobic interaction	68.3	15.65	0.229	60.5	6.89

[a] Activity was determined using the quantitative coupled assay.
[b] 1 unit is defined as the consumption of 1 μmol NADPH per sec.

Figure 3.3 *contd.*

	Protein (mg)	Total activity[a] (units[b])	Specific activity (units/mg)	Yield (%)	Degree of purification (fold)
DHDPS-Q234D					
Crude extract	803.8	27.99	0.035	-	-
$(NH_4)_2SO_4$ fractionation	295.5	17.55	0.059	62.7	1.71
Ion exchange	197.6	13.49	0.068	48.2	1.96
Hydrophobic interaction	28.8	8.83	0.306	31.5	8.80

[a] Activity was determined using the quantitative coupled assay.
[b] 1 unit is defined as the consumption of 1 µmol NADPH per sec.

Figure 3.9 *SDS-PAGE of the pure preparations of the DHDPS variants. Lanes are as follows: 1 - DHDPS-L197D, 2 - DHDPS-L197Y, 3 - DHDPS-Q196D, 4 - DHDPS-D193A, 5 - DHDPS-D193Y, 6 - DHDPS-Q234D.*

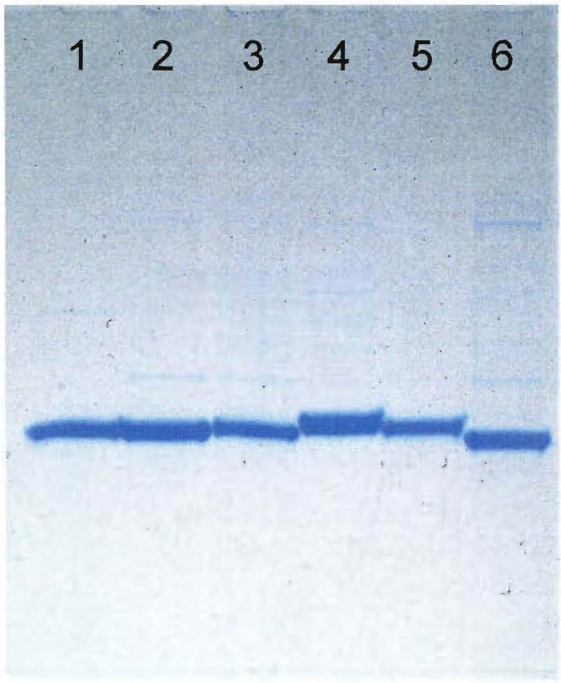

3.5 Synthesis of (*S*)-ASA

Preparations of (*S*)-ASA of sufficient purity and quantity were required for the detailed kinetic characterisation of DHDPS and its variants (Chapter five), and for semi-qualitative activity assays during enzyme purification and preliminary analysis.

(*S*)-ASA utilised in the kinetic characterisation of DHDPS and its variants for this study was synthesised from aspartate by a procedure developed in this lab.

3.5.1 Syntheses of (*S*)-ASA from allylglycine

(*S*)-ASA syntheses published before the outset of this work were generally derived from the original report (19) in which the carbonyl functionality is produced *via* oxidative cleavage of the double bond of (*S*)-allylglycine by ozonolysis in acid (Figure 3.10). Due to its simplicity, this single step synthesis has historically been the method of choice for production of (*S*)-ASA for kinetic characterisation of DHDPS (12,20). However, ozonolysis of allylglycine has been found to result in (*S*)-ASA of variable purity (5,21,22) as the reaction can generate a number of different products that have proven difficult to remove from the preparation (21,22). Furthermore, studies in this lab have shown that (*S*)-ASA produced in this way is unsuitable for accurate characterisation of DHDPS, as an unidentified side product of the preparation produces artefactual substrate inhibition kinetic behaviour (23).

Figure 3.10 *Synthesis of (S)-ASA by ozonolysis of allylglycine (19).*

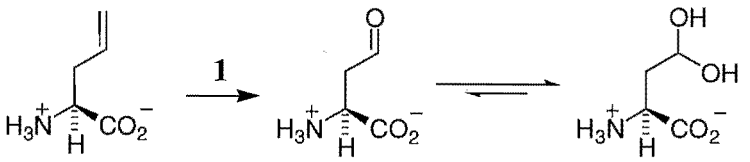

(*S*)-Allylglycine (*S*)-Aspartate-β-semialdehyde

Reaction conditions: **1** ozone, 1 M HCl.

Like many aminoaldehydes, (*S*)-ASA displays a strong tendency to polymerise in solution, and is stable only in strong acid, introducing added difficulty to the synthesis of this molecule (22,24). Thus, the production of (*S*)-ASA from α-amine- and α-carboxyl-protected derivatives of allylglycine by ozonolysis (22) and other methods (5,8,21) have been explored. The oxidation of the double bond of diprotected allylglycine using catalytic osmium tetroxide and sodium periodate was first proposed by Gerrard (5). This oxidation reaction cannot proceed past the aldehyde, eliminating many of the side products of the ozonlysis reaction, and producing product of suitable quality for kinetic characterisation of DHDPS. (*S*)-ASA synthesised by this method

has, therefore, routinely been used in this lab in the past. However, the high cost of allylglycine in both enantiopure and racemic forms, coupled with the relatively low yield and time consuming nature of the synthesis, has lead to development of a novel three step synthesis from diprotected aspartate.

3.5.2 Synthesis of (*S*)-ASA *via* Weinreb amide activation of aspartate

(*S*)-ASA for this study was produced from aspartate by selective reduction of the side chain carboxyl to generate the aldehyde moiety (1) (Figure 3.11). Selective activation of the side chain for reduction can be achieved by generation of either a thioester derivative (25) or a Weinreb amide (26) and requires prior protection of the α-carboxyl group. As synthesis *via* the Weinreb amide is less time consuming and results in a higher product yield (1), this method has been adopted here. The diprotected aspartate derivative α-*tert*-butyl (*S*)-N-*tert*-butoxycarbonyl aspartate was chosen as starting material for synthesis as this derivative incorporates acid labile protecting groups, is commercially available, and is substantially less expensive than allylglycine.

Weinreb amide activation

α-*tert*-Butyl (*S*)-N-*tert*-butoxycarbonyl aspartate was converted to the corresponding *N*-methoxy-*N*-methylamide (Weinreb amide) in a reaction involving (benzotriazol-1-yloxy)-tris(dimethyl-amino)phosphonium hexafluorophosphate ($BOP.PF_6$), triethylamine and N,O-dimethylhydroxylamine hydrochloride (step 1). The yield of the reaction after purification of the product by flash chromatography was routinely around 90%. The aldehyde was generated by reduction of the Weinreb amide using diisobutyl aluminium hydride at -78°C (step 2). This reaction produced diprotected (*S*)-ASA in quantitative yield, which required no further purification before deprotection.

Figure 3.11 *Synthesis of (S)-ASA from α-tert butyl (S)-N-tert-butoxycarbonyl aspartate* via *Weinreb amide activation of the side chain carboxyl (1).*

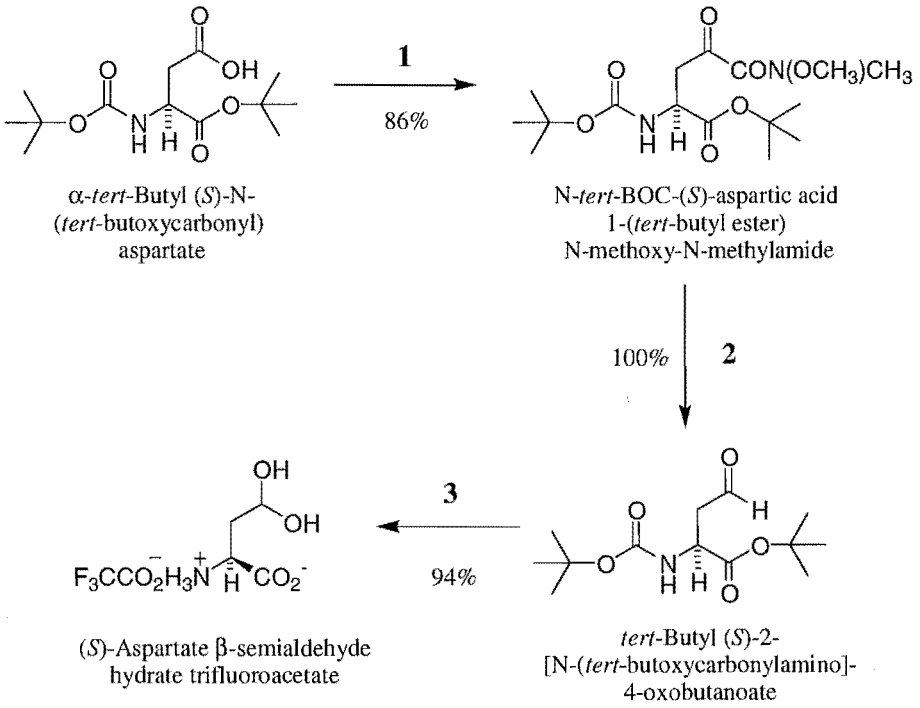

Reaction conditions: **1**, Et_3N, $BOP.PF_6$; **2**, DIBAL, THF, -78°C; **3**, CF_3CO_2H, DCM

Deprotection of (S)-ASA

The method of Tudor *et al.* (22) was used to deprotect the aldehyde, by stirring in trifluoroacetic acid and dry dichloromethane (step 3). (*S*)-ASA was isolated as the hydrated trifluoroacetate salt, a pale yellow solid, in approximately 94% yield. The purity of the final product, as estimated by titration using the DHDPS coupled assay (section 8.9.4), was excellent at around 95-99%. This three step procedure provided an efficient, high yielding route to (*S*)-ASA of excellent quality, while eliminating the use of the poisonous reducing agent osmium tetroxide.

3.6 Summary

The single point mutations described in Chapter two were produced by site-directed mutagenesis of the *dap*A gene contained on the plasmid pJG001, and the correct mutations were confirmed by restriction digest and sequencing. The mutated plasmids were transformed into the *dap*A- *E. coli* strain, AT997r$^-$, to allow overexpresison of

the variant enzymes in the absence of wild-type DHDPS. Wild-type DHDPS, DHDPR, and the DHDPS variants were successfully overexpressed and purified to homogeneity using both previously described methods and methods developed in this work.

Synthesis of the substrate, (*S*)-ASA, was achieved with an overall yield of 81% using an improved synthesis developed in this lab. This method produced highly pure product, at 95-99%.

3.7 References

1. Roberts, S. J., Morris, J. C., Dobson, R. C., and Gerrard, J. A. (2003) The preparation of (*S*)-aspartate semi-aldehyde appropriate for use in biochemical studies. *Bioorg Med Chem Lett* **13**, 265-267
2. Ling, M. M., and Robinson, B. H. (1997) Approaches to DNA mutagenesis: an overview. *Anal Biochem* **254**, 157-178
3. Kunkel, T. A. (1985) Rapid and efficient site-specific mutagenesis without phenotypic selection. *Proc Natl Acad Sci, U S A* **82**, 488-492
4. Stratagene. (1998) *QuikChange site-directed mutagenesis kit: instruction manual*
5. Gerrard, J. A. (1992) Studies on dihydrodipicolinate synthase. *D. Phil. thesis*, Oxford University
6. Maniatis, T., Fritsch, E., and Sanbrook, J. (1990) *Molecular cloning: a laboratory manual*, 2nd Ed., Cold Spring Harbor Press, Cold Spring Harbor, New York
7. Kraunsoe, J. A. E. (1992) Studies in lysine biosynthesis. BSc. Hons. Part II, Oxford University
8. Coulter, C. V. (1997) Studies in lysine biosynthesis. *PhD thesis*, University of Canterbury
9. Coulter, C. V., Gerrard, J. A., Kraunsoe, J. A. E., and Pratt, A. J. (1999) *Escherichia coli* dihydrodipicolinate synthase and dihydrodipicolinate reductase: Kinetic and inhibition studies of two putative herbicide targets. *Pestic Sci* **55**, 887-895
10. Mirwaldt, C., Korndorfer, I., and Huber, R. (1995) The crystal structure of dihydrodipicolinate synthase from *Escherichia coli* at 2.5 Å resolution. *J Mol Biol* **246**, 227-239
11. Tamir, H., and Gilvarg, C. (1974) Dihydrodipicolinic acid reductase. *J Biol Chem* **249**, 3034-3040
12. Reddy, S. G., Sacchettini, J. C., and Blanchard, J. S. (1995) Expression, purification, and characterization of *Escherichia coli* dihydrodipicolinate reductase. *Biochemistry* **34**, 3492-3501

13. Farkas, W., and Gilvarg, C. (1965) The reduction step in diaminopimelic acid biosynthesis. *J Biol Chem* **240**, 4717-4722

14. Bukhari, A. I., and Taylor, A. L. (1971) Genetic analysis of diaminopimelic acid- and lysine-requiring mutants of *Escherichia coli*. *J Bacteriol* **105**, 844-854

15. Yeh, P., Sicard, A. M., and Sinskey, A. J. (1988) General organization of the genes specifically involved in the diaminopimelate-lysine biosynthetic pathway of *Corynebacterium glutamicum*. *Mol Gen Genet* **212**, 105-111

16. Dobson, R. C., Valegard, K., and Gerrard, J. A. (2004) The crystal structure of three site-directed mutants of *Escherichia coli* dihydrodipicolinate synthase: Further evidence for a catalytic triad. *J Mol Biol* **338**, 329-339

17. Shedlarski, J. G., and Gilvarg, C. (1970) The pyruvate-aspartic semialdehyde condensing enzyme of *Escherichia coli*. *J Biol Chem* **245**, 1362-1373

18. Grover, P., and Ryall, R. L. (2004) Critical appraisal of salting-out and its implications for chemical and biological sciences. *Chem Rev* **105**, 1-10

19. Black, S., and Wright, N. G. (1955) Aspartic β-semialdehyde dehydrogenase and aspartic β-semialdehyde. *J Biol Chem* **213**, 39-50

20. Karsten, W. E. (1997) Dihydrodipicolinate synthase from *Escherichia coli*: pH dependent changes in the kinetic mechanism and kinetic mechanism of allosteric inhibition by L-lysine. *Biochemistry* **36**, 1730-1739

21. Coulter, C. V., Gerrard, J. A., Kraunsoe, J. A. E., Moore, D. J., and Pratt, A. J. (1996) (*S*)-Aspartate semi-aldehyde: Synthetic and structural studies. *Tetrahedron* **52**, 7127-7136

22. Tudor, D. W., Lewis, T., and Robins, D. J. (1993) Synthesis of the trifluoroacetate salt of aspartic-acid β-semialdehyde, an intermediate in the biosynthesis of *L*-lysine, *L*-threonine, and *L*-methionine. *Synthesis* **11**, 1061-1062

23. Dobson, R. C., Gerrard, J. A., and Pearce, F. G. (2004) Dihydrodipicolinate synthase is not inhibited by its substrate, (*S*)-aspartate β-semialdehyde. *Biochem J* **377**, 757-762

24. Meffre, P. (1999) Syntheses of optically active 2-amino-4-oxobutyric acid and *N*,*O*-protected derivatives. *Amino Acids* **16**, 251-272

25. Bergmeier, S. C., Cobas, A. A., and Rapoport, H. (1993) Chirospecific synthesis of (1*S*,3*R*)-1-amino-3-(hydroxymethyl) cyclopentane, precursor for carbocyclic nucleoside synthesis - dieckmann cyclization with an α-amino acid. *J Org Chem* **58**, 2369-2376

26. Wernic, D., Dimaio, J., and Adams, J. (1989) Enantiospecific synthesis of *L*-α-aminosuberic acid: Synthetic applications in preparation of atrial natriuretic factor analogs. *J Org Chem* **54**, 4224-4228

Chapter Four

Biophysical characterisation of wild-type DHDPS and the variants.

4.1 Introduction

After production and purification of sufficient quantities of *E. coli* DHDPS and the DHDPS variants, a rigorous biophysical characterisation was undertaken to ascertain the quaternary structure of the enzymes. For this, three complementary techniques were employed.

In the first instance, blue-native PAGE (BN-PAGE) was used to provide a preliminary indication of the quaternary structure of each variant. This is a relatively simple native protein electrophoresis technique that offers reasonable size resolution and thus allows qualitative and semi-quantitative analysis of the size of oligomeric structures. Analytical gel permeation liquid chromatography, a more precise treatment, was also employed for estimation of the molecular weights of wild-type DHDPS and the variants.

The quaternary structure and solution properties of the DHDPS variants were also characterised by analytical ultracentrifugation. Both sedimentation velocity and sedimentation equilibrium experiments were carried out, allowing accurate measurement of the sedimentation coefficient, shape, and molecular weights of the proteins in aqueous solution, and also analysis of structural dynamics.

4.2 Blue-native PAGE

BN-PAGE (1-3) was utilised as an initial determinant of the quaternary structure of the variants with respect to the wild-type enzyme. This is a non-denaturing electrophoretic technique that separates proteins by size in their native state.

BN-PAGE differs from standard native PAGE in that it is based on a charge-shift principle whereby the anionic dye, Coomassie blue G-250, is complexed with the

proteins of interest, imparting a uniform negative charge to the surface of the molecules without disrupting their structural integrity. The binding of a large number of negatively charged dye molecules to the surface shifts the isoelectric point of the proteins to more negative values and as a result, the Coomassie blue-protein complex will migrate towards the anode upon electrophoresis at mildly basic pH, irrespective of the original isoelectric point of the free protein (3).

The electrophoretic mobility of the proteins under this technique is therefore mainly determined by the charge-shift imparted by the dye, which is largely proportional to the size of the protein molecule (1). However, the primary separating principle of BN-PAGE is not the charge/mass ratio, but the decreasing pore size of the polyacrylamide-gradient gel used. The gradient gel effectively reduces the protein migration velocity during the process of electrophoresis, according to the mass of the protein, and can completely stop protein migration at a mass-specific pore-size limit (3).

Under this electrophoretic system, size resolution is obviously dependent on factors such as the shape and physical properties of the protein of interest. Nevertheless, reasonable size resolution of a range of different sorts of proteins can be achieved using this technique (2). An added effect of the charge-shift system is that dye associated proteins will repel each other, and thus the tendency for aggregation of the proteins during native electrophoresis is greatly reduced (3).

4.2.1 Modified BN-PAGE used in this study

BN-PAGE was originally developed as a means for isolation of membrane protein complexes (1,4) and published protocols have employed complex measures to ensure that proteins remain soluble during preparation and throughout the procedure (3). Since all proteins investigated in this study were water soluble, it was possible to alter the protocol, omitting the addition of costly detergents from the sample-treatment and running buffers. Trial electophoresis experiments were then performed in order to ascertain appropriate running conditions for the modified protocol. Bovine serum albumin (BSA) was routinely used as a molecular weight marker in BN-PAGE experiments performed for this study. The slow equilibrium between the BSA monomer and dimer in solution allows resolution of these species by this technique, affording semi-quantitative analysis of unknown molecular weights.

BN-PAGE was performed by treating protein samples with treatment buffer containing a high concentration of Coomassie blue G-250. Samples were then electrophoresed at 200 V on a 4-15% polyacrylamide gel with cathode buffer containing Coomassie blue G-250 to ensure constant dye-protein association. Under this system Coomassie blue dye is permeated into the gel during electrophoresis and thus subsequent staining was not required. Gels were developed by fixing and destaining.

4.2.2 BN-PAGE of wild-type DHDPS and the variants

BN-PAGE provided the first evidence that the two variants DHDPS-L197D and DHDPS-L197Y existed as stable dimers in solution. Both variants reproducibly produced a single stained band of higher electrophoretic mobility under BN-PAGE than that of wild-type DHDPS (Figure 4.1).

Figure 4.1 *BN-PAGE of wild-type DHDPS, DHDPS-L197D and DHDPS-L197Y. Lane 1 was loaded with wild-type DHDPS at a concentration of 0.5 mg/ml. Lane 2 was loaded with DHDPS-L197D at a concentration of 0.5 mg/ml. Lane 3 was loaded with DHDPS-L197D at a concentration of 0.3 mg/ml. Lane 4 was loaded with DHDPS-L197Y at a concentration of 0.5 mg/ml. Lane 5 shows two major zones of staining corresponding to the BSA monomer and dimer (molecular weights marked).*

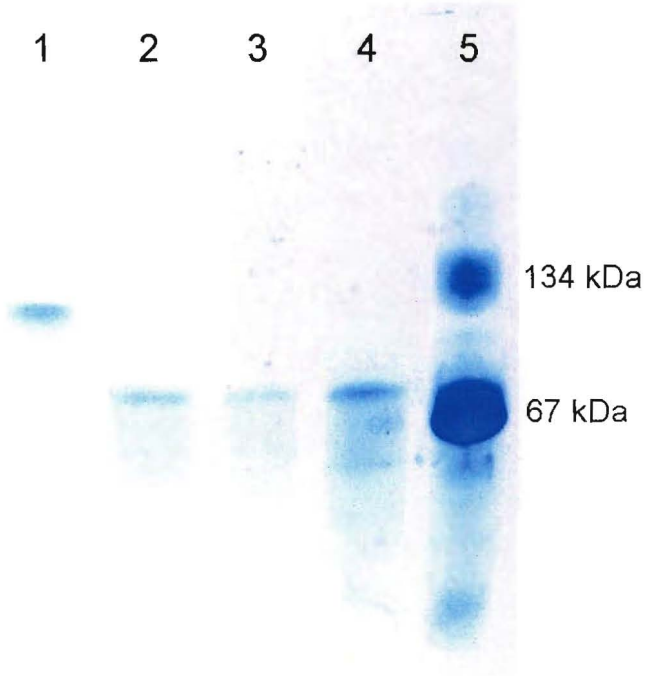

The single band observed for wild-type DHDPS under BN-PAGE shows slightly higher electrophoretic mobility than the 134 kDa marker, consistent with the expected

tetrameric molecular weight of 125 kDa. In contrast, the band observed for DHDPS-L197D and DHDPS-L197Y agrees reasonably well with the 67 kDa marker, consitent with the molecular weight of the dimer. Varying the loading concentration of DHDPS-L197D (Figure 4.1 lanes 2 and 3) and DHDPS-L197Y did not result in altered eletrophoretic behaviour or resolution of multiple bands. This indicated that under the conditions of this technique, the observed shift in quaternary structure was not concentration dependent.

DHDPS-Q196D, DHDPS-D193A, DHDPS-D193Y, and DHDPS-Q234D displayed essentially identical electrophoretic mobility to wild-type DHDPS under BN-PAGE, suggesting that these variants electorphoresed as tetramers. Variation of loading concentrations for these variants did not alter the observed electrophoretic behaviour.

4.3 Analytical gel permeation liquid chromatography

Gel permeation liquid chromatography provides a simple and effective means for the characterisation and size estimation of macromolecules (5-11). This is a well established technique that has been progressively developed in terms of materials, theory, and practice, since its inception over 45 years ago (12). The major analytical application of gel chromatography has been the estimation of solute molecular weights from the elution volume, V_e, and modern analytical gel permeation liquid chromatography is generally performed by one of two methods for the determination of V_e: frontal analysis or zonal analysis.

4.3.1 Frontal analysis

Frontal, also known as large zone analysis, (10,11) involves applying sufficient volume of solute solution to the column to ensure that the elution profile contains a plateaux region where the effluent solute concentration is equal to that of the applied solution. By this method, advancing and trailing fronts are produced by axial dispersion of the original zone boundary and V_e may be obtained as the centroid of either the advancing front or the trailing front. This technique is severely limited by the quantity of protein required for the procedure and for this reason has not been employed in this study.

4.3.2 Zonal analysis

Most analytical gel permeation liquid chromatography studies employ zonal analysis. This is the most familiar technique where a small zone of solute, typically less than 2% of the bed volume, is applied to a gel column previously equilibrated with buffer (8). Axial dispersion during migration on the gel causes dilution of the zone resulting in a smooth, curved peak, with an elution concentration considerably lower than that of the applied solution. Here, V_e is usually taken as the effluent volume corresponding to the peak, rather than the centroid, of the eluted zone (8). It is this method that has been employed to determine V_e in this study.

4.3.3 Protein molecular mass estimation

Molecular mass estimation of proteins by gel permeation liquid chromatography requires calibration of the gel column by determining elution volumes for an appropriate series of protein standards of known molecular size and shape characteristics. The measured V_e of the protein of interest can then be converted to an apparent molecular mass by means of a calibration plot (8).

Generally, the calibration plot comprises the dependence of V_e upon the log of the molecular mass of the protein. However, this representation of the data relies on the validity of two main assumptions. Firstly, the major parameter governing V_e is the Stokes' radius, that is, the radius of the equivalent hydrodynamic sphere (8). Molecular mass estimation by partition on a gel column, therefore, requires that the Stokes' radius is directly proportional to the molecular mass for the range of proteins studied. Secondly, the interpretation of V_e in terms of mass rather than the Stokes' radius implies constancy of the partial specific volume and the frictional ratio across the range of proteins investigated. Thus, the approximation breaks down in the case of proteins that lie well outside the typical values for these parameters, for example, glycoproteins.[†]

Fortunately, these assumptions are valid provided that the range of proteins used for calibration is chosen carefully and that the nature of the protein of interest is reasonably well known (8). Andrews (6,7) has reported a likely uncertainty of ± 10%

[†] Winzor (8) offers a succinct mathematical treatment of these assumptions.

in molecular mass estimates by this method, based on assumed normal gel permeation behaviour.

4.3.4 Molecular mass estimation of wild-type DHDPS and DHDPS-L197D by zonal analysis

Since early BN-PAGE experiments indicated that DHDPS-L197D was dimeric, analytical gel permeation liquid chromatography studies were conducted for wild-type DHDPS and DHDPS-L197D. A Sephadex G-200 superfine (GE Healthcare) column of approximately 175 ml bed volume was assembled and calibrated with yeast alcohol dehydrogenase (150 kDa), bovine serum albumin (67 kDa), ovalbumin (43 kDa), and ribonuclease A (13.7 kDa). These proteins were chosen as they have been shown to exhibit close to ideal elution behaviour on Sephadex columns (7). Each calibration standard was run in duplicate and chromatograms were produced by measurement of the absorbance at 280 nm as a function of elution volume. V_e was determined as the ordinate maximum of the eluted zone, which was generally symmetrical, and the average of the duplicate values was calculated.

Figure 4.2 *Analytical gel permeation liquid chromatography of wild-type DHDPS and DHDPS-L197D. The molecular masses of the calibration standards are indicated. Wild- type DHDPS and DHDPS-L197D are plotted as elution volume, V_e, against the natural log of their expected molecular masses of 125 kDa and 62.5 kDa respectively. r^2 for the four point calibration curve was 0.99.*

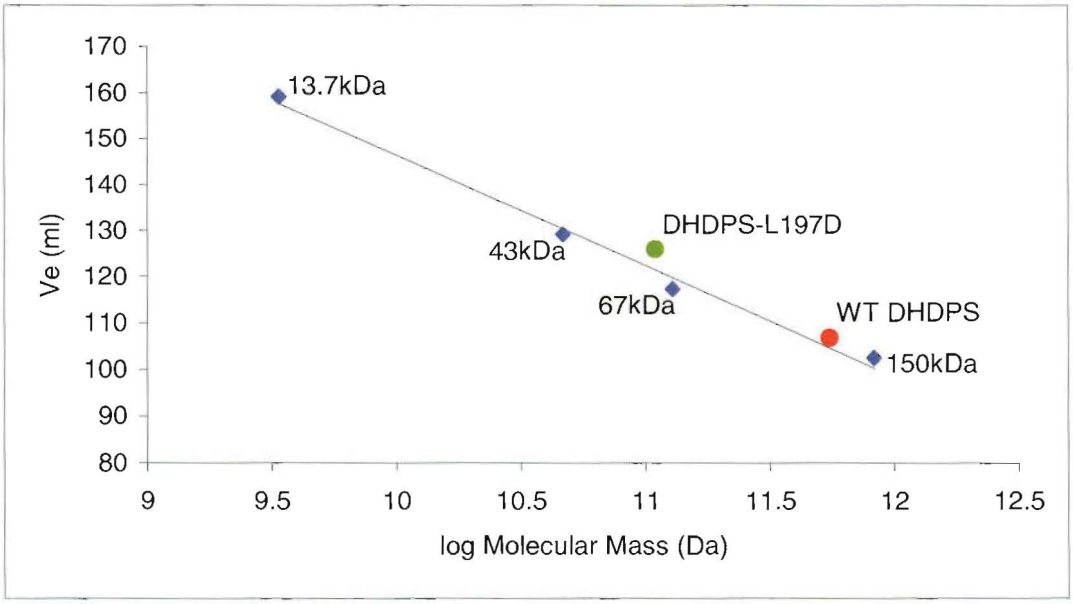

Wild-type DHDPS and DHDPS-L197D were chromatographed on the gel column in a similar way. Elution profiles were produced from DHDPS activity measurements using the coupled assay (section 5.2.3) in both cases and, again, V_e was determined as the ordinate maximum of the eluted zone. Figure 4.2 shows the calibration curve generated from the four point calibration. Wild-type DHDPS and DHDPS-L197D are plotted as elution volume, V_e, against the natural log of their expected molecular masses of 125 kDa and 62.5 kDa respectively. It is clear from the graph that neither protein follows the calibration curve exactly; however, there is a clear difference in V_e between the two, consistent with the predicted masses of the tetramer and dimer.

The relationship between V_e and molecular mass (M) was determined from the linear regression to the four point calibration curve and is shown in Equation 4.1. Molecular masses were calculated from the measured elution volumes using this equation.

$$M = e^{\left[\frac{V_e - 386.13}{23.975}\right]} \qquad \text{Equation 4.1}$$

The molecular mass of 114.8 kDa calculated for wild-type DHDPS is just within the 10% precision error of the expected molecular mass quoted by Andrews (6,7) and indicates that this protein may be displaying non-ideal behaviour on this column. Likewise, the value of 51.9 kDa calculated for DHDPS-L197D represents a 20% deviation from the expected molecular mass of the dimer. This deviation may be due to the shape of the dimer, since a long, thin, molecule might be expected to display altered elution behaviour. Alternatively, these deviations from expected values may be due to dissociation and re-association of the alternative oligomeric structures (8).

The shift in V_e between wild-type DHDPS and DHDPS-L197D, combined with the observation of a single, well formed elution zone for DHDPS-L197D, allow us to conclude that the L197D mutation has resulted in disruption of the dimer-dimer interface of DHDPS, producing a dimeric species.

4.3.5 Qualitative gel permeation liquid chromatography of wild-type DHDPS and the variants

Since quantitative molecular mass estimation by analytical gel permeation liquid chromatography on the Sephadex G-200 column required over 48 hours for each experiment, a faster qualitative system was employed for initial characterisation of the

remaining variants. The gel matrix of Sephacryl chromatography media is less compressible than that of the Sephadex media (8) and therefore tolerates much higher flow rates. Thus, a column of Sephacryl S-400 (GE Healthcare) was assembled and used for semi-qualitative analytical gel permeation liquid chromatography using wild-type DHDPS and DHDPS-L197D as reference measurements.

Each protein was chromatographed separately and chromatograms were produced by measurement of the absorbance at 280 nm as a function of elution volume. The absorbance profiles of the elution zone for each protein are shown in Figure 4.3.

Figure 4.3 *Zonal analysis of wild-type DHDPS and the variants.*

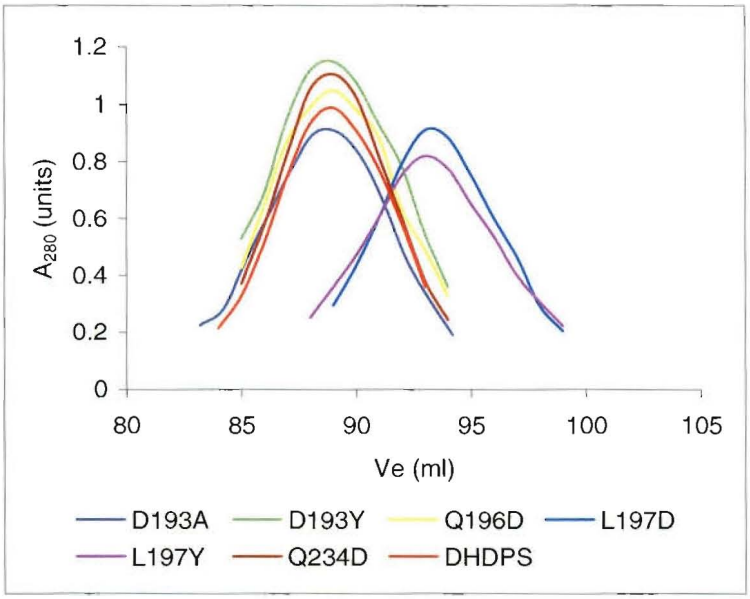

Elution volumes determined by zonal analysis for DHDPS-Q196D, DHDPS-D193A, DHDPS-D193Y, and DHDPS-Q234D, differed from that of wild-type DHDPS (88.5 ml) by less than 0.5 ml in all cases. This is in contrast to a shift in elution volume of 4.5 ml to approximately 93 ml for the DHDPS-L197D and DHDPS-L197Y variants. This result indicates that the DHDPS-L197D and DHDPS-L197Y variants display a significant shift in quaternary structure from that of wild-type DHDPS, consitent with that predicted for a dimeric form.

4.4 Analytical ultracentrifugation

Analytical ultracentrifugation is a powerful technique that can provide highly accurate hydrodynamic and thermodynamic information on macromolecules over a wide range of solvent conditions and solute concentrations (13). The technique can provide two complementary views of solution behaviour by employing different experimental protocols using the same instrumentation. Sedimentation velocity analysis primarily provides hydrodynamic information about the size and shape of a molecule. Sedimentation equilibrium analysis provides thermodynamic information including the solute molecular mass and association constants and stoichiometries (13).

Analytical ultracentrifugation experiments are generally carried out using the XL-A or XL-I ultracentrifuges. These instruments are equipped with complex scanning optics and transparent cells that allow direct measurement of the solute concentration profile during centrifugation. Unlike gel permeation liquid chromatography, data from analytical ultracentrifugation are obtained without solute interaction with a matrix, and are based on the mass and friction of the solute of interest, rather than the Stokes' radius (14). Thus, the technique provides a more direct method for determining the hydrodynamic and thermodynamic properties of macromolecules.

Analytical ultracentrifugation, using both the sedimentation velocity and sedimentation equilibrium techniques, was employed for the high resolution biophysical characterisation of wild-type DHDPS and the variants in this study.

4.4.1 Sedimentation velocity analytical ultracentrifugation

The application of a large centrifugal force to a solution of macromolecules results in the depletion of the solute at the meniscus and the formation of a boundary that moves toward the bottom of the solution column as a function of time (14). Diffusion causes the boundary to spread as it migrates, resulting in a solute concentration distribution around this boundary. The data measured in a sedimentation velocity experiment are, therefore, solute concentration profiles over the length of the cell in a radial direction. Sequential profile scans at defined time periods during centrifugation allow direct observation of the migration and development of this concentration boundary.

Data from a sedimentation velocity experiment can be analysed in a number of different ways (13,14). Most recently, a method for the production of a continuous sedimentation coefficient distribution has been developed (15,16). This analysis is based on the direct modelling of the boundary by a distribution of solutions of the Lamm equation. Mathematical methods for the determination of these solutions have been implemented in the program SEDFIT (15). Using this program, conversion of the continuous sedimentation coefficient distribution into a continuous molecular mass distribution is possible. However, this assumes a good estimate of the frictional ratio (f/f_0) has been extracted from the experimental data (14).

4.4.2 Sedimentation equilibrium analytical ultracentrifugation

At centrifugal fields lower than those generally used for sedimentation velocity experiments, sedimentation of solutes is opposed to a certain extent by diffusion. Sedimentation equilibrium is attained when the flux of sedimenting molecules is exactly balanced by the flux of diffusing molecules (13,14). This situation can easily be established by centrifugation at a constant centrifugal field until the solute concentration distribution appears to be invariant with time (14).

Analysis of the shape of the equilibrium radial concentration profile yields precise thermodynamic information, including molecular mass and equilibrium association constants for associating systems.

4.4.3 Analytical ultracentrifugation analysis of wild-type DHDPS and the variants

The hydrodynamic and thermodynamic properties of wild-type DHDPS and the variant enzymes were analysed by sedimentation velocity and sedimentation equilibrium experiments performed in a Beckman Model XL-A analytical ultracentrifuge equipped with UV/Vis scanning optics.

Sedimentation velocity experiments were performed by centrifugation of the proteins at a concentration of 1 mg/ml at 40,000 rpm and 20°C. Radial absorbance scans were collected at 280 nm every 6 min. Sedimentation velocity data were then fitted to a continuous sedimentation coefficient distribution ($c(s)$) model using the program SEDFIT (15). The sedimentation coefficient, s, was then taken as the ordinate maximum of this distribution. Plots of the raw data overlaid with the calculated fits

were produced for visual inspection of the data. Additionally, plots of raw residuals were created to allow assessment of the goodness of the fits.

SEDFIT was also used to calculate continuous mass distributions (*c(M)*), using the value of f/f_0 determined for the *c(s)* fit. The apparent molecular mass, M_{app}, was taken as the ordinate maximum of this distribution.

Based on the results obtained from the sedimentation velocity experiments, wild-type DHDPS and the four variants DHDPS-L197D, DHDPS-L197Y, DHDPS-Q196D, and DHDPS-D193A, were selected for further analysis by sedimentation equilibrium ultracentrifugation. For these experiments, samples at initial protein concentrations of 0.1, 0.3 and 1.0 mg/ml were centrifuged at 10,000 rpm or 16,000 rpm until sedimentation equilibrium was attained (~24 hours). Radial absorbance scans were obtained at 280 nm and the data acquired at both speeds were fitted globally using the program SEDPHAT (17) to yield the equivalent molar mass assuming a single species (M_{eq}) according to Equation 4.2 below.

$$c(r) = c(r_0)\exp^{[\frac{\omega^2}{2RT}M_{eq}(1-\bar{v}\rho)(r^2-r_0^2)]} + E \qquad \text{Equation 4.2}$$

where, *c(r)* is the mass concentration at radius *r* (cm), $c(r_0)$ is the concentration at the reference radius r_0, ω is the rotor angular velocity (radians/sec), *R* is the gas constant, *T* is temperature (K), $\bar{v}$ is the partial specific volume of the solute (g/ml), ρ is the solvent density, and E is the baseline offset.

To assess the state of association of wild-type DHDPS and the variant enzymes, sedimentation equillibrium data were fitted to various models including the monomer-dimer and monomer-dimer-tetramer self-association models implemented in SEDPHAT.[‡]

The hydrodynamic and thermodynamic parameters determined for wild-type DHDPS and the variant enzymes are presented in Table 4.1.

[‡] Where the monomer-dimer self-association model was used analytically, the tight-dimer was assumed as a monomeric unit and, thus, this model was effectively used as a dimer-tetramer self-association model. This was reasonable, since it was shown that no dissociation of the wild-type tetramer or the variant dimers into monomer was detectable.

Table 4.1 *Hydrodynamic and thermodynamic properties determined for wild-type DHDPS and the variant enzymes.* s *is the sedimentation coefficient, in Svedberg, taken from the ordinate maximum of the* c(s) *distribution,* f/f_0 *is the frictional ratio calculated from the continuous size-distribution best-fit,* M_{app} *is the apparent molecular mass taken from the ordinate maximum of the* c(M) *distribution.* M_{eq} *is the equivalent molecular mass, assuming a single species, calculated from sedimentation equilibrium analyses, and* $K_{a\ dimer\text{-}tetramer}$ *is the association constant for the rapid dimer-tetramer equilibrium calculated from sedimentation equilibrium analyses.*

	Wild-type DHDPS	DHDPS-L197D	DHDPS-L197Y	DHDPS-Q196D	DHDPS-D193A
s (S)	6.6	4.1	4.2	6.5	6.4
f/f$_0$	1.24	1.29	1.24	1.26	1.29
M_{app} (kDa)	123	63.4	63.1	121	126
M_{eq} (kDa)	121	62.3	67.3	111	109
$K_{a\ dimer\text{-}tetramer}$ (M^{-1})	-	-	-	$10^{5.6}$	$10^{5.8}$

	DHDPS-D193Y	DHDPS-Q234D
s (S)	6.4	6.5
f/f$_0$	1.29	1.25
M_{app} (kDa)	123	124
M_{eq} (kDa)	-	-
$K_{a\ dimer\text{-}tetramer}$ (M^{-1})	-	-

For both sedimentation velocity and sedimentation equilibrium experiments, the partial specific volume of the protein, the buffer density, and the buffer viscosity were computed using the program SEDNTERP (18).

4.4.4 Analytical ultracentrifugation analysis of wild-type DHDPS

Sedimentation velocity analytical ultracentrifugation

The sedimenting boundary of the wild-type enzyme shows minimal spreading with time, which is consistent with a largely homogeneous sample (Figure 4.4). However, sample heterogeneity can not be ruled out based on the radial scans alone and the data were subsequently fitted to the continuous size-distribution model. The *c(s)* distribution shows a single, narrow, symmetrical peak, confirming that wild-type DHDPS was predominantly a single species in solution. The ordinate maximum of the peak corresponded to a sedimentation coefficient of 6.6 S (Figure 4.4B). The quality of the fit is indicated by the low r.m.s.d of 0.0108 and the random distribution of residuals (Figure 4.4A). Data were subsequently fitted to a continuous-mass distribution. From the ordinate maximum of the peak observed in the *c(M)* distribution the apparent molar mass of the 6.6 S species was 123 kDa. This agrees well with the theoretical tetrameric mass of wild-type DHDPS (125 kDa).

Sedimentation equilibrium analytical ultracentrifugation

Global analysis of the multi-speed sedimentation equilibrium data also confirmed that the wild-type enzyme was tetrameric in aqueous solution with an equivalent molar mass of 121 kDa (Figure 4.5). Again, this agrees very favourably with the predicted molar mass. Similar molecular mass results were also obtained by fitting data from the separate initial protein concentration experiments, indicating that the self-association of the native and mutant forms is not concentration-dependent in the range detectable here. Additionally, neither the monomer-dimer nor the monomer-dimer-tetramer self-association models produced meaningful fits to the data, indicating that the equilibrium between oligomeric structures in the self-asssociation of the tetramer was not detectable by this analysis.

Figure 4.4 *Sedimentation velocity analysis of wild-type DHDPS. A - Absorbance at 280 nm plotted as a function of radial position from the axis of rotation (cm). The raw data are represented as open symbols (○) plotted at time intervals of 12 min. Raw data are overlaid with the nonlinear least squares best-fit to a continuous-size distribution model. Residuals for the nonlinear least squares best-fit are also shown. B - The continuous sedimentation coefficient [c(s)] distribution plotted as a function of sedimentation coefficient (Svedberg, S). The fit was obtained using a resolution of 100 species between s_{min} of 2 S and s_{max} of 15 S with $P = 0.95$, $\nu = 0.7405$, $\rho = 1.005$ g/ml, $\eta = 1.0214$ cp, and $f/f_0 = 1.24$. The r.m.s.d and runs test average for the fit were calculated to be 0.0108 and 3.39, respectively.*

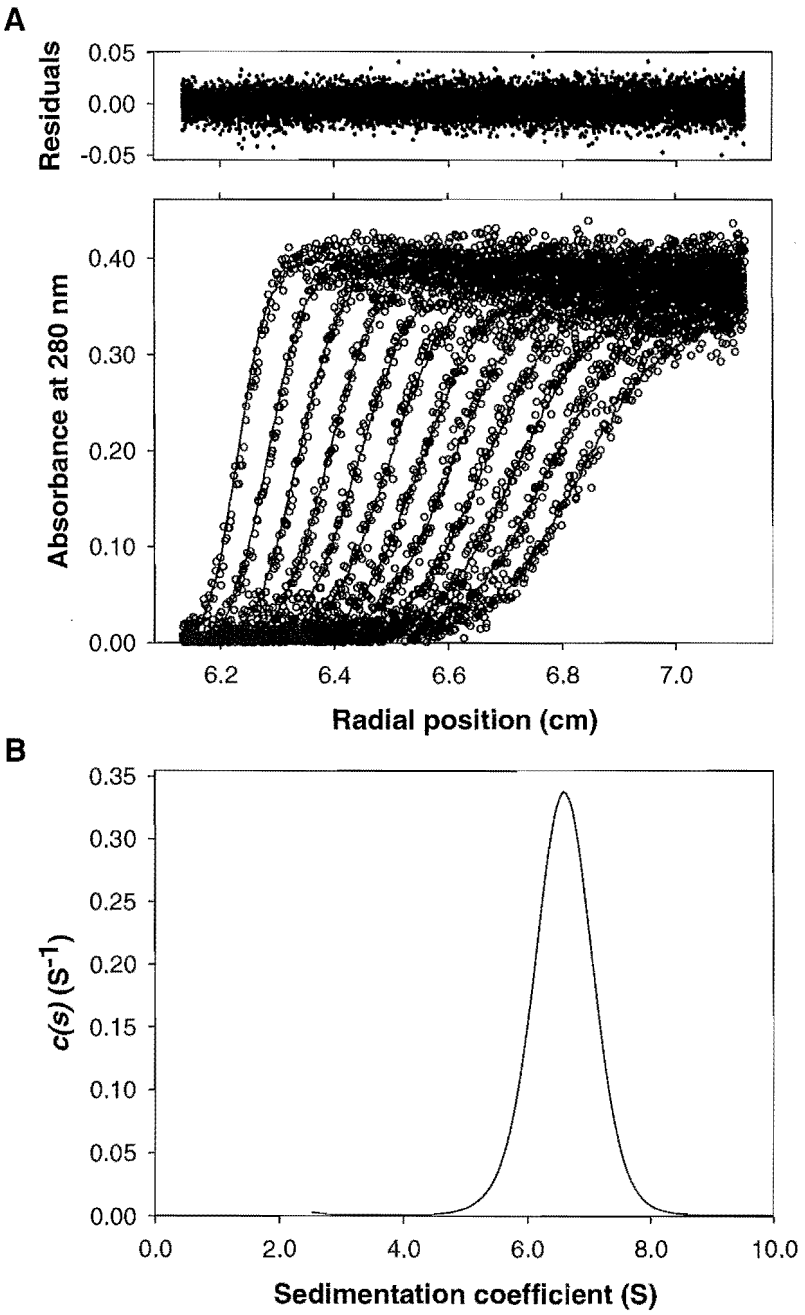

Figure 4.5 *Sedimentation equilibrium analysis of wild-type DHDPS. The absorbance at 280 nm is plotted as a function of radial position from the axis of rotation (cm). The raw data (open symbols, ○) obtained at two speeds, 10,000 rpm and 16,000 rpm, and an initial concentration of 1.0 mg/ml are shown overlaid with the nonlinear least squares best-fit to Equation 1 (solid lines). The r.m.s.d of the fits was < 0.005.*

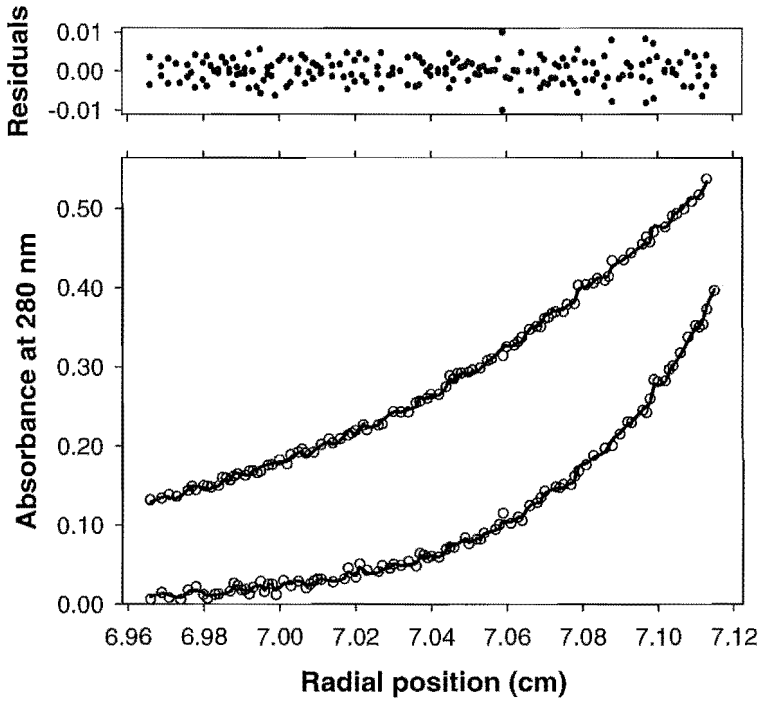

4.4.5 Analytical ultracentrifugation analysis of DHDPS-L197D

Sedimentation velocity analytical ultracentrifugation

The *c(s)* distribution generated from the sedimentation velocity data obtained for DHDPS-L197D showed a single major peak with ordinate maximum at 4.1 S (Figure 4.6). This is in obvious contrast to the value of 6.6 S determined for the wild-type enzyme and indicates that DHDPS-L197D is predominantly a single species of lower sedimentation mass than the wild-type. The corresponding *c(M)* distribution yields an apparent molecular mass of 63.4 kDa, which is in excellent agreement with the predicted molecular mass of the tight-dimer unit of 62.5 kDa. The randomly distributed residuals and low r.m.s.d (0.0115) indicate a good fit to the data.

Close inspection of the *c(s)* distribution reveals the existence of a second species with a sedmentation coefficient of approximately 7.2 S, suggesting that there is a small proportion of higher order oligomer present in the DHDPS-L197D sample. However,

it is not possible from this analysis to determine whether this indicates the presence of a small fraction of tetramer.

Figure 4.6 *Sedimentation velocity analysis of DHDPS-L197D. A - Absorbance at 280 nm plotted as a function of radial position from the axis of rotation (cm). The raw data are represented as open symbols (○) plotted at time intervals of 12 min. Raw data are overlaid with the nonlinear least squares best-fit to a continuous-size distribution model. Residuals for the nonlinear least squares best-fit are also shown. B - The continuous sedimentation coefficient [c(s)] distribution plotted as a function of sedimentation coefficient (Svedberg, S). The fit was obtained using a resolution of 100 species between s_{min} of 2 S and s_{max} of 15 S with P = 0.95, $\bar{v}$ = 0.7394, ρ = 1.005 g/ml, η = 1.0214 cp, and f/f_0 = 1.29. The r.m.s.d and runs test average for the fit were calculated to be 0.0115 and 2.95, respectively.*

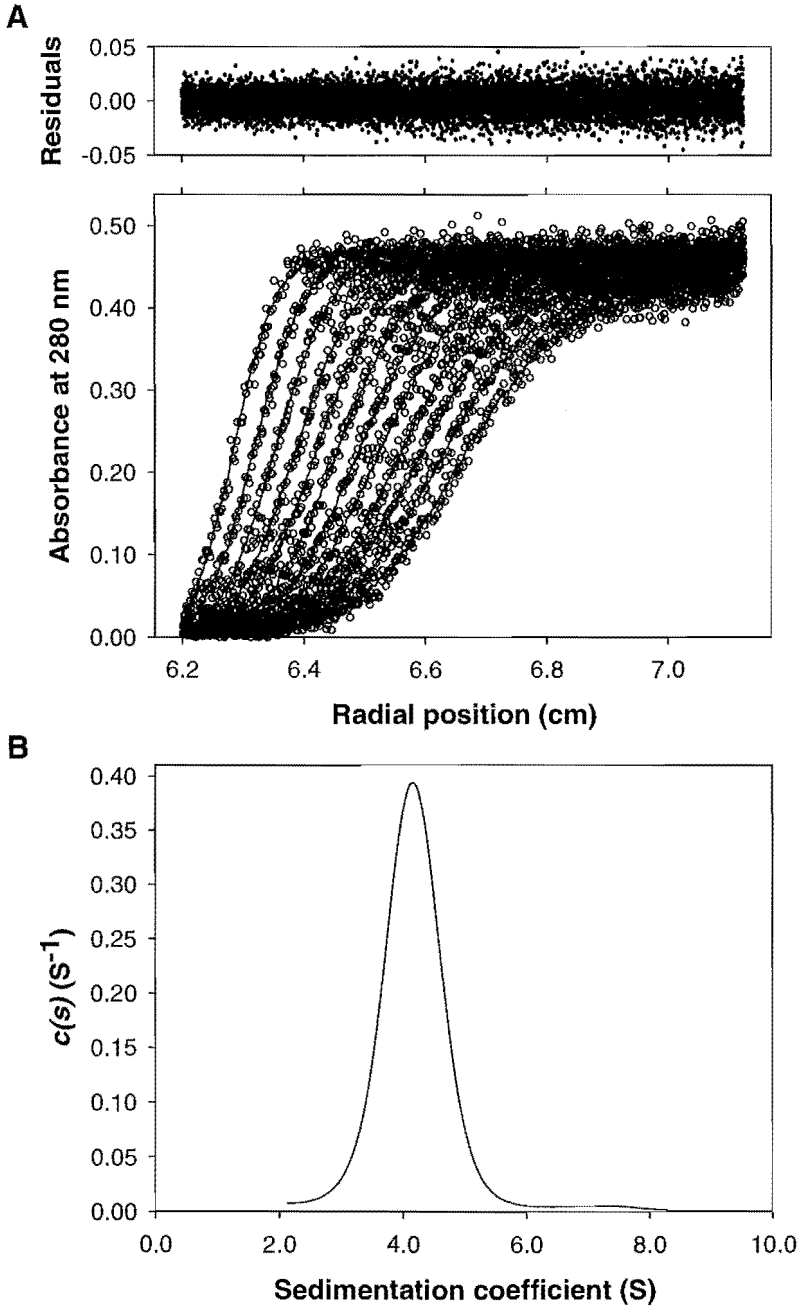

Sedimentation equilibrium analytical ultracentrifugation

The equivalent molecular mass value determined from the global analysis of sedimentation equilibrium data collected for DHDPS-L197D was 62.3 kDa, indicating unequivocally that this variant exists primarily as a dimer in solution (Figure 4.7). Again, analysis of data at different intial protein concentration ranges gave similar results, indicating that the oligomeric state of the variant is not concentration dependent. This was confirmed by unsucessful attempts to fit the data to monomer-dimer and monomer-dimer-tetramer self-association models. Thus, equilibrium between monomeric, dimeric, and tetrameric forms of DHDPS-L197D is below the level detectable by this analysis indicating that the 7.2 S species observed in the sedimentation velocity experiments (Figure 4.6B) may be an artefact of the high protein concentration used.

Figure 4.7 *Sedimentation equilibrium analysis of DHDPS-L197D. The absorbance at 280 nm is plotted as a function of radial position from the axis of rotation (cm). The raw data (open symbols, ○) obtained at two speeds, 10,000 rpm and 16,000 rpm, and an initial concentration of 1.0 mg/ml are shown overlaid with the nonlinear least squares best-fit to Equation 1 (solid lines). The r.m.s.d of the fits was < 0.005.*

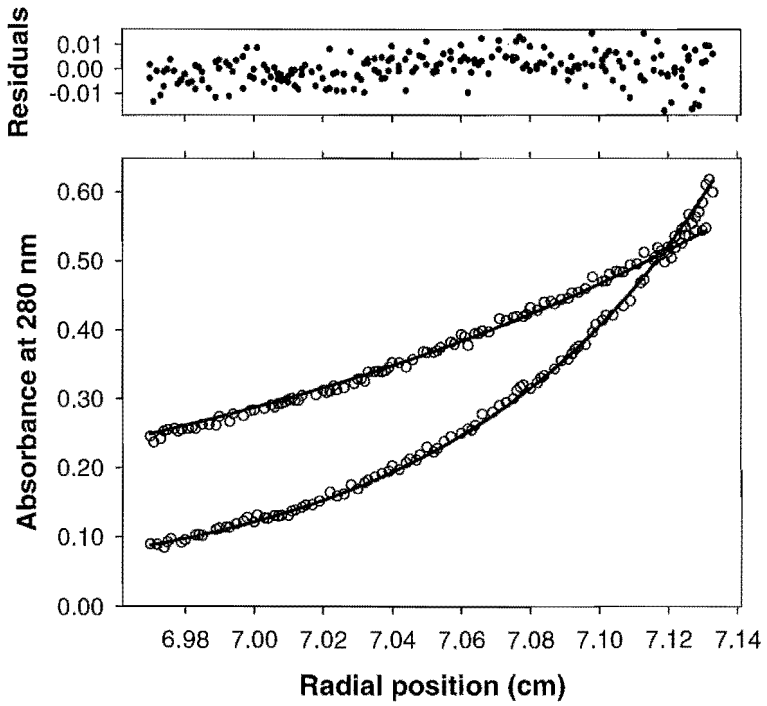

4.4.6 Analytical ultracentrifugation analysis of DHDPS-L197Y

Sedimentation velocity analytical ultracentrifugation

Analysis of the sedimentation velocity data for DHDPS-L197Y produced a *c(s)* distribution very similar to that of DHDPS-L197D (Figure 4.8). The ordinate maximum of the peak gave a sedimentation coefficient value of 4.2 S, which corresponded to an apparent molecular mass of 63.1 kDa. Again, the random distribution of residuals and the low r.m.s.d of 0.0111 for the fit indicated that the quality of the continuous distribution model fit was high.

Similar to DHDPS-L197D, the *c(s)* distribution obtained for DHDPS-L197Y shows a shoulder of higher sedimentation velocity species indicating the presence of a second species with a sedimentation coefficient of approximately 7.0 S. In this case, no defined peak is apparent, and, again, it is impossible to determine from this analysis whether this may be a tetrameric species or some other sedimenting aggregate.

Sedimentation equilibrium analytical ultracentrifugation

The equivalent molecular mass value determined from the global analysis of sedimentation equilibrium data collected for DHDPS-L197Y was 63.1 kDa (Figure 4.9), again indicating unequivocally that this variant exists primarily as a dimer in solution. Analysis of data at different protein concentration ranges gave similar M_{eq} values, indicating that the oligomeric state of the variant is not concentration dependent. The failure to obtain fits to the self-association models confirms that equilibrium between the possible oligomeric structures is below the level detectable by this method.

Figure 4.8 *Sedimentation velocity analysis of DHDPS-L197Y. A - Absorbance at 280 nm plotted as a function of radial position from the axis of rotation (cm). The raw data are represented as open symbols (○) plotted at time intervals of 12 min. Raw data are overlaid with the nonlinear least squares best-fit to a continuous-size distribution model. Residuals for the nonlinear least squares best-fit are also shown. B - The continuous sedimentation coefficient [c(s)] distribution plotted as a function of sedimentation coefficient (Svedberg, S). The fit was obtained using a resolution of 100 species between s_{min} of 2 S and s_{max} of 15 S with P = 0.95, $\bar{\nu}$ = 0.7398, ρ = 1.005 g/ml, η = 1.0214 cp, and f/f_0 = 1.24. The r.m.s.d and runs test average for the fit were calculated to be 0.0111 and 2.26, respectively.*

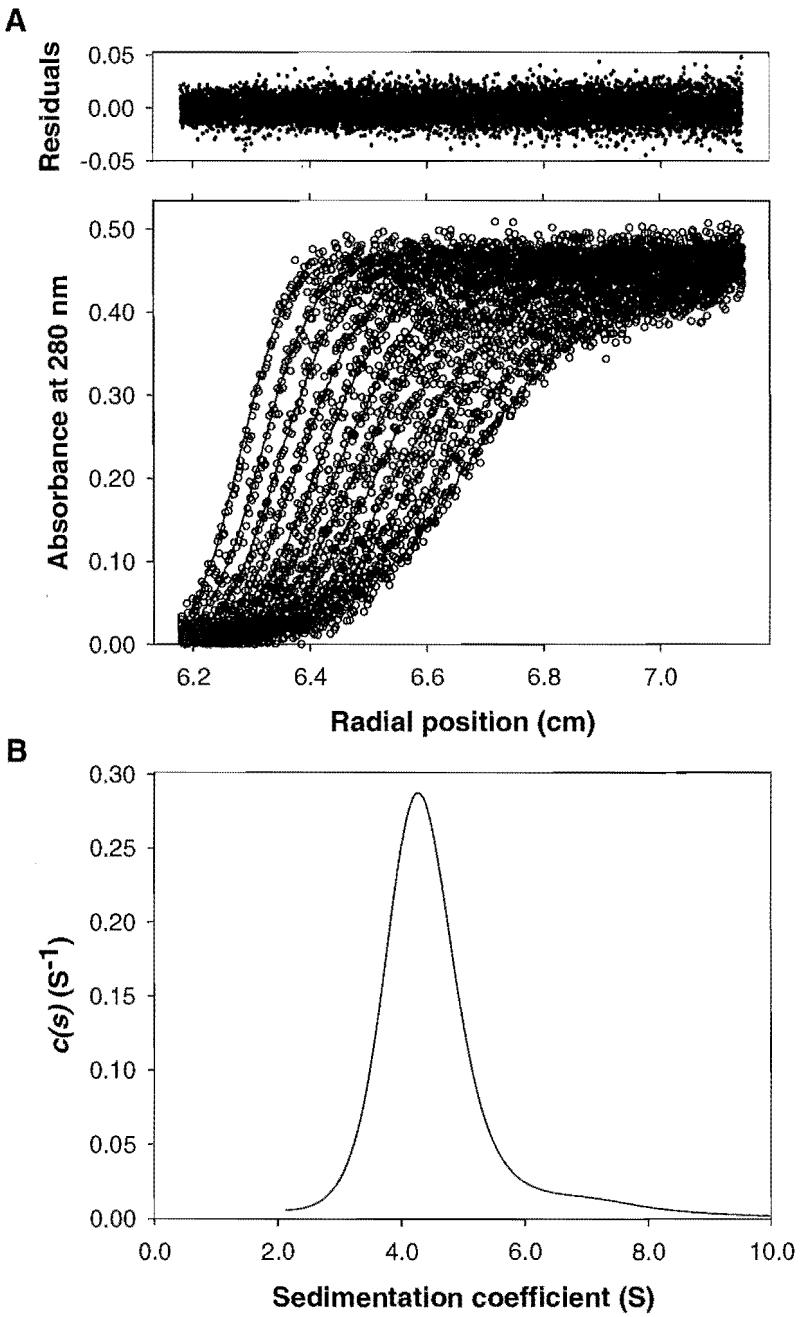

Figure 4.9 *Sedimentation equilibrium analysis of DHDPS-L197Y. The absorbance at 280 nm is plotted as a function of radial position from the axis of rotation (cm). The raw data (open symbols, ○) obtained at two speeds, 10,000 rpm and 16,000 rpm, and an initial concentration of 1.0 mg/ml are shown overlaid with the nonlinear least squares best-fit to Equation 1 (solid lines). The r.m.s.d of the fits was < 0.004.*

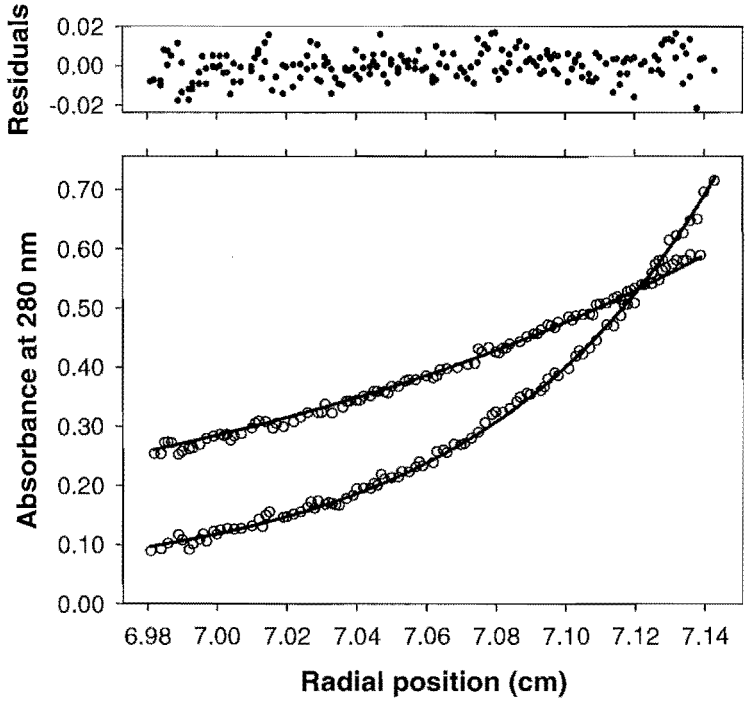

4.4.7 Analytical ultracentrifugation analysis of DHDPS-Q196D

Sedimentation velocity analytical ultracentrifugation

Sedimentation velocity data indicated that DHDPS-Q196D was primarily tetrameric at a protein concentration of 1 mg/ml. The *c(s)* distribution derived from the data showed a single peak with ordinate maximum at 6.5 S, in good agreement with that of the wild-type. The r.m.s.d of 0.0106 calculated for this fit and the random distribution of residuals indicate that this distribution represents a good fit to the raw data (Figure 4.10). However, closer inspection of the shape of the distribution reveals an asymmetrical peak that is skewed towards species of lower S values and does not return to baseline *c(s)* values below the peak S value.

Figure 4.10 *Sedimentation velocity analysis of DHDPS- Q196D. A - Absorbance at 280 nm plotted as a function of radial position from the axis of rotation (cm). The raw data are represented as open symbols (○) plotted at time intervals of 12 min. Raw data are overlaid with the nonlinear least squares best-fit to a continuous-size distribution model. Residuals for the nonlinear least squares best-fit are also shown. B - The continuous sedimentation coefficient [c(s)] distribution plotted as a function of sedimentation coefficient (Svedberg, S). The fit was obtained using a resolution of 100 species between s_{min} of 2 S and s_{max} of 15 S with P = 0.95, $\bar{\nu}$ = 0.7403, ρ = 1.005 g/ml, η = 1.0214 cp, and f/f_0 = 1.26. The r.m.s.d and runs test average for the fit were calculated to be 0.0106 and 3.35, respectively.*

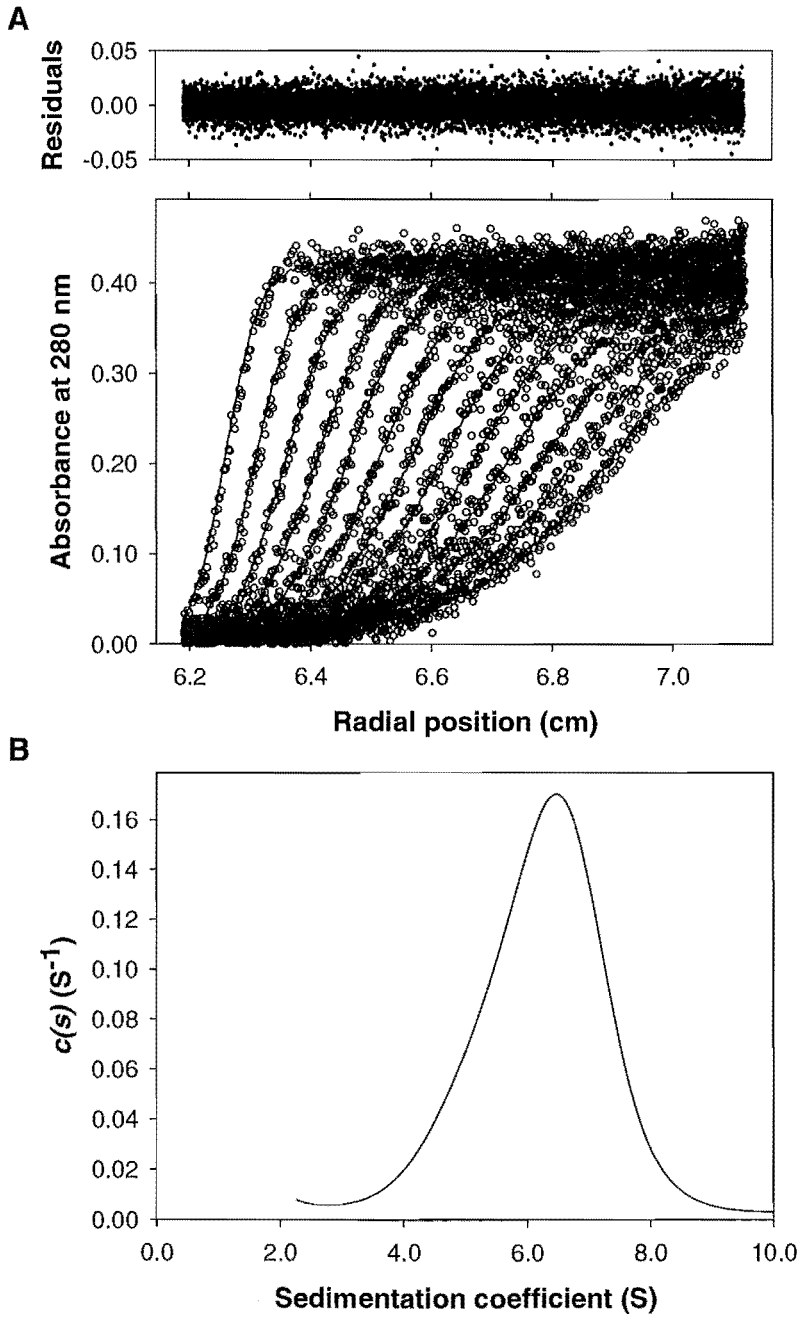

Direct comparison with the distribution obtained for wild-type DHDPS (Figure 4.11), shows that the *c(s)* distribution for DHDPS-Q196D is significantly broader than the wild-type enzyme, particularly at lower sedimentation coefficient values. This suggests that the DHDPS-Q196D tetramer may reside in a rapid equilibrium with lower order species. Previous studies have demonstrated that *c(s)* distribution analyses of a self-associating system residing in a slow equilibrium mixture results in baseline separation of each oligomeric species (19). However, the *c(s)* distribution analyses of proteins existing in rapid equilibria are predicted to result in broader, non baseline-resolved distributions (Perugini, M. A., *pers comm*). The data shown in Figure 4.9B is consistent with this phenomenon. Alternatively, this could be due to a significant change in the shape of the tetramer brought about by the Q196D mutation. However, there is only a slight increase in the frictional ratio from 1.24 for wild-type DHDPS (Figure 4.4) to 1.26 (Figure 4.10) for the Q196D variant. Sedimentation equilibrium experiments were therefore performed to provide further insight into the state of association of DHDPS-Q196D.

Figure 4.11 *Direct comparison of the* c(s) *distributions calculated for DHDPS-Q234D (solid line) and wild-type DHDPS (dashed line)*

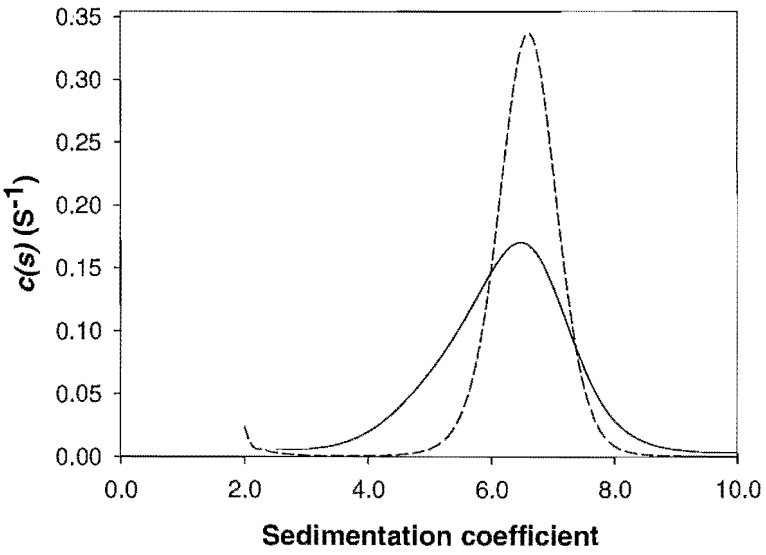

Sedimentation equilibrium analytical ultracentrifugation

The equivalent molecular mass value determined from the analysis of high concentration sedimentation equilibrium data collected for DHDPS-Q196D was 111

kDa (Figure 4.12). This is lower than the equivalent molecular mass estimate obtained for the wild-type enzyme, supporting the hypothesis that DHDPS-Q196D exists as an equilibrium between tetramer and a lower order species, most likely dimer.

Accordingly, the data from all protein concentration ranges were globally fitted to the monomer-dimer self-association model using the molecular weight and sedimentation coefficient of the tight-dimer unit, as determined for DHDPS-L197D, as the monomeric unit for the purposes of the model. This analysis yielded an association constant for the rapid dimer-tetramer equilibrium of $10^{5.6}$ M^{-1}, indicating that DHDPS-Q196D exists as a mixture of dimer and tetramer in rapid equilibrium in solution. This result means that the solution concentration of dimer is equal to the solution concentration of tetramer when the protein concentration is equal to ~5 μM. The r.m.s.d for this fit was calculated as less than 0.007, suggesting an excellent fit to the model.

Figure 4.12 *Sedimentation equilibrium analysis of DHDPS-Q196D. The absorbance at 280 nm is plotted as a function of radial position from the axis of rotation (cm). The raw data (open symbols, ○) obtained at two speeds, 10,000 rpm and 16,000 rpm, and an initial concentration of 1.0 mg/ml are shown overlaid with the nonlinear least squares best-fit to Equation 1 (solid lines). The r.m.s.d of the fits was < 0.007.*

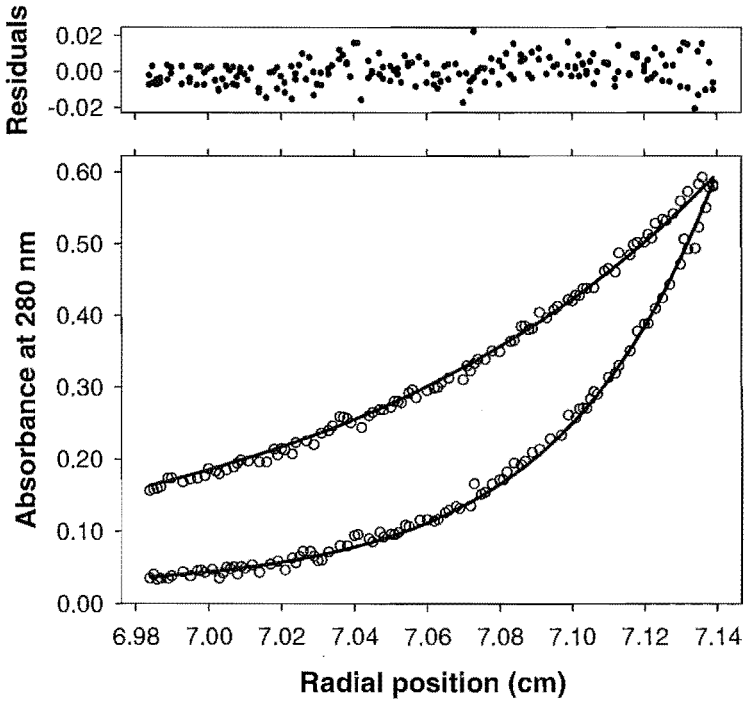

4.4.8 Analytical utracentrifugation analysis of DHDPS-D193A

Sedimentation velocity analytical ultracentrifugation

Sedimentation velocity data indicated that DHDPS-D193A was primarily tetrameric at a protein concentration of 1 mg/ml. The *c(s)* distribution derived from the data showed a single peak with ordinate maximum at 6.4 S (Figure 4.13). The r.m.s.d of 0.0106 calculated for this fit and the random distribution of residuals indicate that this distribution represents a good fit to the raw data. Again, the shape of the *c(s)* distribution peak obtained was asymmetrical and skewed towards species with lower S values, similar to the data obtained for DHDPS-Q196D (Figure 4.10).This indicates that DHDPS-D193A displays altered hydrodynamic behaviour under sedimentation velocity analysis, and suggests that this variant may reside in dimer-tetramer equilibrium, as demonstrated for DHDPS-Q196D.

Sedimentation equilibrium analytical ultracentrifugation

The equivalent molecular mass value, assuming a single species, calculated for DHDPS-D193A at an initial concentration of 1 mg/ml was 109 kDa (Figure 4.14). This supports the hypothesis that this variant exists as a mixture of tetramer and lower order species in aqueous solution.

The data from all protein concentration ranges were globally fitted to the monomer-dimer self-association model as for DHDPS-Q196D. The association constant calculated for the rapid dimer-tetramer equilibrium of $10^{5.8}$ M^{-1} indicates that DHDPS-D193A exists as a mixture of dimer and tetramer in rapid equilibrium in solution. This result means that the solution concentration of dimer is equal to the solution concentration of tetramer when the protein concentration is approximately equal to ~3 μM. The r.m.s.d for this fit was calculated as less than 0.007 suggesting an excellent fit to the experimental data.

Figure 4.13 *Sedimentation velocity analysis of DHDPS-D193A. A - Absorbance at 280 nm plotted as a function of radial position from the axis of rotation (cm). The raw data are represented as open symbols (○) plotted at time intervals of 12 min. Raw data are overlaid with the nonlinear least squares best-fit to a continuous-size distribution model. Residuals for the nonlinear least squares best-fit are also shown. B - The continuous sedimentation coefficient [c(s)] distribution plotted as a function of sedimentation coefficient (Svedberg, S). The fit was obtained using a resolution of 100 species between s_{min} of 2 S and s_{max} of 15 S with $P = 0.95$, $\nu = 0.741$, $\rho = 1.005$ g/ml, $\eta = 1.0214$ cp, and $f/f_0 = 1.29$. The r.m.s.d and runs test average for the fit were calculated to be 0.0107 and 1.73, respectively.*

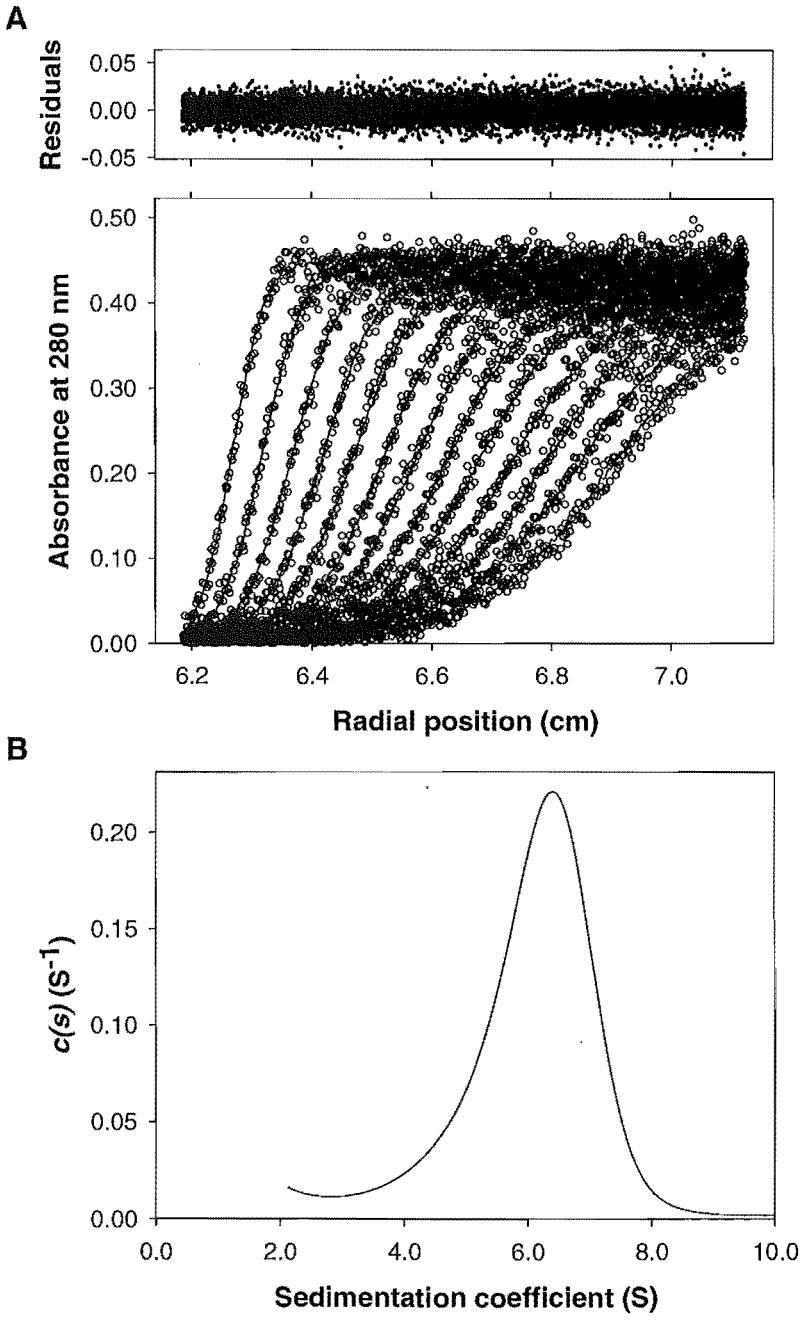

Figure 4.14 *Sedimentation equilibrium analysis of DHDPS-D193A. The absorbance at 280 nm is plotted as a function of radial position from the axis of rotation (cm). The raw data (open symbols, ○) obtained at two speeds, 10,000 rpm and 16,000 rpm, and an initial concentration of 1.0 mg/ml are shown overlaid with the nonlinear least squares best-fit to Equation 1 (solid lines). The r.m.s.d of the fits was < 0.008.*

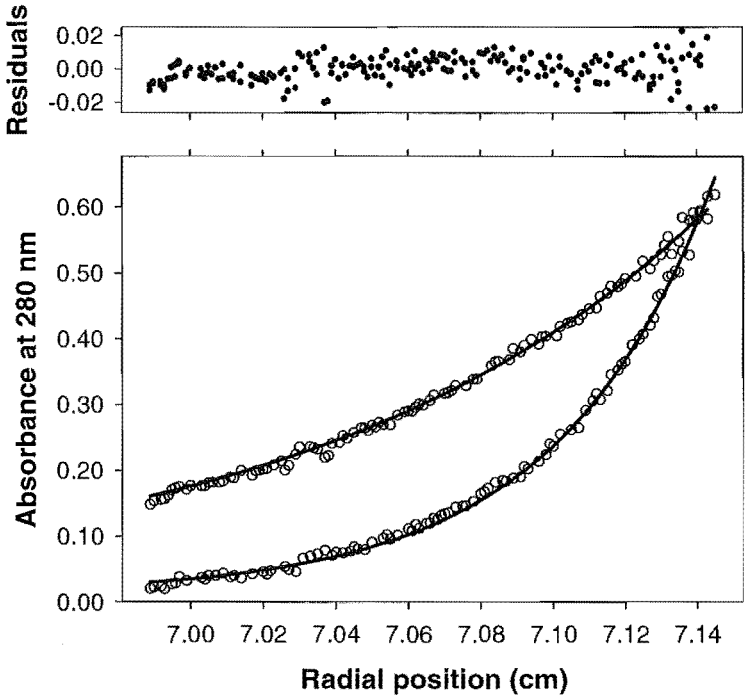

4.4.9 Analytical utracentrifugation analysis of DHDPS-D193Y

Sedimentation velocity analytical ultracentrifugation

The *c(s)* distribution derived from sedimentation velocity data indicated that DHDPS-D193Y was primarily tetrameric at a protein concentration of 1 mg/ml, showing a single peak with ordinate maximum at 6.4 S (Figure 4.15). The shape of the *c(s)* distribution peak obtained showed a similar asymmetric pattern to DHDPS-Q196D and DHDPS-D193A but here this was far less pronounced. Thus, further analysis by sedimentation equilibrium was not carried out for this variant.

Figure 4.15 *Sedimentation velocity analysis of DHDPS-D193Y. A - Absorbance at 280 nm plotted as a function of radial position from the axis of rotation (cm). The raw data are represented as open symbols (○) plotted at time intervals of 12 min. Raw data are overlaid with the nonlinear least squares best-fit to a continuous-size distribution model. Residuals for the nonlinear least squares best-fit are also shown. B - The continuous sedimentation coefficient [c(s)] distribution plotted as a function of sedimentation coefficient (Svedberg, S). The fit was obtained using a resolution of 100 species between s_{min} of 2 S and s_{max} of 15 S with P = 0.95, $\bar{v}$ = 0.7412, ρ = 1.005 g/ml, η = 1.0214 cp, and f/f_0 = 1.29. The r.m.s.d and runs test average for the fit were calculated to be 0.0108 and 1.68, respectively.*

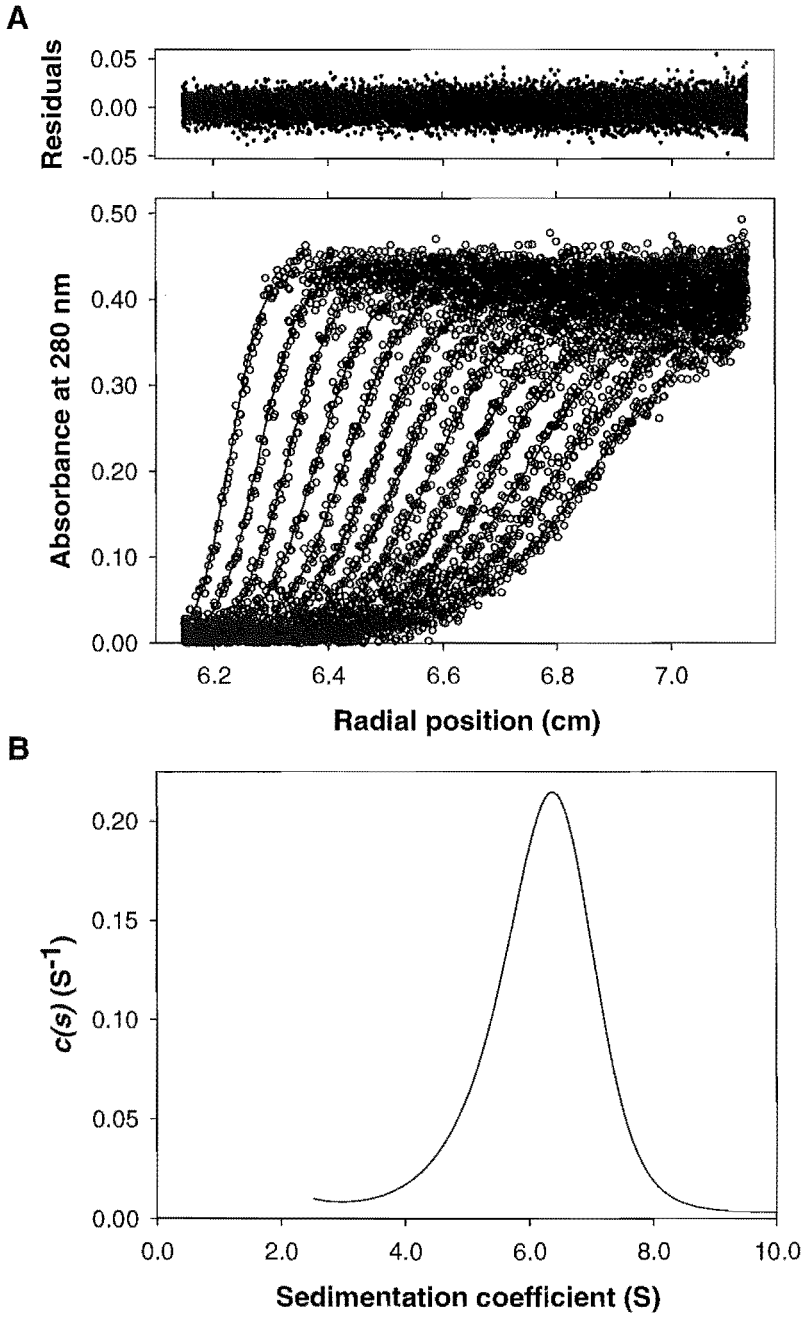

Figure 4.16 *Sedimentation velocity analysis of DHDPS-Q234D. A - Absorbance at 280 nm plotted as a function of radial position from the axis of rotation (cm). The raw data are represented as open symbols (○) plotted at time intervals of 12 min. Raw data are overlaid with the nonlinear least squares best-fit to a continuous-size distribution model. Residuals for the nonlinear least squares best-fit are also shown. B - The continuous sedimentation coefficient [c(s)] distribution plotted as a function of sedimentation coefficient (Svedberg, S). The fit was obtained using a resolution of 100 species between s_{min} of 2 S and s_{max} of 15 S with P = 0.95, v = 0.7403, ρ = 1.005 g/ml, η = 1.0214 cp, and f/f_0 = 1.29. The r.m.s.d and runs test average for the fit were calculated to be 0.0109 and 3.67, respectively.*

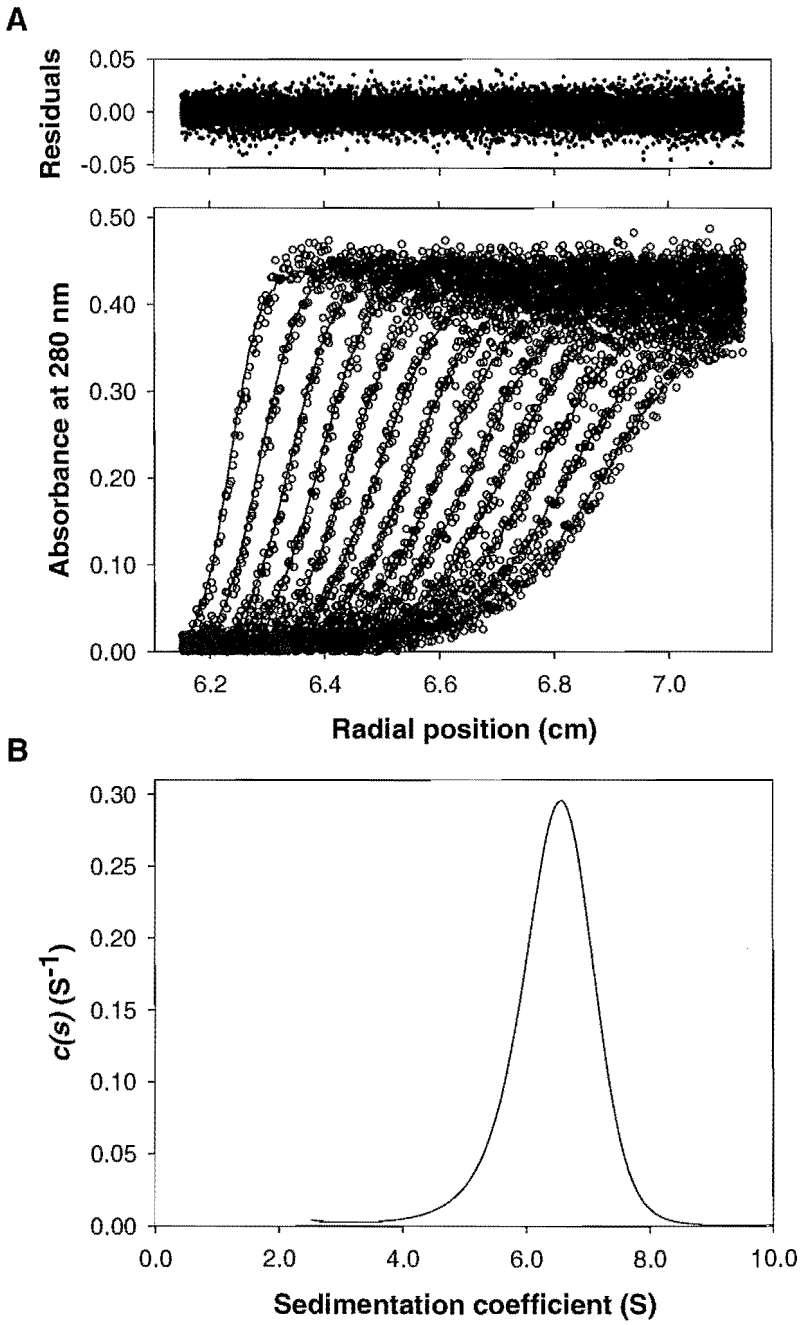

4.4.10 Analytical utracentrifugation analysis of DHDPS-Q234D

Sedimentation velocity analytical ultracentrifugation

Sedimentation velocity data indicated that DHDPS-Q234D was tetrameric. The ordinate maximum of the *c(s)* distribution at 6.5 S is in good agreement with that of the wild type (Figure 4.16). The random distribution of residuals and r.m.s.d of 0.0106 calculated for this fit indicate that the distribution represents an excellent fit to the raw data. A small amount of asymmetry is apparent in the *c(s)* peak; however, this relatively minor in comparison to the other variants studied. Therefore, sedimentation equilibrium experiments were not performed for DHDPS-Q234D

4.5 Discussion

Detailed biophysical characterisation of wild-type DHDPS and the variants reveals that all point mutations produced have affected the quaternary structural characteristics of the variants with respect to the wild-type enzyme.

BN-PAGE provided initial indication that both point mutations at position 197, L197D and L197Y, had produced variants of dimeric nature. Analytical size exclusion chromatography confirmed that the molecular weight of DHDPS-L197D was around that expected for a dimeric species. The apparent molecular masses calculated by this method for wild-type DHDPS and DHDPS-L197D were 114.8 kDa and 51.9 kDa respectively. These values agree reasonably well with the predicted values of 125 kDa and 62.5 kDa; however, it is clear that in this case this system is not sufficiently accurate for quantitative molecular mass estimation. Semi-qualitative size exclusion chromatography showed that the DHDPS-Q196D, DHDPS-D193A, DHDPS-D193Y, and DHDPS-Q234D variants eluted at a similar elution volume to the wild-type enzyme, indicating that these were predominantly tetrameric under the conditions used. The elution volumes determined for DHDPS-L197D and DHDPS-L197Y, were significantly displaced from that of the wild-type, indicating that the quaternary structure of these variants had been altered. As the loading protein concentration for these experiments was high (15-20 mg/ml), equilibrating mixtures of dimer and tetramer would be expected to be forced toward the tetramer. Thus, smaller scale alterations to the quaternary structure in the variants would not necessarily be observed in this type of analysis.

Analytical ultracentrifugation analysis of the DHDPS enzymes offered accurate and detailed information on the solution properties of the proteins in terms of molecular mass measurement and self association characteristics. The sedimentation coefficient of wild-type DHDPS calculated from sedimentation velocity data was 6.6 S. This is in reasonable agreement with the published value of 7.1 S obtained by sucrose density gradient centrifugation (20), which is known to be a less accurate technique (13). The equivalent molecular mass calculated from this data was 123 kDa, in excellent agreement with values determined by sequence analysis (21,22) and mass spectrometry (23,24), which confirms a tetramer of 125 kDa. The equivalent molecular mass calculated from sedimentation equilibrium data was 121 kDa, again showing excellent agreement with the predicted value. The fact that self-association models failed to fit the raw data satisfactorily indicates that the levels of lower order oligomers in the equilibrium, that is monomers or dimers, are below that detectable by the models as implemented in SEDPHAT.

Analysis of sedimentation velocity and sedimentation equilibrium data from DHDPS-L197D and DHDPS-L197Y showed unequivocally that these two variants exist in solution as stable, obligate dimers. This change in quaternary structure was reflected in the calculated sedimentation coefficients of 4.1 S and 4.2 S for DHDPS-L197D and DHDPS-L197Y respectively. Additionally, calculated molecular masses for DHDPS-L197D of M_{app} = 63.4 kDa and M_{eq} = 62.3 kDa agreed well with the predicted molecular mass for the tight-dimer of 62.5 kDa, as did the values calculated for DHDPS-L197Y of M_{app} = 63.1 kDa and M_{eq} = 67.3 kDa.

The observation of a small, secondary peak or shoulder in the *c(s)* distributions for DHDPS-L197D and DHDPS-L197Y is an interesting result. These ancillary distributions, at higher S values than the major peak, could be due to a fraction of a tetrameric species in equilibrium with the dimer. However, this would seem unlikely as the M_{eq} values determined from sedimentation equilibrium data for these variants were found to be largely independent of the protein concentration range fitted, and self-association models failed to detect this equilibrium. Fitting the data to a non-interacting, two-species model indicated that these higher sedimentation coefficient species constituted approximately 10% and 13% of the DHDPS-L197D and DHDPS-L197Y preparations respectively. This fit suggests that the secondary species is a

non-specific aggregate, since equilibrium between dimer and tetramer would be expected for a specific interaction. Additionally, fast equilibrium in a self-association reaction would be expected to broaden the observed peak under this analysis (*cf.* DHDPS-Q196D) instead of introducing a second peak.

The appearance of species at higher S values than the dimer in the *c(s)* distributions may be explained in terms of the conditions used for the experiment. Both DHDPS-L197D and DHDPS-L197Y displayed much lower stability in solution than the wild type enzyme, and at concentrations around and above 1 mg/ml, were found to produce significant amounts of amorphous aggregate over hour time scales at 4°C. Since the sedimentation velocity experiments were performed at 20°C and a protein concentration of 1 mg/ml it is reasonable to assume that the process of non-specific aggregation occurred during the time course of data collection. Nucleation of these non-specific aggregates rapidly leads to larger particulates which would sediment almost immediately under the large centrifugal field used. It is, therefore, possible that the observed higher molecular weight species are these low order non-specific aggregates.

Sedimentation velocity data for DHDPS-Q196D, DHDPS-D193A, DHDPS-D193Y, and DHDPS-Q234D suggested that these variants were tetrameric, but had altered hydrodynamic properties with respect to wild-type DHDPS. Sedimentation equilibrium data revealed significant equilibrium between dimeric and tetrameric species in the DHDPS-Q196D and DHDPS-D193A variants. This suggests that the relatively high protein concentration used in the sedimentation velocity experiments resulted in a bias toward the observation of the tetrameric species. In fact, it is likely that all four of these variant enzymes exist as equilibrating mixtures of substantial populations of dimer and tetramer in solution.

The K_a values determined for DHDPS-Q196D and DHDPS-D193A suggest that these variants exist as equal populations of dimer and tetramer in the low micro molar range. This has implications for the kinetic characterisation of these variants as initial rate activity assays are typically carried with the protein at very low concentrations.

The fact that mutation of the dimer-dimer interface residues identifed in this work has caused significant alteration to the quaternary structure of DHDPS indicates that these

amino acid positions are important in the tetramerisation of the protein. Mutation of residues Q196 and D193 had the greatest effect on tetramerisation, presumably due to removal of the inter-dimer hydrogen bonds that these residues provide. Interestingly, the D193A mutation appears, from sedimentation velocity data, to have disrupted the quaternary structure to a greater extent than the D193Y mutation. Sedimentation equilibrium data for DHDPS-D193A will be required to confirm this. Introduction of the Q234D mutation appears to have had the least effect on the quaternary structure of the enzyme. This is as may be expected considering the mobile nature of this side chain (section 2.6.2)

4.6 Summary

A comprehensive biophysical characterisation of wild-type DHDPS and the DHDPS-variants was carried out to ascertain the effect of each of the single point mutations on the quaternary structure of the protein. DHDPS-L197D and DHDPS-L197Y were shown to be obligate dimers in solution. Sedimentation equilibrium data demonstrated that DHDPS-Q196D and DHDPS-D193A reside in equilibrium between dimer and tetramer, with K_a values in the micromolar range. Sedimentation velocity data suggested that DHDPS-L197Y and DHDPS-Q234D also displayed altered quaternary stracture; however, this was not quantified for these variants.

4.7 References

1. Schagger, H., and von Jagow, G. (1991) Blue native electrophoresis for isolation of membrane protein complexes in enzymatically active form. *Anal Biochem* **199**, 223-231
2. Schagger, H., Cramer, W. A., and von Jagow, G. (1994) Analysis of molecular masses and oligomeric states of protein complexes by blue native electrophoresis and isolation of membrane protein complexes by two-dimensional native electrophoresis. *Anal Biochem* **217**, 220-230
3. Schagger, H. (2001) Blue-native gels to isolate protein complexes from mitochondria. *Methods Cell Biol* **65**, 231-244
4. Schagger, H. (1995) Native electrophoresis for isolation of mitochondrial oxidative phosphorylation protein complexes. *Methods Enzymol* **260**, 190-202
5. Whitaker, J. R. (1963) Determination of molecular weights of proteins by gel filtration on Sephadex. *Anal Chem* **35**, 1950-1953
6. Andrews, P. (1965) The gel filtration behaviour of proteins related to their molecular weights over a wide range. *Biochem J* **96**, 595-606

7. Andrews, P. (1964) Estimation of the molecular weights of proteins by Sephadex gel filtration. *Biochem J* **91**, 222-233

8. Winzor, D. J. (2003) Analytical exclusion chromatography. *J Biochem Biophys Methods* **56**, 15-52

9. Winzor, D. J. (2003) The development of chromatography for the characterization of protein interactions: A personal perspective. *Biochem Soc Trans* **31**, 1010-1014

10. Ackers, G. K., and Thompson, T. E. (1965) Determination of stoichiometry and equilibrium constants for reversibly associating systems by molecular sieve chromatography. *Proc Natl Acad Sci, U S A* **53**, 342-349

11. Winzor, D. J., and Scheraga, H. A. (1963) Studies of chemically reacting systems on Sephadex. I. Chromatographic demonstration of the Gilbert theory. *Biochemistry* **172**, 1263-1267

12. Porath, J., and Flodin, P. (1959) Gel filtration: A method for desalting and group separation. *Nature* **183**, 1657-1659

13. Laue, T. M., and Stafford, W. F., 3rd. (1999) Modern applications of analytical ultracentrifugation. *Annu Rev Biophys Biomol Struct* **28**, 75-100

14. Lebowitz, J., Lewis, M. S., and Schuck, P. (2002) Modern analytical ultracentrifugation in protein science: a tutorial review. *Protein Sci* **11**, 2067-2079

15. Schuck, P. (2000) Size-distribution analysis of macromolecules by sedimentation velocity ultracentrifugation and Lamm equation modeling. *Biophys J* **78**, 1606-1619

16. Schuck, P., Perugini, M. A., Gonzales, N. R., Howlett, G. J., and Schubert, D. (2002) Size-distribution analysis of proteins by analytical ultracentrifugation: strategies and application to model systems. *Biophys J* **82**, 1096-1111

17. Vistica, J., Dam, J., Balbo, A., Yikilmaz, E., Mariuzza, R. A., Rouault, T. A., and Schuck, P. (2004) Sedimentation equilibrium analysis of protein interactions with global implicit mass conservation constraints and systematic noise decomposition. *Anal Biochem* **326**, 234-256

18. Laue, T. M., Shah, B. D., Ridgeway, T. M., and Pelletier, S. L. (1992) in *Analytical ultracentrifugation in biochemistry and polymer science*, pp. 90-125, The Royal Society of Chemistry, Cambridge

19. Perugini, M. A., Schuck, P., and Howlett, G. J. (2000) Self-association of human apolipoprotein E3 and E4 in the presence and absence of phospholipid. *J Biol Chem* **275**, 36758-36765

20. Shedlarski, J. G., and Gilvarg, C. (1970) The pyruvate-aspartic semialdehyde condensing enzyme of *Escherichia coli*. *J Biol Chem* **245**, 1362-1373

21. Gerrard, J. A. (1992) Studies on dihydrodipicolinate synthase. *D. Phil. thesis*, Oxford University

22. Richaud, F., Richaud, C., Ratet, P., and Patte, J. C. (1986) Chromosomal location and nucleotide sequence of the *Escherichia coli dap*A gene. *J Bacteriol* **166**, 297-300

23. Dobson, R. C., Valegard, K., and Gerrard, J. A. (2004) The crystal structure of three site-directed mutants of *Escherichia coli* dihydrodipicolinate synthase: further evidence for a catalytic triad. *J Mol Biol* **338**, 329-339

24. Borthwick, E. B., Connell, S. J., Tudor, D. W., Robins, D. J., Shneier, A., Abell, C., and Coggins, J. R. (1995) *Escherichia coli* dihydrodipicolinate synthase: characterization of the imine intermediate and the product of bromopyruvate treatment by electrospray mass spectrometry. *Biochem J* **305**, 521-524

Chapter Five

Kinetic analysis of wild-type DHDPS and the DHDPS variants.

5.1 Introduction

Kinetic analysis of wild-type and variant DHDPS was undertaken in order to ascertain the functional consequences of altering of the quaternary structure of the enzyme. Accurate and detailed analysis of DHDPS reaction kinetics, as catalysed by the wild-type and variant enzymes, required a quantitative assay system for the determination of reaction rate in the absence, or near absence, of product. Thus, initial rate measurement is routinely achieved by monitoring the depletion of substrates or accumulation of products over time, directly after the initiation of the reaction.

Three assay systems have been reported for the detection of DHDPS activity. The *o*-aminobenzaldehyde assay (1,2) yields largely qualitative measurements and is, therefore, primarily useful as a simple method of enzyme detection during purification. While the imidazole buffer assay (1,2) has been used in basic kinetic analysis of DHDPS from various sources (3-5), this system is unsuitable for detailed analysis. The coupled assay system, in which DHDPR is utilised as a coupling enzyme (1,2), has been developed to produce accurate time resolved rate data for DHDPS and has, therefore, been employed for kinetic analysis in this study.

Presented in this chapter is the rigorous kinetic and regulatory characterisation of wild-type DHDPS and the DHDPS variants. Kinetic descriptions and kinetic parameters of the altered enzymes are compared, both quantitatively and qualitatively, with those determined for the wild-type.

5.2 Assay systems for DHDPS activity

5.2.1 The *o*-aminobenzaldehyde assay

The assumption by early workers that the product of the condensation of pyruvate and (*S*)-ASA was a Δ^1-piperidine derivative led to the employment of *o*-aminobenzaldehyde for detection of DHDPS activity (1). The assumed product was expected to form a yellow dihydroquinazolium adduct with *o*-aminobenzaldehyde. However, addition of this compound to DHDPS reaction mixtures produced a purple chromophore under neutral or acidic conditions, providing the first evidence that the identity of the true product of DHDPS may be elusive (1). Nonetheless, this procedure provides a very simple method of qualitative detection of DHDPS activity, as the characteristic deep purple colouration develops specifically in the presence of the enzyme and its substrates. For this reason, the *o*-aminobenzaldehyde was routinely employed throughout this study for detection of DHDPS activity during purification of wild-type DHDPS and the DHDPS variants.

The absorbance at 540 nm of the purple chromophore allows its production to be monitored easily, and this assay has been used in semi-quantitative rate analysis of DHDPS by a number of groups (6-10). However, the use of this assay in initial rate determination makes a key assumption: that the rate of enzymatic reaction, rather than the rate of coloured adduct formation, is limiting. As a substantial lag time (~20 min) is observed between the initiation of the DHDPS reaction and the increase in absorbance at 540 nm, this assumption may not be valid. Additionally, as the identity of the coloured compound is unknown, quantification of the product is difficult.

5.2.2 The imidazole buffer assay

Incubation of DHDPS and its substrates in imidazole buffer at pH 7.4 results in a rise in concentration of a chromophore with a peak absorbance at 270 nm. This assay is simple and easy to perform, however, as with the *o*-aminobenzaldehyde assay, the chromophore formed has not been identified and the reaction follows a lag phase before linear increase of absorbance at 270 nm. This system continues to be used for kinetic analysis of DHDPS by other groups (4,5,11,12), but has been deemed unsuitable for the purposes of detailed analysis in this study for the same reason as outlined in section 5.2.1 above.

5.2.3 The coupled assay with DHDPR

Where the reaction of the enzyme of interest is difficult to monitor, a coupled assay system can be employed (13). The product of the enzymatic reaction of interest is used as the substrate for a second, coupling, enzymatic reaction, which can be easily monitored. The rate of reaction of the second enzyme can then be related directly to the rate of reaction of the first, assuming the product of the first does not accumulate. To ensure that the intermediate product reacts quickly, the activity of the coupling enzyme must be kept well in excess of the target enzyme activity.

Due to the difficulties in direct spectrophotometric measurement of the substrates and products of the DHDPS reaction, a coupled enzyme assay was developed (Figure 5.1), in which the product of the DHDPS reaction, dihydrodipicolinate, is reduced by the next enzyme of the DAP pathway, DHDPR, with concomitant oxidation of NADPH (1,2). As NADPH absorbs strongly at 340 nm, while $NADP^+$ exhibits little absorbance at this wavelength, the rate of oxidation of the cofactor can easily be quantified photometrically (ε_{340} = 6220 M^{-1} cm^{-1}). By ensuring that DHDPR activity in the reaction mixture is well in excess of DHDPS activity, the time resolved rate of oxidation of NADPH can be related in a 1:1 stoichiometry to the production of dihydrodipicolinate, since under these conditions the reaction catalysed by DHDPS is rate limiting.

Figure 5.1 *The coupled assay for DHDPS activity. The oxidation of NADPH by the coupling enzyme, DHDPR, is monitored at 340 nm.*

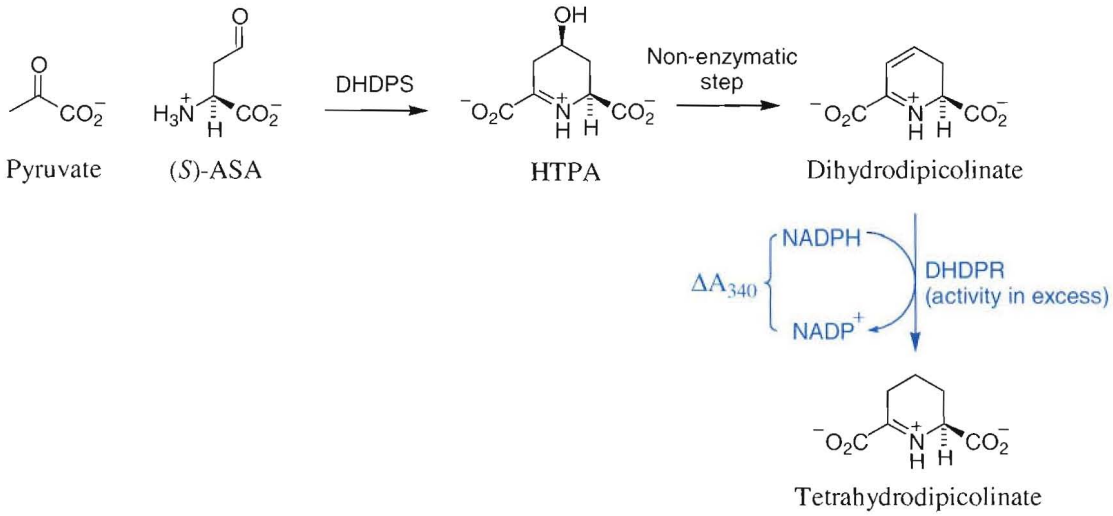

Despite the fact that this coupled assay is more favourable for initial rate determination than both the *o*-aminobenzaldehyde and the imidazole buffer assays, it has not been widely adopted for DHDPS rate determination, perhaps due to the necessity for large quantities of purified DHDPR. However, reports describing comprehensive kinetic analysis of DHDPS have largely employed this assay system (14-20).

Modifications to the coupled assay for use in this study

The coupled assay procedure used in this study followed that of Karsten (15) with slight modifications to optimise effectiveness for the range of kinetic investigations conducted. Assays were conducted at pH 8.0 in HEPES buffer. While it is often desirable to conduct initial activity measurements at close to physiological pH, this pH was chosen as it is close to the optimal pH for DHDPS activity of 8.4 (1), and there is no significant difference between kinetic parameters obtained at pH 8.0 and those obtained at pH 7.2 (21). Additionally, purification and storage of all enzymes was carried out at pH 8.0 (sections 3.3 and 3.4), as the enzyme is most stable at this pH. Alterations in pH are obviously undesirable, especially in the case of the variants with altered structural stability. All assays were conducted at a constant temperature of 30°C using a circulating water bath to heat the spectrophotometer stage. Reactions were incubated for defined times at this temperature and initiated in all cases by addition of a minimal volume of chilled (*S*)-ASA solution to prevent temperature alteration.

DHDPR activity was typically held at ten times the maximal DHDPS activity being investigated. Controls were routinely run by varying the concentration of DHDPR around this level, to ensure no deviation in apparent activity. These conditions allowed measurement of initial rates of DHDPS reaction within the appropriate range and, subsequently, determination of accurate kinetic parameters for the wild-type and variant enzymes.

5.3 Steady state kinetics of *E. coli* DHDPS.

As described in section 1.3.3, the ping-pong kinetic mechanism has been assigned to DHDPS (3,4,15,22). The ping-pong mechanism describes a system where catalysis proceeds through a covalent enzyme-substrate complex with an irreversible step

between the ordered binding of substrates. Typically, this irreversible step is the release of the first product on formation of the covalent intermediate, and thus the enzyme can exist in a free or substituted form (13).

In the case of DHDPS, the binding of pyruvate to the free enzyme (E) leads to formation of a Schiff base with the release of water (section 1.3.5). The subsequent tautomerisation of this Schiff base to an enamine with release of a proton is thought to constitute the irreversible step (15) and has been shown to occur before binding of (*S*)-ASA (2). (*S*)-ASA then binds to the stable substituted form (F), allowing product formation and release, and regeneration of free enzyme:

$$E + Pyr \underset{k_{-1}}{\overset{k_1}{\rightleftharpoons}} E.Pyr \xrightarrow{k_2} F + ASA \underset{k_{-3}}{\overset{k_3}{\rightleftharpoons}} F.ASA \xrightarrow{k_4} E + HTPA$$

The kinetic behaviour of *E. coli* DHDPS has been thoroughly investigated previously (15). The observed initial velocity patterns that produce parallel lines on a double reciprocal plot suggested the ping-pong mechanism and confirmed the findings of others (3,4,22). However, this observation alone is not sufficient evidence upon which to base the assignment of the mechanism.

Substrate inhibition studies showed competitive substrate inhibition with respect to pyruvate, which is diagnostic of the ping-pong mechanism (15). Substrate inhibition by (*S*)-ASA, was also observed (15); however, this behaviour was subsequently found to be artefactual (19). This does not preclude the assignment of the ping-pong model, and the identification of the covalent enzyme-pyruvate complex in the absence of (*S*)-ASA (2,4,23) further supports this mechanism.

5.4 Selwyn's test for enzyme inactivation

An enzyme may lose activity for a large number of reasons. In many cases, enzymes are much more stable at high concentrations than at low concentrations and will therefore lose activity rapidly when diluted from a stock solution into an assay mixture. Thermal lability of the enzyme of interest must also be considered, as the temperature of incubation of the assay mixture may cause gradual structural breakdown of the enzyme, leading to inactivation. Obviously, inactivation during the

time course of the assay must be avoided as it can lead to errors in measurement of the initial rate, and may produce errors in the type of behaviour observed.

The consideration of thermal lability is particularly relevant to the kinetic analysis of the DHDPS variants in this study, as during purification (section 3.4) it was observed that alteration to the quaternary structural properties of the enzyme lead to increased activity loss during the heat shock-step. Accordingly, Selwyn's test for enzyme inactivation (24) was performed for both wild-type and variant enzymes to assess their stability during the time course used in the assay and, thus, their suitability for accurate kinetic analysis. This test involves monitoring the state of the reaction over a given time period using different concentrations of enzyme. If the enzyme is becoming inactivated over this time course, plots of reaction state *vs.* initial enzyme concentration multiplied by time will not overlay. Conversely, overlaying curves indicate that no detectable enzyme inactivation is occurring. A time course of three to five minutes was chosen for analysis by Selwyn's test, corresponding to the period of incubation of the enzymes during initial rate measurements.

Figure 5.2 shows Selwyn's test for all enzymes. Test traces for wild-type DHDPS, DHDPS-Q196D, DHDPS-D193A, DHDPS-D193Y, and DHDPS-Q234D overlay, confirming no detectable inactivation in these enzymes under the conditions of the assay. DHDPS-L197D and DHDPS-L197Y show traces that do not overlay. In the case of DHDPS-L197D, the plot indicates simple inactivation of the enzyme over the time course of the assay (Figure 5.2 DHDPS-L197D#1). Inspection of the plots revealed that the traces for the two highest concentrations of the enzyme showed reasonable agreement. Repetition of Selwyn's test indicated that inactivation was no longer occurring at enzyme concentrations greater than 0.042 mg/ml (Figure 5.2 DHDPS-L197D#2). Thus, a concentration of 0.63 mg/ml DHDPS-L197D was employed for analytical activity assays.

Figure 5.2 *Selwyns test for enzyme inactivation for all studied enzyme variants. $E_0.t$ is the initial enzyme volume in µl multiplied by time in seconds. ΔA_{340} is the the initial A_{340} measurement minus the current A_{340} measurement and gives an indication of the consumption of NADPH. #1 and #2 refer to repeated experiments. Legends refer to the volume of stock enzyme solution added to the assay. Stock concentrations used were as follows: wild-type DHDPS - 0.075 mg/ml, DHDPS-L197D - 0.42 mg/ml, DHDPS-L197Y - 0.32, DHDPS-Q196D - 0.61 mg/ml, DHDPS-D193A - 0.88 mg/ml, DHDPS-D193Y - 0.33 mg/ml, DHDPS-Q234D - 0.20 mg/ml.*

Wild-type DHDPS

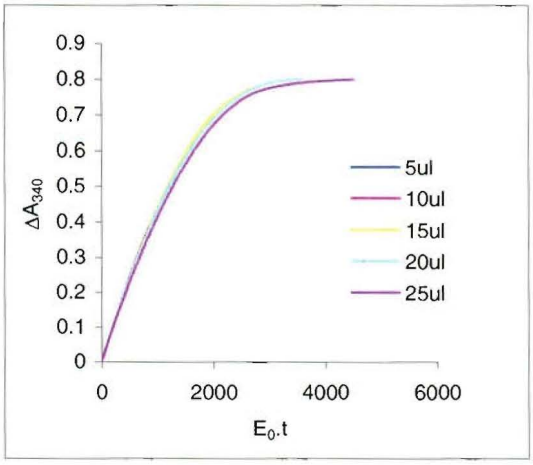

DHDPS-L197D#1

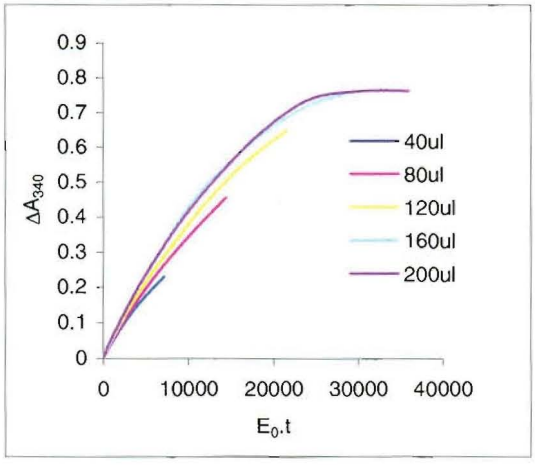

DHDPS-L197D#2

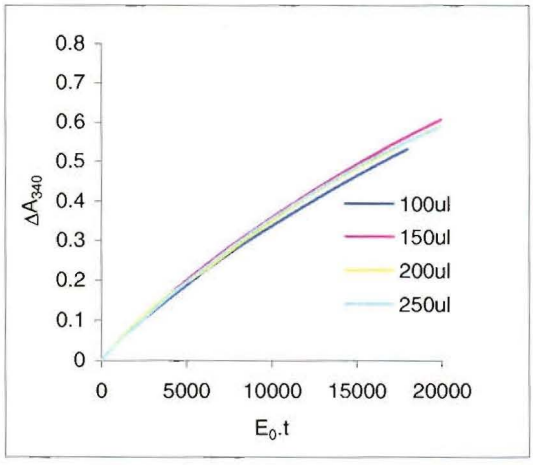

DHDPS-L197Y#1

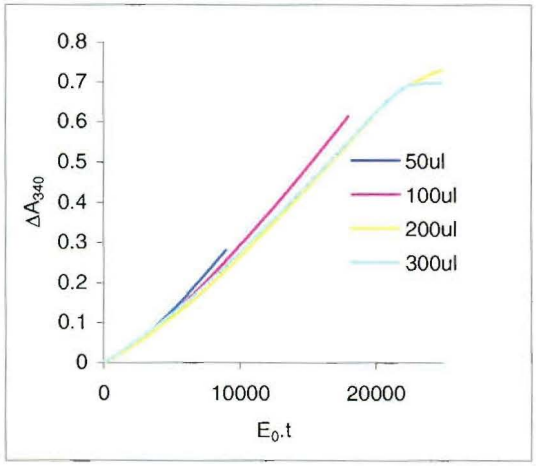

DHDPS-L197Y#2

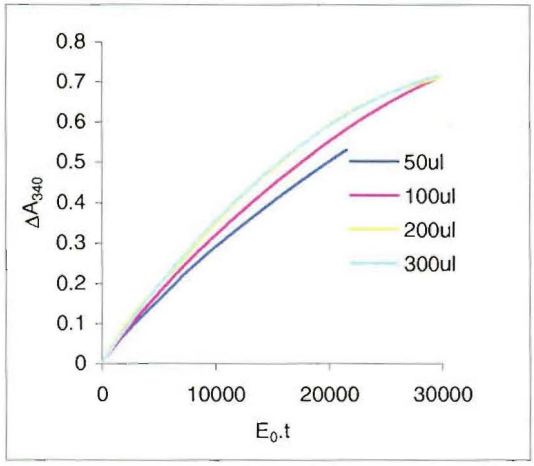

Figure 5.2 *contd.*

DHDPS-Q196D

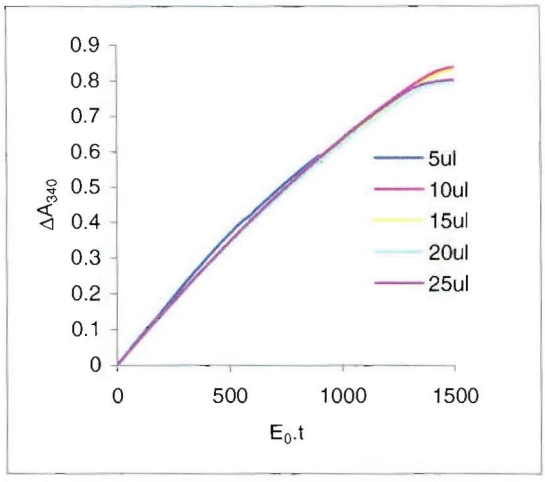

DHDPS-D193A

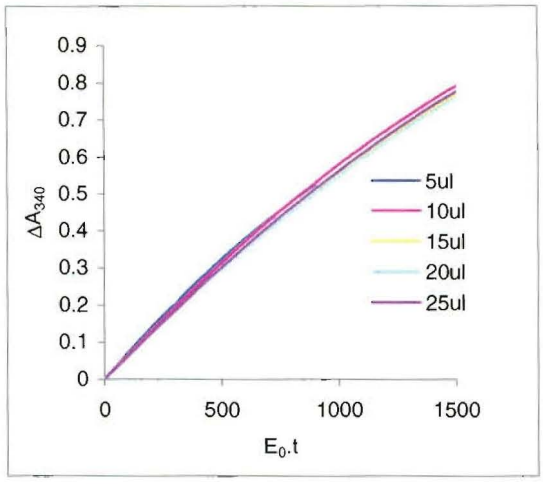

DHDPS-D193Y

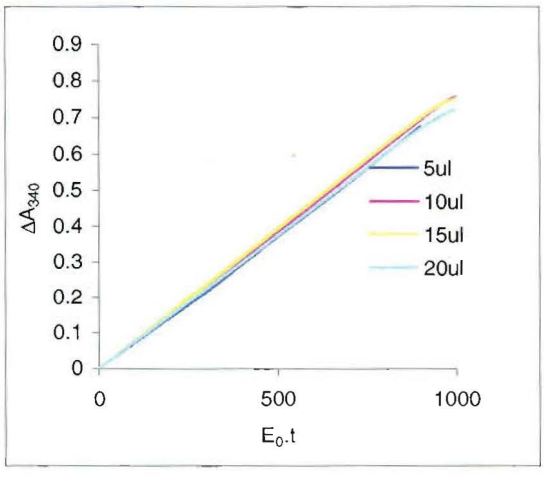

DHDPS-Q234D

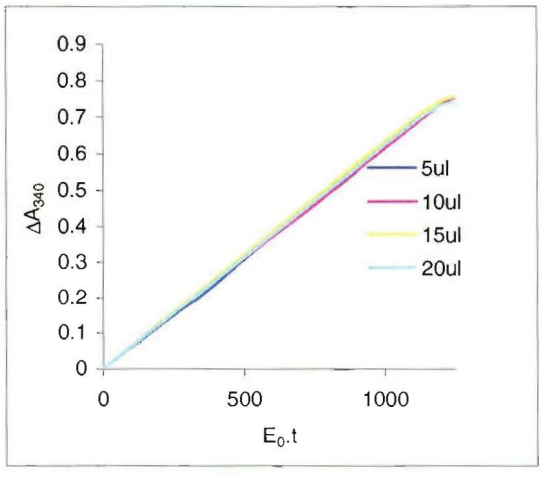

Interestingly, when Selwyn's test was performed for DHDPS-L197Y, plotted data indicated that the enzyme was *activating* during the time course used (Figure 5.2 DHDPS-L197Y#1). Alteration of the preincubation conditions employed for the test circumvented this activation, however, like DHDPS-L197D, DHDPS-L197Y now showed inactivation (Figure 5.2 DHDPS-L197Y#2). Again, this inactivation was found to be concentration dependent and an enzyme concentration of 0.096 mg/ml DHDPS-L197Y was employed for initial rate analysis.

In light of the puzzling observation of activation in DHDPS-L197Y, Selwyn's test was repeated for DHDPS-L197D using the exact conditions employed for DHDPS-L197Y. Under these conditions DHDPS-L197D displayed the same activation behaviour, indicating that the turnover rate of both dimeric enzymes was apparently

increasing over time under the conditions of the assay. This phenomenon was further investigated in a separate study and will be discussed further in Chapter seven.

5.5 Kinetic analysis of wild-type *E. coli* DHDPS and the variants

The steady state kinetic behaviour of all DHDPS enzymes was investigated by measurement of initial rates at varied pyruvate and (*S*)-ASA concentrations, using the coupled assay as described in section 5.2.3. Following Cornish-Bowden (13), substrate concentrations were varied between 0.2 K_m and 10 K_m, using a preliminary single curve estimate of apparent K_m as a starting point. All initial rate measurements were made in triplicate and resulting data were analysed by non-linear curve fitting using the EnzFitter program (Biosoft, Cambridge), allowing determination of k_{cat} and K_m values. Initial rate measurements were converted to standard units, where 1 unit is equal to the consumption of 1 µmol NADPH per minute per milligram of protein in a 1 ml assay.

Kinetic data were fitted to both a ping-pong Bi Bi model (Equation 5.1) and a ternary complex model (Equation 5.2).

$$v = VAB / (K_{mB}A + K_{mA}B + AB) \qquad \text{Equation 5.1 (13)}$$

$$v = VAB / (K_{mB}A + K_{mA}B + AB + K_{sA}K_{mB}) \qquad \text{Equation 5.2 (13)}$$

Here V is the maximal velocity, K_{mA} and K_{mB} are the Michaelis-Menten constants for the two substrates, A and B are the substrate concentrations, and v is the initial velocity. K_{sA}, which appears in Equation 5.2, is the binding constant for substrate A to the E enzyme form. Data were fitted to appropriate models based on the σ value of the non-linear regression and the lowest standard errors associated with the kinetic constants (25). Where the two models showed similar σ values an F test was utilised to assess whether the difference between fits was significant. Table 5.1 shows the kinetic constants resulting from this analysis.

Table 5.1 *Kinetic constants determined for wild-type DHDPS and the variant enzymes. DHDPS-D193Y and DHDPS-Q234D underwent a simplified kinetic analysis yielding apparent kinetic parameters (sections 5.5.6 and 5.5.7).*

	Wild-type DHDPS	DHDPS-L197D	DHDPS-L197Y	DHDPS-Q196D	DHDPS-D193A
k_{cat} (s^{-1})	78.0 ± 0.06	1.97 ± 0.05	1.11 ± 0.05	13.28 ± 0.16	9.15 ± 0.16
Relative k_{cat} (%)	100	2.52	1.42	17.0	11.7
K_{mPyr} (mM)	0.16 ± 0.003	0.68 ± 0.04	1.11 ± 0.10	0.32 ± 0.01	0.44 ± 0.02
k_{cat}/K_{mPyr} (mM^{-1} sec^{-1})	487.5 ± 9.1	2.90 ± 0.19	1.0 ± 0.1	41.5 ± 1.4	20.8 ± 1.0
K_{mASA} (mM)	0.13 ± 0.002	0.15 ± 0.01	0.18 ± 0.01	0.15 ± 0.005	0.17 ± 0.007
k_{cat}/K_{mASA} (mM^{-1} sec^{-1})	600.0 ± 9.2	13.1 ± 0.9	6.17 ± 0.44	88.5 ±3.1	53.8 ± 2.4
K_{SA} (mM)	-	0.032 ± 0.011	0.028 ± 0.014	-	-

	DHDPS-D193Y		DHDPS-Q234D	
Varied substrate	Pyruvate	(*S*)-ASA	Pyruvate	(*S*)-ASA
k_{cat}^{app} (s^{-1})	7.21 ± 0.14	6.46 ± 0.12	11.78 ± 0.15	12.39 ± 0.42
Relative k_{cat} (%)	9.2	8.3	15.1	15.9
K_{mPyr}^{app} (mM)	0.57 ± 0.04	-	0.46 ± 0.02	-
K_{mASA}^{app} (mM)	-	0.15 ± 0.01	-	0.15 ± 0.02
$k_{cat}^{app}/K_{mPyr}^{app}$ (mM^{-1} sec^{-1})	12.6 ± 0.9	-	25.6 ± 1.2	-
$k_{cat}^{app}/K_{mASA}^{app}$ (mM^{-1} sec^{-1})	-	43.1 ± 3.0	-	82.6 ± 11.4

Direct plots of raw data overlaid with calculated fit curves were generated for visualisation of the fitted data. Lineweaver-Burke or double-reciprocal plots (1/rate *vs.* 1/[substrate]) were produced to allow visual inspection of data trends with respect to kinetic patterns. This is the most commonly used type of plot in kinetic studies, however, due to the nature of the reciprocal plot, the visual impression of experimental error is misleading and the impression of residuals is exaggerated as rate decreases (13). The Eadie-Hofstee plot (rate/[substrate] *vs.* rate) was also included as it produces a more accurate indication of the quality of the data. The presence of v in both coordinates results in errors producing deviation towards or away from the origin rather than parallel to the ordinate axis (13). Standardised percentage residual plots *vs.* substrate concentration were also generated as an aid to evaluation of the quality of the data. These are useful for identifying systematic errors in data that can indicate whether an incorrect model has been used. It should be noted here that while residuals should be normally distributed around zero, they will be expected to show less variation as substrate concentration increases. This is because constant experimental error will lead to reduced proportional error as rate increases (13).

5.5.1 Steady state kinetic analysis of wild-type DHDPS

Initial rate data obtained by assay of pure wild-type DHDPS fitted the ping-pong model with an r^2 value of 0.999 and p>F of much less than 0.001. Kinetic constants generated from this regression agreed well with those determined previously both in this laboratory and elsewhere (15). The K_m value of 0.16 ± 0.003 mM determined for pyruvate is consistent with the value determined by Karsten (15) of 0.194 ± 0.033 mM. This value is also consistent with those of other workers. Coulter (14) reports a K_{mPyr} in the range of (0.11–0.13) mM, while Yugari and Gilvarg (1) report a K_{mPyr} of 0.25 mM. Likewise, the K_m value for (*S*)-ASA of 0.13 ± 0.002 mM determined from the regression is essentially identical to the reported value of 0.124 ± 0.011 mM determined by Karsten (15), and also agrees well with other reports from the literature. Coulter (14) reports a K_{mASA} range of (0.1–0.14) mM at a pH of 7.2, Yugari and Gilvarg (1) found the K_{mASA} to be 0.13 mM at a pH of 7.4 while Pearce (21) reports a K_{mASA} range of (0.10–0.46) mM.

The catalytic turnover number (k_{cat}) of 78.0 sec^{-1} calculated here agrees well with values obtained by other workers in this laboratory (Dobson, R. C. J., Roberts, S. J. *pers. comm.*); however, the k_{cat} value of 188.0 sec^{-1} reported by Karsten(15) is

significantly higher than that determined in this study. This difference can most likely be attributed to variation in the conditions employed for the coupled assay. Figures 5.3 and 5.4 show plots of initial rate data collected for wild-type DHDPS overlaid with the fitted data for the ping-pong model. Data is represented with respect to pyruvate concentration (Figure 5.3) and (*S*)-ASA concentration (Figure 5.4).

Figure 5.3 *Kinetic plots of wild-type DHDPS with respect to pyruvate concentration at various (S)-ASA concentrations. A is a direct plot of initial rate data overlayed with fit data for the ping-pong model generated by non-linear regression (curves). B and C are Lineweaver-Burke and Eadie-Hofstee plots of the same data respectively. D is a plot of percentage residuals for each data point* ($100\times(v_{obs}-v_{cal})/v_{cal}$). *v is the mean initial rate in* $\mu mol_{NADPH}\ mg^{-1}\ min^{-1}$, *and [Pyruvate] refers to pyruvate concentration. The* r^2 *value for the fit was 0.999 and p>F was much less than 0.001.*

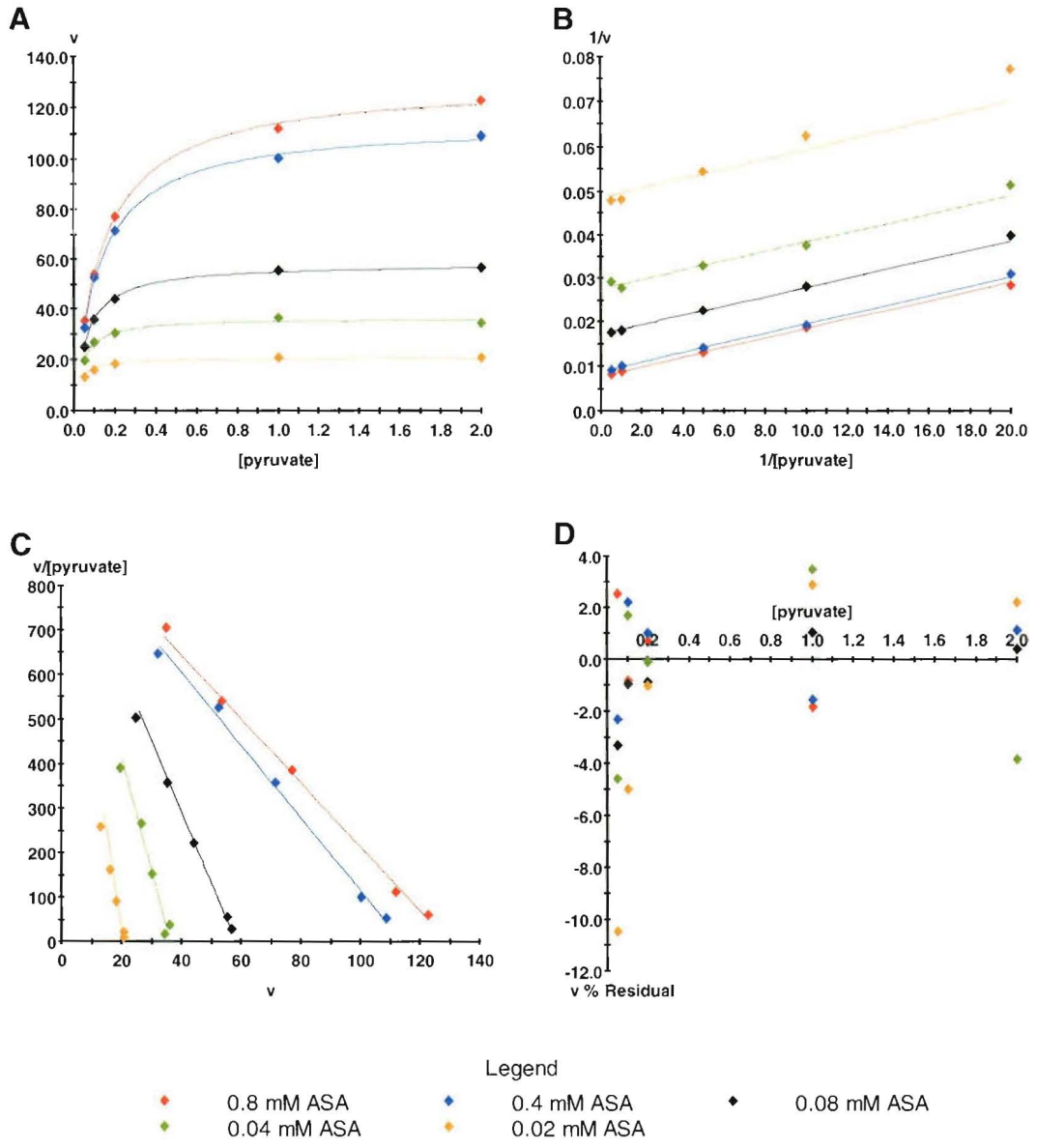

Figure 5.4 *Kinetic plots of wild-type DHDPS with respect to (S)-ASA concentration at various pyruvate concentrations. A is a direct plot of initial rate data overlayed with fit data for the ping-pong model generated by non-linear regression (curves). B and C are Lineweaver-Burke and Eadie-Hofstee plots of the same data respectively. D is a plot of percentage residuals for each data point ($100\times(v_{obs}-v_{cal})/v_{cal}$). v is the mean initial rate in $\mu mol_{NADPH}\ mg^{-1}\ min^{-1}$, and [ASA] refers to (S)-ASA concentration. The r^2 value for the fit was 0.999 and p>F was much less than 0.001.*

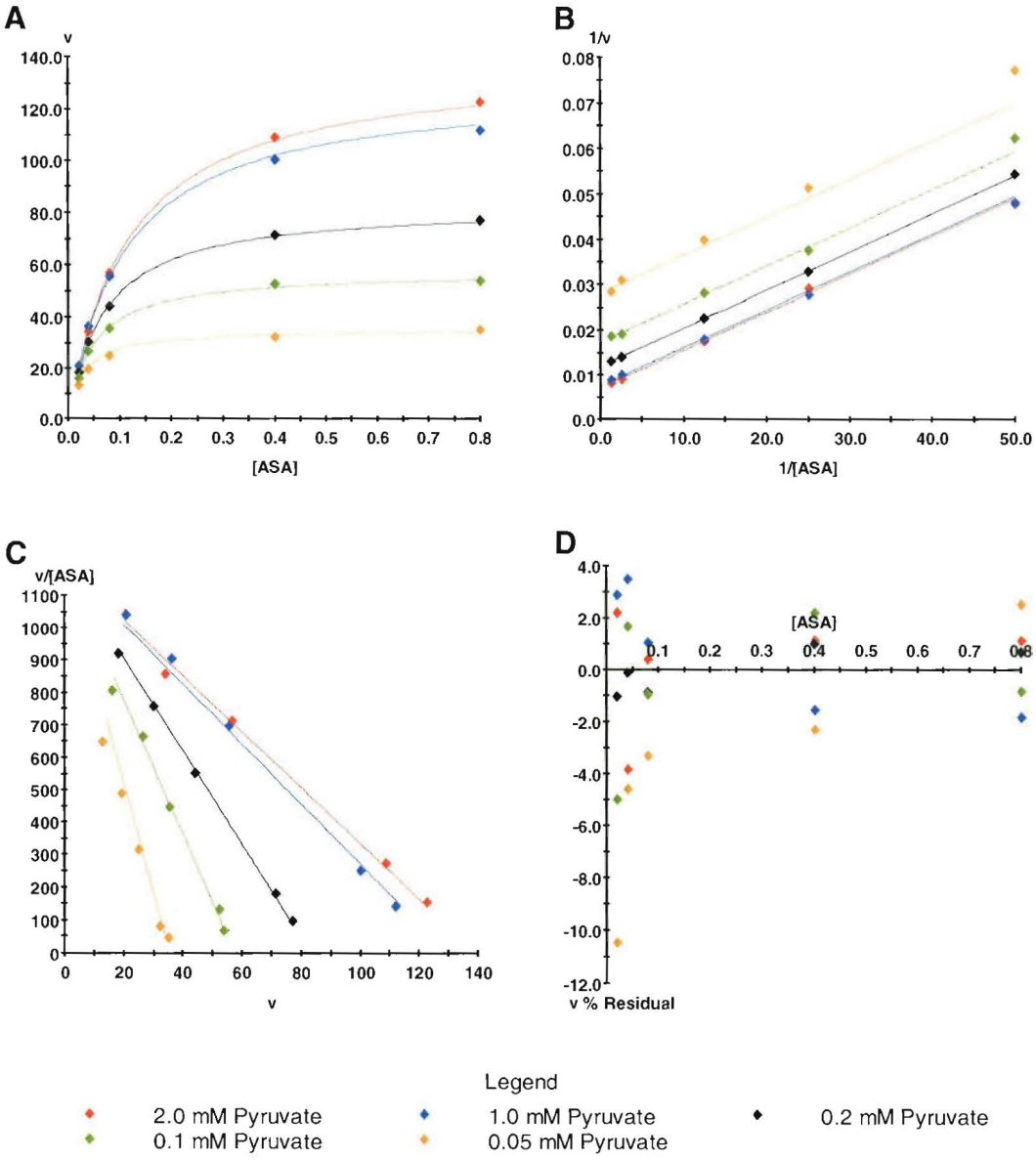

5.5.2 Steady state kinetic analysis of DHDPS-L197D

The activity of the dimeric variant, DHDPS-L197D, was found to be severely attenuated with respect to the wild-type enzyme. The k_{cat} of 1.97 sec^{-1} determined for DHDPS-L197D is only 2.52% of that of wild-type DHDPS and represents an approximate 40-fold reduction in catalytic efficiency. Strikingly, initial rate data for DHDPS-L197D showed a significantly better fit to the compulsory ordered ternary complex kinetic model (r^2 = 0.997 p>F much less than 0.001) than to the ping-pong model, indicating a shift in kinetic mechaninsm. This can be seen in the trend of converging data on the double reciprocal plot in Figures 5.5B and 5.6B. In order to ensure that this shift in data trend was not artefactual, the kinetic experiment was repeated using two concentrations of pyruvate differing by one order of magnitude and a range of (*S*)-ASA concentrations incorporating both higher and lower values than those used in the original experiment (13) (data not shown). Fitting this new data again revealed a converging trend, indicating that the shift in kinetic mechanism was a real observation.

Concomitant with the attenuation of activity was the observation of a greater than four fold increase in the K_m for pyruvate from 0.16 mM (wild-type) to 0.68 mM. This result is interesting, as it suggests that the reduction in catalytic efficiency may be, at least in part, due to perturbation of the binding of pyruvate to the enzyme. The K_m of the enzyme for (*S*)-ASA remains relatively unchanged at 0.15 mM. Figures 5.5 and 5.6 show kinetic plots of initial rate data for DHDPS-L197D and fitted data for the ternary-complex mechanism.

Figure 5.5 *Kinetic plots of DHDPS-L197D with respect to pyruvate concentration at various (S)-ASA concentrations. A is a direct plot of initial rate data overlayed with fit data for the ternary complex model generated by non-linear regression (curves). B and C are Lineweaver-Burke and Eadie-Hofstee plots of the same data respectively. D is a plot of percentage residuals for each data point ($100\times(v_{obs}-v_{cal})/v_{cal}$). v is the mean initial rate in $\mu mol_{NADPH}\ mg^{-1}\ min^{-1}$, and [Pyruvate] refers to pyruvate concentration. The r^2 value for the fit was 0.997 and p>F was much less than 0.001.*

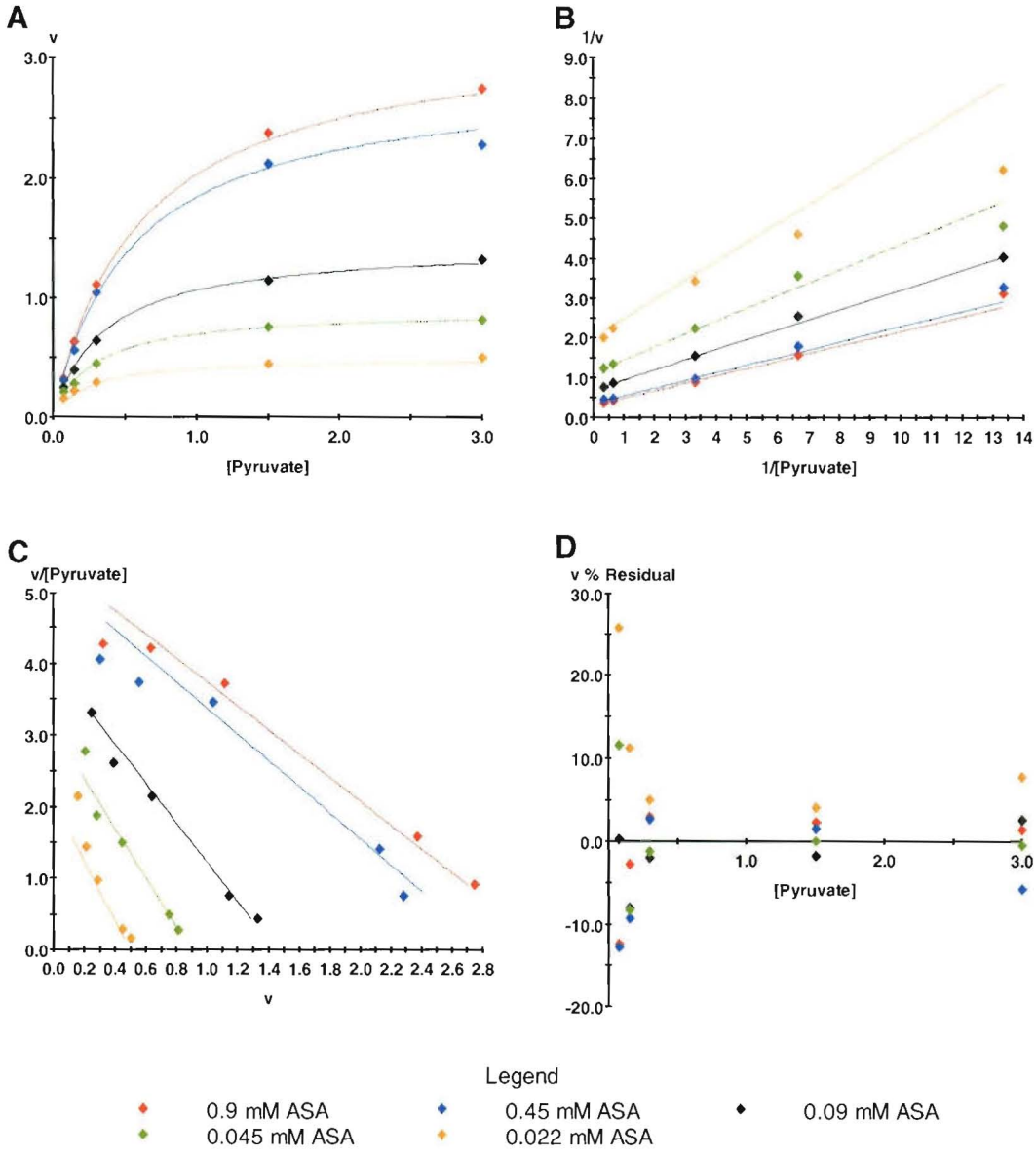

Figure 5.6 *Kinetic plots of DHDPS-L197D with respect to (S)-ASA concentration at various pyruvate concentrations. A is a direct plot of initial rate data overlayed with fit data for the ternary complex model generated by non-linear regression (curves). B and C are Lineweaver-Burke and Eadie-Hofstee plots of the same data respectively. D is a plot of percentage residuals for each data point ($100\times(v_{obs}-v_{cal})/v_{cal}$). v is the mean initial rate in $\mu mol_{NADPH}\ mg^{-1}\ min^{-1}$, and [ASA] refers to (S)-ASA concentration. The r^2 value for the fit was 0.997 and p>F was much less than 0.001.*

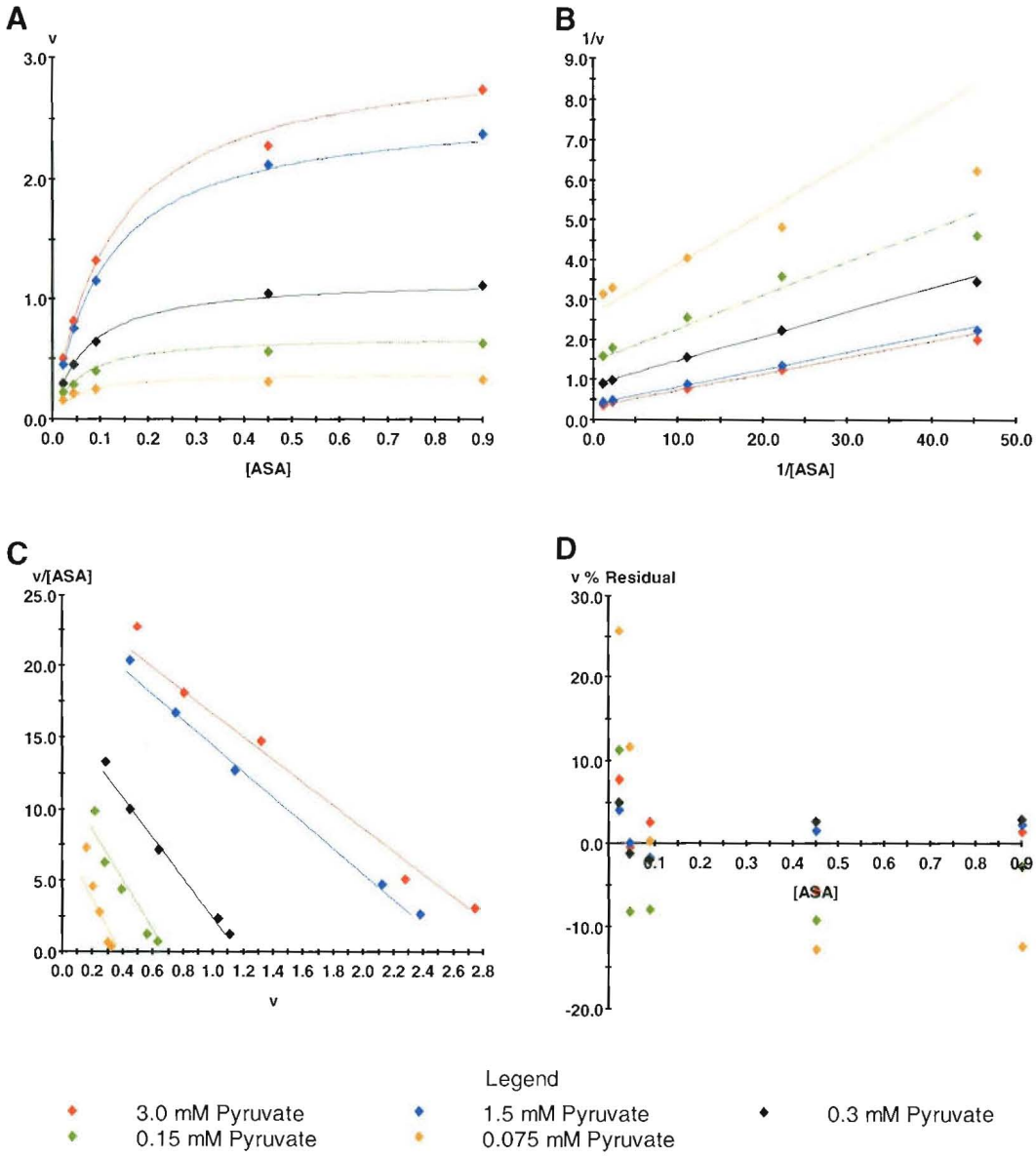

5.5.3 Steady state kinetic analysis of DHDPS-L197Y

The results of the steady state kinetic analysis of the dimeric variant DHDPS-L197Y were very similar to those of DHDPS-L197D. The activity of DHDPS-L197Y, was reduced to 1.42% of that of the wild-type enzyme, with a k_{cat} value of 1.11 sec^{-1}. Again, initial rate data for DHDPS-L197Y showed a better fit to the ternary complex kinetic model (r^2 = 0.997 p>F much less than 0.001) than to the ping-pong model. Here, the significance of the difference between the fits was not as great as with DHDPS-L197D; however, visually, the fit for the ternary complex model (Figure 5.7B and 5.8B) describes the data far better than the fit for the ping-pong model.

The K_m value for pyruvate, determined as 1.11 mM, is almost seven-fold that of the wild-type enzyme. This further increase over the K_m value obtained for DHDPS-L197D may be reflected in the higher attenuation of activity observed in DHDPS-L197Y. Again, the K_m of the enzyme for (*S*)-ASA remains relatively unchanged at 0.18 mM. Figures 5.7 and 5.8 show kinetic plots of initial rate data for DHDPS-L197Y and fitted data for the ternary complex mechanism.

Figure 5.7 *Kinetic plots of DHDPS-L197Y with respect to pyruvate concentration at various (S)-ASA concentrations. A is a direct plot of initial rate data overlayed with fit data for the ternary complex model generated by non-linear regression (curves). B and C are Lineweaver-Burke and Eadie-Hofstee plots of the same data respectively. D is a plot of percentage residuals for each data point ($100\times(v_{obs}-v_{cal})/v_{cal}$). v is the mean initial rate in $\mu mol_{NADPH}\ mg^{-1}\ min^{-1}$, and [Pyruvate] refers to pyruvate concentration. The r^2 value for the fit was 0.997 and p>F was much less than 0.001.*

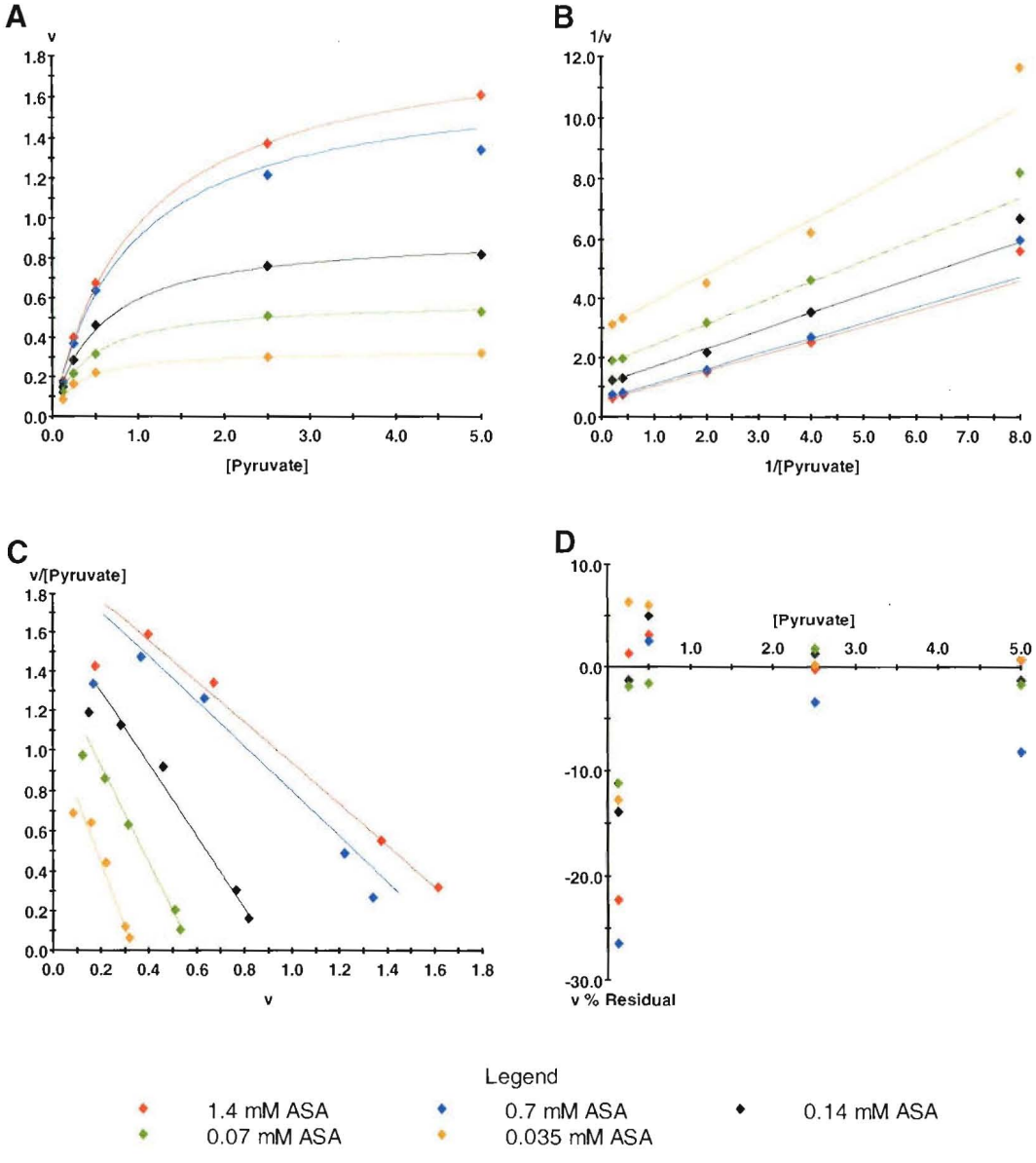

Figure 5.8 *Kinetic plots of DHDPS-L197Y with respect to (S)-ASA concentration at various pyruvate concentrations. A is a direct plot of initial rate data overlayed with fit data for the ternary complex model generated by non-linear regression (curves). B and C are Lineweaver-Burke and Eadie-Hofstee plots of the same data respectively. D is a plot of percentage residuals for each data point ($100\times(v_{obs}-v_{cal})/v_{cal}$). v is the mean initial rate in $\mu mol_{NADPH}\ mg^{-1}\ min^{-1}$, and [ASA] refers to (S)-ASA concentration. The r^2 value for the fit was 0.997 and p>F was much less than 0.001.*

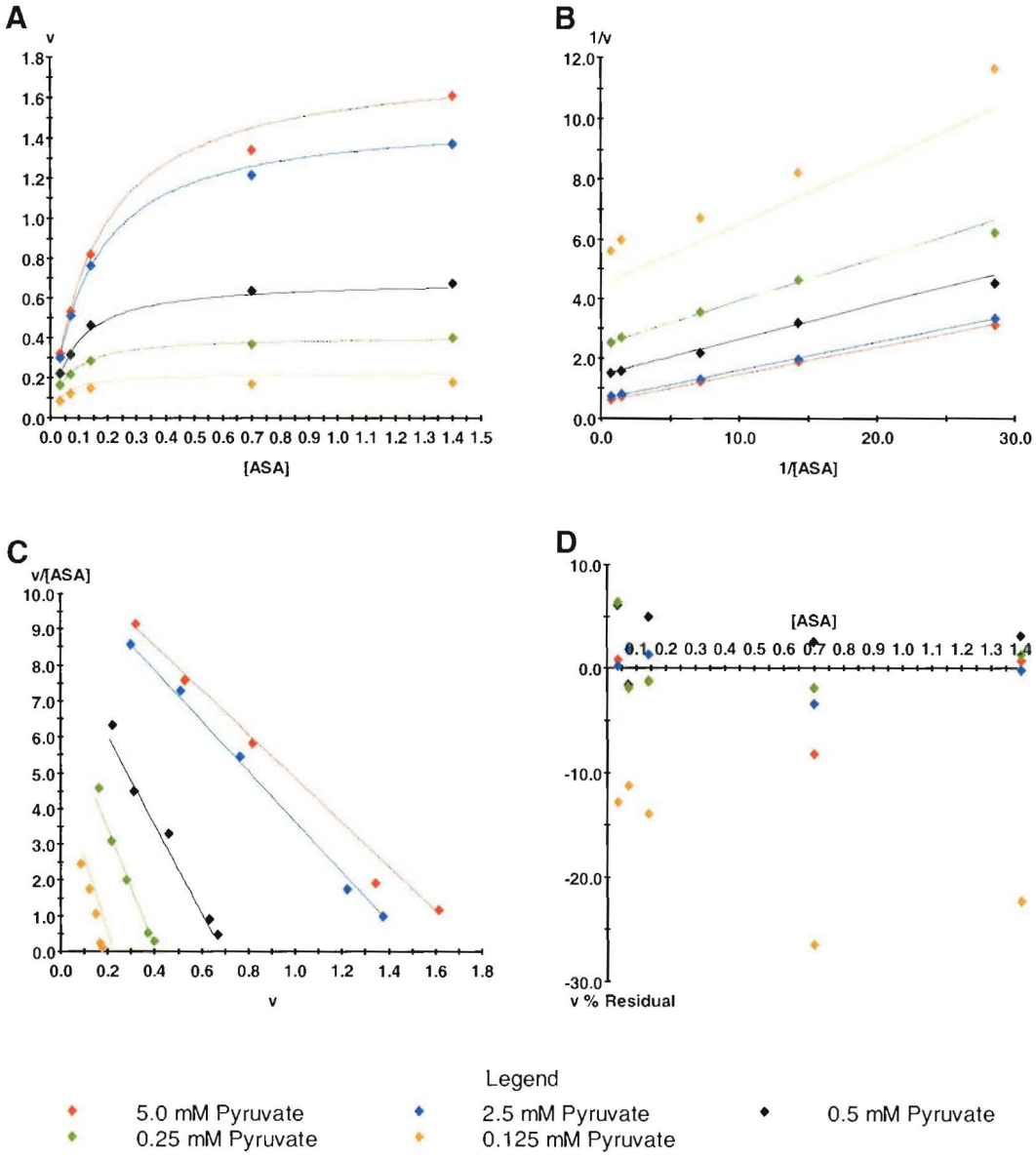

5.5.4 Steady state kinetic analysis of DHDPS-Q196D

Initial rate data collected for DHDPS-Q196D was fitted to the ping-pong model (r^2 = 0.997, p>F much less than 0.001) and shows the characteristic parallel data trends of this mechanism on the double reciprocal plot. Fit of the data to the ternary complex mechanism was attempted, in light of the results obtained for the L197D and L197Y variants. However, as the quality of this fit was poor and the regression produced nonsensical values for kinetic parameters, this mechanism was rejected.

As may be expected, attenuation of catalytic efficiency in this variant was not nearly as pronounced as in the true dimeric variants. DHDPS-Q196D displayed 17.0% (k_{cat} = 13.28 sec^{-1}) of wild type activity and displayed only a two-fold increase in K_m for pyruvate (K_{mPyr} = 0.32 mM). The K_m for (*S*)-ASA was unchanged at 0.15 mM. Figures 5.9 and 5.10 show kinetic plots of initial rate data for DHDPS-Q196D and fitted data for the ping-pong mechanism.

Figure 5.9 *Kinetic plots of DHDPS-Q196D with respect to pyruvate concentration at various (S)-ASA concentrations. A is a direct plot of initial rate data overlayed with fit data for the ping-pong model generated by non-linear regression (curves). B and C are Lineweaver-Burke and Eadie-Hofstee plots of the same data respectively. D is a plot of percentage residuals for each data point ($100\times(v_{obs}-v_{cal})/v_{cal}$). v is the mean initial rate in $\mu mol_{NADPH}\ mg^{-1}\ min^{-1}$, and [Pyruvate] refers to pyruvate concentration. The r^2 value for the fit was 0.997 and p>F was much less than 0.001.*

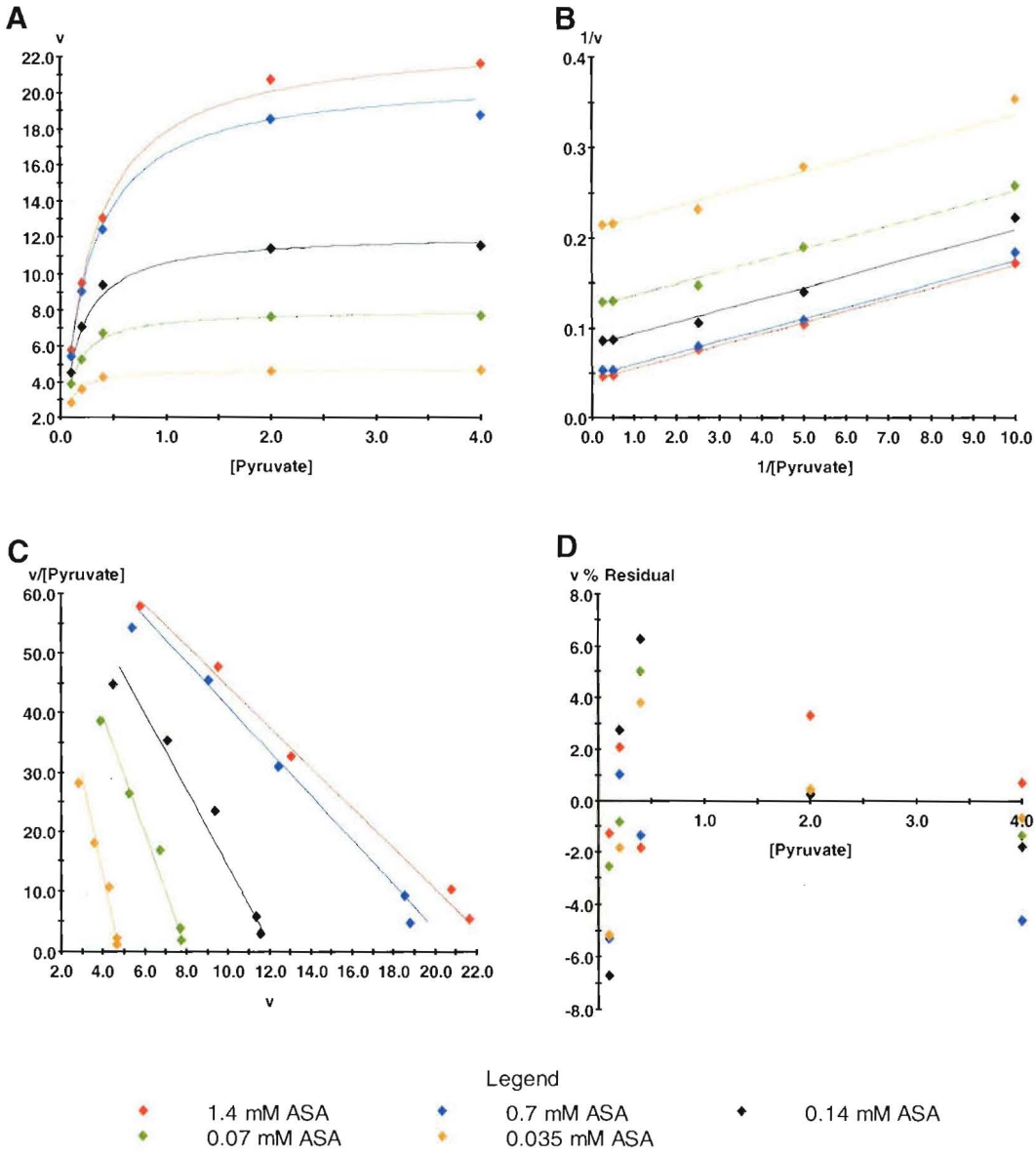

Figure 5.10 *Kinetic plots of DHDPS-Q196D with respect to (S)-ASA concentration at various pyruvate concentrations. A is a direct plot of initial rate data overlayed with fit data for the ping-pong model generated by non-linear regression (curves). B and C are Lineweaver-Burke and Eadie-Hofstee plots of the same data respectively. D is a plot of percentage residuals for each data point ($100\times(v_{obs}-v_{cal})/v_{cal}$). v is the mean initial rate in $\mu mol_{NADPH}\ mg^{-1}\ min^{-1}$, and [ASA] refers to (S)-ASA concentration. The r^2 value for the fit was 0.997 and p>F was much less than 0.001.*

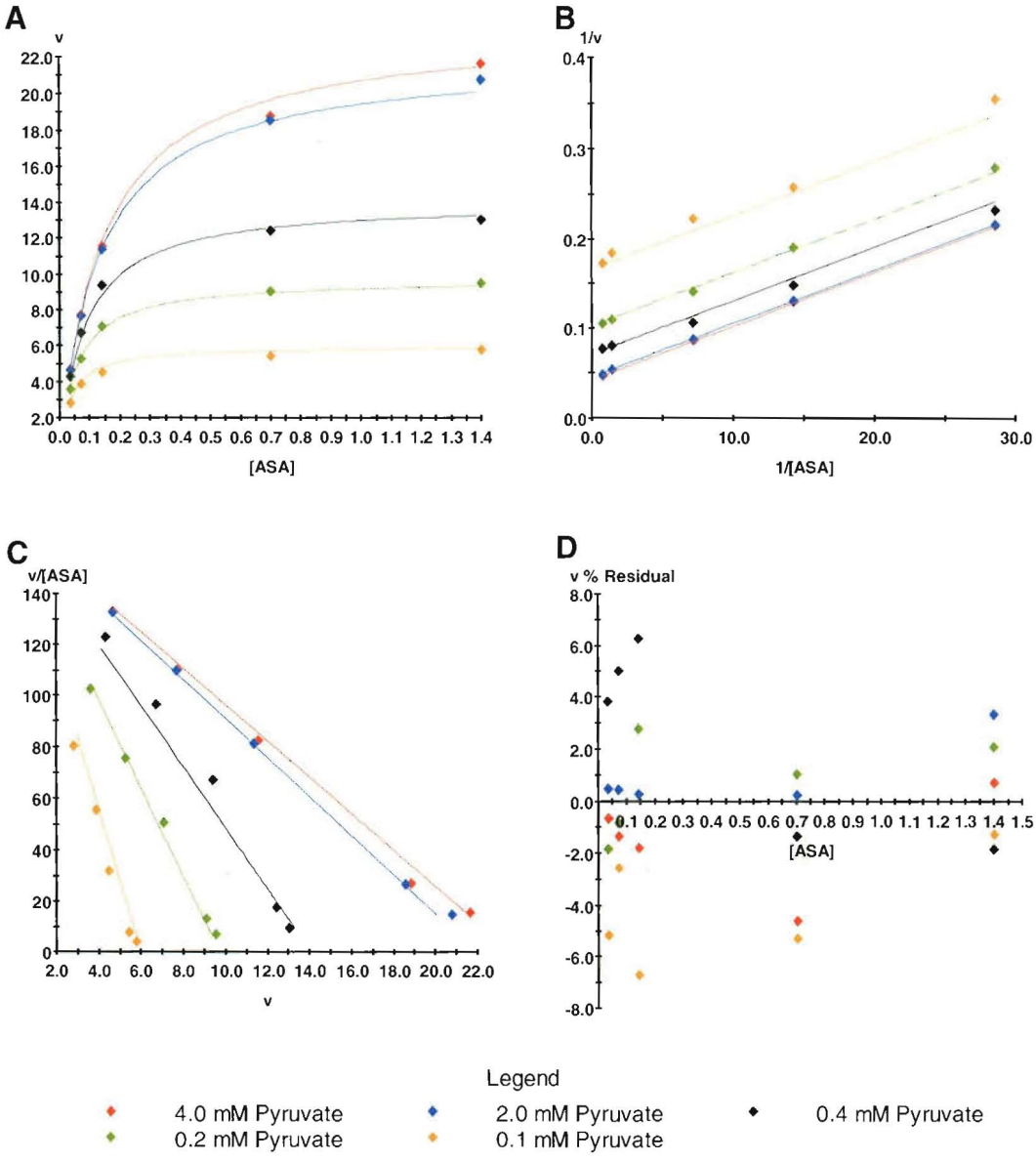

5.5.5 Steady state kinetic analysis of DHDPS-D193A

Like DHDPS-Q196D, initial rate data collected for DHDPS-D193A fitted well to the ping-pong kinetic model ($r^2 = 0.996$, p>F much less than 0.001), but did not produce a meaningful fit to the ternary complex model. The catalytic activity of DHDPS-D193A was determined to be 11.7% ($k_{cat} = 9.15$ sec^{-1}) that of the wild-type. Again, the K_m for pyruvate was raised from that of the wild type to 0.44 mM and the K_m for (*S*)-ASA of 0.17 mM was entirely consistent with that of the wild type.

The fact that the catalytic activity of DHDPS-D193A has been attenuated to a slightly higher degree than that of DHDPS-Q196D is an interesting result because, since DHDPS-Q196D was found to have a slightly higher dimeric character by analytical ultracentrifugation, one might expect DHDPS-Q196D to have the lower catalytic efficiency. Figures 5.11 and 5.12 show kinetic plots of initial rate data for DHDPS-D193A and fitted data for the ping-pong mechanism.

Figure 5.11 *Kinetic plots of DHDPS-D193A with respect to pyruvate concentration at various (S)-ASA concentrations. A is a direct plot of initial rate data overlayed with fit data for the ping-pong model generated by non-linear regression (curves). B and C are Lineweaver-Burke and Eadie-Hofstee plots of the same data respectively. D is a plot of percentage residuals for each data point ($100\times(v_{obs}-v_{cal})/v_{cal}$). v is the mean initial rate in $\mu mol_{NADPH}\ mg^{-1}\ min^{-1}$, and [Pyruvate] refers to pyruvate concentration. The r^2 value for the fit was 0.996 and p>F was much less than 0.001.*

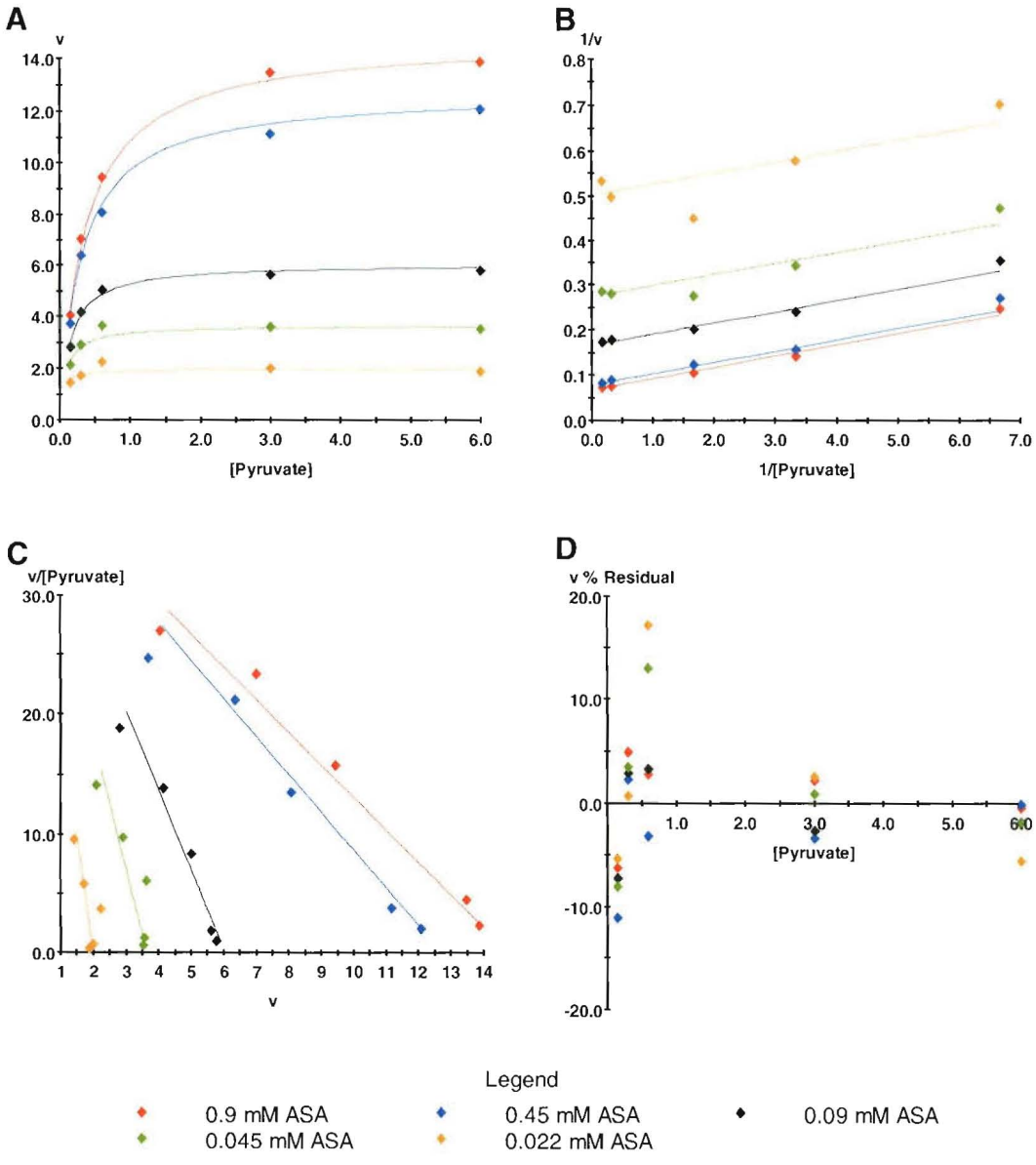

Figure 5.12 *Kinetic plots of DHDPS-D193A with respect to (S)-ASA concentration at various pyruvate concentrations. A is a direct plot of initial rate data overlayed with fit data for the ping-pong model generated by non-linear regression (curves). B and C are Lineweaver-Burke and Eadie-Hofstee plots of the same data respectively. D is a plot of percentage residuals for each data point ($100\times(v_{obs}-v_{cal})/v_{cal}$). v is the mean initial rate in $\mu mol_{NADPH}\ mg^{-1}\ min^{-1}$, and [ASA] refers to (S)-ASA concentration. The r^2 value for the fit was 0.99 and p>F was much less than 0.001.*

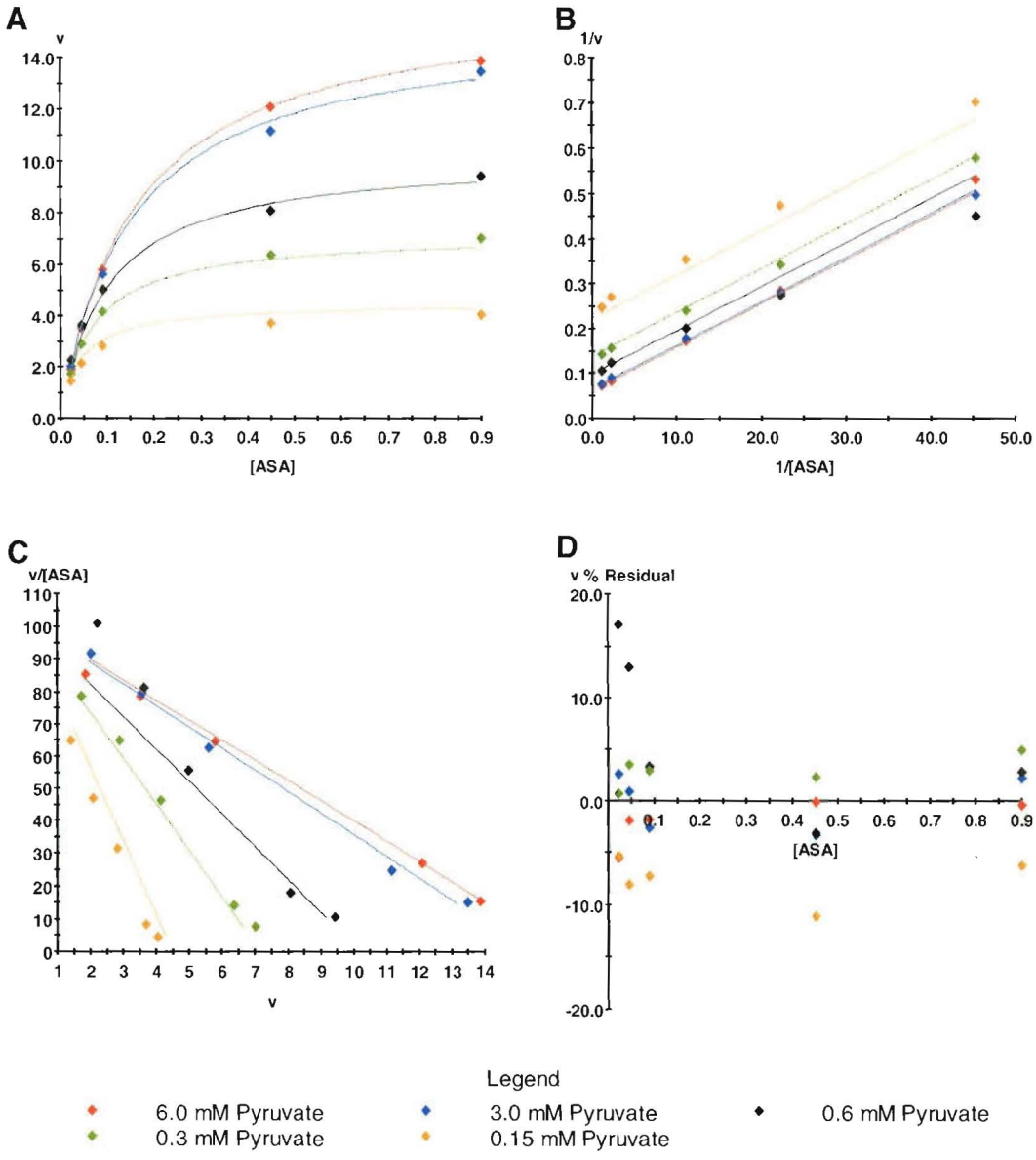

5.5.6 Steady state kinetic analysis of DHDPS-D193Y

Analytical ultracentrifugation studies of DHDPS-D193Y indicated that the variant displayed significantly less alteration in quaternary structure than other variants. Therefore, it was decided that comprehensive kinetic analysis of this variant would not be attempted, due to the time involved in such a study. Thus, steady state kinetic analysis of DHDPS-D193Y was carried out assuming that initial rate data collected at a constant concentration of one substrate while varying the concentration of the other substrate would fit a pseudo single-substrate model (Equation 5.3).

$$v = V^{app}A / (K_{mA}{}^{app} + A) \qquad \text{Equation 5.3}$$

Equation 5.3 is identical to the Michaelis-Menten equation and yields the apparent maximal velocity, V^{app}, and the apparent Michaelis-Menten constant, $K_{mA}{}^{app}$, for the varied substrate, at the concentration of the fixed substrate (25). Experiments were designed with the fixed substrate concentration as close to saturating as possible in order to obtain a meaningful estimate of the true maximal velocity.

Data from these experiments fitted the Michaelis-Menten equation well ($r^2 > 0.997$, p>F much less than 0.001) and apparent k_{cat} values were determined to be 7.21 sec^{-1} when pyruvate concentration was varied and 6.46 sec^{-1} when (*S*)-ASA concentration was varied. Consistent with results from other variants, the apparent K_m for pyruvate ($K_{mPyr}{}^{app}$ = 0.57 mM) was higher than that of wild-type DHDPS and the apparent K_m for (*S*)-ASA ($K_{mASA}{}^{app}$ = 0.15 mM) remained similar to that of the wild-type enzyme. Figures 5.13 and 5.14 show kinetic plots of initial rate data for DHDPS-D193Y and fitted data for the pseudo single-substrate model.

Figure 5.13 *Kinetic plots of DHDPS-D193Y with respect to pyruvate concentration at near saturating (S)-ASA concentration. A is a direct plot of initial rate data overlayed with fit data for the ping-pong model generated by non-linear regression (curve). B and C are Lineweaver-Burke and Eadie-Hofstee plots of the same data respectively. D is a plot of percentage residuals for each data point ($100\times(v_{obs}-v_{cal})/v_{cal}$). v is the mean initial rate in $\mu mol_{NADPH}\ mg^{-1}\ min^{-1}$, and [Pyruvate] refers to pyruvate concentration. The r^2 value for the fit was 0.997 and p>F was much less than 0.001.*

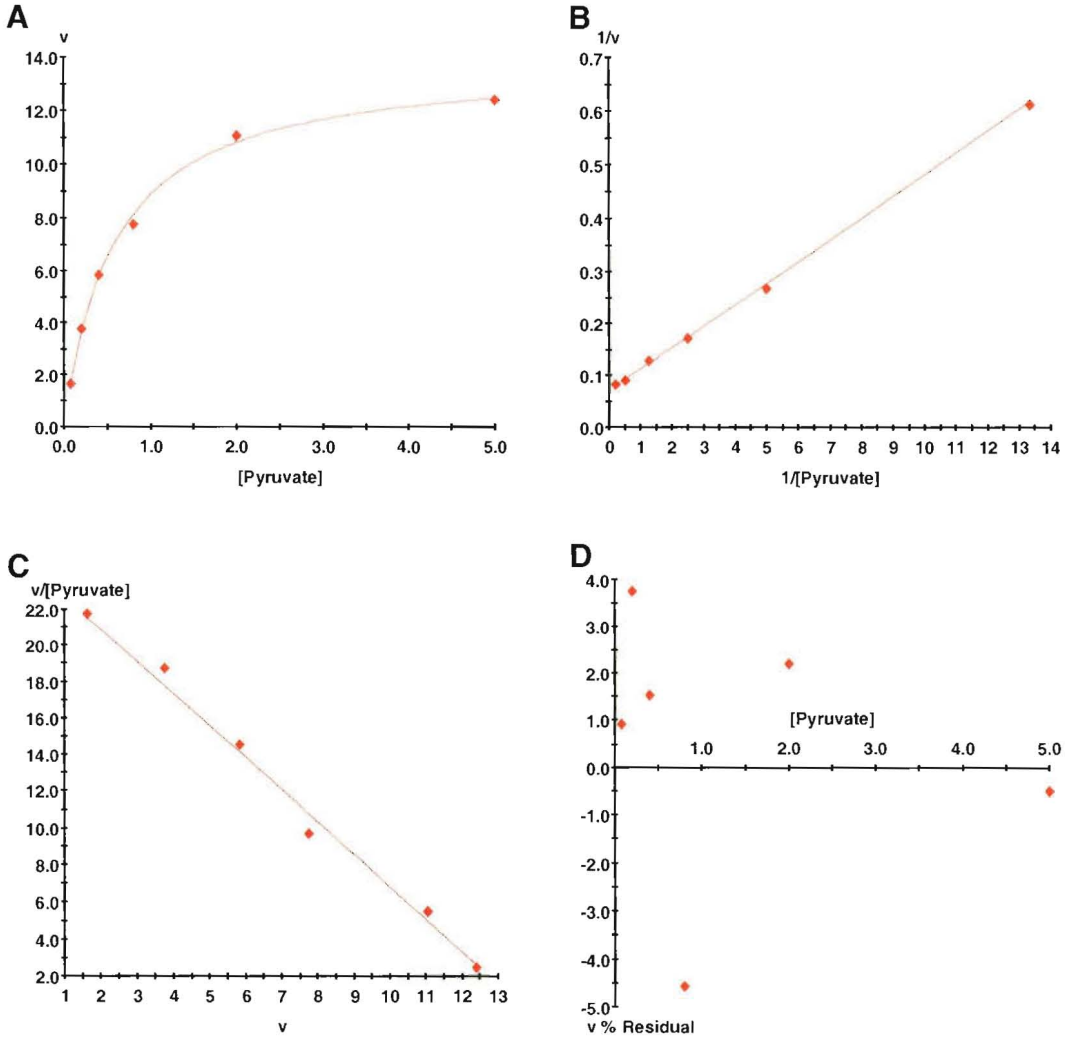

Figure 5.14 *Kinetic plots of DHDPS-D193A with respect to (S)-ASA concentration at near saturating pyruvate concentrations. A is a direct plot of initial rate data overlayed with fit data for the ping-pong model generated by non-linear regression (curve). B and C are Lineweaver-Burke and Eadie-Hofstee plots of the same data respectively. D is a plot of percentage residuals for each data point ($100\times(v_{obs}-v_{cal})/v_{cal}$). v is the mean initial rate in $\mu mol_{NADPH}\ mg^{-1}\ min^{-1}$, and [ASA] refers to (S)-ASA concentration. The r^2 value for the fit was 0.99 and p>F was much less than 0.001.*

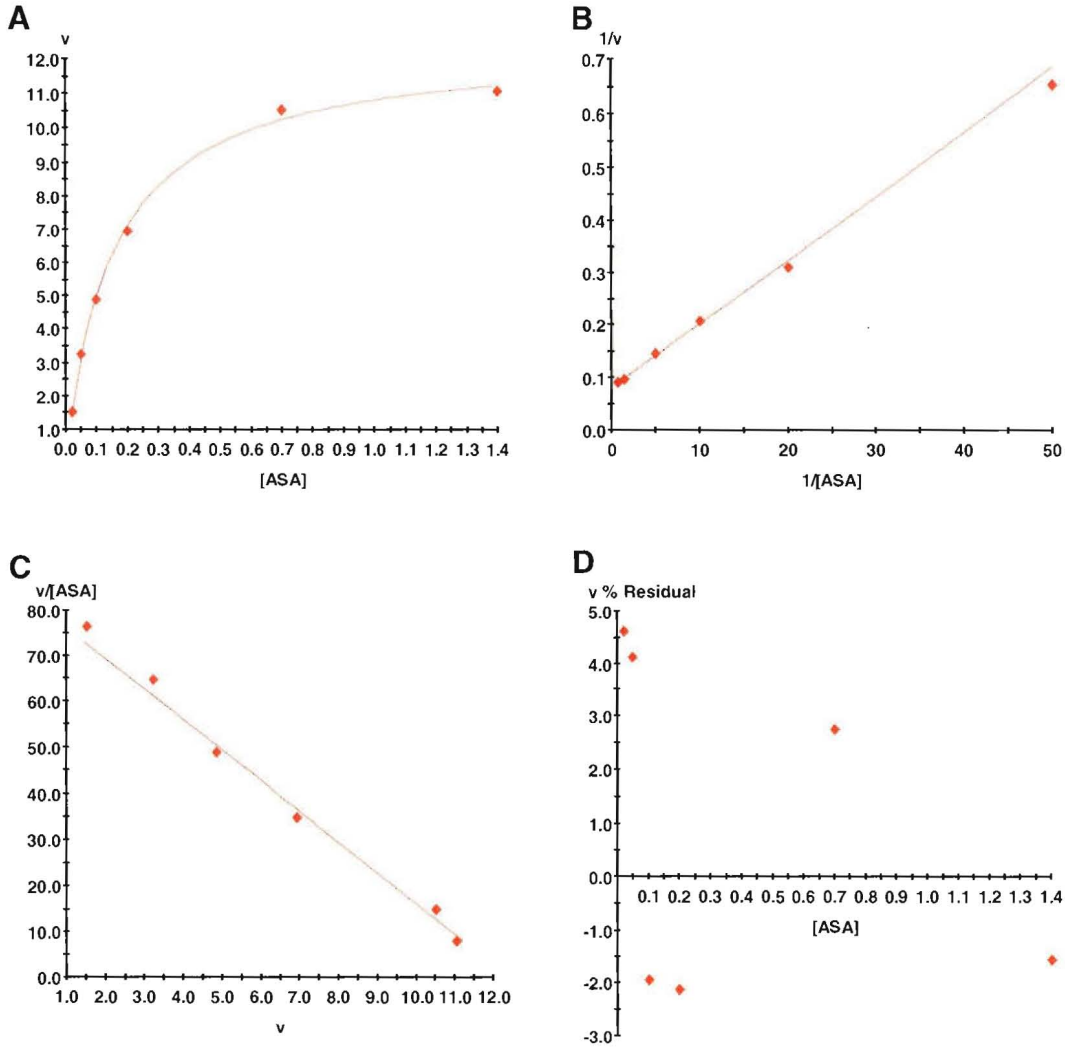

5.5.7 Steady state kinetic analysis of DHDPS-Q234D

As analytical ultracentrifugation studies of DHDPS-Q234D indicated that the variant displayed little alteration in quaternary structure, this variant was analysed in the same way as DHDPS-D193Y to yield apparent kinetic constants. Apparent k_{cat} values were determined to be 11.78 sec^{-1} when pyruvate concentration was varied and 12.39 sec^{-1} when (*S*)-ASA concentration was varied. These values represent 15.1% and 15.9% of the wild-type values respectively. Again, the apparent K_m for pyruvate (K_{mPyr}^{app} = 0.57 mM) was higher than that of wild-type DHDPS and the apparent K_m for (S)-ASA (K_{mASA}^{app} = 0.15 mM) remained similar to that of the wild-type enzyme. Figures 5.15 and 5.16 show kinetic plots of initial rate data for DHDPS-Q234D and fitted data for the pseudo single-substrate model.

Figure 5.15 *Kinetic plots of DHDPS-Q234D with respect to pyruvate concentration at near saturating (S)-ASA concentration. A is a direct plot of initial rate data overlayed with fit data for the ping-pong model generated by non-linear regression (curve). B and C are Lineweaver-Burke and Eadie-Hofstee plots of the same data respectively. D is a plot of percentage residuals for each data point ($100\times(v_{obs}-v_{cal})/v_{cal}$). v is the mean initial rate in $\mu mol_{NADPH}\ mg^{-1}\ min^{-1}$, and [Pyruvate] refers to pyruvate concentration. The r^2 value for the fit was 0.998 and p>F was much less than 0.001.*

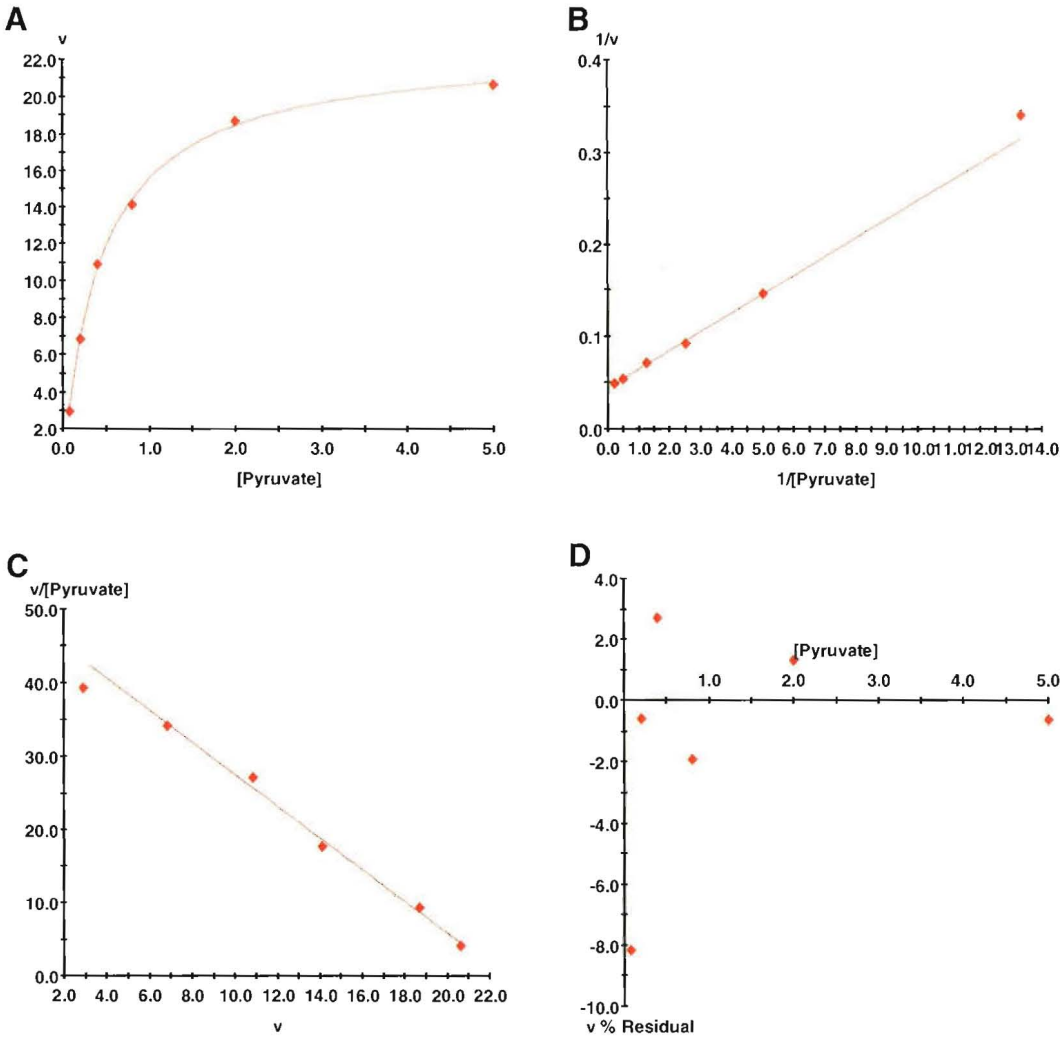

Figure 5.16 *Kinetic plots of DHDPS-Q234D with respect to (S)-ASA concentration at near saturating pyruvate concentrations. A is a direct plot of initial rate data overlayed with fit data for the ping-pong model generated by non-linear regression (curve). B and C are Lineweaver-Burke and Eadie-Hofstee plots of the same data respectively. D is a plot of percentage residuals for each data point ($100\times(v_{obs}-v_{cal})/v_{cal}$). v is the mean initial rate in $\mu mol_{NADPH}\ mg^{-1}\ min^{-1}$, and [ASA] refers to (S)-ASA concentration. The r^2 value for the fit was 0.991 and p>F was much less than 0.001.*

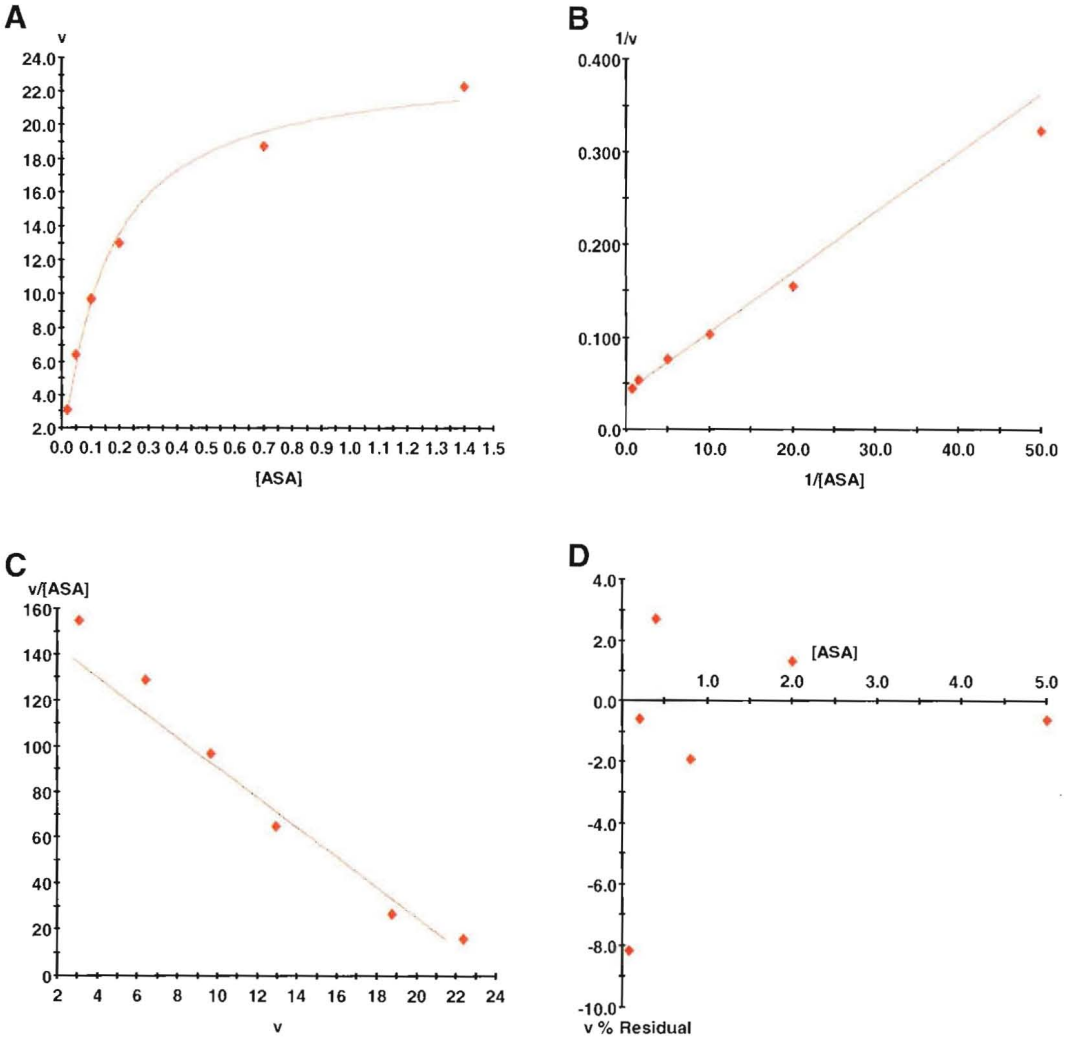

5.6 Feedback inhibition by lysine of *E. coli* DHDPS

As discussed in Chapter one, DHDPS is the final branch point enzyme in the synthesis of (*S*)-lysine. As the committed step in (*S*)-lysine biosynthesis, DHDPS represents the key point in regulation of the pathway, and undergoes allosteric feedback regulation by the end product of the pathway, (*S*)-lysine. The precise mechanism by which lysine exerts regulatory control over DHDPS is unclear, although kinetic and structural studies support the proposal that lysine is an allosteric inhibitor (1,4,5,15,26,27). DHDPS has been reported to show partial inhibition properties at high lysine concentrations. Karsten has shown that Dixon plots (1/rate *vs.* [inhibitor]) asymptotically approach a finite maximal velocity at saturating (*S*)-lysine concentrations, of about 10% that of the maximal velocity without (*S*)-lysine (15).

DHDPS displays different mechanisms of inhibition with respect to each of its substrates. Prior to this study, *E. coli* DHDPS was thought to display a partial uncompetitive mechanism of inhibition by lysine with respect to the first substrate, pyruvate (15). When an enzyme displays pure uncompetitive inhibition, the inhibitor binds only to the enzyme-substrate complex, decreasing both the maximal velocity and K_m values with increasing inhibitor concentrations (13). However, work published in collaboration with Dobson and Roberts during this research revealed that inhibition data obtained by our hands fitted significantly better to a partial mixed inhibition mechanism (20). With respect to its second substrate, (*S*)-ASA, *E. coli* DHDPS has been found to exhibit partial non-competitive inhibition (15).

5.6.1 Partial mixed inhibition

In its simplest form, mixed inhibition describes a mechanism in which the inhibitor can bind to both the free enzyme and to the enzyme-substrate complex, altering both K_m^{app} and the maximal velocity, V (13). At saturating levels of inhibitor, E.S.I predominates, but the enzyme still functions, albeit at a decreased rate ($k > k`$). Equation 5.4 is the steady-state kinetic equation that describes the partial mixed inhibition models shown in Figure 5.17.

$$v = V/([K_m^{app}/A] + [1 + I/K_i`]/[1 + I/K_i]) \qquad \text{Equation 5.4 (28)}$$

Here v is the initial velocity, V is the maximal velocity, and A is the substrate concentration, K_m^{app} is the apparent Michaelis-Menten constant and K_i and $K_i`$ are the inhibition constants for I binding to the E and E.S complex respectively. $V`$ represents the maximal velocity in the presence of saturating inhibitor. Note that $K_i/K_i` = V/V`$ allowing $V`$ to be calculated. The ratio of $V$ to $V`$ reflects the degree of partial inhibition

Figure 5.17 *Schematic representation of mixed inhibition. E represents the enzyme, S the substrate, I the inhibitor, P the product, and k the rate constant.*

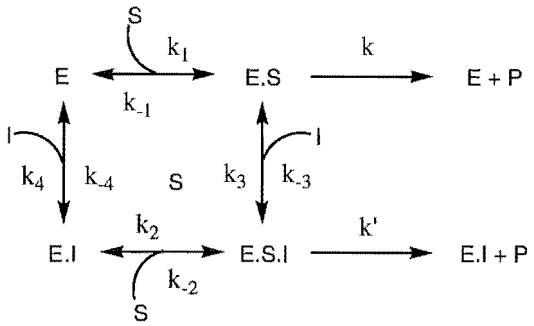

5.6.2 Partial non-competitive inhibition

Pure non-competitive inhibition represents a special case of mixed inhibition (13) (Figure 5.17), where the inhibitor constant $K_i = k_{-4}/k_4 = k_{-3}/k_3$, and the apparent substrate binding constant $K_s = k_{-1}/k_1 = k_{-2}/k_2$. As such, V is decreased and K_m remains constant with increasing inhibitor concentration. Equation 5.5 is the steady-state kinetic equation that describes partial non-competitive inhibition (29).

$$v = 1 / \{[(K_i + I)/(V` K_i + V I)][1+K_s / S]\} \qquad \text{Equation 5.5 (29)}$$

V is the maximal velocity in the absence of inhibitor and $V`$ is the maximal velocity in the presence of saturating inhibitor concentration. As above, the ratio of $V$ to $V`$ reflects the degree of partial inhibition.

5.7 Analysis of the lysine inhibition kinetics of wild-type DHDPS and the variants

Comprehensive lysine inhibition studies were carried out on wild-type DHDPS and the L197D, L197Y, Q196D, and D193Y variants by collection of initial rate data at a range of inhibitor and substrate concentrations. For each enzyme, two experiments were conducted in which data were collected at varying concentrations of the inhibitor and one substrate, while the other substrate was kept at a sub-saturating level around its determined K_m, in accordance with Karsten (15). (*S*)-Lysine concentrations were varied between 0.0 and 5.0 mM. (*S*)-ASA and pyruvate concentrations were varied between 0.2 K_m and 10 K_m, in accordance with Cornish-Bowden (13). The kinetic data were fitted to inhibition models using the EnzFitter program, yielding the associated kinetic and inhibition constants. The ratio of V to $V`$ was used to calculate the percentage residual activity at saturating inhibitor levels, α, for the partial inhibition models. Kinetic plots were produced as for section 5.5 (Appendix one).

Kinetic constants for the enzymes studied are shown in Table 5.2. K_i and $K_i`$ values obtained for the inhibition of wild-type DHDPS with respect to pyruvate are entirely consistent with published results (20), as is the percentage residual activity at saturating (*S*)-lysine concentration (20). Likewise, kinetic constants yielded for the inhibition of wild-type DHDPS with respect to (*S*)-ASA agree well with those published in all cases (15).

Inhibition data with respect to pyruvate fitted the partial mixed inhibition model for all variants studied. In all cases, kinetic constants yielded from the analysis of each mutant were entirely consistent with those determined for the wild-type enzyme Residual activity levels at saturating inhibitor concentration also showed good agreement with that of the wild-type enzyme.

Inhibition data with respect to (*S*)-ASA collected for each variant fitted the partial non-competitive inhibition model in all cases. Again kinetic constants and residual activity levels at saturating inhibitor concentration determined for each variant were completely consistent with those of wild-type DHDPS.

Table 5.2 *Inhibition of DHDPS mutant enzymes. In all cases the enzymes displayed partial inhibition with respect to lysine.*

	Wild-type DHDPS	DHDPS-L197D	DHDPS-L197Y	DHDPS-Q196D	DHDPS-D193A
With respect to pyruvate					
Inhibition Type	Mixed	Mixed	Mixed	Mixed	Mixed
V^{app} (units/mg)[a]	7.52 ± 0.07	2.21 ± 0.05	1.13 ± 0.04	14.7 ± 0.50	9.41 ± 0.35
$V`^{app}$ (units/mg)[a]	0.29 ± 0.06	0.11 ± 0.04	0.033 ± 0.02	0.47 ± 0.32	0.54 ± 0.25
α (%)[b]	3.9	5.2	2.9	3.3	5.7
K_{mPyr}^{app} (mM)	0.084 ± 0.003	0.40 ± 0.03	0.70 ± 0.09	0.23 ± 0.03	0.30 ± 0.04
K_i (mM)	3.55 ± 0.72	2.62 ± 0.9	4.12 ± 3.08	4.13 ± 2.72	2.21 ± 0.97
$K_i`$ (mM)	0.14 ± 0.007	0.14 ± 0.02	0.12 ± 0.02	0.14 ± 0.02	0.13 ± 0.02
With respect to ASA					
Inhibition Type	Non-competitive	Non-competitive	Non-competitive	Non-competitive	Non-competitive
V^{app} (units/mg)[a]	8.74 ± 0.27	2.14 ± 0.08	1.19 ± 0.04	16.8 ± 0.5	9.81 ± 0.32
$V`^{app}$ (units/mg)[a]	0.29 ± 0.28	0.05 ± 0.07	0.04 ± 0.03	0.72 ± 0.41	0.86 ± 0.24
α (%)[b]	3.4	2.1	3.7	4.3	8.8
K_{mASA}^{app} (mM)	0.09 ± 0.009	0.13 ± 0.01	0.13 ± 0.01	0.10 ± 0.01	0.11 ± 0.01
K_i (mM)	0.40 ± 0.05	0.30 ± 0.05	0.16 ± 0.03	0.19 ± 0.03	0.18 ± 0.03

[a] One unit is equal to 1 $\mu mol_{NADPH}\, min^{-1}$.

[b] α is defined as the ratio of V, the maximal velocity in the absence of inhibitor, and V', the maximal velocity at saturating inhibitor concentration.

5.8 Discussion

Comparison of detailed kinetic data from the DHDPS variants with that acquired from the wild-type enzyme revealed a number of remarkable functional and mechanistic features of the variants. Both dimeric variants, DHDPS-L197D and DHDPS-L197Y, retain significant catalytic activity showing, as proposed, that the free tight-dimer unit of DHDPS is able to function autonomously. The level of activity of all DHDPS variants was sufficient to allow complete kinetic characterisation.

Among the most striking results of this kinetic study is the shift in kinetic mechanism observed in the two dimeric mutants, DHDPS-L197D and DHDPS-L197Y, from the ping-pong model to the compulsory ordered ternary complex model. This shift indicates that there has been a subtle change in the order of reaction steps during catalysis by these variants. The reason for this apparent alteration in the kinetic mechanism is not immediately obvious from these kinetic studies alone. However, inspection of kinetic parameters reveals that all K_{mPyr} values determined for the variants are significantly raised with respect to that of wild-type DHDPS, while K_{mASA} values remain consistent with that of the wild-type enzyme. This suggests that the first half reaction, involving pyruvate binding and Schiff base formation, is affected in the variants, and is further discussed in Chapter seven.

The observed attenuation of catalytic efficiency in the two dimeric variants, to 2.5% and 1.4% of the wild-type level respectively, is a surprising result. Since the site of the mutation is approximately 25 Å distant from the active site, structural rearrangements that may cause loss of catalytic efficiency would not be expected to be transmitted from the mutation to the active site. Weakening of the dimer-dimer association in the variants DHDPS-Q196D, DHDPS-D193A, DHDPS-D193Y, and DHDPS-Q234D also results in attenuation of catalysis, but to a lesser degree. This level of activity, intermediate between the dimeric variants and the tetramer, is consistent with the presence of significant populations of both dimer and tetramer in the initial rate assay preparation.

All variants display K_m values for pyruvate that are significantly higher than that of the wild-type. This increase appears to be inversely proportional to the rate of catalytic turnover, indicating that perturbation of pyruvate binding may play a

significant part in the attenuation of activity in the mutants. However, structural data is required to ascertain whether attenuation of activity in the variants is due directly to structural factors brought about by the shift in quaternary structure in the variants (Chapter six).

Inihibition patterns and mechanisms displayed by the variants are essentially identical to those of the wild-type enzyme. This is as expected since the lysine binding site is situated adjacent to the interface between the two monomers of the tight dimer and it is known that no cooperativity exists between the two tight-dimers of the tetramer. This, combined with the consistency of K_{mASA} values determined for the wild-type and variant enzymes, constitutes strong evidence that the structural details of the wild-type DHDPS tight-dimer are conserved in the mutants.

5.9 Summary

The experiments detailed in this chapter were undertaken in order to ascertain the functional effect, if any, of the alteration of the quaternary structure of *E. coli* DHDPS. This has been achieved by comprehensive kinetic analysis of wild-type DHDPS and the variants. Kinetic data show that all variants have attenuated catalytic activity, and that this attenuation is most marked in the two dimeric variants DHDPS-L197D and DHDPS-L197Y. Data also indicate that the binding of pyruvate is perturbed in the variants. Conversely, lysine inhibition remains fully intact in all variants, suggesting that the integrity of the (*S*)-lysine binding site, at the tight-dimer interface, is preserved.

5.10 References

1. Yugari, Y., and Gilvarg, C. (1965) The condensation step in diaminopimelate synthesis. *J Biol Chem* **240**, 4710-4716
2. Shedlarski, J. G., and Gilvarg, C. (1970) The pyruvate-aspartic semialdehyde condensing enzyme of *Escherichia coli*. *J Biol Chem* **245**, 1362-1373
3. Kumpaisal, R., Hashimoto, T., and Yamada, Y. (1987) Purification and characterization of dihydrodipicolinate synthase from wheat suspension-cultures. *Plant Physiol* **85**, 145-151
4. Laber, B., Gomis-Ruth, F. X., Romao, M. J., and Huber, R. (1992) *Escherichia coli* dihydrodipicolinate synthase. Identification of the active site and crystallization. *Biochem J* **288**, 691-695

5. Blickling, S., Renner, C., Laber, B., Pohlenz, H. D., Holak, T. A., and Huber, R. (1997) Reaction mechanism of Escherichia coli dihydrodipicolinate synthase investigated by X-ray crystallography and NMR spectroscopy. *Biochemistry* **36**, 24-33

6. Ghislain, M., Frankard, V., and Jacobs, M. (1990) Dihydrodipicolinate synthase of *Nicotiana sylvestris*, a chloroplast-localized enzyme of the lysine pathway. *Planta* **180**, 480-486

7. Frisch, D. A., Gengenbach, B. G., Tommey, A. M., Sellner, J. M., Somers, D. A., and Myers, D. E. (1991) Isolation and characterization of dihydrodipicolinate synthase from maize. *Plant Physiol* **96**, 444-452

8. Shaver, J. M., Bittel, D. C., Sellner, J. M., Frisch, D. A., Somers, D. A., and Gengenbach, B. G. (1996) Single-amino acid substitutions eliminate lysine inhibition of maize dihydrodipicolinate synthase. *Proc Natl Acad Sci ,U S A* **93**, 1962-1966

9. Stahly, D. P. (1969) Dihydrodipicolinic acid synthase of *Bacillus licheniformis*. *Biochim Biophys Acta* **191**, 439-451

10. Wallsgrove, R. M., and Mazelis, M. (1981) Spinach leaf dihydrodipicolinate synthase: partial-purification and characterization. *Phytochemistry* **20**, 2651-2655

11. Bugg, T. D., and Walsh, C. T. (1992) Intracellular steps of bacterial cell wall peptidoglycan biosynthesis: enzymology, antibiotics, and antibiotic resistance. *Nat Prod Rep* **9**, 199-215

12. Couper, L., Mckendrick, J. E., Robins, D. J., and Chrystal, E. J. T. (1994) Pyridine and piperidine derivatives as inhibitors of dihydrodipicolinic acid synthase, a key enzyme in the diaminopimelate pathway to *L*-lysine. *Bioorg Med Chem Lett* **4**, 2267-2272

13. Cornish-Bowden, A. (1999) *Fundamentals of enzyme kinetics*, 2nd Ed., Portland Press Ltd, London

14. Coulter, C. V., Gerrard, J. A., Kraunsoe, J. A. E., and Pratt, A. J. (1999) *Escherichia coli* dihydrodipicolinate synthase and dihydrodipicolinate reductase: Kinetic and inhibition studies of two putative herbicide targets. *Pestic Sci* **55**, 887-895

15. Karsten, W. E. (1997) Dihydrodipicolinate synthase from *Escherichia coli*: pH dependent changes in the kinetic mechanism and kinetic mechanism of allosteric inhibition by *L*-lysine. *Biochemistry* **36**, 1730-1739

16. Gerrard, J. A. (1992) Studies on dihydrodipicolinate synthase. *D. Phil. thesis*, Oxford University

17. Paiva, A. M., Vanderwall, D. E., Blanchard, J. S., Kozarich, J. W., Williamson, J. M., and Kelly, T. M. (2001) Inhibitors of dihydrodipicolinate reductase, a key enzyme of the diaminopimelate pathway of *Mycobacterium tuberculosis*. *Biochim Biophys Acta* **1545**, 67-77

18. Dobson, R. C., Valegard, K., and Gerrard, J. A. (2004) The crystal structure of three site-directed mutants of *Escherichia coli* dihydrodipicolinate synthase: Further evidence for a catalytic triad. *J Mol Biol* **338**, 329-339

19. Dobson, R. C., Gerrard, J. A., and Pearce, F. G. (2004) Dihydrodipicolinate synthase is not inhibited by its substrate, (*S*)-aspartate β-semialdehyde. *Biochem J* **377**, 757-762

20. Dobson, R. C., Griffin, M. D., Roberts, S. J., and Gerrard, J. A. (2004) Dihydrodipicolinate synthase (DHDPS) from *Escherichia coli* displays partial mixed inhibition with respect to its first substrate, pyruvate. *Biochimie* **86**, 311-315

21. Pearce, F. G. (1999) Kinetic studies of dihydrodipicolinate synthase. *B.Sc (Hons)*, University of Canterbury

22. Dereppe, C., Bold, G., Ghisalba, O., Ebert, E., and Schar, H. P. (1992) Purification and characterization of dihydrodipicolinate synthase from pea. *Plant Physiol* **98**, 813-821

23. Borthwick, E. B., Connell, S. J., Tudor, D. W., Robins, D. J., Shneier, A., Abell, C., and Coggins, J. R. (1995) *Escherichia coli* dihydrodipicolinate synthase: characterization of the imine intermediate and the product of bromopyruvate treatment by electrospray mass spectrometry. *Biochem J* **305**, 521-524

24. Selwyn, M. J. (1965) A simple test for inactivation of an enzyme during assay. *Biochim Biophys Acta* **105**, 193-195

25. Cleland, W. W. (1979) Statistical analysis of enzyme kinetic data. *Methods Enzymol* **63**, 103-138

26. Blickling, S., Beisel, H. G., Bozic, D., Knablein, J., Laber, B., and Huber, R. (1997) Structure of dihydrodipicolinate synthase of *Nicotiana sylvestris* reveals novel quaternary structure. *J Mol Biol* **274**, 608-621

27. Kumpaisal, R., Hashimoto, T., and Yamada, Y. (1989) Inactivation of wheat dihydrodipicolinate synthase by 3-bromopyruvate. *Agric Biol Chem* **53**, 355-359

28. Tipton, K. F. (1996) in *Enzymology* (Engel, P. C., ed), pp. 115-174, Academic Press, San Diego

29. Keleti, T. (1986) *Basic enzyme kinetics*, 1st Ed., Trans. Freidrich, P., and Kramer, M., Akademiai Kiado, Budapest

Chapter Six

The crystal structures of DHDPS-L197Y and DHDPS-L197D

6.1 Introduction

Data presented in Chapter four demonstrated that the two DHDPS variants, DHDPS-L197Y and DHDPS-L197D, existed as obligate dimers in solution, as opposed to the tetrameric structure of the wild-type enzyme. The detailed kinetic characterisation presented in Chapter five revealed that these two variants exhibit highly attenuated catalytic efficiency with respect to wild-type DHDPS, with a concomitant rise in the K_m for the first binding substrate, pyruvate. Interestingly, all other kinetic and inhibition parameters determined for these variants were found to be entirely consistent with those of the wild-type.

Beyond the assertion that the reduced catalysis of the dimeric variants is due, at least in part, to the impaired binding of pyruvate, no satisfactory explanation for the altered kinetic properties of the two variants was obvious from the functional and biophysical data presented in previous chapters. Thus, the question was raised of whether the observed changes in the kinetic behaviour in the dimeric variants, with respect to the wild-type enzyme, were due to structural factors introduced by the large-scale shift in quaternary structure from obligate tetramer to obligate dimer. X-ray crystal structures of these variants were, therefore, required in order to place these results in the context of atomic resolution structural data.

This chapter details the X-ray crystal structures of both DHDPS-L197Y and DHDPS-L197D, and compares these with the 1.9 Å resolution crystal structure of the unliganded wild-type enzyme solved in this laboratory during this research (1).

6.2 Protein X-ray crystallography of DHDPS-L197D and DHDPS-L197Y

The technique of single crystal protein X-ray crystallography involves the interpretation of the diffraction of X-rays from the ordered array of protein molecules in a crystal, ultimately allowing the three-dimensional resolution of individual atoms (2). This method requires the production of protein crystals of sufficient size and quality to produce interpretable diffraction patterns in diffraction experiments. This is not a trivial task, and is the process that constitutes the bottleneck in modern macromolecular crystallography (3,4).

Crystallisation experiments were undertaken for both DHDPS-L197Y and DHDPS-L197D, following the recommendations of Bergfors (3). All crystallisation experiments were conducted at 4°C, in light of the observed reduced stability of these variants. Attempts to crystallise both dimeric variants under the same buffer conditions failed, presumably due to differences in solubility between the two.

6.2.1 Crystallisation of DHDPS-L197Y and diffraction data collection

Crystallisation conditions for DHDPS-L197Y were found initially using the sparse-matrix crystallisation screen, Crystal Screen (Hampton Research), using the hanging-drop vapour-diffusion technique. The protein was found to form needle-shaped crystals in a range of drops containing polyethylene glycol of different molecular weights and at different concentrations.

Further trials, screening around the conditions under which crystals had been observed, yielded well formed crystals of approximately 0.2 mm x 0.2 mm x 0.5 mm in drops equilibrated against a well solution of 30% polyethylene glycol 1500 in 20 mM Tris.HCl pH 8. Drops were prepared by adding 2 µl of well solution to 2 µl of 7.5 mg/ml protein in 20 mM Tris.HCl pH 8. Crystals grown in this way formed slowly over a period of 2 to 3 months; however, crystallisation under these conditions was shown to be reproducible.

X-ray intensity data collection was performed at 110 K from a single, mounted crystal that had been flash-frozen in liquid nitrogen after soaking in cryoprotectant consisting

of 10% glycerol in mother liquor. The crystal prepared in this way diffracted well to beyond 1.7 Å resolution.

6.2.2 Crystallisation of DHDPS-L197D and diffraction data collection

Crystals of DHDPS-L197D of sufficient size for X-ray diffraction were produced using the hanging-drop vapour-diffusion method. Inital attempts at the crystallisation of DHDPS-L197D using the sparse-matrix crystallisation screen, Crystal Screen (Hampton Research), did not yield any promising leads for crystallisation using the hanging-drop method. Thus, a range of narrow grid screens was undertaken in which crystallisation conditions were chosen and varied based on prior knowledge of the properties of the protein gained during purification and characterisation.

A screen in which ammonium sulfate was used as a precipitant at varied concentrations and pH yielded many, extremely small, but well shaped crystals in drops containing 2 µl of 7.2 mg/ml protein and 2 µl of well solution, and equilibrated against 2.6 M ammonium sulfate, 100 mM Tris.HCl, pH 7.5-8.5. As the nucleation rate in crystallisation experiments is often related to the degree of protein supersaturation (3), further grid screens were designed using lower precipitant and protein concentrations in an effort to produce few, but larger crystals.

Optimisation in this way yielded well formed crystals of approximately 0.3 mm x 0.3 mm x 0.5 mm in drops prepared with 2 µl of 7.2 mg/ml protein and 2 µl of well solution, and equilibrated against 2.4 M ammonium sulfate, 100 mM Tris.HCl, pH 8.15. Growth of crystals of similar quality was routinely reproducible using these conditions. Sitting-drop crystallisation experiments were also conducted under identical conditions; however the morphology of crystals produced by this technique was deemed unsuitable for X-ray diffraction data collection.

X-ray diffraction data were collected as for DHDPS-L197Y. The cryoprotectant solution used here was mother liquor containing 25% w/v sucrose. This was chosen as trials had revealed that mounting of these crystals in standard cryoprotectant solutions, for example 10% v/v glycerol, resulted in rapid deterioration of both the appearance of the crystal and the resulting diffraction pattern. The crystal mounted in this way diffracted to beyond 2.0 Å resolution.

6.2.3 Structure solution and refinement

Diffraction data sets were processed and scaled using the program CrystalClear (5). The merging *R* values were 0.072 and 0.051 for the DHDPS-L197Y and DHDPS-L197D data sets respectively. The crystal structures were solved by molecular replacement using AMoRe (6,7), utilising the *E. coli* DHDPS monomer (1), as the search model. The crystal structure of DHDPS-L197Y was solved in the space group $P2_12_12_1$ and contained a dimer in the asymmetric unit. The DHDPS-L197D structure was solved in the space group $P4_32_12$, with a single monomer in the asymmetric unit.

Refinement of the molecular replacement solutions was achieved using REFMAC5 (7,8). For this step, a glycine residue was placed at the position of the mutation. Manual model corrections were carried out using the program O (9,10) and new models were further refined using REFMAC5. The final refinement rounds involved the placement of solvent molecules using the program ARP (7,11) followed again by manual corrections using O. The quality of the structures at all stages of the refinements was assessed using the program Procheck (7,12), which also served as a guide for rebuilding and corrections at each refinement round. In some cases, the side chains of amino acid residues could not be completely resolved due to insufficient electron density for rebuilding. In these cases, atoms that could not be accurately placed were deleted from the coordinate file. Data collection and refinement statistics are presented in Table 6.1.

For the purposes of direct comparison of the structures of the variants with that of the wild-type, overlays were produced using the least-squares alignment functions of O. Initially, alignments were produced by pairwise fitting of the α-carbon coordinates. These alignments were then improved by an algorithm for matching of structural fragments (13), and the coordinates were transformed according to this fit to produce the overlay. Alignments were produced by matching of a single monomer from each structure, and also by matching of the variant dimers with the dimeric asymmetric unit solved for the wild-type.

Table 6.1 *Data collection and refinement statistics for the DHDPS-L197Y and DHDPS-L197D crystal structures.*

	DHDPS-L197D	DHDPS-L197Y
Data Collection		
Number of images	247	316
Oscillation range (°)	0.3	0.3
Number of Crystals	1	1
Exposure Time (s)	240	240
Camera length (mm)	170	100
Data Processing		
Resolution (outer shell)	37.50-2.00 (2.052-2.00)	39.97-1.70 (1.76-1.70)
Number of reflections (unique)	101273 (20562)	313262 (86208)
Completeness (outer shell)	98.6 (89.3)	99.5 (99.8)
Space group	$P4_32_12$	$P2_12_12_1$
Unit Cell a,b,c (Å)	50.71, 50.71, 222.82	60.48, 106.71, 120.66
α,β,γ (°)	90.0, 90.0, 90.0	90.0, 90.0, 90.0
R_{merge}[a] (outer shell)	0.051 (0.309)	0.072 (0.337)
Refinement		
R_{Free} (outer shell)[b]	0.344 (0.425)	0.236 (0.348)
R_{Cryst} (outer shell)[c]	0.307 (0.327)	0.198 (0.337)
Solvent molecules	12	747
Mean B-value	40.05	16.82
r.m.s.d from ideal geometry		
Bond lengths (Å)	0.035	0.006
Bond angles (°)	2.077	1.013

[a] R_{merge} = SUM (ABS(I – <I>)) / SUM (I).
[b] R_{free} based on 5% of the total reflections.
[c] $R_{cryst} = \Sigma(|F_{obs}|-|F_{calc}|)/\Sigma|F_{obs}|$.

6.3 The crystal structure of DHDPS-L197Y

DHDPS-L197Y crystallised as a dimer analogous to the tight-dimer unit of wild-type DHDPS (Figure 6.1). Inspection of the crystal packing produced by space group

symmetry operations showed that crystal contacts between dimers in no way resembled the packing of dimers to form the tetramer in the wild-type enzyme. In fact, no crystal contacts were found involving the exposed dimer-dimer interface surface. The final model contained two molecules in the asymmetric unit, each comprising the full sequence of 292 amino acid residues. The R_{Cryst} and R_{Free} values for the fully refined structure were 0.198 and 0.236 respectively.

Figure 6.1 *The crystal structure of DHDPS-L197Y. Subunits A and B associate to form a dimer analogous to the tight-dimer unit of wild-type* E. coli *DHDPS.*

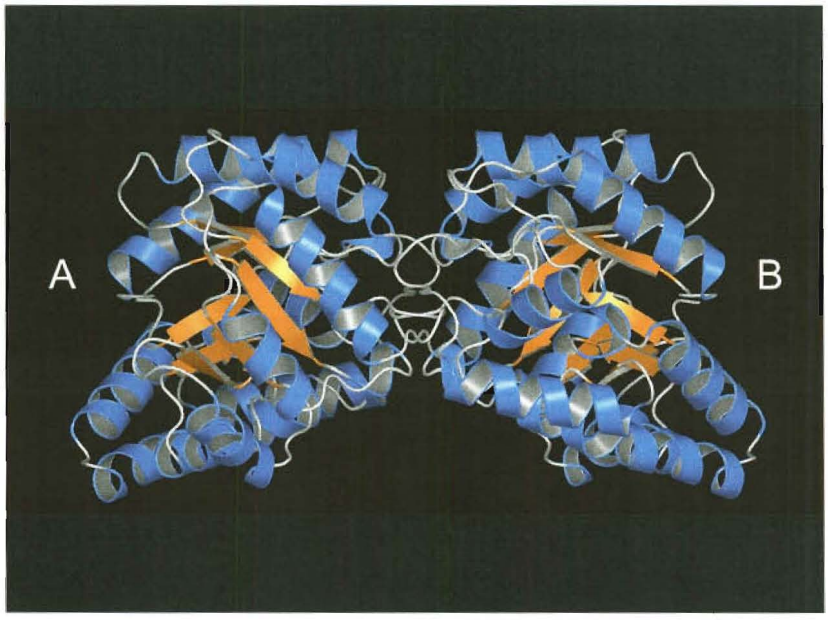

6.3.1 General features of the structure

The tertiary structure of wild-type DHDPS, as revealed by our structure (1) and reported elsewhere (14-16), is maintained in its entirety throughout the structure of DHDPS-L197Y (Figure 6.1). Each monomer comprises two domains: the N-terminal $(\alpha/\beta)_8$ barrel, consisting of residues 1-224, and the C-terminal α-helical domain, consisting of residues 225-292 (Figure 6.2). All details of the interface between the two monomers of DHDPS-L197Y are essentially identical to those of the major tight-dimer interface of the wild-type enzyme.

Inspection of the Ramachandran plot (17) (Figure 6.3) revealed that the majority of non-glycine residues fell within the allowed regions for peptide torsion angles. However, two residues, Y107 and N156, lay outside these regions. Y107 from both

monomers lay in the disallowed region of the plot. This observation is entirely consistent with observations of our own structure (1) and with previous reports (14,16).

Figure 6.2 *The structure of the DHDPS-L197Y monomer showing the position of K161 (yellow) a) shows a view looking through the $(\alpha/\beta)_8$ barrel b) shows a view of the side of the $(\alpha/\beta)_8$ barrel.*

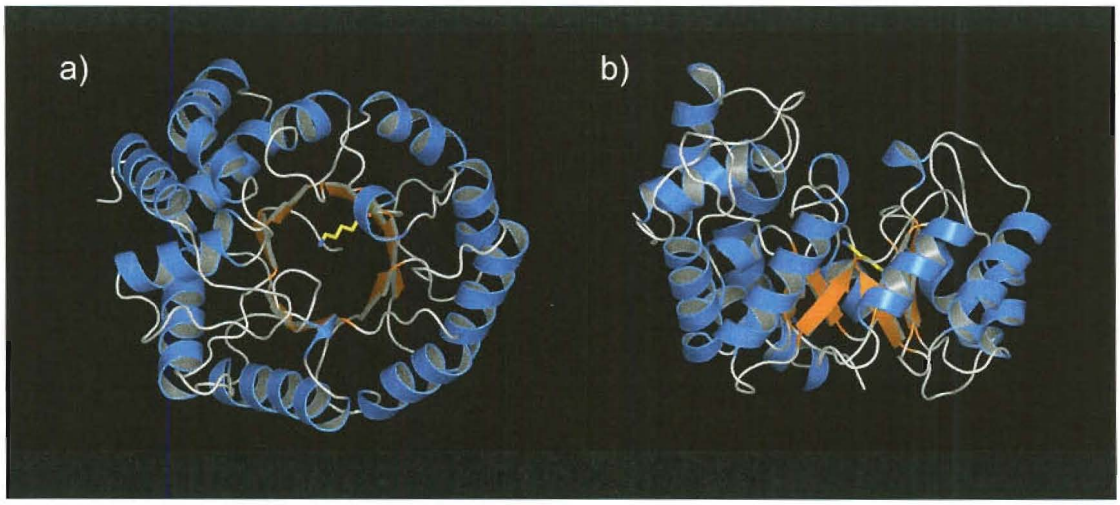

Figure 6.3 *Ramachandran plot of chains A and B in the asymmetric unit of DHDPS-L197Y. a, b, l, and p are allowed regions for torsion angles, ~a, ~b, ~l, and ~p are generously allowed regions for torsion angles, white regions are disallowed regions. ▲ represents glycine residues and ■ represents other residues. ■ denotes residues in disallowed or generously allowed regions.*

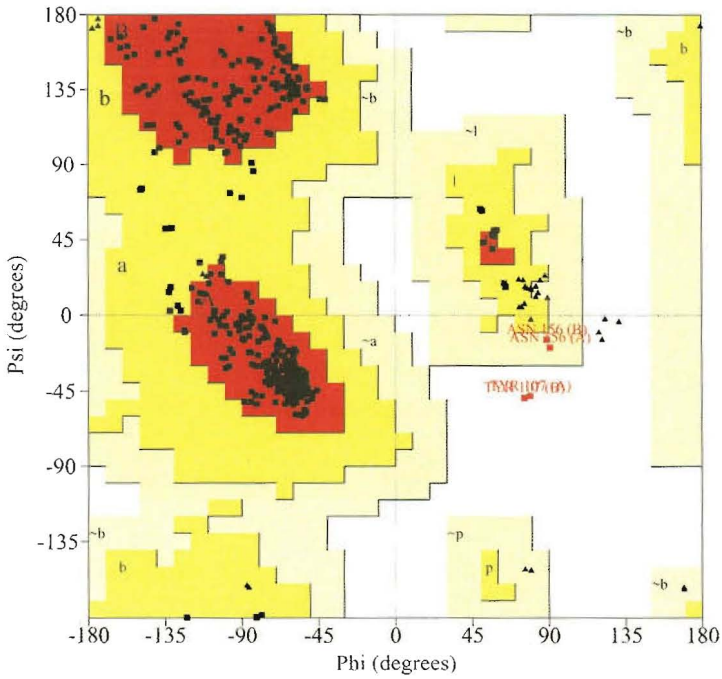

As detailed in sections 1.3.5 and 1.4.1, Y107 protrudes into the active site of one monomer from the neighbouring monomer of the tight-dimer unit and forms part of an essential catalytic triad motif that is involved in proton movement to and from the active site (18). Thus, torsional strain on this residue has been proposed to be associated intimately with catalytic function (14). The conformation of Y107 and the proton relay triad is completely conserved in the structure of DHDPS-L197Y.

N156 residues from both monomers of the DHDPS-L197Y dimer lay in a generously allowed region for peptide torsion angles. Torsional strain on this residue has not been observed in structures of the wild-type enzyme (14-16) or other mutants (18). This observation is addressed in section 6.3.3.

6.3.2 Alignment of the DHDPS-L197Y and wild-type DHDPS structures

Alignment of monomer A of DHDPS-L197Y with monomer A of the wild-type structure resulted in an r.m.s.d for the α-carbon atoms of 0.23 Å. Alignment of the full DHDPS-L197Y dimer with the tight-dimer unit of the wild-type enzyme yielded an r.m.s.d of 0.29 Å for α-carbon atoms. An overlay of the α-carbon traces of the two structures produced from the dimer alignment is shown in Figure 6.4.

Figure 6.4 *Alignment of the DHDPS-L197Y dimer (red spline) with the tight-dimer unit of wild-type DHDPS (light blue spline).*

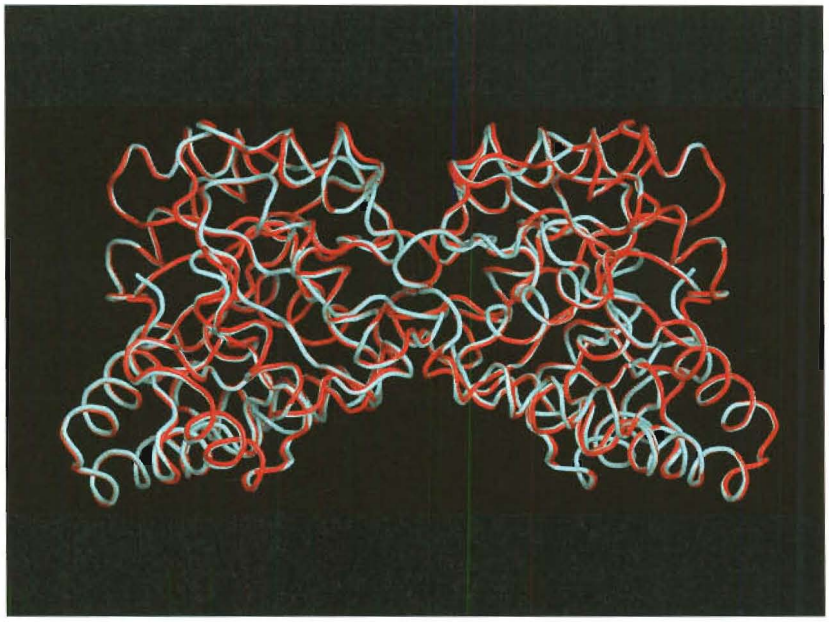

From this overlay, it is clear that all secondary structural elements align throughout the structure with a high degree of similarity and that the monomers of the L197Y variant hold the same orientation, with respect to each other, as those of the wild-type. Where variations between the structures exist, these are generally small displacements of loop regions. However, it should be noted here that all loop regions carrying catalytic residues, lysine or substrate binding residues, and monomer-monomer interface residues show good alignment with those of the wild-type.

6.3.3 Strained residue N156

As mentioned in section 6.3.1, residue N156 was found to hold strained peptide torsion angles. Closer inspection of the structure of DHDPS-L197Y reveals that N156 forms part of a loop region linking helix α5 to strand β6 in the $(\alpha/\beta)_8$ barrel structure (Figure 6.5). The alignment indicates that this loop region had been displaced slightly and that the side chain of N156 had adopted a different rotamer in DHDPS-L197Y with respect to the wild-type structure. These changes are essentially identical in both monomers of DHDPS-L197Y; however, the reasons for the rearrangements are unclear.

Figure 6.5 *Close up of the single monomer alignment of the crystal structure of DHDPS-L197Y (red spline) with that of wild-type DHDPS (light blue spline) showing the displacement of the loop region connecting helix α5 to strand β6.*

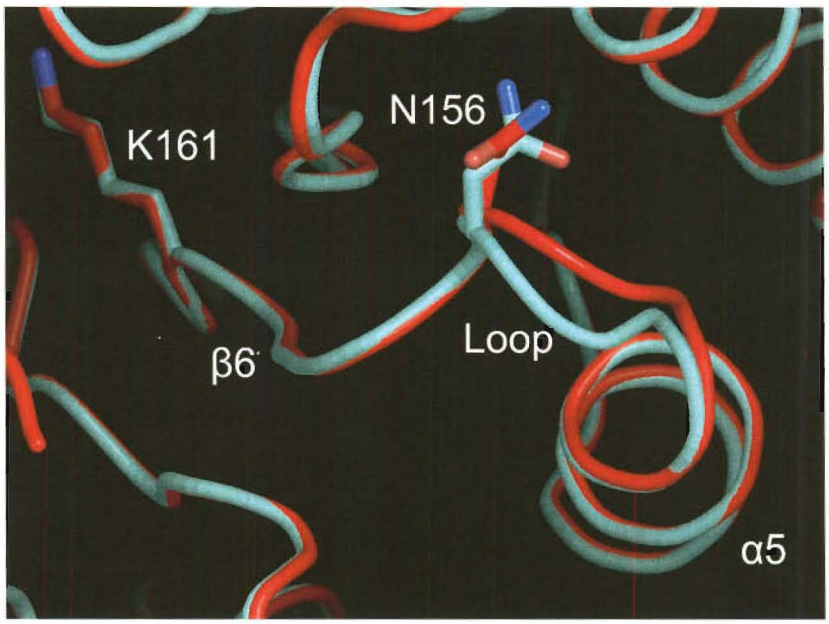

Since the end of strand β6 distal to this loop holds the pyruvate binding residue, K161, the observed structural change was of interest. However, all atomic coordinates for K161 show excellent agreement with those of the wild-type enzyme (Figure 6.5) indicating that the structural shifts are local. Neither helix α5 nor strand β6 were significantly displaced, and no rearrangements in main chain or side chain atoms of structural elements surrounding the loop are apparent from the alignment. Additionally, inspection of crystal packing reveals no crystal contacts in the vicinity of the loop. Thus, explanation of why this loop has shifted causing N156 to adopt a strained conformation in the crystal structure of DHDPS-L197Y has proven difficult.

6.3.4 The mutation site, Y197

Figure 6.5 *Residue Y197 of DHDPS-L197Y covered by electron density calculated for a model omitting this side chain. 2Fo-Fc electron density (blue) is contoured at 1σ.*

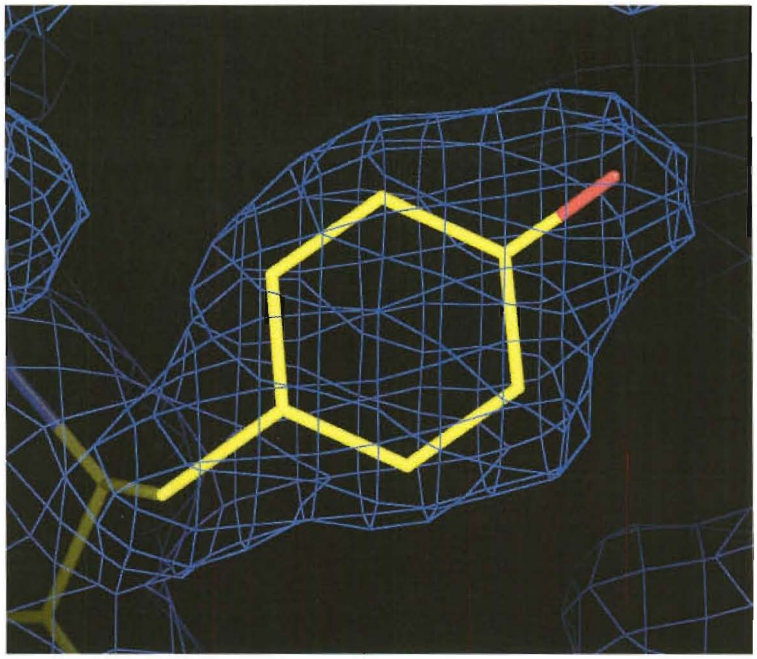

A tyrosine residue was modelled at the site of the mutation during refinement as electron density appeared to guide rebuilding. 'Omit' electron density maps were produced to ensure this residue had been modelled correctly in the final model for DHDPS-L197Y. In order to remove model bias from the calculation of electron density maps around the mutated residue, the side chain atoms of both Y197 residues were deleted from the final coordinate file. This edited model was then used to calculate structure-factors and produce electron density maps. Figure 6.5 shows that

the electron density calculated for the omit map agrees well with the modelled tyrosine side chain, indicating that this side chain had been modelled correctly. This also demonstrates that the required mutation is present, as was indicated by gene sequencing in section 3.2.5.

Figure 6.6 *Overlay of the mutation site of DHDPS-L197Y (yellow) with wild-type DHDPS (light blue) produced from the alignment of single monomers from the structures.*

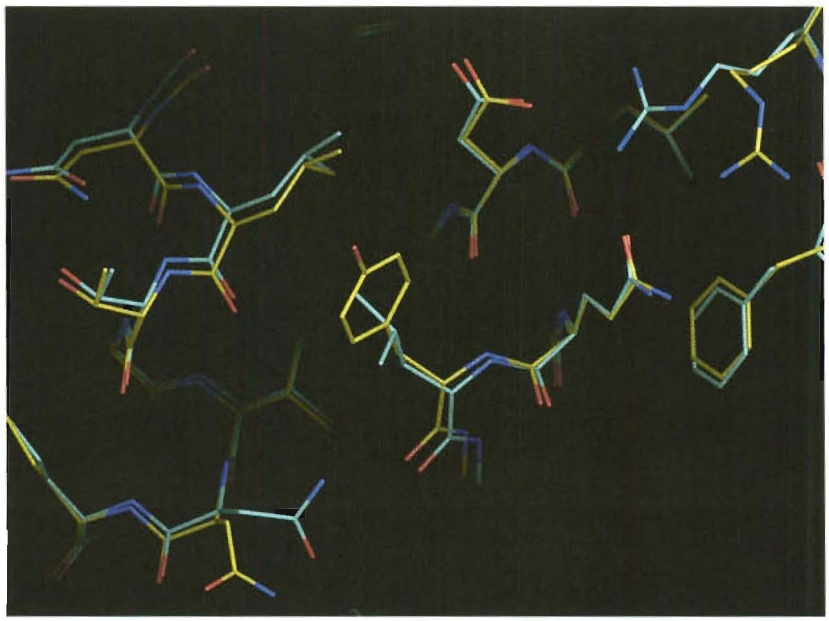

The alignment of monomer A of DHDPS-L197Y with monomer A of the wild-type enzyme showed that the structure in the vicinity of the mutation was conserved, despite the introduction of the bulky tyrosine side chain (Figure 6.6). Y197 has adopted a rotamer similar to that of the leucine residue it replaced, which was as predicted from modelling experiments conducted prior to the production of the mutation. Secondary structural elements have not been displaced around the site of the mutation and side chains in direct contact with Y197 hold the same conformation as in the wild-type structure. R230 and N171, which, as described in section 2.6.2, are situated at the edge of the dimer-dimer interface contact area, both hold different side chain rotamers in DHDPS-L197Y with respect to the wild-type structure. This is likely to be an indirect result of the exposure of the interface surface, since main chain atoms have not been displaced. Also, electron density from wild-type structures has indicated that these two residues may have two possible side chain conformations. Thus, the introduction of the L197Y mutation into the DHDPS structure has not

caused gross structural rearrangements that may be transmitted throughout the protein structure.

6.3.5 The active site

As detailed in Chapter five, DHDPS-L197Y displayed greatly attenuated catalytic efficiency when compared to wild-type DHDPS. It was suggested that, while unlikely, structural rearrangements within the active site of the variant may have caused this reduction in activity. However, the crystal structure of DHDPS-L197Y shows no gross rearrangements in the critical catalytic and binding residues of the active site that may account for the altered kinetic behaviour observed in this variant.

Figure 6.7 *Overlay of the active sites of DHDPS-L197Y (yellow) and wild-type DHDPS (light blue) produced from the alignment of single monomers from the structures.*

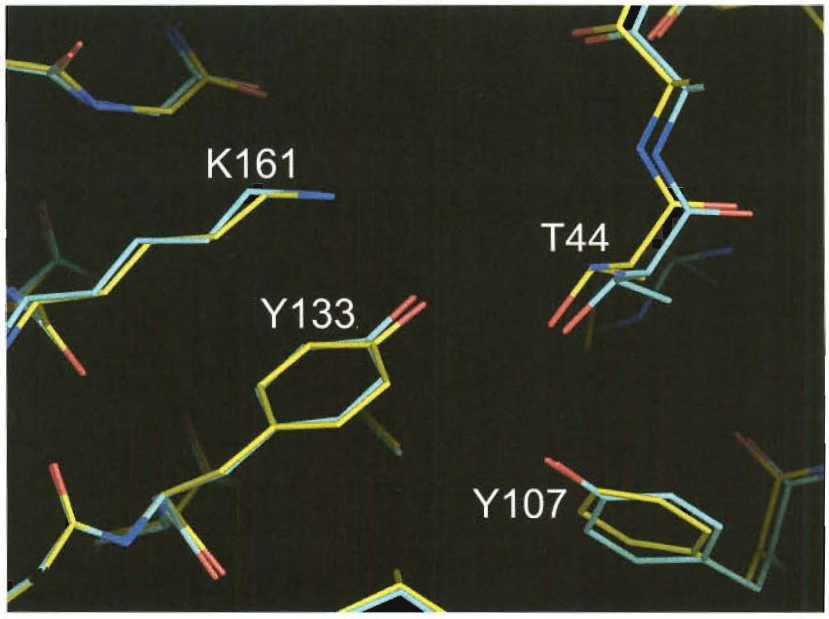

The single monomer alignment of the wild-type and DHDPS-L197Y structures showed that all active site binding and catalytic motifs were intact in the DHDPS-L197Y structure and that no gross structural displacements had occurred with respect to the wild type structure. Figure 6.7 shows the overlay of the active sites detailing the the pyruvate binding residue, K161, and the intact proton relay triad consisting of Y133, T44, and Y107. The atomic coordinate errors estimated from the refinements of the two structures were 0.10 Å and 0.11 Å, for DHDPS-L197D and the wild-type enzyme, respectively. Deviations between coordinates of corresponding

atoms in critical residues were generally below, or in the range of, the cumulative coordinate error for the two structures, indicating that no significant structural changes were present in the active site of DHDPS-L197Y.

6.3.6 Unexplained density at K161

Inspection of the electron density around the active site lysine residue, K161, during refinement, and after production of the final model and maps, revealed unexplained density connected to the end of the side chain (Figure 6.8). Initially, it was presumed that this density was pyruvate, covalently bound as an imine or enamine to the side chain nitrogen of K161. This was a surprising result, since DHDPS-L197Y had been crystallised without the addition of pyruvate to the crystallisation buffer. Moreover, pyruvate had not been added to the protein preparation at any step during purification. Thus, the only exposure of the protein to pyruvate, prior to crystallisation, was inside the cell and in the crude cell lysate.

Figure 6.8 *Positive electron density (green) observed at K161 of DHDPS-L197Y. 2Fo-Fc density is contoured at 1σ (blue), and Fo-Fc density is contoured at 3σ (green) and -3σ (red).*

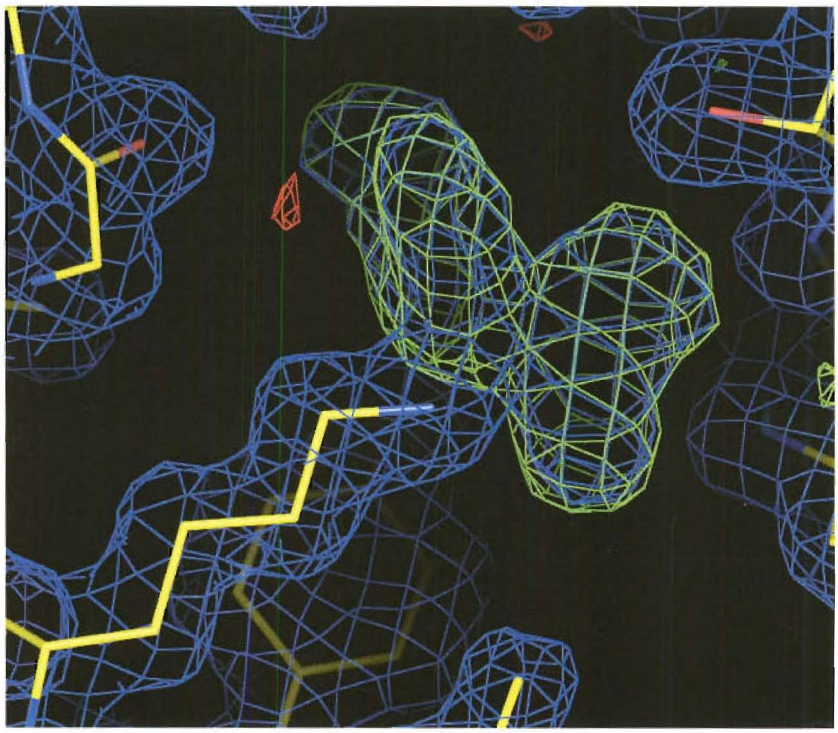

Coordinates and restraint libraries for the various lysine-pyruvate adducts (Figure 6.9) were produced using the programs Sketcher (7) and Libcheck (7). Attempts to model

the planar imine or enamine into the extra density failed to satisfy suitably the observed electron density. The position of the carboxyl group of the bound pyruvate is clearly evident from the density and is consistent with published reports of the pyruvate bound wild-type structure (14). However, the remaining density lies in a different plane and is inconsistent with the position of the C_3 atom of the bound, planar pyruvate.

Figure 6.9 *Possible structures of the pyruvate-bound active site lysine residue, K161.*

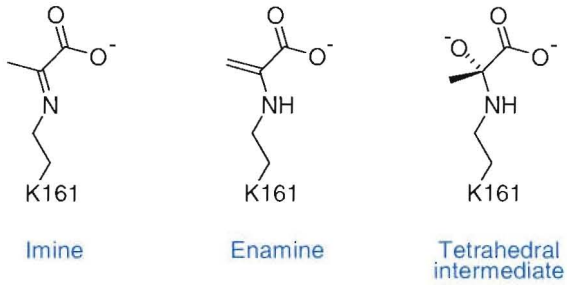

Consideration of the shape of the unsatisfied electron density indicated that the observed adduct may be tetrahedral. Thus, the tetrahedral reaction intermediate was modelled at this position. Refinement of this model produced a good fit to the density with only small peaks in the difference map (Figure 6.10) indicating that this was likely to be the identity of the observed adduct. Positive density observed beyond the oxyanion oxygen is presumed to be a hydrogen bonded water molecule. Negative density at and below the oxyanion oxygen may be due to incomplete occupancy at this position.

Since this reaction intermediate would be expected to be highly unstable, the observation of this trapped adduct in DHDPS-L197Y is an extremely interesting result. The fact that this tetrahedral intermediate has remained bound throughout purification, repeated dialysis, and crystallisation of the protein is remarkable. This electron density has not been observed in the wild-type DHDPS structures solved by us, where purification and preparation of protein for crystallisation was essentially the same as that for DHDPS-L197Y (1). Obviously, different buffer conditions were employed for crystallisation of wild-type DHDPS, but, again pyruvate, was not added.

Figure 6.10 *Model of the tetrahedral reaction intermediate covalently attached to K161 of DHDPS-L197Y. 2Fo-Fc density is contoured at 1σ (blue), and Fo-Fc density is contoured at 3σ (green) and -3σ (red).*

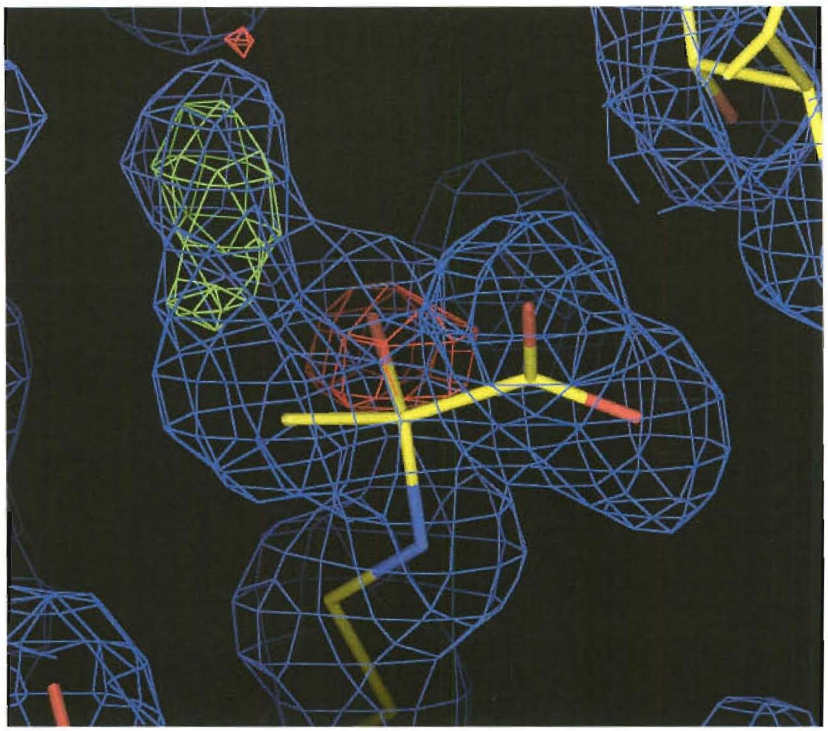

A possible reason for the persistence of the covalently bound tetrahedral intermediate at K161 may be found in the hydrogen bonding pattern of the adduct (Figure 6.11). The carboxyl of the bound pyruvate is hydrogen bonded to the backbone nitrogens of both T44 and T45, and the side chain oxygen of T45. This is as observed in the pyruvate-bound wild-type DHDPS structures where pyruvate has been modelled as a planar adduct (14). Inspection of the position of the oxyanion oxygen atom reveals that this is in very close contact with the hydroxyl group of Y133, with an oxygen-oxygen distance of 2.31 Å. This fact, combined with the presence of excellent geometry for hydrogen bonding, suggests that these atoms are very tightly hydrogen bonded. Stabilisation of the oxyanion in this way may lead to stabilisation of the tetrahedral reaction intermediate and thus account for its persistence. This is explored further in Chapter seven.

Figure 6.11 *Hydrogen bond coordination of the tetrahedral intermediate as modelled at K161 of DHDPS-L197Y.*

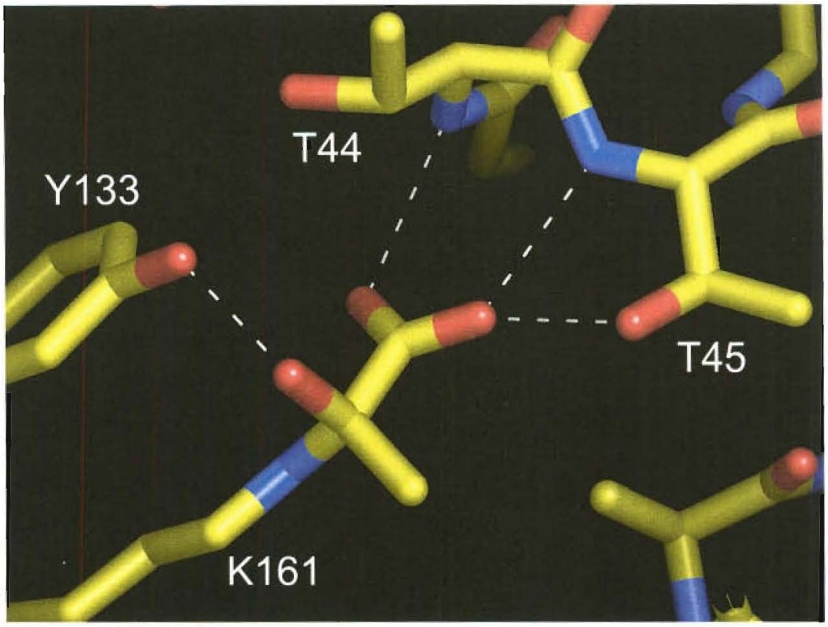

6.4 The crystal structure of DHDPS-L197D

DHDPS-L197D crystallised as a dimer that was produced by crystallographic two-fold symmetry operation on the single monomer in the asymmetric unit (Figure 6.11). Like DHDPS-L197Y, crystal packing in no way resembled the packing of dimers in the tetramer and no crystal contacts were conveyed *via* the exposed interface surface.

Refinement of the molecular replacement solution of this structure in space group $P4_32_12$ proved troublesome. The full length of the protein chain was resolved in electron density maps produced during refinement. However, many side chains towards the periphery of the protein lacked sufficient clear electron density to guide rebuilding, and side chains that were resolved were found to have much higher B values than those on the interior. Additionally, peaks corresponding to ordered water molecules were not evident in the numbers expected, based on prior experience. Density modification by solvent flattening failed to significantly improve electron density and attempts to solve the structure in alternative space groups of Laue class P4/mmm resulted in structures with unsatisfactory *R* values.

Inspection of the Wilson plots revealed that the Wilson B-factor for the data set was estimated at 33.9 $Å^2$. This is in contrast to a value of 19.1 $Å^2$ estimated for the DHDPS-L197Y data set, and values of around 20 $Å^2$ for the two wild-type structures and two other mutant structures (Dobson, R. C. J. *pers. comm.*) solved in this lab.

Since the Wilson B-factor gives an indication of the average B value obtainable on model refinement, it is likely that the observation of thermal disorder in the DHDPS-L197D is real. Thus, difficulties experienced in the refinement of this structure may be due to this factor, perhaps combined with space group ambiguity.

6.4.1 General features of the structure

Rebuilding and refinement of the DHDPS-L197D model in the tetragonal spacegroup, $P4_32_12$, followed by placement of 12 resolved water molecules resulted in a final R_{Cryst} value of 0.307 and an R_{Free} value of 0.344. Figure 6.12 shows that the tertiary structure of the DHDPS-L197D dimer is essentially identical to that of the tight-dimer unit of wild-type DHDPS, and that the details of the monomer-monomer interface are conserved.

Figure 6.12 *The crystal structure of DHDPS-L197D. Subunits A and B associate* via *a crystallographic two-fold symmetry axis, to form a dimer analogous to the tight-dimer unit of wild-type* E. coli *DHDPS.*

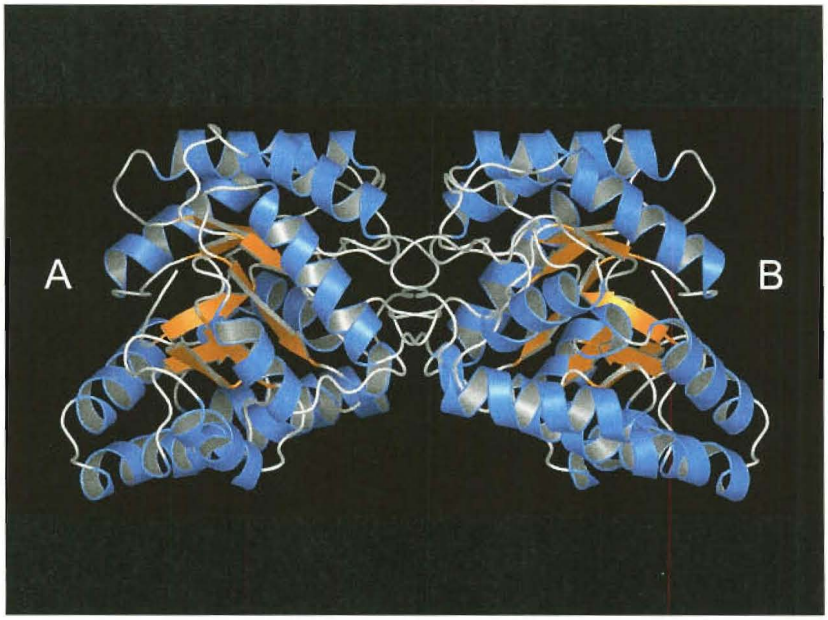

Analysis of peptide torsion angles in the solved monomer revealed that Y107 remains in a strained conformation in the DHDPS-L197D variant (Figure 6.13), suggesting that this residue has adopted the correct position in the proton relay triad. As was found in DHDPS-L197Y, a second residue, in this case K155, was found in the generously allowed region of the Ramachandran plot. K155 forms part of the same loop region linking helix α5 to strand β6 in the $(\alpha/\beta)_8$ barrel structure that was found to be displaced in the DHDPS-L197Y structure. Inspection of the alignment of the DHDPS-L197D and wild-type DHDPS monomers (section 6.4.2) reveals that this loop is also displaced in DHDPS-L197D from its position in the wild-type structure, while helix α5 and strand β6 remain in position (data not shown). Again the reason for this displacement is unclear from the DHDPS-L197D structure.

Figure 6.13 *Ramachandran plot of the peptide chain in the asymmetric unit of DHDPS-L197D. a, b, l, and p are allowed regions for torsion angles, ~a, ~b, ~l, and ~p are generously allowed regions for torsion angles, white regions are disallowed regions.* ▲ *represents glycine residues and* ■ *represents other residues.* ■ *denotes residues in disallowed or generously allowed regions.*

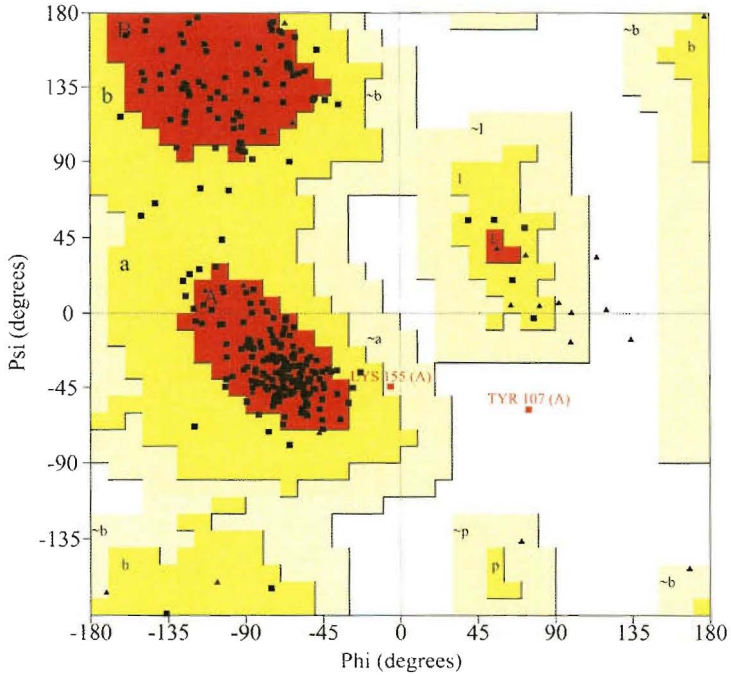

6.4.2 Alignment of the DHDPS-L197D and wild-type DHDPS structures

Alignment of monomer A of DHDPS-L197D with monomer A of the wild-type structure resulted in an r.m.s.d for the α-carbon atoms of 0.40 Å. Alignment of the symmetry produced DHDPS-L197D dimer with the tight-dimer unit of the wild-type

enzyme yielded an r.m.s.d of 0.45 Å, indicating very high conservation of secondary, tertiary and quaternary structural details. Figure 6.14 shows the overlay of the α-carbon traces of the two structures produced from the dimer alignment.

Figure 6.14 *Alignment of the DHDPS-L197D dimer (red spline) with the tight dimer unit of wild-type DHDPS (light blue spline).*

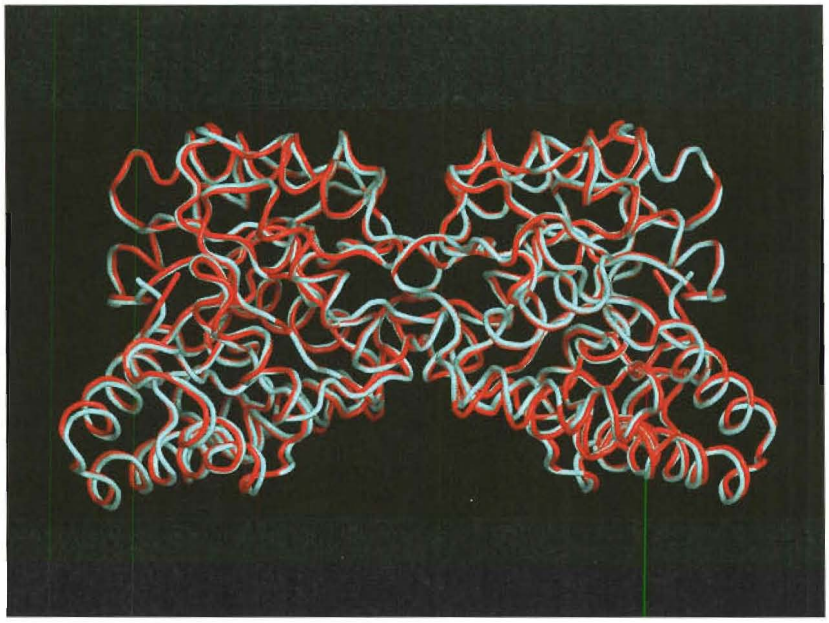

Inspection of these alignments reveals that all secondary structural elements are intact and correctly positioned within the monomeric model of the structure of DHDPS-L197D. Inspection of the orientation of the monomers with respect to each other in the symmetry produced dimer shows a small shift in DHDPS-L197D with respect to the wild-type structure (Figure 6.14). The angle that the monomers make to each other, when viewed in the plane shown in Figure 6.14, has been altered in DHDPS-L197D, suggesting a slight hinging across the short dimension of the elliptical interface. This may be due to crystal packing causing subtle bending of the dimer.

6.4.3 The mutation site, D197

Modelling of the mutated residue, D197, proceeded as for DHDPS-L197Y. Density around this side chain calculated from an omit-map indicated an essentially planar side chain allowing the correct modelling of aspartate at this site (Figure 6.15).

Figure 6.15 *Residue D197 of DHDPS-L197D covered by electron density calculated for a model omitting this side chain. 2Fo-Fc electron density (blue) is contoured at 1σ.*

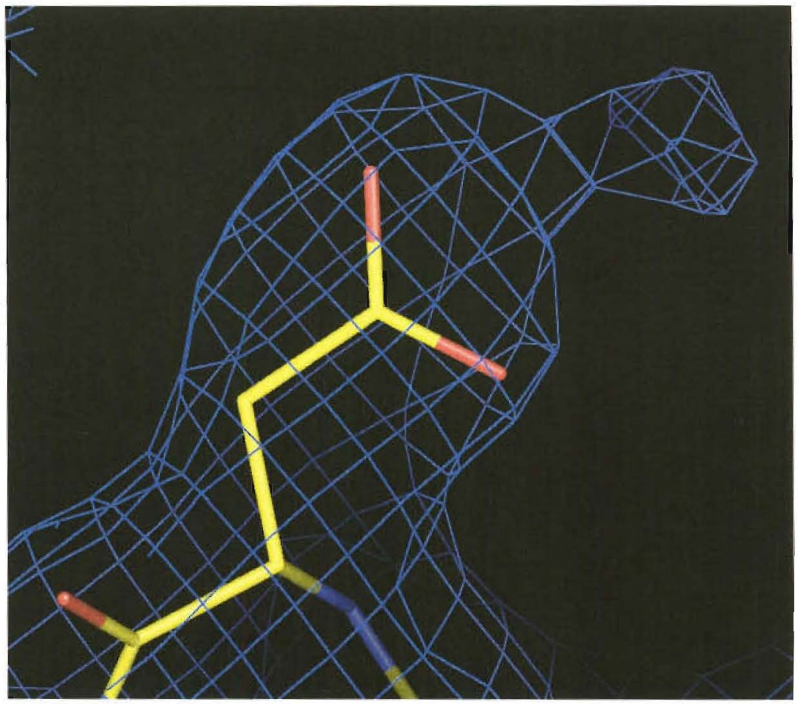

Figure 6.16 *Overlay of the mutation site of DHDPS-L197Y (yellow) with wild-type DHDPS (light blue) produced from the alignment of single monomers from the structures.*

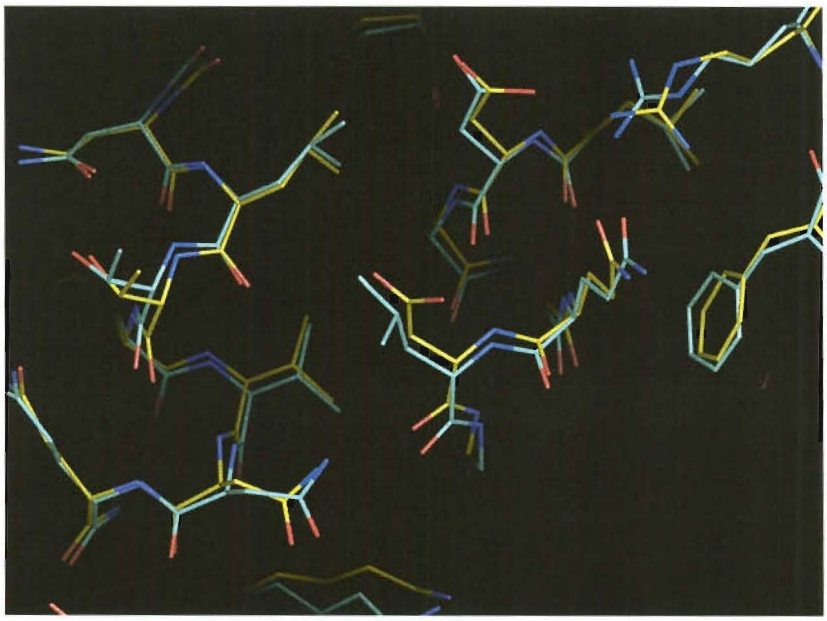

The single monomer alignment of DHDPS-L197D and the wild-type structures showed that the structure in the vicinity of the mutation was conserved in the variant (Figure 6.16). D197 has adopted a rotamer similar to that of the leucine residue it

replaced and side chains in direct contact with D197 hold the same conformation as in the wild-type structure. Secondary structural elements have also not been displaced around the site of the mutation, showing that gross structural alteration has not occurred as a direct result of the L197D point mutation.

6.4.4 The active site

Alignment of monomer A of DHDPS-L197D with monomer A of the wild-type enzyme showed that all active site binding and catalytic motifs were intact in the DHDPS-L197D structure. Figure 6.17 shows the overlay of the active sites detailing the pyruvate binding residue, K161, and the proton relay triad consisting of Y133, T44, and Y107. Slight displacements of the side chains of the three residues forming the proton relay are evident from this alignment; however, given the limitations of the final model for DHDPS-L197D these may be exaggerated. Interatomic distances between relevant groups forming the proton shuttle in the variant remain consistent with strong hydrogen bonding, indicating that this motif remains intact.

Figure 6.17 *Overlay of the active sites of DHDPS-L197Y (yellow) and wild-type DHDPS (light blue) produced from the alignment of single monomers from the structures.*

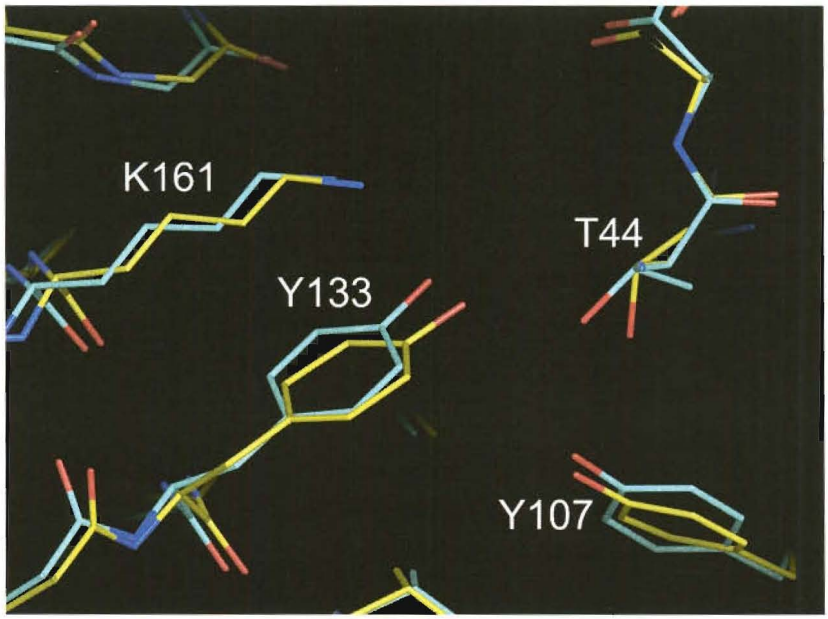

6.4.5 Density at K161

Like DHDPS-L197Y, DHDPS-L197D displayed extra electron density at the side chain of K161 (Figure 6.18). As the structure of DHDPS-L197D could not be fully refined, or perhaps due to incomplete occupancy, the form of this density is not as well defined as that in DHDPS-L197Y. Nevertheless, it is clear that the density does not represent a planar adduct at K161, and that the shape of the unsatisfied density is similar to that seen in DHDPS-L197Y. The position of the carboxyl group of pyruvate, as suggested by the density, is consistent with both DHDPS-L197Y and wild-type structures determined from pyruvate soaked crystals (14). The shape of the remaining density is consistent with the tetrahedral intermediate as modelled for DHDPS-L197Y and comprises a bulge corresponding to the putative water molecule hydrogen bonded to the oxyanion moiety.

Figure 6.18 *Positive electron density (green) observed at K161 of DHDPS-L197Y. 2Fo-Fc density is contoured to 1σ (blue), and Fo-Fc density is contoured to 3σ (green) and -3σ (red).*

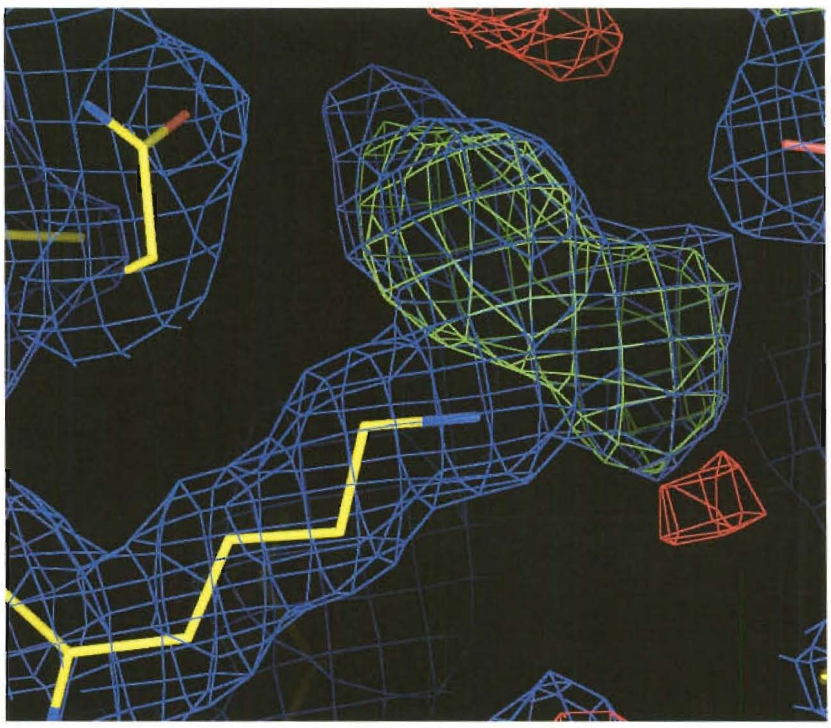

Again, DHDPS-L197D had been crystallised without the addition of pyruvate to the crystallisation buffer and pyruvate had not been added to the protein preparation during purification. Thus, the bound pyruvate was carried through processing of the

protein from the crude cell lysate, indicating that this variant was displaying behaviour similar to DHDPS-L197Y that has not been seen in the wild-type structures.

6.5 Summary

The crystal structures of the two obligate dimeric variants, DHDPS-L197Y and DHDPS-L197D, were solved to resolutions of 1.7 Å and 2.0 Å respectively. The structures demonstrate that all details of the wild-type DHDPS tight-dimer structure, including active site motifs, are highly conserved in both variants. Electron density observed at K161, indicates that pyruvate is covalently bound to this residue in the form of the tetrahedral reaction intermediate, despite crystallisation in the absence of the substrate. This trapping of a K161-pyruvate adduct will be discussed further in Chapter seven.

6.6 References

1. Dobson, R. C. J., Griffin, M. D. W., Jameson, G. B., and Gerrard, J. A. (2005) The crystal structures of native and (*S*)-lysine bound dihydrodipicolinate synthase from *Escherichia coli* with improved resolution show new features of biological significance. *Acta Crystallogr D Biol Crystallogr*, (Submitted)
2. Rhodes, G. (2000) *Crystallography made crystal clear*, Academic Press, San Diego
3. Bergfors, T. M. (1999) *Protein crystallization*, International University Line, La Jolla
4. Drenth, J. (1999) *Principles of protein X-ray crystallography (2nd ed.)*, Springer-Verlag, New York
5. Pflugrath, J. W. (1999) The finer things in X-ray diffraction data collection. *Acta Crystallogr D Biol Crystallogr* **55**, 1718-1725
6. Navaza, J., and Saludjian, P. (1997) AMoRe: An automated molecular replacement program package. *Methods Enzymol* **276**, 581-594
7. Collaborative computational project, n. (1994) The CCP4 suite: programs for protein crystallography. *Acta Crystallogr D Biol Crystallogr* **50**, 760-763
8. Murshudov, G. N., Vagin, A. A., and Dodson, E. J. (1997) Refinement of macromolecular structures by the maximum-likelihood method. *Acta Crystallogr D Biol Crystallogr* **53**, 240-255
9. Jones, T. A., Zou, J. Y., Cowan, S. W., and Kjeldgaard. (1991) Improved methods for building protein models in electron density maps and the location of errors in these models. *Acta Crystallogr A* **47**, 110-119

10. Jones, T. A., and Kjeldgaard, M. (1997) Electron-density map interpretation. *Methods Enzymol* **277**, 173-208

11. Lamzin, V. S., and Wilson, K. S. (1997) Automated refinement for protein crystallography. *Methods Enzymol* **277**, 269-305

12. Laskowski, R. A., Macarthur, M. W., Moss, D. S., and Thornton, J. M. (1993) Procheck: A program to check the stereochemical quality of protein structures. *J Appl Crystallogr* **26**, 283-291

13. Kleywegt, G. J., and Jones, T. A. (1997) Detecting folding motifs and similarities in protein structures. *Methods Enzymol* **277**, 525-545

14. Blickling, S., Renner, C., Laber, B., Pohlenz, H. D., Holak, T. A., and Huber, R. (1997) Reaction mechanism of *Escherichia coli* dihydrodipicolinate synthase investigated by X-ray crystallography and NMR spectroscopy. *Biochemistry* **36**, 24-33

15. Blickling, S., Beisel, H. G., Bozic, D., Knablein, J., Laber, B., and Huber, R. (1997) Structure of dihydrodipicolinate synthase of *Nicotiana sylvestris* reveals novel quaternary structure. *J Mol Biol* **274**, 608-621

16. Mirwaldt, C., Korndorfer, I., and Huber, R. (1995) The crystal structure of dihydrodipicolinate synthase from *Escherichia coli* at 2.5 Å resolution. *J Mol Biol* **246**, 227-239

17. Ramachandran, G. N., and Sasisekharan, V. (1968) Conformation of polypeptides and proteins. *Adv Protein Chem* **23**, 283-438

18. Dobson, R. C., Valegard, K., and Gerrard, J. A. (2004) The crystal structure of three site-directed mutants of *Escherichia coli* dihydrodipicolinate synthase: further evidence for a catalytic triad. *J Mol Biol* **338**, 329-339

Chapter Seven

Summary and conclusions

A model for the evolution of quaternary structure in *E. coli* DHDPS

7.1 Introduction

The aim of this thesis, as set out in Chapter one, has been to investigate the functional and mechanistic advantages conferred by the tetrameric structure of *E. coli* DHDPS. This project was undertaken in light of structural data that suggested that the tight-dimer unit of the enzyme should display autonomous function, in terms of both catalysis and regulation. Chapters four, five, and six reported and discussed the results of the biophysical, kinetic, and high resolution structural characterisation of wild-type *E. coli* DHDPS, and the point-mutant variants designed and produced in Chapters two and three.

The present chapter draws together and relates the results of all experiments presented in this thesis and offers a functional rationale for the existence of *E. coli* DHDPS as a homotetrameric structure. Finally, based on this rationale, a model for the process of evolution of the quaternary structure in *E. coli* DHDPS is proposed.

7.2 Schiff base formation is affected in dimeric variants of *E. coli* DHDPS

As detailed in section 1.3.5, the first half reaction of DHDPS is initiated by nucleophilic attack of the ε-amino group of K161 on the keto-group of pyruvate (Figure 7.1, step 1), resulting in formation of the Schiff base (step 2), followed by proton abstraction from the methyl carbon of pyruvate to form the enamine (step 3). It is this proton, released on formation of the enamine, that is proposed to constitute the first product of the reaction mechanism, thereby separating the two half reactions with regards to the ping-pong kinetic mechanism (1,2).

Results presented in previous chapters of this thesis, and elaborated below, indicate that the transition from the tetrameric structure of wild-type *E. coli* DHDPS to the dimers of DHDPS-L197D and DHDPS-L197Y, affects this first half reaction.

Figure 7.1 *The first half reaction of DHDPS comprising the formation of an enamine between K161 and pyruvate with the release of a proton.*

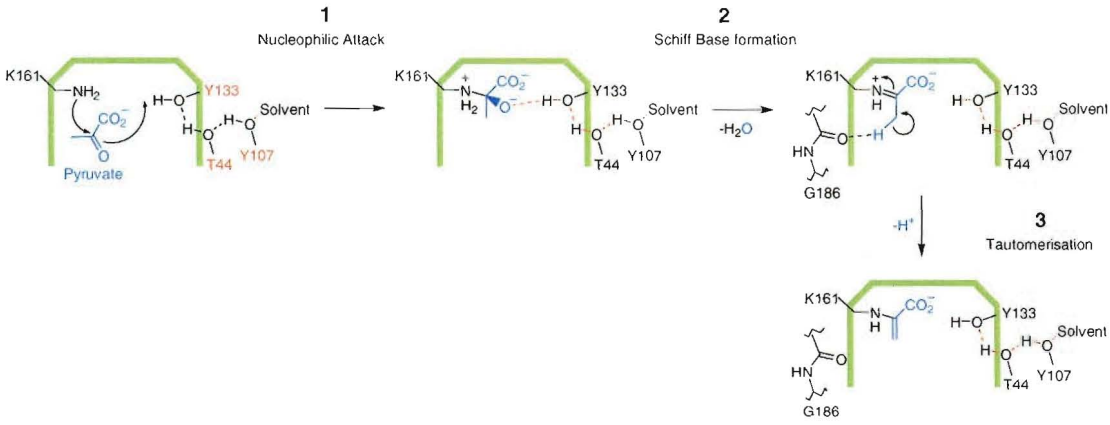

The active site of DHDPS carries out two essential catalytic processes during the first half reaction. The first of these is the stabilisation of the oxyanion intermediate leading to the formation of the Schiff base. Structural (1) and mutagenesis (3) studies have provided evidence that Y133 assists the reaction through a hydrogen bond between the side chain hydroxyl and the keto-oxygen/oxyanion of pyruvate. The second process is the movement of protons into and out of the active site, allowing the dehydration of the tetrahedral intermediate state and the subsequent tautomerisation of the Schiff base to the enamine. This is carried out by the triad of hydrogen bonded side chains, Y133, T44, and Y107, which function to shuttle protons between the active site and bulk solvent (1,3,4) (Figure 7.1).

Figure 7.2 shows the configuration of the two active site proton-relay triads in the tight-dimer. As described in section 1.4.1, Y107 protrudes into the active site of one monomer from the adjacent monomer of the tight-dimer, and forms a hydrogen bond with the side chain hydroxyl of T44. The side chain hydroxyl of Y107 is also hydrogen bonded to an ordered water molecule at the surface of the protein, and thus, completes the proton-relay to bulk solvent.

Figure 7.2 *The two proton-relay triads of the DHDPS tight-dimer. The two monomers of the tight-dimer are shown in light blue and yellow.*

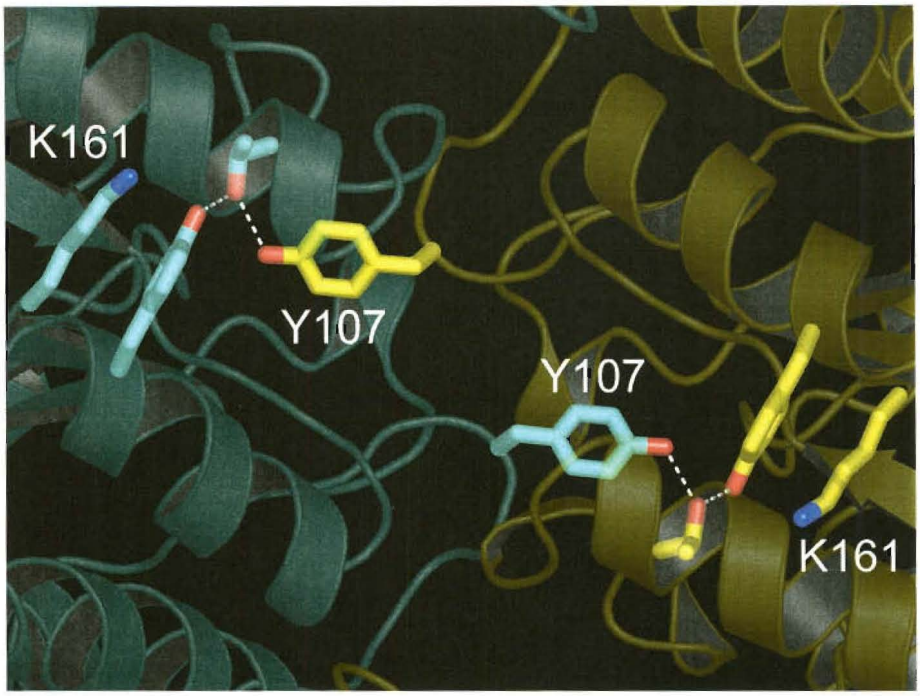

7.2.1 Catalysis is attenuated in all variants

The kinetic analysis presented in Chapter five showed that all variants displayed attenuated catalytic efficiency when compared to the wild-type enzyme. This was most marked in the two obligate dimers, DHDPS-L197D and DHDPS-L197Y, which retained 2.5% and 1.4% of wild-type activity respectively. This demonstrates that the association of two tight-dimer units to form the wild-type DHDPS tetramer is necessary for full catalytic activity. X-ray crystal structures showed that all secondary, tertiary, and quaternary structural details of the wild-type tight-dimer were completely preserved in the two dimeric variants, indicating that gross structural rearrangement in the variants was not responsible for the attenuation of catalysis. Thus, some other factor, present in the tetramer but lacking in the dimeric mutants, must account for the observed differences in catalysis.

DHDPS-Q196D, DHDPS-D193A, DHDPS-D193Y, and DHDPS-Q234D each display activity around 10-15% of that of wild-type DHDPS. DHDPS-Q196D and DHDPS-D193A were found to display equilibria between dimer and tetramer in solution. Thus, significant populations of both dimer and tetramer in rapid equilibrium were present in the assay mixture, consistent with the activities observed, which were

intermediate between that of the wild-type tetramer and the variant dimers. Based on sedimentation velocity analysis, DHDPS-D193Y, and DHDPS-Q234D were also assumed to display partial dimeric character, consistent with their observed activities.

7.2.2 Pyruvate binding is hindered in the variants

Concomitant with the observed reduction in catalytic activity was the observation of an increase in the K_m for pyruvate determined for each variant, indicating that binding of this substrate was hindered. Inspection of the kinetic parameters revealed that the magnitude of the increase in K_{mPyr}, relative to the wild-type enzyme, correlated with the degree of attenuation of catalytic efficiency in the variants. This suggested that attenuation of activity in the variants is related to pyruvate binding. Additionally, the fact that all other raw kinetic parameters for all variants were completely consistent with those of wild-type DHDPS indicated that the major kinetic effect was on the first half reaction.

7.2.3 DHDPS-L197D and DHDPS-L197Y display a shift in kinetic mechanism

The two dimeric variants, DHDPS-L197D and DHDPS-L197Y, displayed the characteristic initial rate patterns of the compulsory-order ternary-complex kinetic mechanism. This is in contrast to the ping-pong mechanism assigned for the wild-type enzyme (2) and means that the strict reaction sequence of wild-type DHDPS has become relaxed in these variants.

In the classical form of the ping-pong mechanism, the formation of a ternary-complex is structurally impossible because the binding sites for the two substrates are either the same or overlapping (5). Thus, the first half reaction must be completed, and the leaving group cleared from the active site, before the second substrate can bind and complete catalysis.

In the context of the DHDPS reaction mechanism a shift in kinetic mechanism from ping-pong to ternary-complex may indicate that (*S*)-ASA is able to bind to the enzyme, after pyruvate binding, but before the formation of the Schiff base or the enamine, breaking down the distinction between the first and second half reactions. Presumably, this would also be possible in the wild-type enzyme, but would become much more apparent if the first half reaction were highly impaired or slowed.

7.2.4 Pyruvate has been trapped at the active site of DHDPS-L197D and DHDPS-L197Y

The remarkable observation of pyruvate, covalently bound to K161 as the tetrahedral reaction intermediate in the structures of DHDPS-L197D and DHDPS-L197Y, is strong evidence that catalysis of the reaction of pyruvate with K161 is impaired in these variants. That this adduct has persisted at the active site over numbers of months, through preparation, storage, and crystallisation, indicates that this intermediate reaction product is truly trapped in the state observed in DHDPS-L197Y.

7.3 The function of the proton-relay triad is impaired in the variants

All results discussed in section 7.2 can be explained by impaired function of the proton relay triad (Figure 7.2) in all variants. It is proposed that the impaired function of this essential motif is due to dynamic flexing of the dimer about the long dimension of the elliptical contact between the monomers. The direct effect of this movement on the proton-relay is to alter the position and orientation of Y107, displacing the side chain hydroxyl and breaking or weakening hydrogen bonding to the side chain of T44 (Figure 7.3). This would affect catalysis by reducing efficiency of proton movement by the triad, thereby raising the activation barrier and reducing the rate of reaction steps requiring proton movement.

A rise in the barrier to dehydration of the tetrahedral intermediate to form the Schiff base in the variants (Figure 7.4) would slow the rate of this reaction, consistent with the reduced catalytic activity observed. In this situation, the bound pyruvate will endure for a much longer period as the tetrahedral intermediate during the reaction cycle of the variants than in wild-type DHDPS. It is proposed that the binding of (*S*)-ASA to this enzyme-pyruvate complex acts, in part, to promote dehydration of the tetrahedral intermediate, allowing the reaction to proceed. In this case the reaction mechanism no longer proceeds through two distinct half reactions, explaining the shift in kinetic mechanism observed in the dimeric variants as discussed in section 7.2.3.

Figure 7.3 *The proposed flexing movement of the monomers of the dimeric variants. a) shows a schematic representation of the orientation of the flex. b) is a view of the proton-relay triads in the orientation depicted in a) and shows the consequence of this flexing on Y107.*

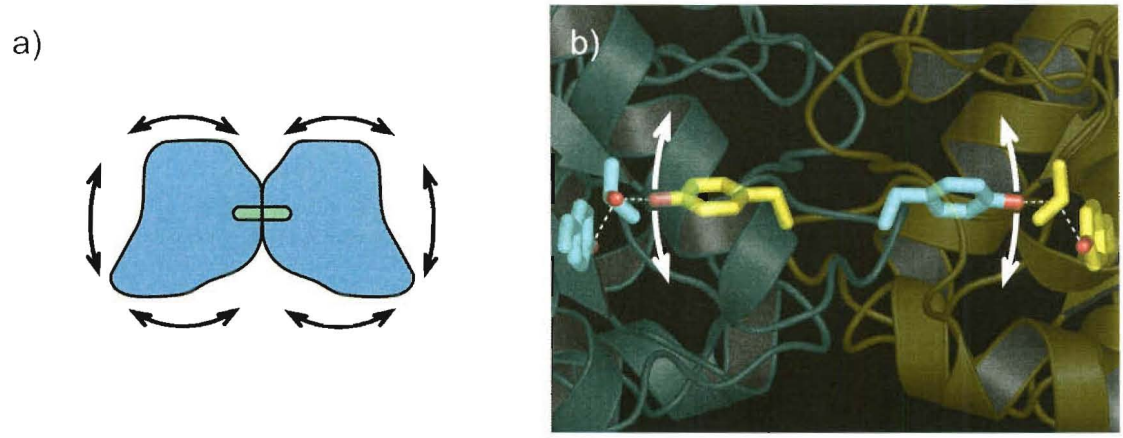

Figure 7.4 *Schematic energy diagrams for the reaction of pyruvate with K161 to form a Schiff base. a) represents the reaction energetics proposed for the reaction in wild-type DHDPS. b) depicts the raised activation barrier to the dehydration step and the stabilisation of the tetrahedral reaction intermediate postulated for the dimeric variants DHDPS-L197D and DHDPS-L197Y.*

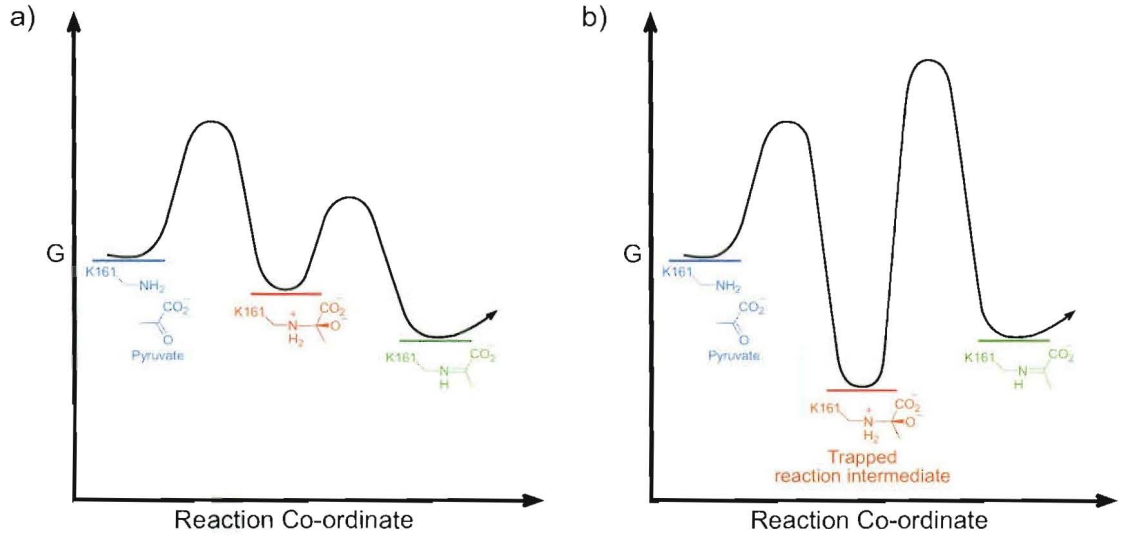

This also provides an explanation for the observed long term trapping of the intermediate in DHDPS-L197D and DHDPS-L197Y. The persistence of the tetrahedral reaction intermediate facilitates further structural stabilisation of this intrinsically unstable adduct (Figure 7.4b). This is consistent with the very close contact observed between the oxyanion oxygen of the pyruvate and the hydroxyl group of Y133, as modelled in DHDPS-L197Y (Figure 6.11). Thus, the tetrahedral

intermediate has become trapped in a state from which the reaction can not proceed forwards or backwards at low temperatures. Since pyruvate is abundant in the cell, this substrate will continue to bind to the variant enzymes while in the crude cell lysate resulting in trapping of the intermediate.

Energetic considerations suggest that the release of the trapped pyruvate adduct may be promoted at raised temperature. This is consistent with the puzzling results of Selwyn's test for DHDPS-L197D and DHDPS-L197Y described in section 5.4 where activation of the dimeric variants during assay was observed at 30°C. Building on this observation, further research carried out in this lab has explored the activation of the dimeric varaints by incubation at constant temperature over extended time periods prior to assay. These experiments showed that the initial velocity of both DHDPS-L197D and DHDPS-L197Y increases steadily over time when the enzymes are incubated at raised temperature with and without the presence of pyruvate. Identical incubations at 4°C failed to produce activation in the variants and no activation was seen in wild-type DHDPS at any temperature (Dobson, R. C. J., Antonio, L. *pers. comm.).*

Figure 7.5 *The heat activation of DHDPS-L197D as a function of time at 4°C (blue) and 42°C (red) in the presence of 20 mM pyruvate. Unpublished data provided by R. C. J. Dobson.*

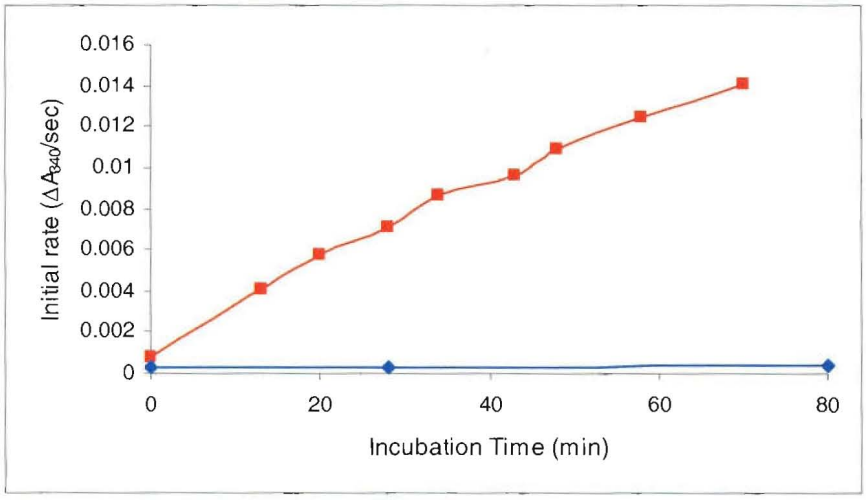

7.4 The tetrameric structure of *E. coli* DHDPS allows efficient functioning of the active site proton-relay triad

From these findings, it is possible to conclude that the tetrameric structure of *E. coli* DHDPS functions to facilitate optimal movement of protons into and out of the active site *via* the proton-relay triad. This is achieved by preventing the breathing or flexing movement discussed above and shown in Figure 7.3. Association of two tight-dimer units in the configuration present in *E. coli* DHDPS effectively rigidifies the dimers, specifically allowing Y107 to maintain its correct position in the proton relay triad. In this way, the problem of pyruvate trapping is avoided and optimal catalysis can proceed in the tetrameric enzyme.

Figure 7.6 *The heat activation of DHDPS-Y107F as a function of time at 4°C (blue) and 42°C (red) in the presence of 20 mM pyruvate. Unpublished data provided by R. C. J. Dobson.*

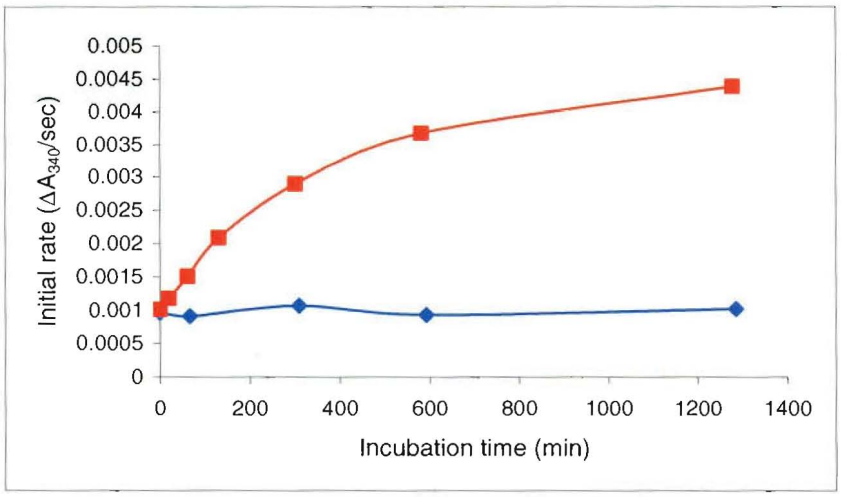

This conclusion predicts that the active site mutant, Y107F, would display similar behaviour to the obligate dimeric variants produced and investigated in this study. This mutation removes the side chain hydroxyl group that completes the proton-relay to bulk solvent and thus would be expected to severely attenuate activity of this motif. The crystal structure of the tetrameric DHDPS-Y107F mutant was solved as part of a separate study carried out in this lab (3) and revealed density at K161 consistent with the tetrahedral reaction intermediate as observed in DHDPS-L197Y. Additionally, kinetic analysis of DHDPS-Y107F showed that activity was reduced when compared to the wild-type enzyme, and that the catalytic turnover of the mutant increased over

time when incubated at raised temperatures (Figure 7.6). These findings add strength to the conclusions reached in this study.

7.5 A model for the evolution of quaternary structure in *E. coli* DHDPS

This conclusion can be extended to postulate a plausible progression for the evolution of the quaternary structure of *E. coli* DHDPS.

Presumably, an ancestral monomeric DHDPS contained a proton-relay diad, comprising Y133 and T44. A bound water molecule, hydrogen bonded to T44, is likely to have completed the proton relay, facilitating proton donation to bulk solvent (Figure 7.7a). This is completely plausible since the crystal structure of DHDPS-Y107F revealed that the position of the side chain hydroxyl of Y107 had been replaced by an ordered water molecule that was hydrogen bonded to the side chain of T44 (3). This water molecule offered surrogate proton-relay activity, thereby avoiding complete abolition of activity in the mutant.

Association of two identical monomers to form a dimeric enzyme completed the proton-relay triad *via* interdigitation of Y107 residues. This made possible an increase in the catalytic rate of the enzyme by increasing efficiency of proton movement, provided the dimer adopted an appropriate configuration for hydrogen bonding of Y107 (Figure 7.7b). Since the dimeric structure can breathe in solution, flexing at the interface hindered placement of the tyrosine side chain, and catalysis remained sub-optimal at mesophilic temperatures.

The structure of DHDPS from the ancient hyperthermophile, *Thermotoga maritima* (6), has recently been deposited in the protein data bank (PDB code 105K). *T. maritima* represents the deepest known branching point in the eubacterial line of descent, and is the most slowly evolving of eubacterial lineages (7). Characterisation of the quaternary structure of this enzyme is incomplete (Lesley, S. A. *pers. comm.*); however, measurements suggest that the protein displays at least partial dimeric character. This lends support to the hypothesis that the enzyme evolved *via* this tight dimer form. Additionally, pyruvate is observed at the active site of *T. maritima* DHDPS despite crystallisation in the absence of this substrate, suggesting that a similar trapping process has occurred. In this case, the problems associated with the

potential trapping of the tetrahedral reaction intermediate are avoided *in vivo*, since the optimal growth temperature of *T. maritima* is around 80°C (6).

Figure 7.7 *A model for the evolution of quaternary structure in DHDPS. a) A putative monomeric ancestor of DHDPS may have had a bound water molecule participating in proton-relay to bulk solvent. b) Dimerisation of identical monomers completed the proton-relay triad by interdigitation of tyrosine residues at the interface but flexing of the dimer hindered efficiency of the catalytic triad. c) Tetramer formation rigidified the dimers, resulting in optimal catalysis by the proton-relay triad.*

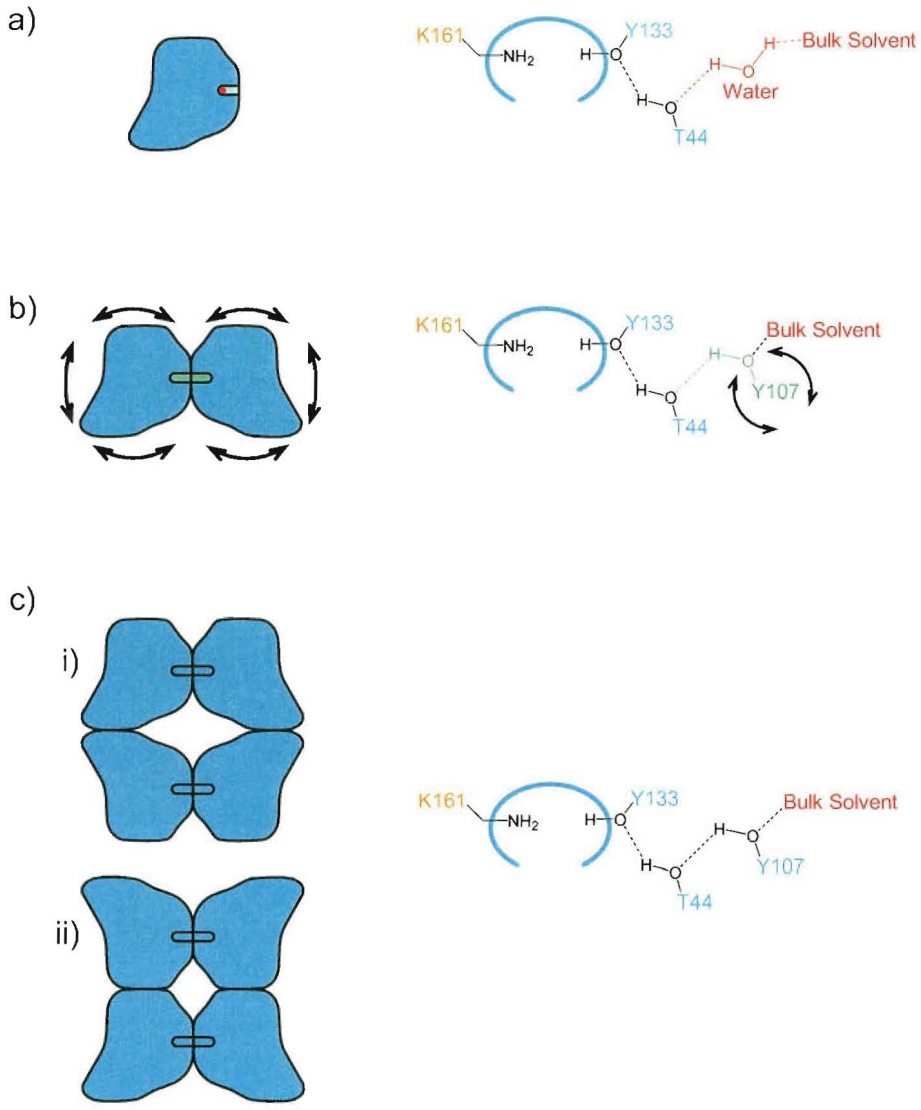

In the modern DHDPS enzymes, breathing is overcome by association of two tight-dimer units and the enzyme reaches optimal catalytic efficiency by restriction of monomer movement within the dimer. Association of the dimers to constrain the proposed flexing of the monomers of the tight-dimer can conceivably occur in two alternate orientations (Figure 7.7c) and both tetrameric architectures have been

observed in nature. Figure 7.7c i) shows the configuration of the *E. coli* enzyme (Figure 7.8a). Alternatively, the configuration shown in Figure 7.7c ii) will have a similar effect. This configuration has been found in plant DHDPS (Figure 7.8b).

Figure 7.8 *The tetrameric structures of* E. coli *DHDPS (a) and* N. sylvestris *DHDPS (b).*

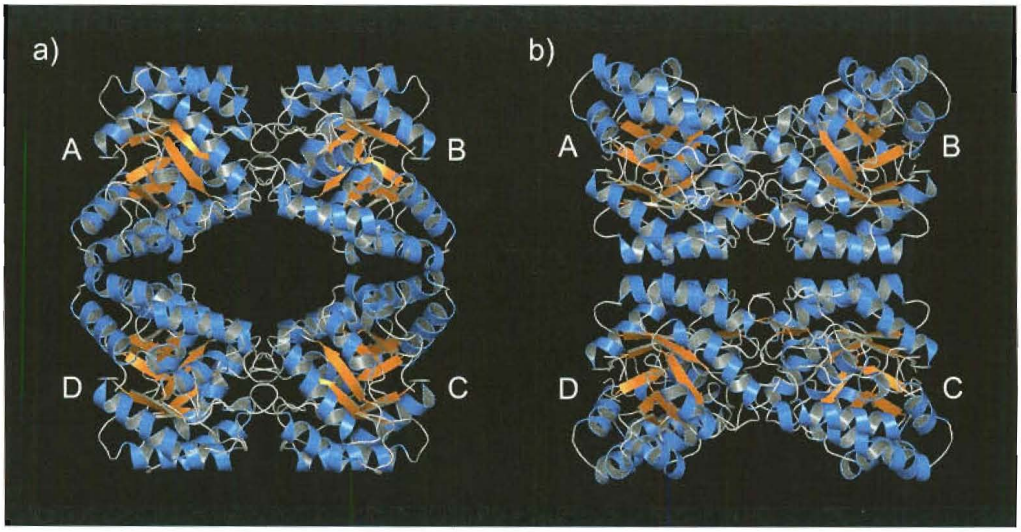

7.6 Conclusion

A functional advantage of the tetrameric structure of *E. coli* DHDPS, over a minimal dimeric structure, has been identified. It has been shown in this study that the tetrameric architecture of the enzyme serves to prevent dynamic breathing or flexing movements within the tight-dimer units of the structure, thereby allowing efficient catalysis *via* a proton-relay motif. It is proposed that, initially, the complete formation of this motif and subsequently, the achievement of optimal catalytic efficiency *via* this motif, have acted as driving forces for the evolution of the tetrameric quaternary structure of *E. coli* DHDPS.

This regulation of structural dynamics offers a functional advantage of oligomeric structure that may be of great importance in a range of oligomeric proteins with widely divergent functions. Such dynamic considerations have perhaps escaped attention in the past due to the focus on static images derived from X-ray crystallography. Greater insights into the role of quaternary structure in protein science will emerge as our appreciation of the dynamics of these structures develops.

7.7 References

1. Blickling, S., Renner, C., Laber, B., Pohlenz, H. D., Holak, T. A., and Huber, R. (1997) Reaction mechanism of *Escherichia coli* dihydrodipicolinate synthase investigated by X-ray crystallography and NMR spectroscopy. *Biochemistry* **36**, 24-33
2. Karsten, W. E. (1997) Dihydrodipicolinate synthase from *Escherichia coli*: pH dependent changes in the kinetic mechanism and kinetic mechanism of allosteric inhibition by *L*-lysine. *Biochemistry* **36**, 1730-1739
3. Dobson, R. C., Valegard, K., and Gerrard, J. A. (2004) The crystal structure of three site-directed mutants of *Escherichia coli* dihydrodipicolinate synthase: Further evidence for a catalytic triad. *J Mol Biol* **338**, 329-339
4. Blickling, S., Beisel, H. G., Bozic, D., Knablein, J., Laber, B., and Huber, R. (1997) Structure of dihydrodipicolinate synthase of *Nicotiana sylvestris* reveals novel quaternary structure. *J Mol Biol* **274**, 608-621
5. Cornish-Bowden, A. (1999) *Fundamentals of enzyme kinetics*, 2nd Ed., Portland Press Ltd, London
6. Huber, R., Langworthy, T. A., Konig, H., Thomm, M., Woese, C. R., Sleytr, U. B., and Stetter, K. O. (1986) *Thermotoga maritima* sp. nov. represents a new genus of unique extremely thermophilic eubacteria growing up to 90°C. *Arch Microbiol* **144**, 324-333
7. Achenbach-Richter, L., Gupta, R., Stetter, K. O., and Woese, C. R. (1987) Were the original eubacteria thermophiles? *Syst Appl Microbiol* **9**, 34-39

Chapter Eight

Experimental

8.1 Materials

Unless otherwise stated, chemicals were purchased from Aldrich Chemicals or Sigma Chemical Company Ltd (Castle Hill, Australia). Media for bacterial cultures was purchased from Invitrogen (Christchurch, New Zealand). SDS-PAGE gels were provided by Gradipore Ltd (Frenchs Forest, Australia). Restriction enzymes were supplied by Roche (Christchurch, New Zealand). Bio-Rad protein assay kit and DNA ladders were purchased from Bio-Rad Laboratories (Auckland, New Zealand). Column chromatography media were purchased from GE Healthcare (Auckland, New Zealand) as Hi-Trap pre-packed columns or as a loose gel, which was packed in Pharmacia XK type columns.

8.2 Microbiology and molecular biology methods

The laboratory texts '*Molecular Cloning: A laboratory Manual*' by Sambrook (1) *et al.* and '*A short course in bacterial genetics; a lab manual and handbook for E. coli and related bacteria*' by Miller (2) were invaluable as references for protocols in the manipulation of bacaterial strains and DNA.

8.2.1 Bacterial Strains

Two bacterial strains were used routinely in this study. *E. coli* XL-1 Blue (genotype - recA1, endA1, gyrA96, thi-1, hsdR17, supE44, relA1, lac [F' proAB lacI ZΔM15) was obtained from Stratagene as part of the QuikChange site-directed mutagenesis kit (3). AT997r$^-$ (genotype - relA1, spoT1, dapA15, thi-1, λ-, recA-) was produced from AT997 by phage transduction and recombination using P_{1vir} by Dobson (4) in this lab. AT997 was a gift from the *E. coli* genetic stock centre, Yale University (CGSC# 4547). The strain was originally characterised as a *dap*C mutant (5) but was later

reassigned as a *dap*A mutant after showing that the *dap*A gene, if in trans, rescued the strain when grown on minimal media (6).

8.2.2 Plasmids

All plasmids utilised in this work (Table 8.1) were based on the vector pBluescript KS+ (Stratagene). The genes *dap*A and *dap*B encode dihydrodipicolinate synthase and dihydrodipicolinate reductase respectively, and had been previously cloned into pBluescript KS+ by others (7-9).

Table 8.1 *Plasmids used for protein expression and their associated genotypes.*

Plasmid	Relevant genotype
pJG001 (8)	::*dap*A, Amp^r
pJK001 (9)	::*dap*B, Amp^r
pL197D	::*dap*A-leu197asp, Amp^r
pL197Y	::*dap*A-leu197tyr, Amp^r
pQ196D	::*dap*A-,gln196asp, Amp^r
pD193A	::*dap*A-,asp193ala, Amp^r
pD193Y	::*dap*A-,asp193tyr, Amp^r
pQ234D	::*dap*A-,gln234asp, Amp^r

8.2.3 Bacterial cultures

All media and equipment for culture of bacteria were sterilised by either autoclave at 121°C for 20 min or by filtration through a 0.2 micron acrodisc (Gellman Sciences), or were purchased sterile. Solutions were prepared in sterile deionised or double distilled water. Standard sterile technique was employed in all manipulations of bacterial cultures and each experiment was accompanied by an appropriate control to monitor for contamination.

8.2.4 Media

Luria-Bertani medium (LB)

LB base was supplied by Gibco BRL in a ready to use powdered form. 20 g of LB base was added to 1 L of water, the pH was adjusted to 7 by addition of NaOH, and the media was autoclaved.

Minimal Media

10.6 g of minimal salts media (Gibco BRL) was added to 1 L of deionised water and autoclaved. 10 ml/L of filter-sterilised 10% glucose was added to this media prior to use.

NZY+ broth

10 g NZ amine, 5 g yeast extract, and 5 g NaCl was added to 1 L of sterile distilled water. The pH was adjusted to 7 with the addition of NaOH before the media was sterilised by autoclave. 12.5 ml of sterile 1 M $MgCl_2$, 12.5 ml of sterile 1 M $MgSO_4$, and 20 ml of sterile 20% glucose were added prior to use of the media.

SOC

Media was prepared in sterile distilled water to final concentrations of 2% w/v bacto-tryptone, 0.5% w/v yeast extract, 10 mM NaCl, 2.5 mM KCl, 10 mM $MgCl_2$, 10 mM $MgSO_4$, and 0.36% w/v glucose. This was then pH adjusted and sterilised by autoclave .

8.2.5 Antibiotics and nutritional supplements

Table 8.2 *Antibiotic concentrations used for bacterial selection.*

Supplement	[Stock] mg ml^{-1}	[Working] µg ml^{-1}
Ampicillin	100	100
Tetracycline	25	25
meso-Diaminopimelate	10	50

1000× or 200× concentration stock solutions of antibiotics and supplements were sterilised by filtration, where required, and stored at -20°C. Stock and working concentrations used for bacterial selection are shown in Table 8.2.

8.2.6 Plate preparation

Molten media containing 15 g/L agar at ~50°C was supplemented with the appropriate antibiotics, and poured directly into sterile petri dishes in a laminar flow hood or close to a flame. Minimal media plates were prepared from agarose, and minimal salt solution that had been sterilised separately and mixed immediately prior to pouring. Any bubbles were removed by flaming of the surface of the plates before setting. The plates were allowed to set overnight before use and could be stored for several weeks if sealed and kept at 4°C. Plates for blue/white selection were prepared by spreading 8 µl of 100 mg/ml IPTG and 40 µl of 20 mg/ml X-gal onto the surface. DMSO, which is used to dissolve the IPTG, was removed by incubation at 37°C for 2 hours.

8.2.7 Bacterial culture

Agar plates were streaked with the appropriate strain from a glycerol freeze, an overnight culture, or a single colony on an agar plate using a flame-sterilised nichrome wire. The plates were incubated overnight at 37°C. Individual colonies were selected and used to inoculate 3 ml of liquid medium. Starter cultures were grown overnight in a shaker incubator at 37°C with shaking at 180 rpm and subsequently used to inoculate larger quantities of media.

8.2.8 Preparation of glycerol freeze stocks for strain storage

1.5 ml of overnight culture was centrifuged at 5000 *g* for 5 min in a screw top cryo-storage tube and the supernatant aspirated. 750 µl of 20% glycerol in LB media was then added and the pellet resuspended gently before storage at -80°C.

8.2.9 Electroporation transformation of AT997r$^-$

Competent cell preparation

3 ml of media containing the appropriate antibiotics and supplements, was inoculated with bacteria from a freshly streaked agar plate, and the culture was grown overnight.

A 1/50 volume of this overnight culture was then used to inoculate fresh media, which was incubated at 37°C with shaking at 180 rpm. Cells were grown to an A_{600} of approximately 0.8, chilled on ice for 15 min, and harvested by centrifugation at 4000 *g* and 4°C for 5 min. The cell pellet was washed with one culture volume of cold sterile water and centrifuged as before. This wash process was repeated twice using 0.5 and 0.05 culture volumes of cold sterile water. The final cell pellet was re-suspended in 1/200 culture volumes of ice-cold 10% v/v glycerol in water, and 40 µl aliquots were stored at -80°C.

Transformation

Competent cells were removed from the storage and defrosted on ice 15 min prior to transformation. Plasmid DNA (usually 1 µl dissolved in either distilled water or low ionic strength buffer) was added to the cells before transferral to a pre-chilled, 0.2 cm gap, electroporation cuvette. Electroporation was performed on a Bio-Rad Gene Pulser set to 2.5 kV at 25 µF with the pulse controller set at 200 Ω. After delivery of a single pulse, the cells were immediately re-suspended in 1 ml of SOC medium, and elaborated at 37°C with gentle shaking for 1–2 hours. This elaborated culture was spread on LB agar plates with the appropriate selection and supplements, and incubated overnight. A transformation control, containing no plasmid DNA, was prepared in parallel with each transformation performed.

8.2.10 Transformation of AT997r$^-$ by the calcium chloride method

Competent cell preparation

3 ml of media containing the appropriate antibiotics and suplements, was inoculated with bacteria from a freshly streaked agar plate, and the culture was grown overnight. A 1/50 volume of this overnight culture was used to inoculate fresh media, which was incubated at 37°C with shaking at 180 rpm. Cells were grown to an A_{600} of approximately 0.8, chilled on ice for 15 min, and harvested by centrifugation at 4000 *g* and 4°C for 5 min. Cells were washed with 1/4 culture-volume of ice cold 10 mM NaCl, then centrifuged as before. A second wash in 1/8 culture volume of ice cold 100 mM $CaCl_2$ was performed and again centrifuged. The cells were finally re-suspended in a 1/15 volume of ice cold 100 mM $CaCl_2$ and 100 µl aliquots were stored on ice for 5 hours before transformation.

Transformation

1 µl of DNA was added to an aliquot of competent cells and incubated on ice for 0.5-1 hours. 1 ml of SOC medium was then added to the transformation before elaboration at 37°C with gentle shaking for 1 hour. The elaborated culture was spread on LB agar plates, with the appropriate selection and supplements, and incubated overnight. A transformation control, containing no plasmid DNA, was prepared in parallel with each transformation performed.

Standard $CaCl_2$ transformation protocols employ a heat pulse at 42°C after transformation (1); however, this step was found to cause a low rate of reversion (section 3.4.1) of the *dap*A$^-$ phenotype in AT997r$^-$, and was therefore omitted.

8.2.11 Standard plasmid preparation by alkaline lysis

Solution 1	50 mM glucose 10 mM EDTA 25 mM Tris.HCl pH 8.0
Solution 2	0.2 M sodium hydroxide 1% SDS
Solution 3	3 M sodium acetate pH 4.8 11.5% v/v glacial acetic acid
$T_{10}E_1$ buffer	40 mM Tris-acteate pH 8.0 1 mM EDTA

A single bacterial colony was used to inoculate 3 ml of LB broth containing appropriate antibiotics which was incubated overnight at 37°C with shaking at 180 rpm. 1.5 ml of culture was then transferred to a centrifuge tube and centrifuged at 10,000 *g* and 4°C for 2 min. The supernatant was removed by aspiration and the pellet resuspended in 100 µl of ice-cold solution 1 before incubation on ice for 10 min. 200 µl of freshly prepared solution 2 was then added, mixed by gentle inversion, and incubated on ice for 5 min. 150 µl of ice-cold solution 3 was added to this preparation and mixed gently until a white precipitate formed. This was incubated on ice for 20 min before centrifugation at 12,000 *g* for 5 min. 250 µl of 95% ethanol was added to the decanted supernatant, mixed, and incubated on ice for 5 min. After centrifugation

at 12,000 *g* for 5 min, the supernatant was carefully removed and the DNA pellet rinsed twice with 1 ml of 70% ethanol at 4°C followed again by centrifugation. The final pellet was dissolved in 200 µl of 3 M sodium acetate and vortexed briefly. 400 µl of 100% ethanol at 4°C was then added and the solution stored on ice for 10 min. The tube was finally centrifuged at 12,000 *g* for 5 min and the supernatant was aspirated. The pellet was dried in a 37°C incubator and, if no further purification was required, dissolved in 10 µl of $T_{10}E_1$ buffer or distilled water.

RNA precipitation and removal

The dried, ethanol washed, pellet was re-dissolved in 100 µl of ice cold $T_{10}E_1$ and incubated on ice for 30 min. 100 µl of ice cold 3 M LiCl was then added, and the resultant solution incubated on ice for 30 min. This was then centrifuged at 11,000 *g* for 10 min and the supernatant poured into a fresh centrifuge tube containing 0.54 volumes isopropanol. After incubation on ice for 10 min and centrifugation at 11,000 *g* for 10 min the pellet was washed with ethanol and dried as above. The pellet from this RNA precipitation step was re-suspended in 200 µl of $T_{10}E_1$ and any residual RNA was digested by addition of RNase A and incubation at 37°C for 30 min.

Phenol/chloroform protein extraction

After incubation, 200 µl phenol and 200 µl chloroform:isopropanol (1:1) was added, the solution gently mixed, and centrifuged at 13,000 *g* for 5 min at room temperature. The aqueous layer was then transferred to a new centrifuge tube containing 200 µl phenol and 200 µl chloroform:isopropanol and the process repeated 2-3 times. Finally, the aqueous layer was removed and added to 0.125 volumes of 2 M potassium acetate in 2 volumes of cold ethanol in a new tube. This was mixed, incubated on ice for 10 min, and centrifuged at 13,000 *g* and 4°C for 10 min. The DNA pellet was then rinsed with ice-cold ethanol, briefly centrifuged, and dried as above. The dried, purified DNA pellet was re-suspended in 10 µl of $T_{10}E_1$ buffer or distilled water.

8.2.12 Restriction digests

Restriction digests were performed in 10 µl volumes. A typical protocol is illustrated with the double digest of pJG001 with the restriction enzymes *Eco*R I and *Hin*d III. The reaction mixture contained 7 µl distilled water, 1 µl DNA solution (~300 ng

DNA), 1 µl 10× reaction buffer, 0.5 µl *Eco*R I (5 Units), and 0.5 µl *Hind* III (5 Units). This was incubated for 2 hours at 37°C before electrophoresis.

8.2.13 Agarose gel electrophoresis

Loading dye	30% v/v glycerol
	0.25% w/v bromophenol blue
	0.25% w/v xylene cyanol
TAE buffer	40 mM Tris-actate pH 8.0
	1 mM EDTA

Restriction fragments were typically mapped on a 1% w/v agarose gel against a 1 kb and/or a 100 bp ladder. When the fragments to be viewed were small (<500 bp) a 1.5% agarose gel was used. 30 ml of agarose in TAE buffer was cooled to ~50°C and poured into a gel casting tray. The gel was allowed to set completely (~30 min) before the well comb was removed and the casting tray was transferred into a gel tank containing TAE buffer. The gel was loaded with digested or uncut DNA in loading buffer, and DNA ladder. Electrophoresis was conducted at 60 V for two to three hours or until the bromophenol blue band was nearing the end of the gel. The gel was stained with 0.5 mg/ml ethidium bromide for 20 min and the DNA fragments were visualised under 302 nm UV radiation.

8.2.14 PCR site-directed mutagenesis

Site-directed mutagenesis was carried out as described in the Stratagene QuikChange site-directed mutagenesis manual (3).

Primer Design

Mutagenic primers introduce specific alterations into each strand of the template DNA by incorporation into the plasmid during the PCR step. Primers were designed according to the recommendations of the QuikChange site-directed mutagenesis manual (3) as follows.

Firstly, both primers contained the desired mutation and annealed to the same sequence on opposite strands of the plasmid. The primers were between 25 and 45

bases in length and had a calculated melting temperature (T_m) > 78°C according to Equation 8.1.

$$T_m = 81.5 + 0.41(\%GC) - 675/N - \%\ \text{mismatch} \qquad \text{Equation 8.1 (3)}$$

where N is the primer length in base pairs. The base substitutions were placed in the middle of the primer with at least 10-15 bases of correct flanking sequence. Finally, the primers were designed with a GC content of over 40% and with one or more C/G bases at each terminus.

The primer design process can be followed using the primers for the L197D mutation as an example. The *dap*A sequence around L197 (red) is shown below.

5'GAT GCG AGC GCG CTG GAC TTC ATG CAA TTG GGC GGT CAT GGG GTT ATT3'
L197

Possible codons for aspartate are GAT and GAC, thus a three base mutation was necessary for the substitution at L197. By introduction of the silent mutation, CAA to CAG, in the previous codon, Q196, a recognition site for the restriction endonuclease, *Fok* I, was generated at the mutation site. The 40-mer primers incorporating a four base mutation (blue) are shown below.

Primer L197D#1

5'GCG AGC GCG CTG GAC TTC ATG CAG GAT GGC GGT CAT GGG G3'
(23) D197 (13)

Primer L197D#2

5'C CCC ATG ACC GCC ATC CTG CAT GAA GTC CAG CGC GCT CGC3'
(13) D197 (23)

Primers were purified by Gibco BRL using PAGE.

PCR Reaction conditions

Three PCR reactions were prepared containing 10, 20, and 50 ng of template DNA. The reversion mutation of pWhitescript with mutagenic primers was used as a diagnostic control for this step. The pWhitescript plasmid has a point mutation in the *lacZ* gene (β-galactosidase) generating a stop codon at the ninth position of the coding

region. Mutagenic primers replace the stop codon with a glutamine codon restoring activity to the enzyme and allowing the determination of mutational efficiency by the proportion of blue/white colonies on IPTG/X-Gal plates. Mutagenesis reactions were prepared using plasmid pJG001 as template DNA. This was isolated from *E. coli* XL-1-pJG001 by alkaline lysis, and purified by RNA precipitation and phenol chloroform protein extraction (section 8.2.11). The DNA was quantified spectrophotometerically and the reactions where performed in thin walled PCR tubes as in tables 8.3 and 8.4.

Table 8.3 *Preparation of mutagenesis reaction for the L197D mutation of* dap*A.*

	[Initial]	Volume (µl)	Amount (ng)
10× reaction buffer		5	
pJG001 template 4.1-kb plasmid	18.5 ng/µl	2.7	10-50
L197D#1	9.41 ng/µl	13.28	125
L197D#2	7.21 ng/µl	17.17	125
dNTP mix		1	
double-distilled water (ddH_2O)		9.85	
Pfu Turbo DNA polymerase	2.5 Units/µl	1	

Table 8.4 *Preparation of the pWhitescript control mutagenesis reaction.*

	[Initial]	Volume (µl)	Amount (ng)
10× reaction buffer		5	
pWhitescript4.5-kbcontrol plasmid	5 ng/µl	2	10
oligonucleotide control primer#1	100 ng/µl	1.25	125
oligonucleotide control primer#2	100 ng/µl	1.25	125
dNTP mix		1	
Double-distilled water (ddH_2O)		37.5	
Pfu Turbo DNA polymerase	2.5 Units/µl	1	

Each reaction was overlaid with mineral oil to prevent evaporation and the PCR reaction carried out in a thermocycler equipped with a "hot bonnet", which also helped to prevent evaporation.

Table 8.5 *PCR cycling parameters used for mutagenesis reactions*

step	Temperature (°C)	Time (min)
1	95	0.5
2	95	0.5
3	55	1
4	68	12
5	steps 2–4 repeated 12 times	

Agarose gel electrophoresis was performed using 10 µl of the reaction product to confirm amplification of the template plasmid. 50 ng of template DNA was also electrophoresed in parallel to aid comparison.

Template Digestion

1 µl of *Dpn* I (10 Units), was added to each of the amplification reactions below the mineral oil. *Dpn* I is a methylated and hemimethylated specific enzyme, which digests the super coiled parental template DNA while leaving the mutated cDNA intact. The reaction mixture was gently, but thoroughly, mixed and incubated at 37°C for 1 hour.

Transforming Epicurean coli XL-1 Blue supercompetent cells

Epicurean coli XL-1 Blue competent cells were gently thawed on ice and 50 µl aliquots transferred to pre-chilled Falcon 2059 polypropylene tubes. 1 µl of mutated DNA was added to separate aliquots, mixed gently by pipetting and incubated on ice for 30 min. The transformation reaction was heat pulsed for 45 seconds at 42°C, and then placed on ice for 2 min. 0.5 ml of NZY+ broth, preheated to 42°C, was added and incubated 37°C for 1 hour with shaking at 225–250 rpm.

DNA sequencing

DNA sequencing reactions were performed at the Auckland Genomics Unit. Plasmids to be sequenced were prepared to the highest quality, quantified

spectrophotomectrically, and sequenced using BigDye dye terminator chemistry (Applied Biosystems).

8.3 Biochemistry general methods

Unless otherwise stated, enzymes were manipulated on ice or at 4°C. All enzymes were routinely stored in 20 mM Tris.HCl pH 8 at 4°C (buffer A) at -20°C in 1 ml aliquots. pH measurements were made using a standard pH meter fitted with a Russell Combination (Tris compatible) Electrode type number TR/CMAW711/TB. Centrifugation was performed in an Eppendorf Centrifuge 5430, on a small scale (<1.5 ml) at up to 15,000 rpm using a 16 F24-11 rotor, and on a large scale (< 50 ml) at up to 11,000 rpm using a 16A4-44 rotor at 4°C. Chromatography columns were run using Gilson Minipuls M312 peristaltic pumps with Gilson Model 740 system control software and a Gilson FC-203B fraction collector. PAGE was routinely run on a Bio-Rad Gel Electrophoresis Unit, using a Bio-Rad 300 power pack. Ultraviolet (UV) spectroscopy was performed on a Hewlett Packard 8452A Diode Array Spectrophotometer with a circulating water bath to maintain a constant temperature.

8.3.1 Standard Bradford assay for determining protein concentration

800 µl of appropriately diluted protein solution was added to 200 µl of Bradford reagent (10) and mixed thoroughly. The solution was incubated at room temperature for exactly 10 min before measurement of the absorbance at 595 nm against a blank consisting of 800 µl of sample buffer and 200 µl of Bradford reagent. Protein concentrations were obtained from a calibration curve generated in parallel using BSA obtained from Sigma. All measurements were prepared in duplicate.

8.3.2 Sodium dodecyl sulfate polyacrylamide gel electrophoresis

Electrophoresis tank buffer	0.3% w/v Tris.HCl
	14.4 % w/v glycine
	1% w/v SDS
Coomassie Blue Stain	1% w/v Coomassie blue
	50% v/v methanol
	10% v/v glacial acetic acid

Destain	5% v/v methanol
	10% v/v glacial acetic acid
2× Sample treatment buffer	0.125 M Tris.HCl pH 8.0
	4% w/v SDS
	20% v/v glycerol
	10% v/v 2-mercaptoethanol
	0.25% w/v bromophenol blue

For routine analysis of protein samples, pre-cast 8–16% gradient gels were used. Samples to be loaded were diluted with buffer to allow the loading of ~20 μg of total protein, and then mixed with an equal volume of 2× treatment buffer. Samples were incubated at 100°C for 2 min then briefly centrifuged before loading into the wells of the gel. Electrophoresis was conducted at 4°C at a constant voltage of 150 V until the bromophenol blue had run to the bottom of the resolving gel. The gel was then stained with Coomassie blue stain for 30 min, followed by destaining.

8.3.3 Preparation of dialysis tubing

Dialysis tubing was boiled for 10 min in a solution of 2% w/v sodium bicarbonate and 0.05% w/v EDTA. Care was taken to ensure the tubing remained submerged at all times. The tubing was then boiled for a further 10 min in deionised water, and this step was then repeated. The solution was cooled and the tubing stored in 0.02% w/v sodium azide for up to three months.

8.4 Overexpression and purification of wild-type and mutant DHDPS enzymes - modified from (11)

Buffer A	20 mM Tris.HCl pH 8 at 4°C

8.4.1 Growth of *E. coli* XL-1 Blue-pJG001 and *E. coli* AT997r$^-$

Cultures of *E. coli* XL-1 Blue-pJG001 or *E. coli* AT997r$^-$ containing the appropriate variant plasmid were streaked on LB agar plates containing appropriate antibiotic selection and grown overnight (37°C). A single colony was then selected and used to inoculate 3 ml of LB broth containing antibiotics, which was incubated overnight at 37°C with shaking at 180 rpm. From this overnight culture, 1 ml was used to

inoculate 1 L of LB broth containing selection and incubated for 20 hours as above. The cells were chilled on ice for 30 min and harvested by centrifugation at 5,000 *g* for 10 min. Cells were washed by re-suspending in 0.5 culture volumes of buffer A with gentle pipetting. The cell suspension was centrifuged at 5,000 *g* for 10 min and the supernatant was discarded. The cell pellet was re-suspended in a small volume of buffer A and centrifuged again as before. The final cell pellet was resuspended in 30 ml of buffer A. One L of inoculated LB broth gave approximately 4 g wet-weight of cells.

8.4.2 Preparation of a crude cell free extract by freeze thaw cycling

Harvested resuspended cells were flash frozen in liquid nitrogen and gently thawed by incubation on ice overnight. Repetition of this process for 7 cycles allowed gentle, selective release of cell contents. The cell free extract was then obtained by centrifugation at 10,000 *g* for 10 min and collection of the supernatant.

8.4.3 Preparation of a crude cell free extract by sonication

Harvested resuspended cells were subjected to ultrasonication in cycles of 3 sec bursts followed by 10 sec pauses. Sonication was continued until the cell suspension had received approximately 5,000 J. The supernatant was collected after centrifugation at 10,000 *g* for 15 min and the remaining pellet was re-suspended in buffer A. The sonication process was repeated once and the supernatant cell free extracts pooled.

8.4.4 Heat Shock of wild-type DHDPS

1 ml aliquots of the crude sonication extract were added to sterile centrifuge tubes. These were heat pulsed for 2 min at 70°C and immediately cooled on ice. After centrifugation at 15,000 *g* for 10 min, the supernatants were collected and pooled.

8.4.5 Ammonium sulfate precipitation of the DHDPS variants

Method development

0.5 ml aliquots of crude cell free lysate, was placed in centrifuge tubes and ammonium sulfate was added to final concentrations of 20, 25, 30, 35, 40, 45, and 50% w/v. Samples were kept on ice with periodic mixing for 45 minutes and were then centrifuged at 10,000 *g* for 10 min to remove precipitated proteins. The supernatants were placed in new tubes and the pellets were resuspended gently in

0.5 ml of buffer A. Activities of all fractions were determined using the coupled assay for DHDPS activity.

Preparative ammonium sulfate fractionation

The total crude cell free extract was brought to 30% ammonium sulfate by incremental addition of solid salt with mixing. This preparation was then mixed at 4°C for 45 min and precipitated proteins were removed by centrifugation at 10,000 *g* for 10 min and discarded. Further solid ammonium sulfate was added incrementally to the resulting supernatant, bringing the concentration to 40% w/v, and this solution was mixed at 4°C for 45 minutes. Precipitated proteins were collected by centrifugation at 10,000 *g* for 10 min and the supernatant discarded. The resulting pellet was resuspended in an equal volume of buffer A and dialysed twice against 100 volumes of buffer A at 4°C for 2 hours.

8.4.6 Ion exchange chromatography

The pooled sample from the heat shock, freeze thaw cycling, or ammonium sulfate precipitaiton was loaded on to a Q Sepharose ion exchange column (bed volume 75 ml, 15 × 2.6 cm) that had been pre-equilibrated with 5 bed volumes of buffer A. The column was then washed with 5 bed volumes of buffer A and the enzyme was eluted with a 0-1 M NaCl gradient in buffer A. The column was washed with three bed volumes of regeneration buffer (1 M NaCl in buffer A). Eluted fractions were tested for DHDPS activity using the *o*-aminobenzaldehyde micro assay described in Table 8.6.

Table 8.6 *The o-aminobenzaldehyde micro assay for DHDPS activity.*

	[Initial] (mM)	Volume (μL)	[Final] (mM)
Tris.HCl (pH 8 at 25°C), pyruvate	200, 40	150	166, 33
o-Aminobenzaldehyde (in ethanol)	400	5	10
DHDPS test solution		5	
(*S*)-ASA	40	15	1.2
Total volume		175	

The assay mixture was incubated at 30°C for 30 min, after which the reaction was quenched by the addition of 100 µl of 10% w/v TCA. Active fractions showed purple coloration and were pooled. Control reactions without enzyme or substrate were also prepared.

8.4.7 Hydrophobic interaction chromatography (HIC)

Ammonium sulfate was added to the pooled dialysed fractions from the ion exchange step to a final concentration of 0.5 M. This was then loaded onto a phenyl Sepharose column (bed volume 125 ml, 25 × 2.6 cm) that had been pre-equilibrated with at least five bed volumes of 0.5 M ammonium sulfate in buffer A. The column was then washed with five bed volumes of the start buffer (0.5 M ammonium sulphate in buffer A) and the enzyme was eluted with a 0.5–0 M ammonium sulfate gradient in buffer A. The column was then washed with three bed volumes of buffer A. The eluted fractions were tested for enzyme activity using the *o*-aminobenzaldehyde micro assay (Table 8.6). Active fractions eluted between 0.2 and 0.1 M ammonium sulfate and were pooled.

8.4.8 Hi-trap ion exchange

Where required, active fractions from the phenyl-sepharose column were loaded onto a Hi-Trap Q-Sepharose column (bed volume 1 ml) that had been pre-equilibrated with 5 bed volumes of buffer A. The column was washed with 5 bed volumes of buffer A and the enzyme eluted with a 0–1 M NaCl salt gradient in buffer A. The column was washed with three bed volumes of regeneration buffer (1 M NaCl in buffer A). The eluted fractions were tested for DHDPS activity using the *o*-aminobenzaldehyde micro assay (Table 8.6).

8.4.9 Dialysis

The purified enzyme was dialysed twice against 100 volumes of buffer A at 4°C for 2 hours.

8.5 Overexpression and purification of DHDPR - modified from (12,13)

Buffer A 20 mM Tris.HCl pH 8 at 4°C

8.5.1 Growth of *E. coli* XL-1 Blue (pJK001)

A frozen stock of *E. coli* strain XL-1 Blue-pJK001 was streaked on LB agar and incubated overnight at 37°C. A single colony was selected and used to inoculate 3 ml of LB broth containing both ampicillin and tetracycline, and incubated overnight at 37°C with shaking at 180 rpm. 1 ml of overnight culture was used to inoculate 1 L of LB broth containing antibiotics, and incubated as above. The culture was chilled on ice for 30 min before cells were harvested by centrifugation at 5,000 *g* for 10 min. Cells were washed by re-suspending in 0.5 culture volumes of buffer A with gentle pipetting. The cell suspension was centrifuged at 5,000 *g* for 10 min and the supernatant was discarded. The cell pellet was re-suspended in a small volume of buffer A and centrifuged again as before. The final cell pellet was resuspended in 30 ml of buffer A. One litre of inoculated LB broth gave approximately 4.5 *g* wet weight of cells.

8.5.2 Preparation of a crude cell free extract by sonication

Harvested resuspended cells were subjected to ultrasonication in 3 sec bursts followed by a 10 sec pause. Sonication was continued until the cell suspension had received approximately 5,000 J. The supernatant was collected after centrifugation at 10,000 *g* for 15 min and the remaining pellet was re-suspended in buffer A. The sonication process was repeated once and the supernatants pooled.

8.5.3 Heat shock

1 ml aliquots of the crude sonication extract were added to sterile centrifuge tubes. These were heat pulsed for 3 min at 70°C and immediately cooled on ice. Precipitated proteins were removed by centrifugation at 15,000 *g* for 10 min, and the supernatant was collected.

8.5.4 Ion exchange

The sample was loaded onto a Q Sepharose ion exchange column (bed volume 75 ml, 15 × 2.6 cm) that had been pre-equilibrated with 5 bed volumes of buffer A. The column was washed with five bed volumes of buffer A and the DHDPR was eluted with a 0-1 M NaCl salt gradient in buffer A. The column was then washed with three bed volumes of regeneration buffer (1 M NaCl, buffer A). The eluted fractions were tested for DHDPR activity using the coupled assay (Table 8.7). Active fractions eluted between 0.6 and 0.9 M NaCl, and were pooled.

Table 8.7 *The semi-quantitative assay for DHDPR activity.*

	[Initial] mM	Volume (μL)	[Final] mM
HEPES (pH 8), pyruvate	200, 80	500	100, 40
NADPH	5.4	30	0.162
DHDPR test sample	-	10	-
DHDPS (in excess)	-	50	-
(*S*)-ASA	40	30	1.2
dH_2O	-	380	-
Total		1000	

Table 8.7 describes the preparation of the assay used for detection of DHDPR activity. The reaction mixture, excluding the DHDPR test sample, was incubated in the preheated auto-sampler of the diode array for exactly 15 min to allow the temperature to reach 30°C and for the generation of the substrate of DHDPR, which is catalysed by DHDPS. Catalysis was initiated by the addition of the DHDPR sample (typically 10 μl) and the initial rate recorded by monitoring the change in absorbance at 340 nm. Water was used as a blank.

8.5.5 Blue-Sepharose affinity chromatography

Active fractions from the ion-exchange column were then loaded onto a Hi-Trap Blue column (bed volume 1 ml) that had been pre-equilibrated with three bed volumes of buffer A. The column was then washed with five bed volumes of buffer A and the enzyme was eluted with 1 M NaCl buffer A. The column was washed with three bed

volumes of regeneration buffer (1 M NaCl in buffer A). The eluted fractions were tested for enzyme activity using the coupled assay (Table 8.7).

8.5.6 Dialysis

The purified enzyme was dialysed twice against 100 volumes of buffer A at 4°C for 2 hours.

8.6 Biophysical methods

Buffer B	150 mM NaCl
	20 mM Tris.HCl pH 8.0 at 4°C

8.6.1 Circular dichroism spectroscopy

CD spectra were recorded at the University of Sydney on a Jasco-720 spectrophotometer at 4°C in 20 mM phosphate buffer containing 150 mM NaF pH 8.0 in a 0.1 mm quartz cell. The spectrometer was calibrated with *D*-(+)-camphorsulfonic acid monohydrate. The slit bandwidth used was 1 nm with a step size of 0.5 nm. Measurements were taken with a signal averaging time of 1.0 sec.

8.6.2 Blue-native polyacrylamide gel electrophoresis

Anode buffer	100 mM Tris. HCl pH 8.0
Cathode buffer	50 mM Tricine
	30 mM Tris. HCl pH 8.0
	0.02% Coomassie blue G-250
2×Sample treatment buffer	200 mM Tris. HCl pH 8.0
	0.7% Coomassie blue G-250
	10% glycerol
Fix	50% v/v methanol
	10% v/v glacial acetic acid

Samples were mixed with an equal volume of 2× sample treatment buffer before being loaded onto a BioRad Tris.HCl 4-15% precast RediGel. Electrophoresis was performed at 4°C and a constant a voltage of 200 V for approximately 60 minutes or

until the Coomasie blue die had run off the end of the gel, apparent by colouration of the anode buffer. Gels were then fixed and destained.

8.6.3 Quantitative analytical gel permeation chromatography

A Sephadex G-200 superfine column of 180 ml bed volume (35 × 2.6 cm) was assembled and equilibrated with buffer B. The column was calibrated with yeast alcohol dehydrogenase, BSA, ovalbumin, and ribonuclease A. Between 10 and 15 mg of each protein was loaded onto the pre-equilibrated column in 2 ml of Buffer B and collection of eluent was started when 1 ml of the sample had been loaded. Approximately 60 ml of void volume was collected before fraction collection was started. Fractions of 1.75 ml were collected at a flow rate of 0.175 ml/minute. With the fraction collector in drop mode, it was found that the error in fraction volume was ~0.5%. The absorbance of each fraction was then measured at 280 nm and these data were used to build elution peaks for each of the standard proteins. Standard proteins were run on the column in duplicate and each fraction reading was made in duplicate. In each case the peak of the elution curve was taken as the elution volume (V_e) for the standard. The resulting data were used to create a calibration curve of V_e against the natural log of the molecular weight of the protein. Wild-type DHDPS and DHDPS-L197D were chromatographed on the column as above. Activity was detected in fractions by the coupled assay and elution peaks were ascertained from these.

8.6.4 Qualitative analytical gel permeation chromatography

A Sephacryl S-400 column of 100 ml bed volume (50 × 1.6 cm) was employed for semi-qualitative analytical gel permeation chromatography. Pure samples of wild-type DHDPS and each of the variants were concentrated to between 15 and 20 mg/ml and 1 ml was applied to the column in buffer B. The column was eluted at a flow rate of 0.5 ml/min and 1 ml fractions were collected. Elution profiles were found by measurement of the absorbance of each fraction at 280 nm and in each case the peak of the elution curve was taken as the elution volume (V_e).

8.6.5 Analytical ultracentrifugation

Analytical ultracentrifugation experiments were performed in a Beckman Model XL-A analytical ultracentrifuge equipped with UV/Vis scanning optics and An-60 Ti

4-hole rotor. Protein samples were prepared in buffer B. Protein and reference (buffer B) solutions were loaded into 12 mm double sector cells with quartz windows. Prior to sedimentation, the protein samples were purified to homogeneity by size-exclusion liquid chromatography on a 16 × 600 mm Sephacryl S-400 column as in section 8.6.4.

Sedimentation velocity analytical ultracentrifugation

Samples at an initial protein concentration of 1.0 mg/ml (380 µl) and reference (400 µl) were centrifuged at 40,000 rpm at 20°C and data were collected at 280 nm every 6 min without averaging. Sedimentation velocity data were fitted to a continuous size-distribution model using the program SEDFIT (14). The partial specific volume ($\bar{v}$) of the sample and buffer density and viscosity of the reference solution were computed using the program SEDNTERP (15).

Sedimentation equilibrium analytical ultracentrifugation

For experiments, samples at initial protein concentrations of 0.1, 0.3 and 1.0 mg/ml (100 µl) and reference solution (120 µl) were centrifuged at 10,000 rpm or 16,000 rpm until sedimentation equilibrium was attained (~24 hours). Radial absorbance scans were taken at 280 nm with 5 averages and the data obtained at both speeds were fitted globally using the program SEDPHAT (16).

8.7 Kinetic analysis of wild-type DHDPS and the DHDPS variants

Two-substrate steady-state rate analysis was employed. DHDPS activity was measured using the coupled assay to DHDPR.

8.7.1 Selwyn's test

The stability of the variants during the time course of the assay was examined using Selwyn's test (17). The test was conducted over a time course of 3 min for all enzymes using a range of enzyme concentrations. Analysis was achieved by plotting the consumption of NADPH, indicated by the change inabsorbance at 340 nm, against the volume of enzyme multiplied by time. If enzyme activity was stable over the time course investigated, the resulting progress curves, when over-laid, did not deviate from one another.

8.7.2 Initial rate determination and kinetic analysis (4,18)

Assays were performed in 100 mM HEPES buffer pH 8 at 30°C, which was kept constant using a circulating water bath, and distilled water was used as a reference. In all cases, it was ensured that enzyme concentration was proportional to initial rate. DHDPR activity was typically kept at 10 times the maximum velocity to be measured in any set of kinetic data. Addition of further DHDPR, above this level, did not alter the initial rate of the reaction, demonstrating that DHDPR activity was in excess of DHDPS activity. This control was conducted routinely.

In all cases, preparations were allowed to equilibrate to 30°C in the cuvette, before the reaction was initiated with 20 µl (*S*)-ASA and mixed by aspiration with the pipette tip. The reaction was followed by measurement of the change in absorbance at 340 nm, corresponding to the consumption of NADPH by DHDPR. Wild-type DHDPS and the DHDPS variants were used at levels such that the rate of change of A_{340} at high substrate concentration was 0.015-0.02 AU/sec.

Kinetic parameter determination

Determination of the true kinetic constants, K_m and k_{cat}, was accomplished by concurrent variation of both substrate concentrations using an approximate range of $0.2 \times K_m$ to $10 \times K_m$. Initial velocities were routinely reproducible within 10%.

Table 8.8 *The quantitative coupled assay used for initial rate determination of wild-type DHDPS and the variants. Shown is the experimental design used for wild-type DHDPS.*

	[Initial] mM	Volume (µL)	[Final] mM
HEPES (pH 8 at 25°C)	200	500	100
NADPH	5.4	30	0.162
DHDPR		80	
DHDPS wild-type		20	
(*S*)-ASA	1-40	20	0.02-0.8
Pyruvate	1-40	50	0.05-2
dH_2O		300	
Total		1000	

Initial estimates of K_m values were determined by varying the concentration of one substrate while holding the other constant, using a range of substrate concentrations as wide as practically possible.

Table 8.8 details the experimental design used to determine initial rates for wild-type DHDPS. 25 data points were collected for each data series and each data point was measured in triplicate.

Lysine inhibition studies

To evaluate the kinetics of inhibition of DHDPS, kinetic experiments were performed holding the concentration of one substrate constant (close to its K_m), and varying both the concentration of the other substrate and the (*S*)-lysine concentration (Table 8.9). This data yielded K_i and K_i` values where appropriate. V^{app} and V^{app} constants from the inhibition analysis allowed the calculation of the percentage residual activity at saturating (*S*)-lysine concentrations

Table 8.9 *The quantitative coupled assay used for lysine inhibition studies. Shown is the experimental design for the analysis of lysine inhibition with respect to varying (S)-ASA concentration for wild-type DHDPS*

	[Initial] mM	Volume (µL)	[Final] mM
HEPES (pH 8 at 25°C)	200	500	100
NADPH	5.4	30	0.162
DHDPR		80	
DHDPS		20	
(*S*)-ASA	1.625-65	20	0.0325-1.3
pyruvate	10	50	0.2
lysine	0-100	50	0-5
dH_2O		250	
Total		1000	

Data analysis

Initial rate data were analysed using the Enzfitter programme available from Biosoft (Cambridge, UK). Data were fitted to the appropriate models as judged by SIGMA values and the lowest standard error associated with the kinetic constants.

8.8 X-ray crystallography and structural methods

Protein crystal structures were routinely inspected using O (19,20) and PyMOL (21). Unless otherwise stated, structural figures were produced using PyMOL (21). Figures depicting the wild-type *E. coli* DHDPS structure were produced using the coordinates of the structure solved in this lab (22).

8.8.1 Crystallisation Experiments

Protein crystallisation experiments were performed using the hanging-drop vapour-diffusion method and the sitting-drop vapour-diffusion method at 4°C using materials and equipment supplied by Hampton Research. The sparse matrix crystallisation screens, Crystal Screen, and Crystal Screen 2, were employed for identification of lead crystallisation conditions.

Crystallisation of DHDPS-L197Y

Well solution 1	30% w/v PEG 1500
	20 mM Tris.HCl pH 8

Well solution 1 was prepared in a greased VDX 24 well plate and cooled to 4°C. Protein was prepared a concentration of 7.5 mg/ml in 20 mM Tris.HCl pH 8. Hanging-drops and sitting-drops were prepared at 4°C in a cold-room. For hanging-drops 2 µl of protein solution was placed on a siliconised cover slide and 2 µl of well solution 1 was added to this and then mixed by gentle aspiration with the pipette tip. Cover slides were then inverted quickly, placed over wells containing well solution 1 and sealed. For sitting-drops, a plastic sitting-drop bridge was placed in wells containing well solution 1. 2 µl of protein solution was placed on the bridge and 2 µl of well solution 1 was added to this and mixed by gentle aspiration with the pipette tip. Wells were quickly sealed with cover slides.

Crystals formed in both hanging- and sitting-drops over a period of 2-3 months. Before mounting and freezing in liquid nitrogen, crystals were dipped in 10% v/v glycerol in well solution 1.

Crystallisation of DHDPS-L197D

Well solution 2	2.4 M ammonium sulfate
	100 mM Tris.HCl pH 8.15

Well solution 2 was prepared in a greased VDX 24 well plate and cooled to 4°C. Protein was prepared at a concentration of 7.2 mg/ml in 20 mM Tris.HCl pH 8. Hanging-drops and sitting-drops were prepared, as for DHDPS-L197Y, using well solution 2.

Crystals formed in both hanging- and sitting-drops over 3-4 days. Before mounting and freezing in liquid nitrogen, crystals were dipped in 25% w/v sucrose in well solution 2.

X-ray data collection

Intensity data were collected at 110 K using an RAxisIV++ image-plate detector coupled to a Rigaku Micromax 007 X-ray generator operating at 40 kV and 20 mA. Diffraction data sets were processed and scaled using the program CrystalClear (23).

Structure determination and refinement

Structures were solved using AMoRe (24,25), using the *E. coli* DHDPS monomer as solved by us as the search model. Refinement was achieved using REFMAC5 (24,26) with manual model corrections using the program O (19,20). Placement of solvent molecules was achieved using the program ARP (24,27) and water molecules with a B-factor of 50 or greater were removed. Structure quality was assessed by the program Procheck (24,28).

8.9 Synthesis of (*S*)-ASA *via* a Wienreb amide (29)

(*S*)-ASA was synthesised by the method of Roberts *et al.* (29), which was developed in this lab. Unless otherwise stated, all synthetic reactions were performed in dry glassware under an atmosphere of oxygen free nitrogen or argon. All organic extracts

were washed with brine and dried over anhydrous magnesium sulfate. After filtration of solutions to remove drying agents, the solvents were removed under reduced pressure on a Büchi rotary evaporator.

^{1}H NMR spectra were recorded on either a Varian Unity 300 or Varian Inova 500 spectrometer, operating at 300 and 500 MHz respectively. ^{13}C NMR spectra were obtained on either a Varian Unity 300 or Varian Inova 500 spectrometer, operating at 75 and 126 MHz respectively. For ^{1}H NMR, chemical shifts are reported relative to tetramethylsilane (TMS) if run in deuterated chloroform ($CDCl_3$). For samples run in deuterium oxide (D_2O), the spectra were referenced to the residual protonated solvent at 4.7 ppm, and for samples run in deuterated methanol (CD_3OD), the spectra were referenced to the residual protonated solvent peak at 3.3 ppm. For ^{13}C spectra run in deuterated chloroform ($CDCl_3$), the spectra were referenced to the residual protonated solvent at 77 ppm, and for samples run in deuterated methanol (CD_3OD), the spectra were referenced to the residual protonated solvent at 49.3 ppm.

Thin layer chromatography (TLC) was conducted on aluminium-backed Merck Kieselgel KG60F254 silica plates. The developed plates were analysed under short-wave UV light and stained with a potassium permanganate or phosphomolybdic acid dip. Unless otherwise stated, flash chromatography was performed on Merck Silica 60. Solvents and reagents were purified according to well-established procedures. Dichloromethane was freshly distilled from calcium hydride before use. Diethyl ether and tetrahydrofuran were freshly distilled from sodium/benzophenone ketyl before use. The petroleum ether used had a boiling range of 50-70°C. Methanol and ethanol were distilled from the appropriate magnesium alkoxide and stored under dry nitrogen over 4 Å molecular sieves.

8.9.1 N-*tert*-BOC-(*S*)-aspartic acid 1-(*tert*-butyl ester) N-methoxy-N-methylamide

(Benzotriazol-1-yloxy) tris(dimethylamino)phosphonium hexafluorophosphate ($BOP.PF_6$) (163 mg, 0.380 mmol) was added to a stirred solution of N-*tert*-BOC-(*S*)-aspartic acid 1-(*tert*-butyl ester) (100 mg, 0.346 mmol) and triethylamine (54 µL, 0.385 mmol) in dichloromethane (3.5 ml) at room temperature. After 5 min of stirring, O,N-dimethylhydroxyamine hydrochloride (40 mg, 0.397 mmol) was added, followed by triethylamine (54 µL, 0.385 mmol). All solid material dissolved within

10 min and the mixture was stirred for 2 hours at r.t. The reaction mixture was washed with 1 M HCl solution (3× 1 ml), H_2O (1 × 1 ml), 1 M $NaHCO_3$ solution (2 × 1 ml) and H_2O (2 × 1 ml). The solvent was removed *in vacuo* to give a clear yellow oily product, which was purified by flash chromatography on silica, using 30% ethyl acetate/petroleum ether as the eluant, to give N-*tert*-BOC-*S*-aspartic acid 1-(*tert*-butyl ester) N-methoxy-N-methylamide as a colourless oil (100 mg, 86%). ^{1}H NMR (300 MHz, DMSO)—δ_H 1.38 (18H, s, 2 × -$C(CH_3)_3$), 2.8 (2H, m, -CH_2-), 3.06 (3H, s, -CH_3), 3.7 (3H, s, -CH_3), 4.23 (1H, m, -CHNH-), 6.98 (1H, m, -NH-). The ^{1}H NMR data were consistent with those in the literature (30).

8.9.2 1-*tert*-Butyl (*S*)-2-(*tert*-BOC-amino)-4-oxobutanoate

A solution of diisobutylaluminum hydride (DIBAL) in hexane (1 M, 0.55 ml, 0.55 mmol) was added dropwise over 20 min to a stirred solution of N-*tert*-BOC-(*S*)-aspartic acid 1-(*tert*-butyl ester) N-methoxy-N-methylamide (110 mg, 0.36 mmol) in anhydrous THF (1.8 ml) at –78°C . The mixture was allowed to stir at –78 °C for 2 hours. The reaction mixture was partitioned between 0.35 M aqueous $NaHSO_4$ solution (3.6 ml) and diethyl ether (5.5 ml). After separation, the aqueous layer was extracted with diethyl ether (3 × 2 ml). The combined ethereal layers were washed with 1 M HCl solution (3× 1 ml), 1 M $NaHCO_3$ solution (3× 1 ml), and brine (3× 1 ml). Concentration *in vacuo* gave 1-*tert*-butyl (*S*)-2-(*tert*-BOC-amino)-4-oxobutanoate as a colourless oil (92 mg, 95%), which solidified on standing at r.t. ^{1}H NMR (300 MHz, $CDCl_3$)—δ_H 1.43 (9H, s, -$C(CH_3)_3$), 1.44 (9H, s, -$C(CH_3)_3$), 2.98 (2H, m, -CH_2-), 4.45 (1H, m, -CH), 5.38 (1H, m, -NH-), 9.75 (1H, s, -CHO). The ^{1}H NMR data were consistent with those in the literature (31).

8.9.3 (*S*)-Aspartate β-semialdehyde hydrate trifluoroacetate

(*S*)-N-*tert*-Butoxycarbonylaspartate β-semialdehyde *p*-methoxybenzyl ester (1.30 mg, 3.86 mmol) was dissolved in dry dichloromethane (24 ml). The reaction was stirred under nitrogen and trifluoroacetic acid (24 ml) was added *via* a syringe. The reaction was stirred for two hours. The solvent was then removed *in vacuo* to give a yellow oily residue, which was partitioned between water (120 ml) and ethyl acetate (3 × 120 ml). The aqueous layer was then concentrated under high vacuum to yield (*S*)-aspartate β-semialdehyde hydrate trifluoroacetate as a pale yellow solid/oil. The

overall yield for this synthesis was 51%. The yield of (*S*)-aspartate β-semialdehyde hydrate trifluoroacetate was 814 mg (3.27 mmol, 85%). ^{1}H NMR (300 MHz D_2O)—δ_H 1.97–2.21 (2H, m, -CH_2CHNH_2-), 4.01–4.05 (1H, m, -$CHNH_2$), 5.21 (1H, t, -$CH(OH)_2$). ^{13}C NMR (75 MHz D_2O)—δ_c 36.2 (-CH_2CHNH_2), 49.7 (-$CHNH_2$-), 87.7 (-$CH(OH)_2$), 118.0 (-CCF_3), 162 (-CCF_3), 171.2 (-C=O). The ^{1}H and ^{13}C NMR data were consistent with those in the literature (7,31).

8.9.4 Titration of (*S*)-ASA purity by the coupled assay

To determine the purity of (*S*)-ASA, the coupled assay was used to quantify the (*S*)-ASA concentration and this was compared to the calculated concentration based on mass of product. The reaction was followed by a change in the absorbance at 340 nm with the loss of NADPH. The method assumes the reactions are irreversible. Fresh solutions of (*S*)-ASA and NADPH were prepared in distilled water. The reaction was prepared as in Table 8.10

Table 8.10 *Preparation of the coupled assay for quantification of (S)-ASA.*

	[Initial] mM	Volume (μL)	[Final] mM
HEPES (pH 8 at 25°C)	200	500	100
NADPH	5.4	30	0.162
DHDPR		100	
DHDPS		10	
(*S*)-ASA		50	> 0.15
Pyruvate	100	50	20
dH_2O		265	
Total		1000	

Under these conditions, (*S*)-ASA was the limiting substrate. This was confirmed by the addition of further NADPH or pyruvate after the reaction had reached a plateau. Thus the total turnover of NADPH was equivalent to the turnover of (*S*)-ASA.

8.10 References

1. Sambrook, J., Fritsch, E., and Maniatis, T. (1990) *Molecular cloning: A laboratory Manual*, 2nd Ed., Cold Spring Harbor Press, Cold Spring Harbor, New York
2. Miller, J. (1992) *A short course in bacterial genetics; a lab manual and handbook for E. coli and related bacteria*, Cold Spring Harbour, New York
3. Stratagene. (1998) *Quikchange site-directed mutagenesis kit: instruction manual*
4. Dobson, R. C., Valegard, K., and Gerrard, J. A. (2004) The crystal structure of three site-directed mutants of *Escherichia coli* dihydrodipicolinate synthase: Further evidence for a catalytic triad. *J Mol Biol* **338**, 329-339
5. Bukhari, A. I., and Taylor, A. L. (1971) Genetic analysis of diaminopimelic acid- and lysine-requiring mutants of *Escherichia coli*. *J Bacteriol* **105**, 844-854
6. Yeh, P., Sicard, A. M., and Sinskey, A. J. (1988) General organization of the genes specifically involved in the diaminopimelate-lysine biosynthetic pathway of *Corynebacterium glutamicum*. *Mol Gen Genet* **212**, 105-111
7. Coulter, C. V. (1997) Studies in lysine biosynthesis. *PhD thesis*, University of Canterbury
8. Gerrard, J. A. (1992) Studies on dihydrodipicolinate synthase. *D. Phil. thesis*, Oxford University
9. Kraunsoe, J. A. E. (1992) Studies in lysine biosynthesis. *BSc. Hons. Part II*, Corpus Christi College
10. Bradford, M. M. (1976) A rapid and sensitive method for the quantitation of microgram quantities of protein utilizing the principle of protein-dye binding. *Anal Biochem* **72**, 248-254
11. Mirwaldt, C., Korndorfer, I., and Huber, R. (1995) The crystal structure of dihydrodipicolinate synthase from *Escherichia coli* at 2.5 Å resolution. *J Mol Biol* **246**, 227-239
12. Reddy, S. G., Sacchettini, J. C., and Blanchard, J. S. (1995) Expression, purification, and characterization of *Escherichia coli* dihydrodipicolinate reductase. *Biochemistry* **34**, 3492-3501
13. Coulter, C. V., Gerrard, J. A., Kraunsoe, J. A. E., and Pratt, A. J. (1999) *Escherichia coli* dihydrodipicolinate synthase and dihydrodipicolinate reductase: Kinetic and inhibition studies of two putative herbicide targets. *Pestic Sci* **55**, 887-895
14. Schuck, P. (2000) Size-distribution analysis of macromolecules by sedimentation velocity ultracentrifugation and Lamm equation modeling. *Biophys J* **78**, 1606-1619
15. Laue, T. M., Shah, B. D., Ridgeway, T. M., and Pelletier, S. L. (1992) in *Analytical ultracentrifugation in biochemistry and polymer science*, pp. 90-125, The Royal Society of Chemistry, Cambridge

16. Vistica, J., Dam, J., Balbo, A., Yikilmaz, E., Mariuzza, R. A., Rouault, T. A., and Schuck, P. (2004) Sedimentation equilibrium analysis of protein interactions with global implicit mass conservation constraints and systematic noise decomposition. *Anal Biochem* **326**, 234-256

17. Selwyn, M. J. (1965) A simple test for inactivation of an enzyme during assay. *Biochim Biophys Acta* **105**, 193-195

18. Dobson, R. C., Griffin, M. D., Roberts, S. J., and Gerrard, J. A. (2004) Dihydrodipicolinate synthase (DHDPS) from *Escherichia coli* displays partial mixed inhibition with respect to its first substrate, pyruvate. *Biochimie* **86**, 311-315

19. Jones, T. A., Zou, J. Y., Cowan, S. W., and Kjeldgaard. (1991) Improved methods for building protein models in electron density maps and the location of errors in these models. *Acta Crystallogr A* **47** (**Pt 2**), 110-119

20. Jones, T. A., and Kjeldgaard, M. (1997) Electron-density map interpretation. *Methods Enzymol* **277**, 173-208

21. DeLano, W. L. (2002) *The PyMOL molecular graphics system*, DeLano Scientific, San Carlos

22. Dobson, R. C. J., Griffin, M. D. W., Jameson, G. B., and Gerrard, J. A. (2005) The crystal structures of native and (*S*)-lysine bound dihydrodipicolinate synthase from *Escherichia coli* with improved resolution show new features of biological significance. *Acta Crystallogr D Biol Crystallogr*, (Submitted)

23. Pflugrath, J. W. (1999) The finer things in X-ray diffraction data collection. *Acta Crystallogr D Biol Crystallogr* **55** (**Pt 10**), 1718-1725

24. Collaborative computational project, n. (1994) The CCP4 suite: programs for protein crystallography. *Acta Crystallogr D Biol Crystallogr* **50**, 760-763

25. Navaza, J., and Saludjian, P. (1997) AMoRe: An automated molecular replacement program package. *Methods Enzymol* **276**, 581-594

26. Murshudov, G. N., Vagin, A. A., and Dodson, E. J. (1997) Refinement of macromolecular structures by the maximum-likelihood method. *Acta Crystallogr D Biol Crystallogr* **53**, 240-255

27. Lamzin, V. S., and Wilson, K. S. (1997) Automated refinement for protein crystallography. *Methods Enzymol* **277**, 269-305

28. Laskowski, R. A., Macarthur, M. W., Moss, D. S., and Thornton, J. M. (1993) Procheck: A program to check the stereochemical quality of protein structures. *Journal of Applied Crystallography* **26**, 283-291

29. Roberts, S. J., Morris, J. C., Dobson, R. C., and Gerrard, J. A. (2003) The preparation of (*S*)-aspartate semi-aldehyde appropriate for use in biochemical studies. *Bioorg Med Chem Lett* **13**, 265-267

30. Wernic, D., Dimaio, J., and Adams, J. (1989) Enantiospecific synthesis of L-a-aminosuberic acid: synthetic applications in preparation of atrial natriuretic factor analogs. *J Org Chem* **54**, 4224-4228

31. Tudor, D. W., Lewis, T., and Robins, D. J. (1993) Synthesis of the trifluoroacetate salt of aspartic-acid β-semialdehyde, an intermediate in the biosynthesis of L-lysine, L-threonine, and L-methionine. *Synthesis-Stuttgart*, 1061-1062

Appendix One

Analysis of the feedback inhibition kinetics of wild-type DHDPS and the variants

Figure A1.1 *Inhibition of wild-type DHDPS with respect to pyruvate. A is a direct plot of initial rate data overlayed with fit data for the partial mixed inhibition model generated by non-linear regression (curves). B and C are Lineweaver-Burke and Eadie-Hofstee plots of the same data respectively. D is a plot of percentage residuals for each data point ($100\times(v_{obs}-v_{cal})/v_{cal}$). v is the mean initial rate in $\mu mol_{NADPH}\ mg^{-1}\ min^{-1}$, and [Pyruvate] refers to pyruvate concentration. The r^2 value for the fit was 0.999 and p>F was much less than 0.001.*

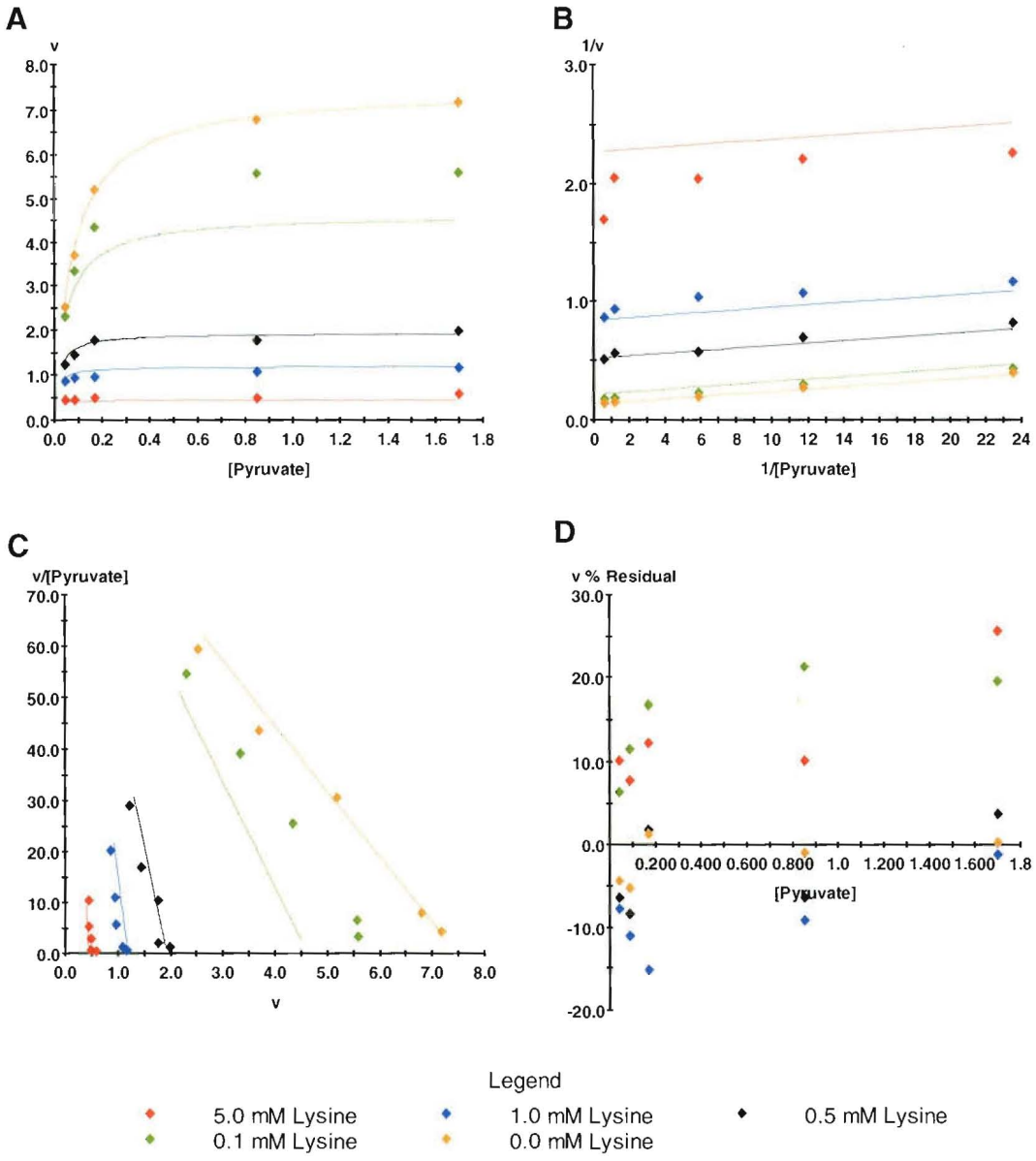

Figure A1.2 *Inhibition of wild-type DHDPS with respect to (S)-ASA. A is a direct plot of initial rate data overlayed with fit data for the partial non-competitive inhibition model generated by non-linear regression (curves). B and C are Lineweaver-Burke and Eadie-Hofstee plots of the same data respectively. D is a plot of percentage residuals for each data point ($100\times(v_{obs}-v_{cal})/v_{cal}$). v is the mean initial rate in $\mu mol_{NADPH}\ mg^{-1}\ min^{-1}$, and [ASA] refers to (S)-ASA concentration. The r^2 value for the fit was 0.98 and p>F was much less than 0.001.*

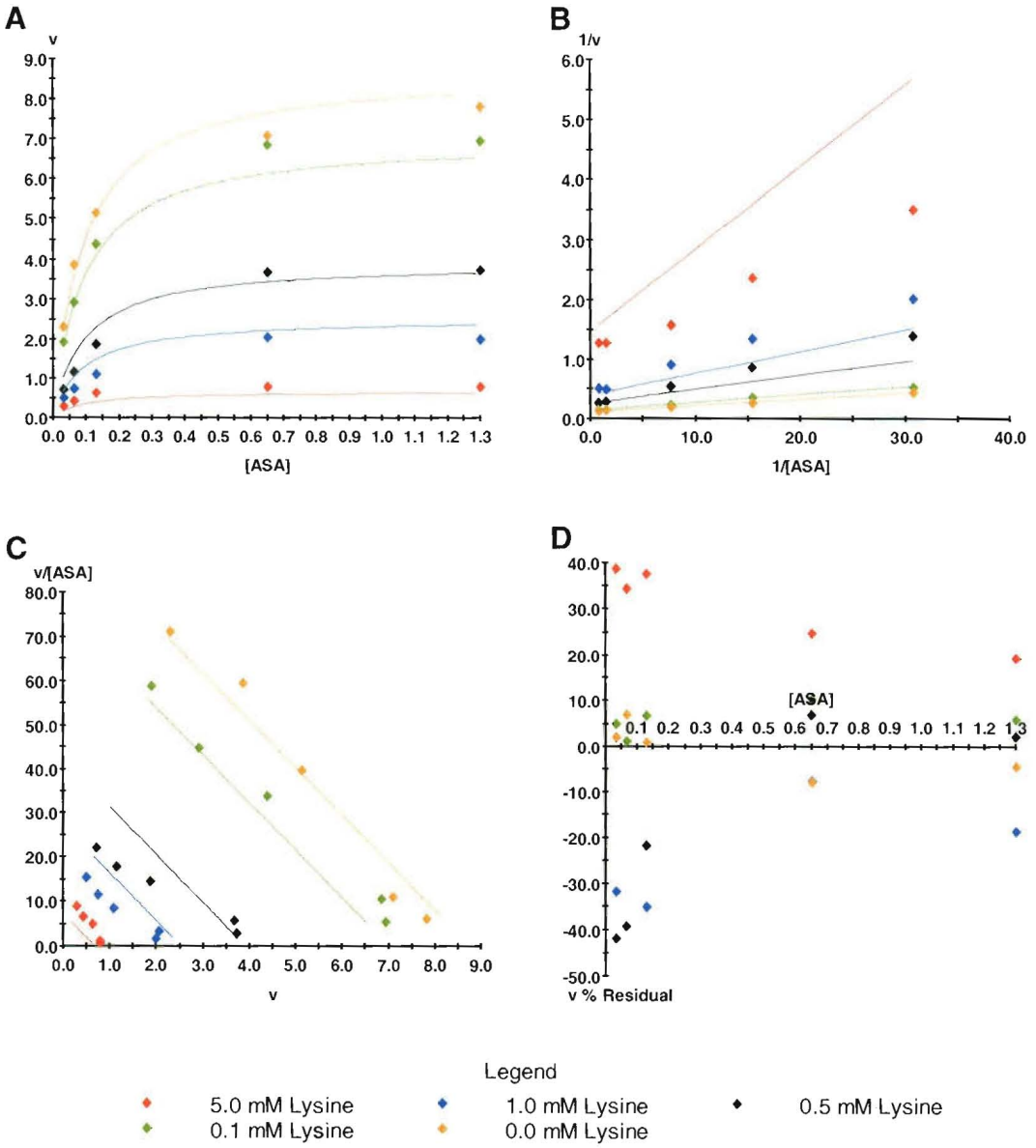

Figure A1.3 *Inhibition of DHDPS-L197D with respect to pyruvate. A is a direct plot of initial rate data overlayed with fit data for the partial mixed inhibition model generated by non-linear regression (curves). B and C are Lineweaver-Burke and Eadie-Hofstee plots of the same data respectively. D is a plot of percentage residuals for each data point ($100\times(v_{obs}-v_{cal})/v_{cal}$). v is the mean initial rate in $\mu mol_{NADPH}\ mg^{-1}\ min^{-1}$, and [Pyruvate] refers to pyruvate concentration. The r^2 value for the fit was 0.99 and p>F was much less than 0.001.*

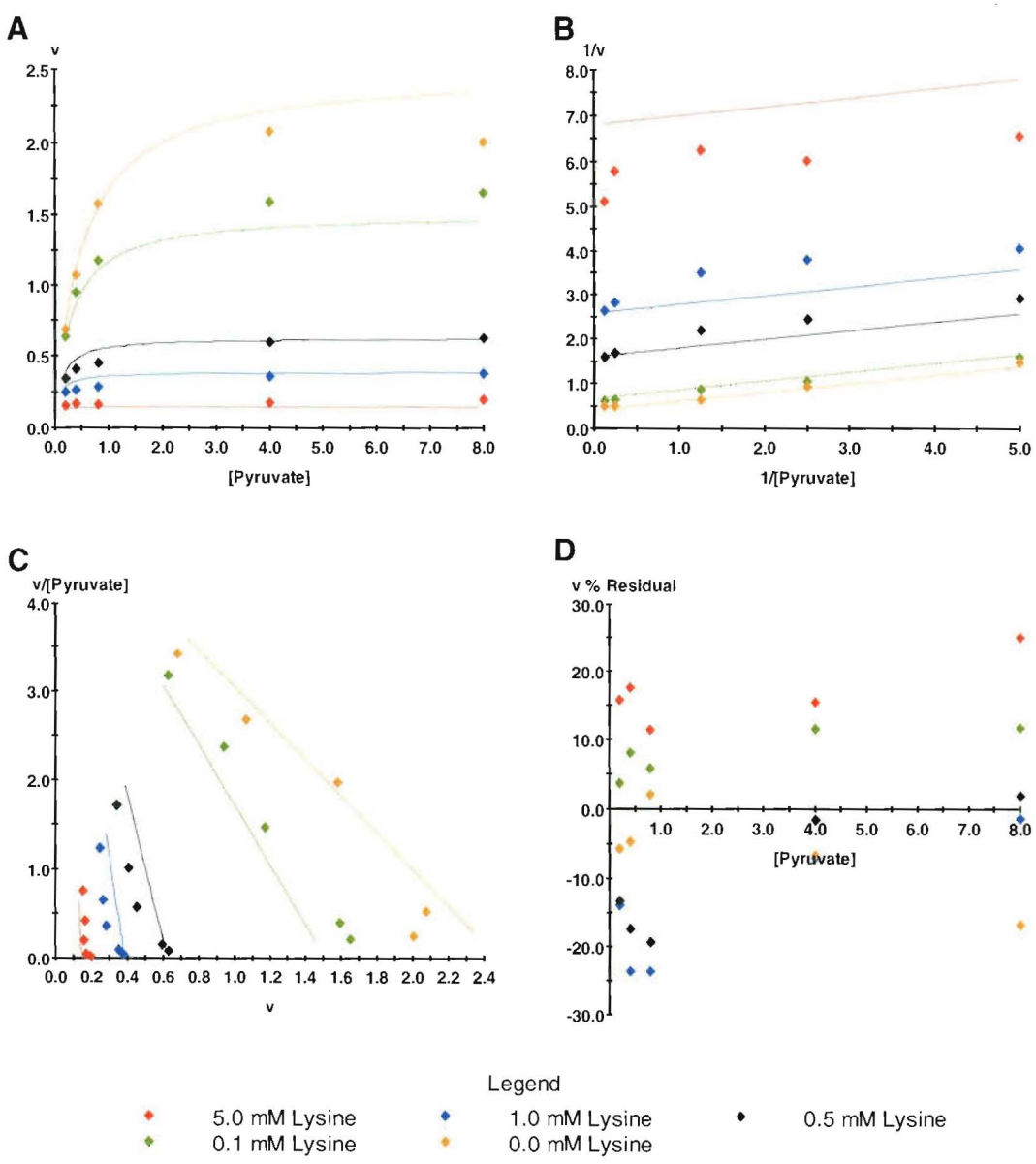

Figure A1.4 *Inhibition of DHDPS-L197D with respect to (S)-ASA. A is a direct plot of initial rate data overlayed with fit data for the partial non-competitive inhibition model generated by non-linear regression (curves). B and C are Lineweaver-Burke and Eadie-Hofstee plots of the same data respectively. D is a plot of percentage residuals for each data point ($100\times(v_{obs}-v_{cal})/v_{cal}$). v is the mean initial rate in $\mu mol_{NADPH}\ mg^{-1}\ min^{-1}$, and [ASA] refers to (S)-ASA concentration. The r^2 value for the fit was 0.98 and p>F was much less than 0.001.*

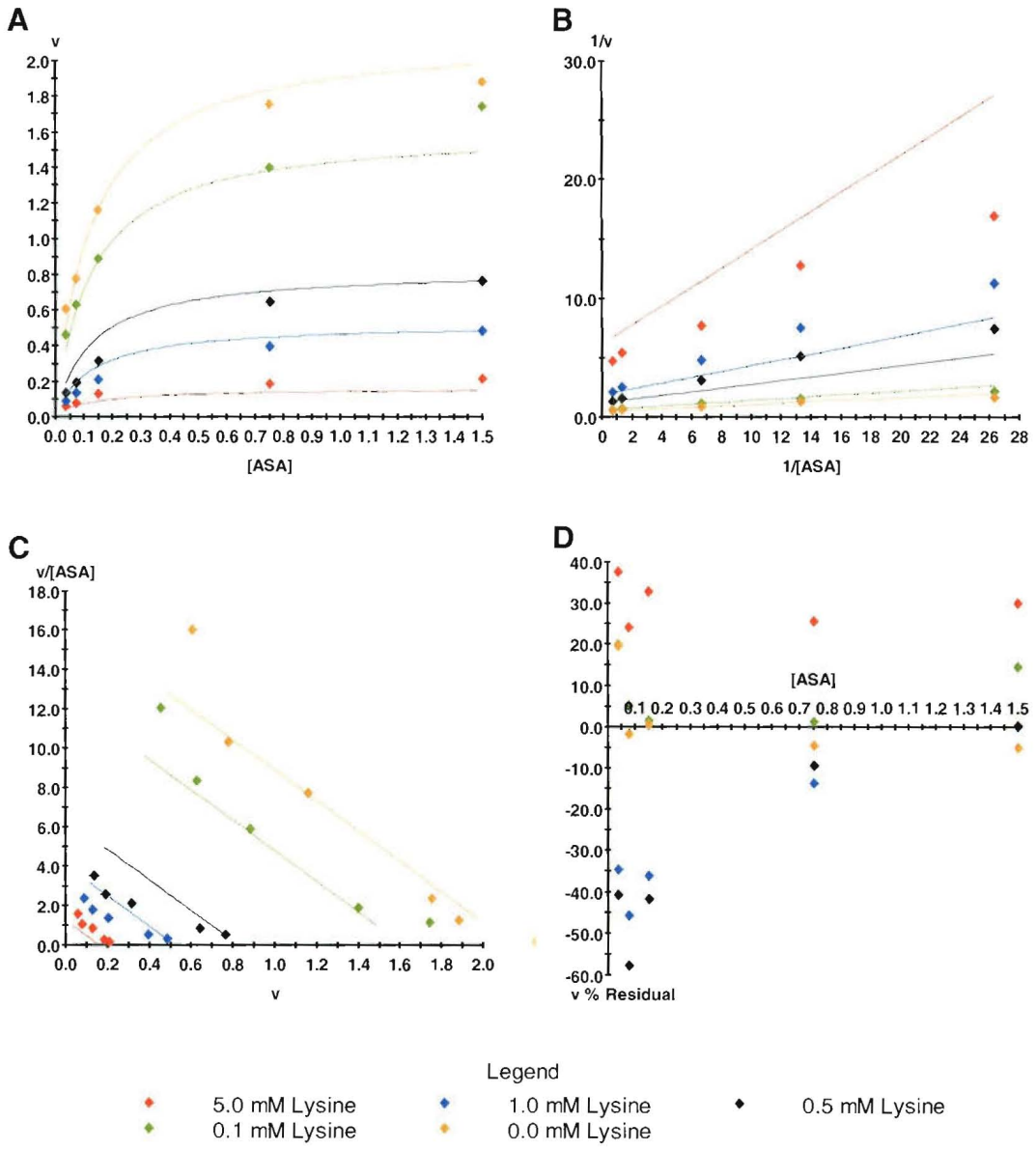

Figure A1.5 *Inhibition of DHDPS-L197Y with respect to pyruvate. A is a direct plot of initial rate data overlayed with fit data for the partial mixed inhibition model generated by non-linear regression (curves). B and C are Lineweaver-Burke and Eadie-Hofstee plots of the same data respectively. D is a plot of percentage residuals for each data point ($100\times(v_{obs}-v_{cal})/v_{cal}$). v is the mean initial rate in $\mu mol_{NADPH}\ mg^{-1}\ min^{-1}$, and [Pyruvate] refers to pyruvate concentration. The r^2 value for the fit was 0.98 and p>F was much less than 0.001.*

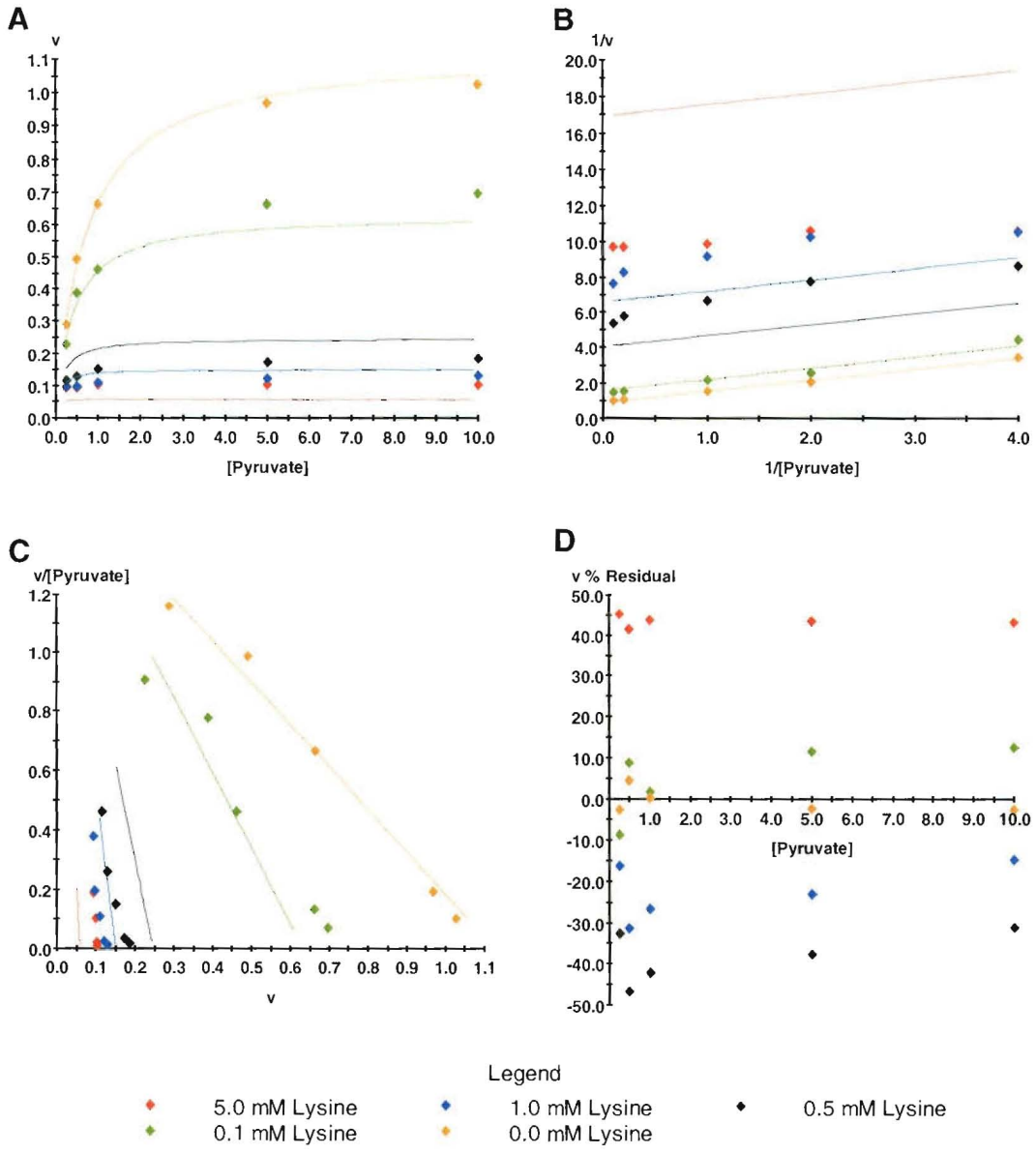

Figure A1.6 *Inhibition of DHDPS-L197Y with respect to (S)-ASA. A is a direct plot of initial rate data overlayed with fit data for the partial non-competitive inhibition model generated by non-linear regression (curves). B and C are Lineweaver-Burke and Eadie-Hofstee plots of the same data respectively. D is a plot of percentage residuals for each data point ($100\times(v_{obs}-v_{cal})/v_{cal}$). v is the mean initial rate in $\mu mol_{NADPH}\ mg^{-1}\ min^{-1}$, and [ASA] refers to (S)-ASA concentration. The r^2 value for the fit was 0.98 and p>F was much less than 0.001.*

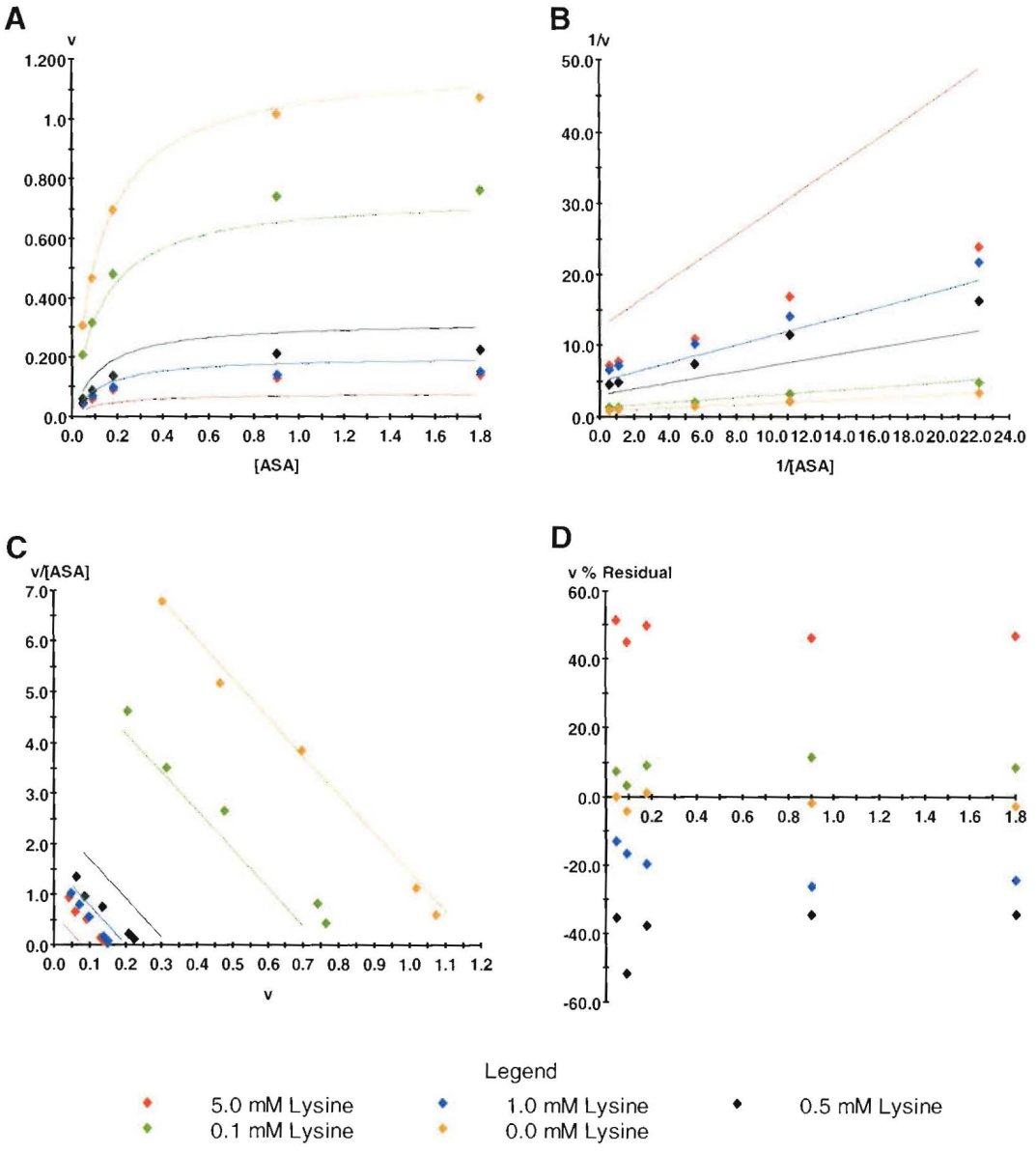

Figure A1.7 *Inhibition of DHDPS-Q196D with respect to pyruvate. A is a direct plot of initial rate data overlayed with fit data for the partial mixed inhibition model generated by non-linear regression (curves). B and C are Lineweaver-Burke and Eadie-Hofstee plots of the same data respectively. D is a plot of percentage residuals for each data point ($100\times(v_{obs}-v_{cal})/v_{cal}$). v is the mean initial rate in $\mu mol_{NADPH}\ mg^{-1}\ min^{-1}$, and [Pyruvate] refers to pyruvate concentration. The r^2 value for the fit was 0.98 and p>F was much less than 0.001.*

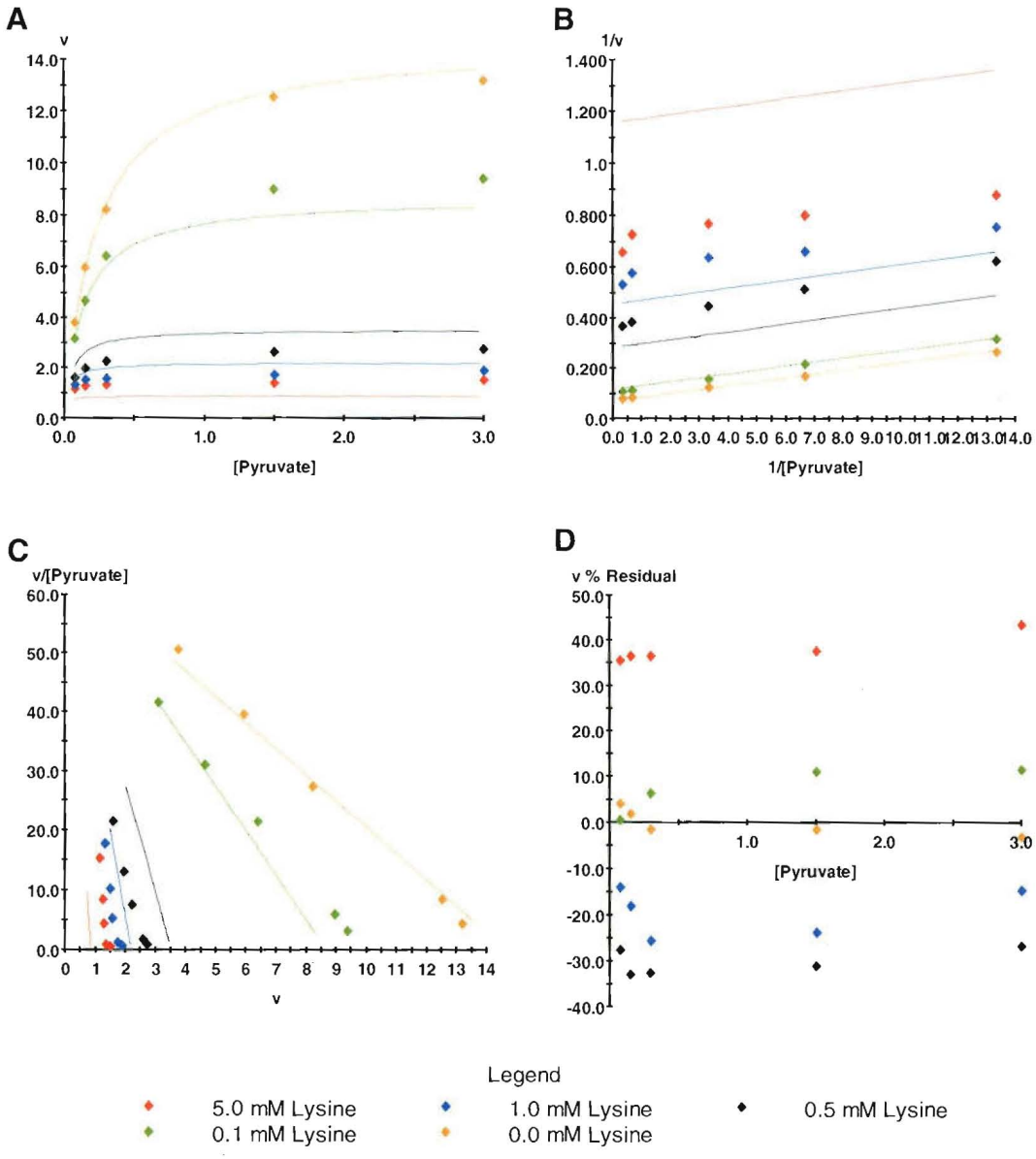

Figure A1.8 *Inhibition of DHDPS- Q196D with respect to (S)-ASA. A is a direct plot of initial rate data overlayed with fit data for the partial non-competitive inhibition model generated by non-linear regression (curves). B and C are Lineweaver-Burke and Eadie-Hofstee plots of the same data respectively. D is a plot of percentage residuals for each data point ($100\times(v_{obs}-v_{cal})/v_{cal}$). v is the mean initial rate in $\mu mol_{NADPH}\ mg^{-1}\ min^{-1}$, and [ASA] refers to (S)-ASA concentration. The r^2 value for the fit was 0.98 and p>F was much less than 0.001.*

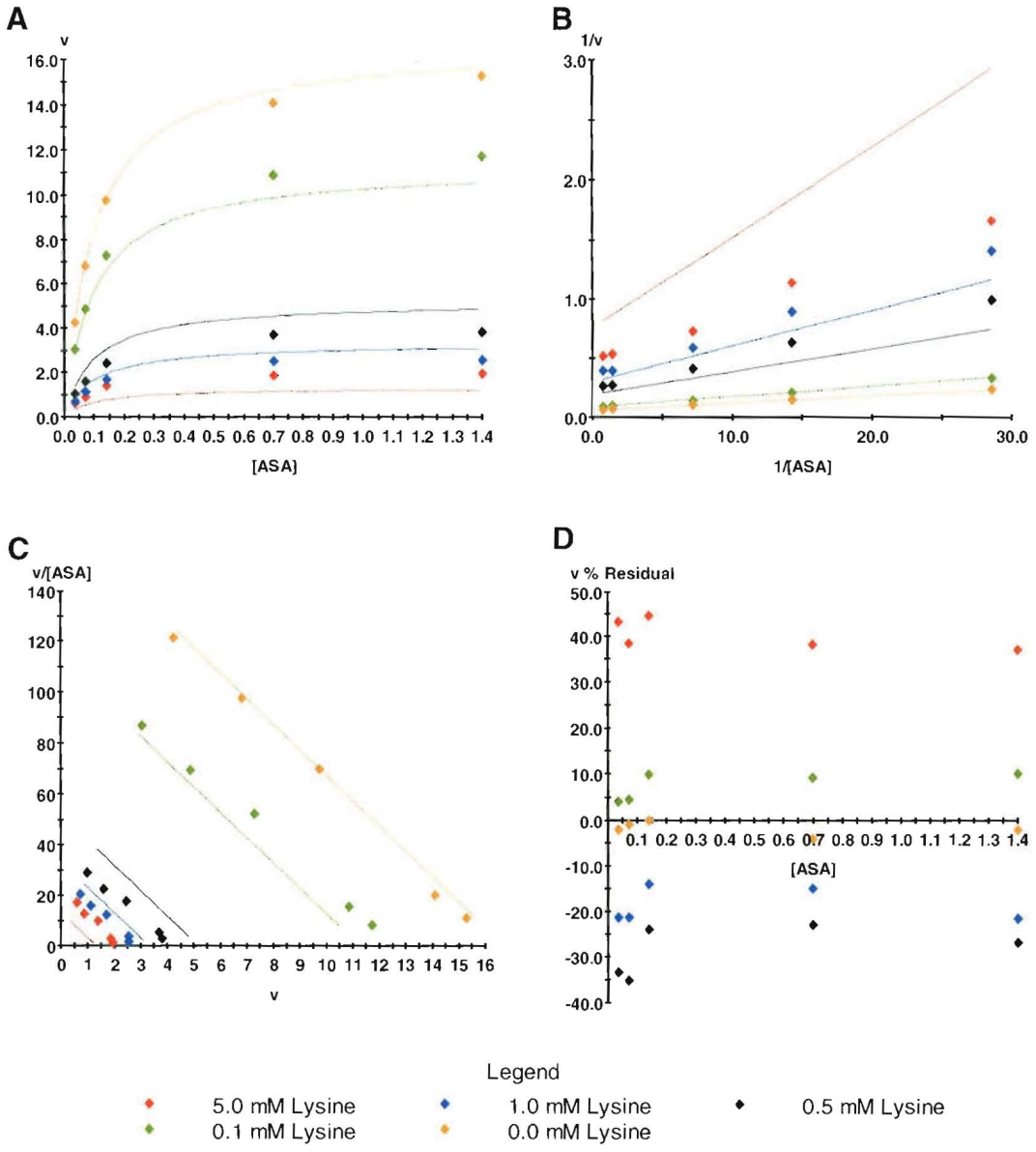

Figure A1.9 *Inhibition of DHDPS-D193A with respect to pyruvate. A is a direct plot of initial rate data overlayed with fit data for the partial mixed inhibition model generated by non-linear regression (curves). B and C are Lineweaver-Burke and Eadie-Hofstee plots of the same data respectively. D is a plot of percentage residuals for each data point ($100\times(v_{obs}-v_{cal})/v_{cal}$). v is the mean initial rate in $\mu mol_{NADPH}\ mg^{-1}\ min^{-1}$, and [Pyruvate] refers to pyruvate concentration. The r^2 value for the fit was 0.98 and p>F was much less than 0.001.*

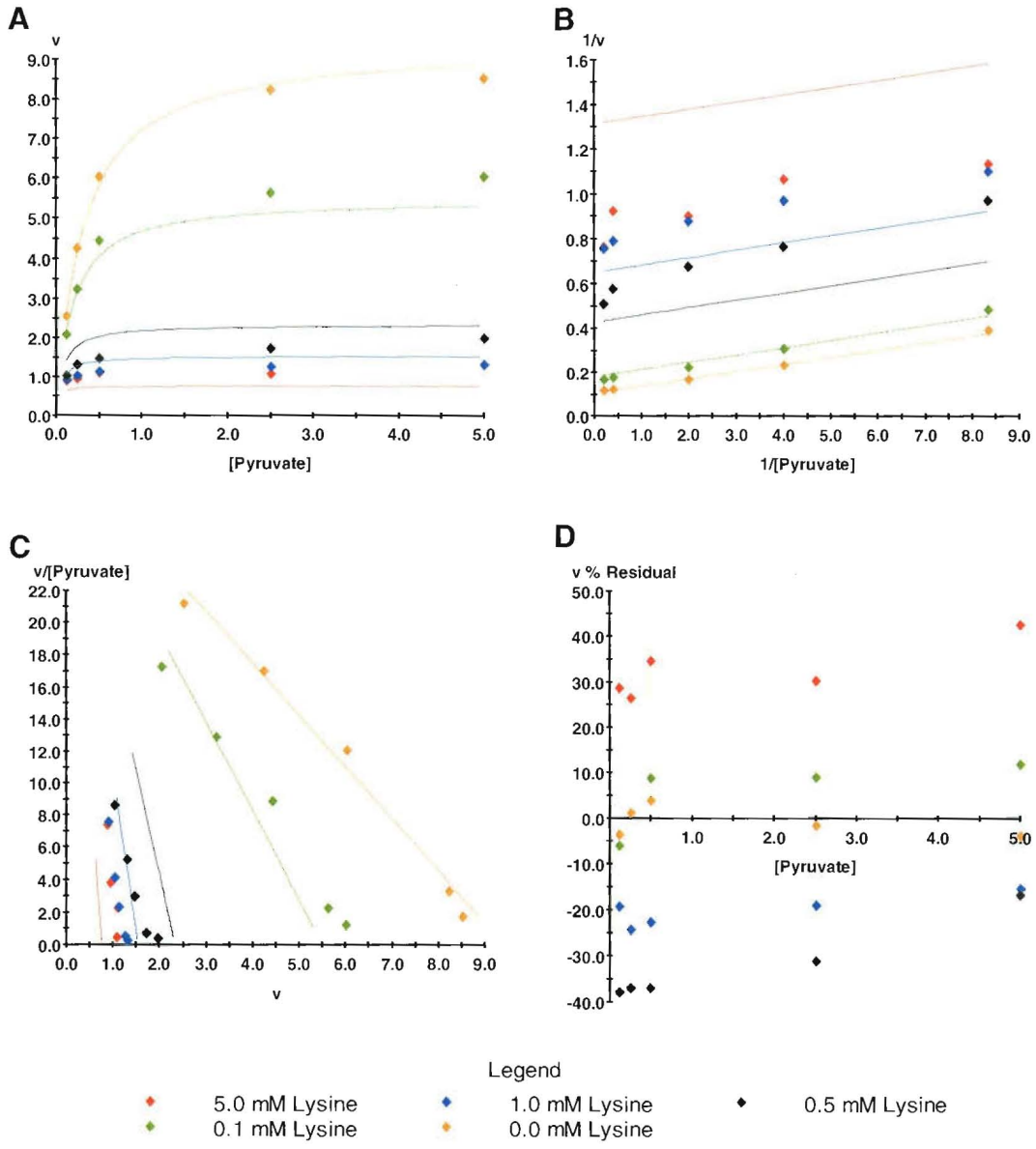

Figure A1.10 *Inhibition of DHDPS-D193A with respect to (S)-ASA. A is a direct plot of initial rate data overlayed with fit data for the partial non-competitive inhibition model generated by non-linear regression (curves). B and C are Lineweaver-Burke and Eadie-Hofstee plots of the same data respectively. D is a plot of percentage residuals for each data point ($100\times(v_{obs}-v_{cal})/v_{cal}$). v is the mean initial rate in $\mu mol_{NADPH}\ mg^{-1}\ min^{-1}$, and [ASA] refers to (S)-ASA concentration. The r^2 value for the fit was 0.98 and p>F was much less than 0.001.*